Consequences of cooperativity in supramolecular polymers

Consequences of Cooperativity in Supramolecular Polymers

PROEFSCHRIFT

ter verkrijging van de graad van doctor aan de
Technische Universiteit Eindhoven, op gezag van de
rector magnificus, prof.dr.ir. C.J. van Duijn, voor een
commissie aangewezen door het College voor
Promoties in het openbaar te verdedigen
op dinsdag 14 juni 2012 om 16.00 uur

door

Seda Cantekin

geboren te Istanbul, Turkije

Dit proefschrift is goedgekeurd door de promotor:

prof.dr. E.W. Meijer

Copromotor:
dr.ir. A.R.A. Palmans

Cover design: ICMS Animation Studio, TU/e
Printing: Gildeprint Drukkerijen, Enschede

A catalogue record is available from the Eindhoven University of Technology Library

ISBN: 978-90-386-3157-8

This work has been financially supported by the National Research School Combination Catalysis

To mum, dad and Ezgi

Dünyayı güzellik kurtaracak, bir insanı sevmekle başlayacak herşey

(Z. Livaneli)

Table of contents

1

COOPERATIVITY AND CHIRAL AMPLIFICATION

Abstract. Cooperativity is widely observed in the self-assembled systems that are found in Nature. Biologically important self-assembled systems embody the principles of cooperative self-assembly i.e., repeating units that form these macromolecular structures are held together by cooperative, non-covalent interactions and they act harmoniously. In addition to cooperativity, chirality plays a dominant role in Nature. Biologically important molecules are homochiral i.e., they constitute a class of molecules with the same absolute configuration. Studying synthetic supramolecular polymers is academically and technologically important in order to gain insights into cooperative interactions and chirality that are observed in complex systems in biology. Owing to their cooperative self-assembly behaviour in dilute solutions, expression of supramolecular chirality and synthetic accessibility, benzene-1,3,5-tricarboxamides (BTAs) serve as a model system. This chapter gives a general overview on cooperativity and chiral amplification in biological and synthetic systems. Cooperativity is described based on the supramolecular polymerization mechanisms. Chiral amplification mechanisms are discussed at different molecular levels. Structural properties, synthesis, self-assembly and chiral amplification behavior of the BTA molecules are described. The chapter is concluded with a summary of the aim and the outline of the thesis.

1.1 Cooperativity and chirality in biological systems

Cooperativity arises from the interplay of two or more interactions leading to collective forces that are negligible in the individual molecules.[1,2] Cooperativity is widely observed in self-assembled systems that are found in Nature. The molecules of life[3], for instance, proteins, DNA, RNA and starch (Figure 1.1) share the principles of cooperation, i.e., they are built by relatively small monomeric units that are held together by cooperative, noncovalent interactions. The monomeric units forming these macromolecules are prone to act harmoniously as a result of this cooperation. The interactions between monomers may also reflect to conformational changes such as protein folding or nucleic acid helix-coil transitions.[4] The term cooperativity can also be used to define the thermodynamics of the formation mechanism of multi-component complexes.[1] A cooperative polymerization is reversible and proceeds to thermodynamic equilibrium —a state determined by environmental conditions such as temperature, pH and the concentrations of monomers.[5] At equilibrium, polymerization and depolymerization take place at the same rate; therefore, the structures of these polymers are dynamic in the sense that they are constantly fluctuating. Under appropriate conditions, these polymerizations are spontaneous, indicating that the polymeric structures are thermodynamically stable. A well-known example is the supramolecular polymerization of the tobacco mosaic virus (TMV), which can be reconstructed from dispersed protein molecules in the presence of nucleic acids at neutral pH. The self-assembly of TMV represents a 'nucleated (cooperative)' polymerization mechanism which requires the dimerization of protein monomers into two-layer discs representing a metastable state. This initial step is followed by the recognition of the virus RNA and further polymerization.[6] Other examples of biological systems in which cooperative growth is observed are nucleated formation of actin[7,8], tubulin[9], and sickle cell hemoglobin.[10,11]

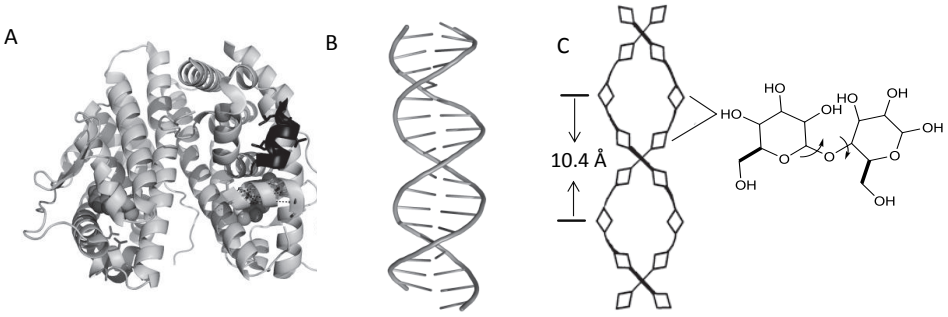

Figure 1.1: Examples of biologically relevant supramolecular polymers that are found in Nature. A) Estrogen receptor beta (3OMO).[12] B) Double-stranded DNA fragment.[13] C) Left-handed double helix of A-type and B-type starch.[14]

In addition to cooperativity, chirality plays a dominant role in Nature. Biologically important monomeric units forming the macromolecular structures such as amino acids, nucleic acids and sugars are chiral. (A chiral molecule is not superimposable with its mirror image.[15] The two molecules with mirror image relationship are named enantiomers (Figure 1.2)). Life is based on homochirality (i.e., a class of chiral compounds having the same absolute configuration dominates in Nature). Sugars such as deoxyribose that contain and transfer the genetic information in DNA have D-configuration and 20 amino acids in proteins (except for glycine) that are responsible for structure and chemical transformations in cells have L-configuration.[16] The evolution of chiral molecules from a presumably racemic, prebiotic world has been a challenging yet invigorating research topic for many years. Several mechanisms have been proposed describing how an initial imbalance between enantiomers occurred, as well as the mechanisms for amplification of this imbalance. Most important among these are the far-from-equilibrium models that include stochastic symmetry breaking coupled with autocatalytic amplification.[17-23]

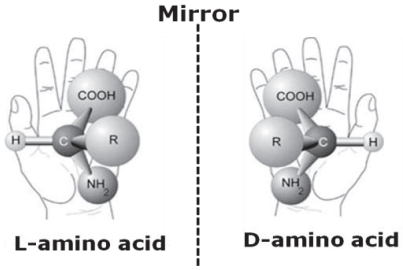

Figure 1.2: Schematic representation of L- and D-amino acids.

Studying synthetic supramolecular polymers which adopt comparable properties to the self-assembled systems that are found in Nature is important in order to gain fundamental knowledge and ultimately use this information to produce functional synthetic materials. Owing to their facile synthetic accessibility and versatility, benzene-1,3,5-tricarboxamide (BTA) molecules represent a model system in order to study cooperative self-assembly and chiral amplification at the supramolecular level.

In the following parts, cooperative interactions within different synthetic macromolecular systems and general aspects of cooperative supramolecular polymerization mechanisms are discussed. Chiral amplification observed in different systems is described. The structural properties, self-assembly and chiral amplification behavior of BTA molecules are summarized. The chapter is concluded by summarizing the aim and outline of the thesis.

1.2 Cooperativity in synthetic macromolecular systems

Poly(*n*-hexylisocyanate)s adopt a stiff helical conformation[24] in solution, the character of which is highly dependent on solvent and temperature changes. Due to the absence of a stereogenic center in the isocyanate units, poly(*n*-hexylisocyanate) forms right-handed (*P*) and left-handed (*M*) helices in equal amounts (Figure 1.3A). Incorporation of stereocenters in the side chain of the polyisocyanates results in strong optical activity suggesting a preference for one helical sense over the other. A new class of polyisocyanates, poly((*R*)-1-deuterio-*n*-hexylisocyanate), was synthesized from deuterated isocyanates which are optically active only by deuterium substitution (Figure 1.3B). The optical activity of these monomers was slightly larger than zero as a result of deuterium chirality ($[\alpha]_D$ = +0.65° for (*R*)- and = −0.43° for (*S*)-enantiomer (neat)). Polymerization of these monomers to give deuterated-poly(isocyanate)s resulted in much larger optical activities (($[\alpha]_D$ = −444° and +302° in *n*-hexane). These results suggested that deuterium substitution influences the relative stabilities of right- and left-handed helical conformations of a racemic polymer leading to an excess helix sense. Considering the small difference between a hydrogen and deuterium (in terms of size and electronic properties), preference for one helical sense only from deuterium substitution would not be possible without cooperation among many residues of the polymer chains.[25-27] The effect of one deuterium per monomeric unit is relatively small but it is cumulative as a result of the cooperative nature of the polymer resulting in an increase of the optical activity going from monomer to polymer. X-ray diffraction analysis revealed that the poly(isocyanate) forms a 8/3 helix in the solid crystal and it was hypothesized that this helical conformation is preserved in the dissolved state. In such a model, several hundreds of residues follow each other in a single helical sequence i.e., helix reversals from one handedness to the other within the polymeric chain are not favored. By this amplification mechanism, small energy differences accumulate and nearly undetectable optical properties under normal circumstances become amplified and thus detectable.

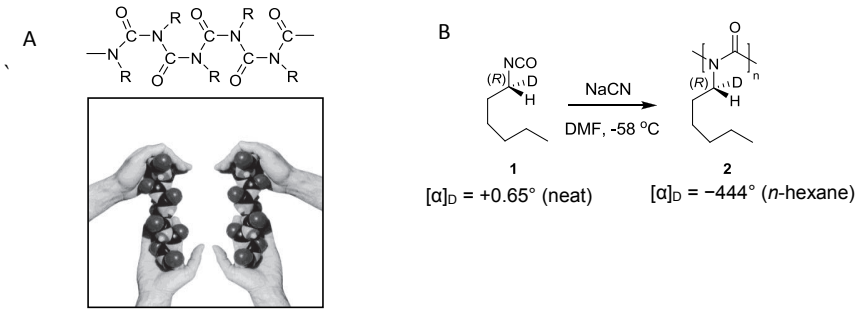

Figure 1.3: A) Right- and left-handed helical poly(isocyanate)s. B) Synthesis of poly((*R*)-1-deuterio-*n*-hexylisocyanate) by polymerization of deuterated isocyanate monomer.[25,26]

In addition to cooperative interactions among monomers within polymers, conformational changes in macromolecules can also be cooperative. An example for such cooperative transition is observed between two types of supramolecular polymers originating from bis-ureas.[28,29] Bis-urea based monomers (**3**) form hydrogen bonded self-assemblies in solution *via* a cooperative mechanism i.e., an unfavorable dimerization step is followed by subsequent favorable association steps. In toluene, these monomers form two types of supramolecular polymers the preference of which is dependent on temperature. At higher temperatures (above 45 °C), hydrogen bonded filaments (**3a**) are formed preferably whereas at lower temperatures (below 40 °C) bis-urea monomers reorganize into rigid tubes (**3b**) (Figure 1.4). This process was monitored by infrared spectroscopy (FT-IR), differential scanning calorimetry (DSC) and isothermal titration calorimetry (ITC). The experimental data fitted with the association model revealed that the transitions between the two states (i.e., between filaments and tubes) in toluene is remarkably sharp and concentration-independent. These results were attributed to the dynamic exchange of the tubes with the monomers and hydrogen-bonded filaments. Furthermore, the tubular structures are stabilized by the solvent molecules that are small enough to reside within the tubes leading to a sort of host-guest system.[30,31]

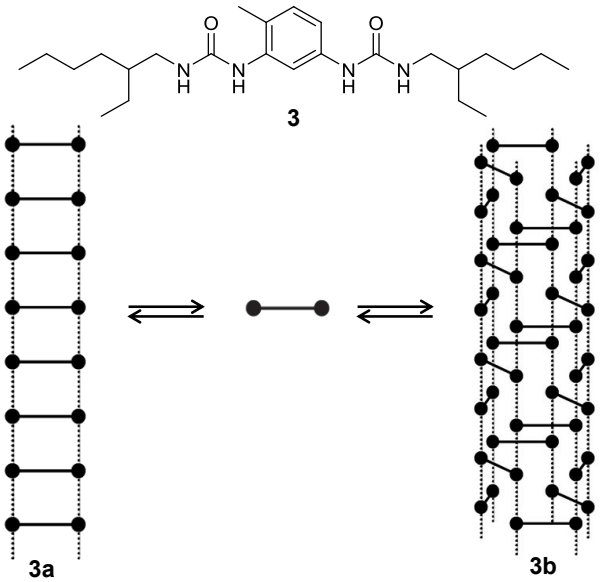

Figure 1.4: Top: bis-urea monomer. Below: schematic representation of filament (**3a**) and tube (**3b**) formed by the monomers.[29]

Another type of cooperative transition was observed in supramolecular polymers originating from C_3 symmetric discotic molecules.[32] The self-assembly of bipyridyl substituted BTAs with chiral penta(ethylene oxide) side chains in polar medium proceeds *via* formation of disordered nonhelical intermediates. Monomers first aggregate into a disordered self-assembled state (coil), which is followed by the formation of ordered 1D helical aggregates (helix). Theory predicts that the helix-coil transition resembles a phase transition and is cooperative[33,34] which is in good agreement with the experimental findings.

1.3 Self-assembly mechanisms: cooperative vs isodesmic

Nucleated (cooperative) and isodesmic are the two common self-assembly mechanisms. Cooperative self-assembly requires the formation of a nucleus initially with an equilibrium constant, K_n. The nucleation proceeds by subsequent elongation steps with an equilibrium constant of K_e, where $K_e > K_n$ (Figure 1.5A). These two steps are absent in isodesmic self-assembly and addition of monomer into the growing chain proceeds equally i.e., equilibrium constant of each step is identical, $K_n = K_e$ (= K) (Figure 1.5B).[35]

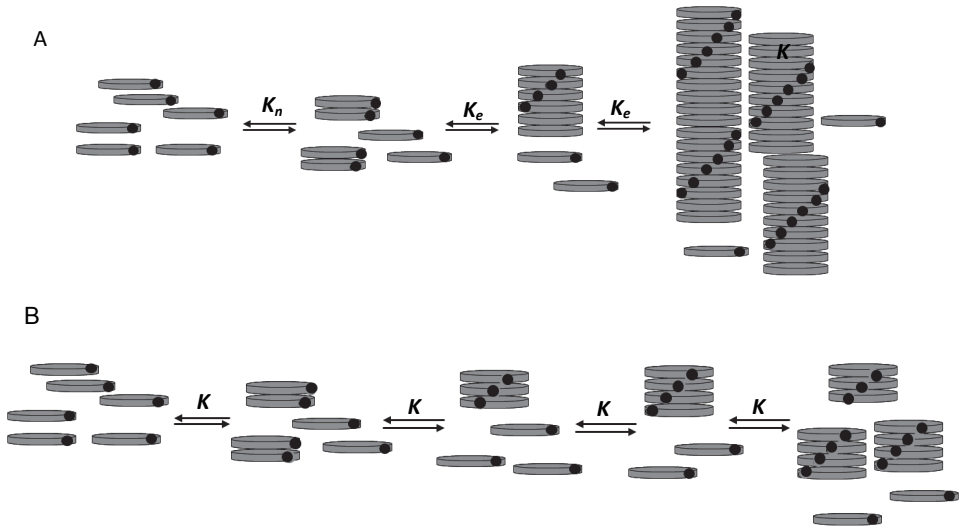

Figure 1.5: A) Schematic representation of A) cooperative, B) isodesmic self-assembly of a single type chiral monomer.

The two mechanisms are compared based on the fraction of the self-assembled material (Φ) as a function of total concentration of monomers (KC_t). This is performed for different cooperativity parameters, $\sigma = K_e / K_n$, (σ = 1, 10^{-2}, and 10^{-5}) (Figure 1.6A). In isodesmic growth (i.e., σ = 1), the concentration of polymeric species increases gradually with increasing

monomer concentration (solid line). In contrast, no polymeric species are formed below a dimensionless concentration of 1 (i.e., critical concentration) in cooperative growth (dashed and dotted lines). Polymers are formed only after the critical concentration is reached. Furthermore, the decrease in the value of σ in the cooperative growth influences the growth profile of the polymeric species (i.e., the transition around the critical concentration is much sharper when $\sigma = 10^{-5}$). Another comparison between the two self-assembly mechanisms is performed based on the equilibrium concentrations of the monomers (K_eM_1) and that of polymers (= $M_2 + M_3 + \ldots$) as a function of total concentration (K_eC_t) (Figure 1.6B). In isodesmic growth, the equilibrium concentrations of monomers (M) and polymers (P) increase simultaneously while in the cooperative growth the concentration of polymers increase only after the critical equilibrium monomer concentration is reached. The monomer concentration does not change anymore upon increasing the total concentration after the equilibrium concentration is reached. Adding more monomers (after the critical concentration is reached) leads to the formation of relatively long polymers in a cooperative system. In the isodesmic case, however, the length of the polymers is smaller due to the absence of the critical concentration regime as the theory predicts.

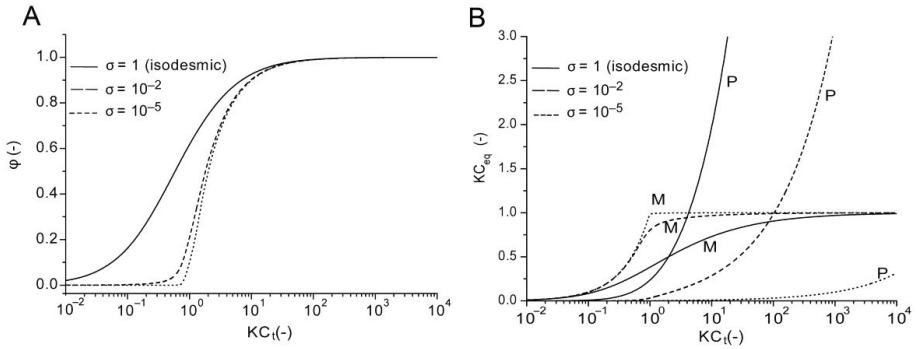

Figure 1.6: A) Fraction of polymerized material, Φ, as a function of the dimensionless concentration, KC_t for three different values of σ. B) Dimensionless concentration of monomers (M) (KM_1) and polymers (defined as $K(M_2 + M_3 + ... + M_i)$) as a function of the dimensionless concentration KC_t for three different values of σ.[35]

The value of the equilibrium constants, K, K_n or K_e can be deduced experimentally by employing concentration-dependent or temperature-dependent measurements for the isodesmic or cooperative mechanisms, respectively. Analytical techniques include UV-vis[36] infrared[37], fluorescence[38], NMR[39], circular dichroism[40] spectroscopy, solution viscometry[41] and calorimetric measurements[42]. The thermodynamic parameters characterizing the supramolecular polymerizations are obtained by fitting the experimental data with suitable mathematical models.[43-46] There are multiple factors determining the nature of the

noncovalent interactions and the polymerization mechanism that is followed. Electronic[47,48], structural[49,50] and hydrophobic effects[51,52] contribute to the cooperative growth of a supramolecular polymer. For instance, perylene bisimides and apolar bipyridyl substituted BTAs[53] self-assemble in an isodesmic fashion whereas the self-assembly of oligo(*p*-phenylenevinylene)[54] (Figure 1.7) exhibits a strongly cooperative behavior. Various C_3-symmetric and asymmetric BTA derivatives (Figure 1.11) self-assemble *via* a cooperative mechanism.[55,56]

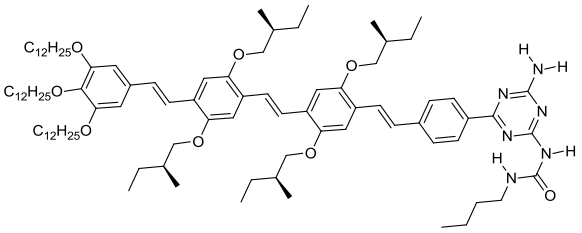

4

Figure 1.7: Molecular structure of oligo(*p*-phenylenevinylene).[54]

1.4 Chiral amplification

1.4.1 At the molecular level: Soai Reaction

The formation of chiral molecules from achiral initial conditions requires an initial imbalance between the two enantiomers and an amplification mechanism. One possible method for this amplification mechanism was first rationalized with a mathematical model by Frank in 1953.[57] This amplification mechanism is based on an autocatalytic system with competitive reactions of two enantiomers that are mutually inhibitory and form inactive products in a dynamic metastable system. The reactions of the two achiral compounds lead to two enantiomeric products that each catalyzes their own formation, thus autocatalysis occurs. Each enantiomer simultaneously reduces the activity of the other−leading to mutual inhibition−resulting in a strong asymmetric amplification.[58] The first experimental evidence for such an autocatalytic reaction is the Soai reaction in which alkylation of pyrimidyl aldehyde **5** with diisopropyl zinc (*i*-Pr_2Zn) gives a chiral alcohol **6** (Scheme 1.1).[60-64] In this reaction, the chiral alcohol catalyzes its own production at a higher rate than that of its enantiomer leading to a very high *e.e.* (> 99.5%)[60] from a prochiral compound. In catalytic asymmetric automultiplication, the product acts as a catalyst and produces itself with the same configuration.[64,65] Thus, the reaction does not require any other chiral auxiliaries and the separation of the catalyst from the reaction mixture is not needed.

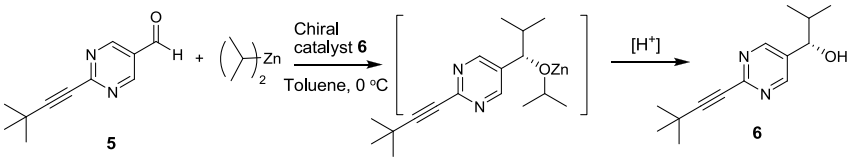

Scheme 1.1: Soai reaction: asymmetric autocatalysis of alcohol **6** by the reduction of aldehyde **5** with *i*-Pr$_2$Zn.[61,66]

Autocatalytic replications in enantioeselective syntheses of alcohol **6** that were induced by chiral quartz[67], *d*- or *l*-crystals of sodium chlorate[68] and helicenes[69] have been reported. Furthermore, hydrogen[70,71] and carbon isotope[72] chirality were used to afford highly enantioenriched alcohol **6**. The application of isotopically chiral amino acids as chiral triggers in the reduction reaction of aldehyde **5** yielded alcohols with *e.e.* > 95% (Scheme 1.2). The isotopically chiral amino acid may induce a slight enantiomeric imbalance during the addition of *i*-Pr$_2$Zn to **5**. The resulting isopropylzinc alkoxide **5a** displays a small *e.e.* and possesses the same absolute configuration as the isotopically chiral amino acid. This *e.e.* is enhanced through the subsequent asymmetric autocatalysis followed by hydrolysis affording the alkanol, (*S*)- or (*R*)-**6** with *e.e* . > 95%.

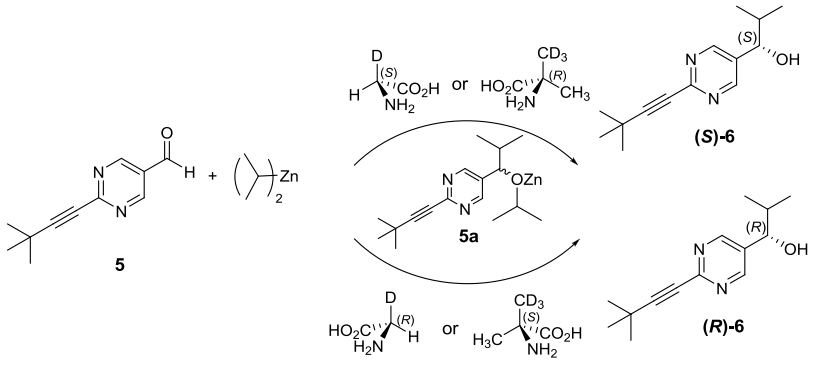

Scheme 1.2: Isotopically chiral amino acid induced asymmetric autocatalysis of 5-pyrimidyl alkanol **6** in the addition of *i*-Pr$_2$Zn to aldehyde **5**.[71]

Since Soai reaction is a remarkable example for autocatalytic reactions, there is a considerable amount of research elucidating the mechanism of this reaction.[74-77] Blackmond and coworkers demonstrated that the Soai reaction is catalyzed by a dimeric species formed by Zn coordination into two molecules of alcohol (derivative of **5a**), the Zn alkoxide.[73,74] Studies showed that there is no difference in the stability between hetero- and homochiral dimers; however, the asymmetric amplification is originated from relative inactivity of the

heterochiral species as a catalyst.[75] Moreover, computational methods in the gas phase were used to unravel the Soai reaction.[77] The calculations demonstrate that the relative orientation of isopropyl groups and γ-pyrimidyl nitrogen atoms plays a critical role. The *anti* arrangement of the molecules allows zinc-bound isopropyl groups to attack the *Re* face of the aldehyde, reproducing the chiral information of the catalyst acting as a template. In contrast, the isopropyl attack on the *Si* face is forbidden due the steric repulsion between isopropyl groups.

Amplification of the *e.e.* has been observed in other types of enantioselective reactions such as the Sharpless expoxidation[78], the alkylation of aldehydes[79,80] and many others.[81,82] In these reactions the *e.e.* values of the products are higher than those of the asymmetric catalysts used; however, these reactions are not autocatalytic and the *e.e.* of the product cannot be increased by repeating the reaction.

1.4.2 Chiral amplification at the macromolecular level

In the 1960s, stereoregular vinyl polymers with chiral, nonracemic pendant groups (e.g., (*R*)- or (*S*)-3-methyl-1-pentene) were prepared.[83,84] The optical activities of such polymers in solution exhibited nonlinear relationships between the configurational enantiomeric characteristics of the monomeric units and the perceived optical activity of the derived polymer. This nonlinear optical activity suggested that the chiral monomeric units affect the chain conformation of the polymers. A full understanding of this phenomenon required an accessible chromophore for a direct observation by circular dichroism as the source of the chiral optical observations. Poly(*n*-hexylisocyanate) −as described in Section 1.2− adopts a stiff helical conformation[24] in solution and forms right-handed (*P*) and left-handed (*M*) helices in equal amounts since there is no stereocenter in the side alkyl groups of the polymer. The copolymer (**7**, Figure 1.8A) was prepared by the copolymerization of 2,6-dimethylheptylisocyanate and *n*-hexylisocyanate (mol%, x:y = 4:96).[85] Incorporation of chiral monomeric units into achiral polyisocyanates resulted in the induction of remarkable optical activity in the copolymers, which changes nonlinearly with the mole fraction of chiral monomers (Figure 1.8A). Moreover, circular dichroism (CD) spectrum of this compound demonstrated that a few units of chiral monomers (sergeants) in the polymer chain are able to disrupt the equal distribution of *P* and *M* among achiral *n*-hexylisocyanate units (soldiers). The term 'sergeants-and-soldiers' was used for the first time to express this nonlinear behavior in covalent polymers. Furthermore, similar nonlinear dependence was observed for the copolymers comprising enantiomeric monomeric units in different ratios. Copolymers with pendant groups, (*R*)- or (*S*)-2,6,-dimethylheptylisocyanate (**8**, Figure 1.8B) form opposite helical senses, as evidenced by the mirror image CD spectra. CD curves reflect the orientation of the helical conformation and demonstrate that the copolymer with an *e.e.* of 12% ((*R*):(*S*) = 56:44) displays the same CD spectrum as the (*R*)-homopolymer.[86] Furthermore,

the optical rotation (measured at the sodium D-line, $[\alpha]_D$) changes nonlinearly with the increasing amount of one enantiomer (Figure 1.8B). These results show that the excess of one enantiomeric unit biases the total helix sense in the polymer; this phenomenon was termed 'majority rules'. Different than in asymmetric synthesis, in a majority rules experiment, the *e.e.* of the monomeric units does not change; however, the observed chirality of the polymer changes.

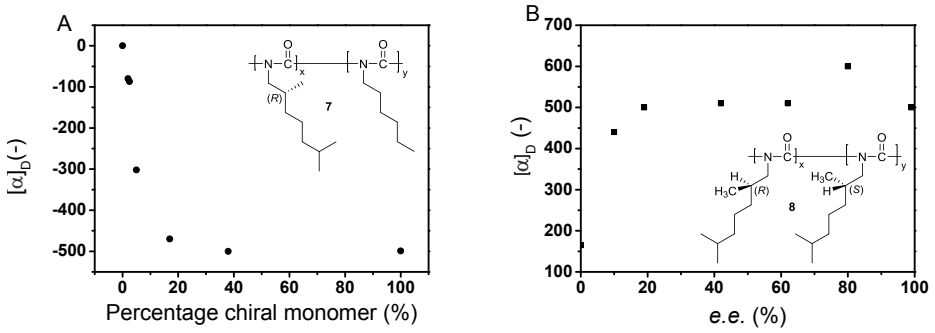

Figure 1.8: Optical rotation at the sodium D-line as a function of A) percentage of the chiral *n*-hexylisocyanate monomer in the polymer chain, sergeants-and-soldiers experiment.[85] B) enantiomeric excess, majority rules experiment.[86]

The two effects observed in covalent polymers, namely the 'sergeants-and-soldiers' and the 'majority rules' phenomena, are applicable to supramolecular systems as well. The very first example was observed in 3,3'-diamino-2,2'-bipyridyl-substituted BTA-based supramolecular polymers (**9**) (Figure 1.9). The sergeants-and-soldiers experiment[87] was performed by mixing achiral BTA **9a** (soldier) with chiral BTA analogue (*S*)-**9b** (sergeant) and the majority-rules experiment[88] was performed by mixing of two enantiomeric BTAs (S)-**9b** and (*R*)-**9c**. Both experiments resulted in a strong nonlinear relationship between observed net helicity and both the fraction of chiral sergeant and the *e.e.* indicating a strong amplification of supramolecular chirality. As a result of the dynamic character of BTA self-assembly (e.g., co-assembled structures are formed within a few seconds), chiral amplification experiments are easily performed in a reasonable time-frame. Despite the differences in the formation mechanisms between a covalent and a noncovalent polymer, the two show remarkable similarities in chiral amplification at the macro- or supramolecular level.

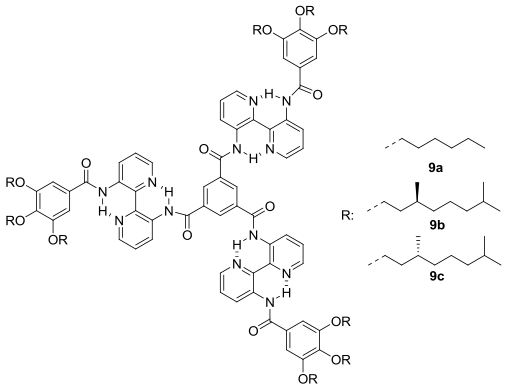

Figure 1.9: Chemical structure of (a)chiral 3,3′-diamino-2,2′-bipyridyl-substituted benzene-1,3,5-tricarboxamides.[32,87-89]

Chiral amplification behavior has been observed in many other supramolecular systems.[90] Amphiphilic hexa-*peri*-hexabenzocoronene (HBC) derivatives assembling into nanotubes in polar organic solvents exhibit majority rules behavior when enantiomeric HBCs are mixed in varying ratios. The mixing experiment resulted in a nonlinear change in CD effect as a function of *e.e.* suggesting that chiral amplification is operative in the co-assembly of the enantiomeric HBCs.[91]

1.4.3 Chiral amplification at solid surfaces

Transfer of chiral information is particularly selective at ordered interfaces owing to the geometrical restrictions introduced by two-dimensional (2D) confinement. As a result, macroscopic chirality can be obtained within self-assemblies of achiral molecules on achiral surfaces by the application of chiral solvent.[92] Molecular homochirality is observed at the interface between a chiral solvent and the surface of highly oriented pyrolytic graphite as a result of the 2D packing of the hydrogen bonded achiral oligo-(*p*-phenylenevinylene) molecules. The results indicate that chiral information of the solvent can be amplified on a larger scale of surface-confined hierarchical supramolecular self-assembly. The sergeants-and-soldiers principle was observed on crystalline surfaces. Achiral *meso*-tartaric acid molecules form 2D enantiomorphous structures on the copper surface as a result of adsorption-induced chirality in the molecular frame combined with a lateral separation of the resulting two enantiomers. The formation of one enantiomorphous domain, however, can be suppressed by co-adsorption of enantiomeric (*S*,*S*)- or (*R*,*R*)-tartaric acid, driving the entire monolayer into homochirality.[93]

1.4.4 Chiral amplification in crystals: chiral symmetry-breaking by enantiomerization

Besides the fundamental importance of understanding the origin of homochirality in Nature, producing enantiopure compounds from achiral or racemic species on the laboratory scale is important for pharmaceutical applications. First example of producing enantiomeric compounds by separating the crystals was demonstrated by Pasteur 150 years ago.[94] Pasteur separated two types of crystals of the sodium ammonium salts of tartaric acid with a mirror image shape (based on their dissymmetric facets inclined to the right or left) by means of a pair of tweezers. He then observed that one type of crystals rotate the polarized light clockwise while the other one rotate the light counterclockwise. He realized that the difference in the rotation of polarized light was a result of dissymmetry in the two crystal types. It is noteworthy to mention that Pasteur made these observations decades before the concepts 'chirality' and 'enantiomerism' were known. After resolution of two enantiomeric crystals of ammonium salts of tartaric acids by Pasteur, crystallization appeared to be a promising method for chiral resolution. For example, achiral $NaClO_3$ molecules crystallize in enantiomerically pure chiral crystals under certain conditions.[95] Viedma recently demonstrated the transformation of these enantiomorphic but intrinsically achiral $NaClO_3$ molecules into a single chirality (i.e., *e.e.* = 100%) by grinding the crystals in a saturated solution.[96,97] Viedma's grinding method was extended to deracemization of biologically relevant enantiomeric molecules such as phenylglycine substituted imine **10** in the presence of organic base, 1,8-diazabicycloundec-7-ene (DBU) (Figure 1.10A).[98] The enantiomeric excesses of the crystals were determined by dissolution and then high performance liquid chromatography (HPLC) and highly enantioenriched compounds were attained over time (*e.e.* = 100%) (Figure 1.10B, left). Similar experiments performed by adding chiral seed, phenylglycine, to the racemizing mixture led to high *e.e.* values over time (Figure 1.10B, right). The driving mechanism in this process is Ostwald ripening, which states that large crystals with the same configuration grow preferentially, while smaller crystals are further ground and eventually disappear under stirring-grinding conditions.[99,100]

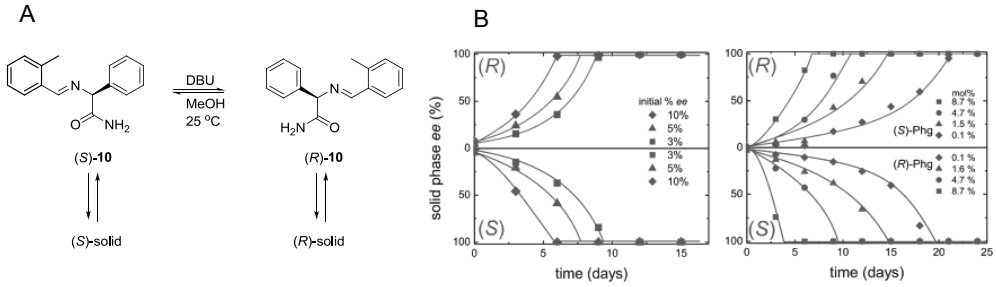

Figure 1.10: A) Chemical and physical equilibria in the racemization and crystallization/dissolution processes for phenylglycine-substituted imine (**10**). B) The change in *e.e.* of **10** over time under racemization and stirring conditions (left). Phenylglycine was used as chiral seed to catalyze the process (right).[98]

Deracemization in crystalline state is a useful technique for obtaining enantioenriched compounds; however, it has a number of requirements; the enantiomers must crystallize as conglomerates and they should be racemizable in solution.[98,98] Tsogoeva and coworkers demonstrated that enantioenriched products can be obtained in a reversible Mannich reaction by enantiomerization through the reverse reaction in combination with stirring (with or without grinding) where labile stereocenter is not a prerequisite in the system.[101,102] Tsunoda *et al.* showed that racemic mixtures of several cyclohexanones can be deracemized in basic suspension by using an optically active host. The formation of more stable inclusion complex between optically active host and one enantiomer of the guest molecule leads to enantioenrichment of racemic guest in quantitative yields.[103]

1.5 BTAs: a model system for studying cooperativity and chiral amplification

Benzene-1,3,5-tricarboxamides (BTAs) are easily accessible small organic molecules that form helical supramolecular polymers by means of threefold intermolecular hydrogen bonding in dilute solutions. These synthetic supramolecular polymers show remarkable similarities to covalent polymers and supramolecular polymers found in Nature (in terms of cooperativity and chiral amplification) despite differing formation mechanisms. Therefore, BTA molecules represent an ideal system for studying complex interactions in supramolecular polymers. Such studies are of great importance for the rational design of molecules that self-assemble into nano-objects of defined structure, stability and shape by the molecular information stored in the chemical structure.

1.5.1 Structural properties and synthesis of BTAs

Structurally, BTA molecules consist of a benzene core and three amide moieties connected to the benzene ring. Amide groups can be readily functionalized with either chiral or achiral units. When the functional groups connected to the amides are the same, BTA molecules are referred to as C_3 symmetric. Furthermore, BTAs can be desymmetrized by introducing different substituents. Although most common BTA structures are carbonyl (C)-centred where carbonyl groups are attached directly to the benzene ring, various types of nitrogen (N)-centred BTAs in which carbonyl and NH groups are replaced, have been reported.[104,105]

The most common synthetic strategy for the preparation of the BTA molecules is the reaction of benzene-1,3,5-tricarbonyl trichloride (trimesic chloride) with the appropriate amine in the presence of base.[55] The trimesic chloride is obtained from benzene-1,3,5-tricarboxylic acid, whereas BTAs can also be prepared *via* direct functionalization of the carboxylic acid with the appropriate amine by using suitable coupling agents.[106] Over the past decades, a broad range of N- and C-centred BTA molecules has been synthesized and analyzed in detail. BTA structures derivatised with R-groups such as alkyl,[55,107] aryl,[105,108,109] pyridyl,[110] bipyridyl,[32,89] porphyryl,[111] triphenylenyl,[112] oligo(*p*-phenylenevinylene),[113] amino acid,[107,115-119] dipeptide,[119] oligopeptide,[120] oligo(ethyleneoxy),[121,122] and benzocrown ethers[123] have been reported. The BTA derivatives have been investigated for a variety of applications such as organogels,[124] hydrogels,[109,124,125] liquid crystals,[107] nanostructured materials,[126] MRI contrast agents,[127] nucleating agents for polymers,[128] metal complexing reagents,[117] and microcapsules for for drug delivery.[129] Figure 1.11 depicts an overview of the selected (a)symmetric, (a)chiral C-centred BTA structures.

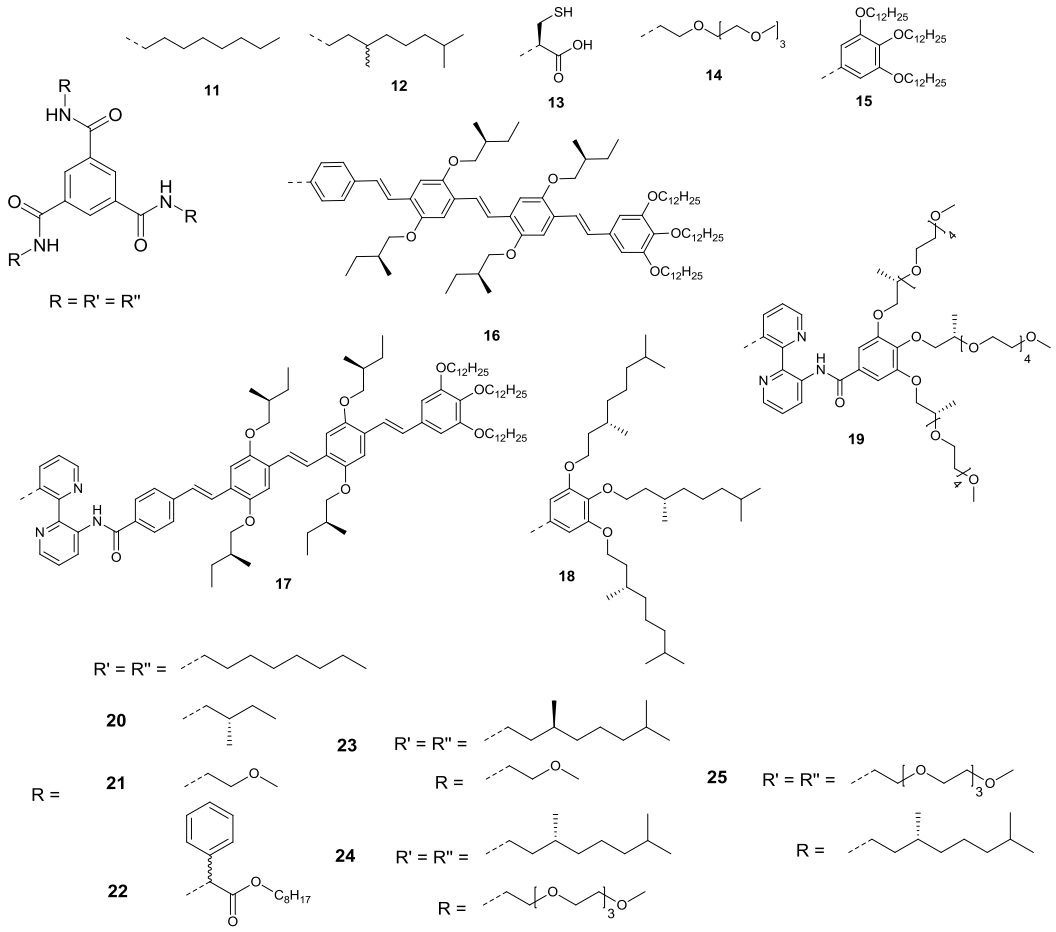

Figure 1.11: The structures of various symmetric and asymmetric (a)chiral C-centred BTAs.[55,32 ,113,122,130,131]

1.5.2 Self-assembly behavior and chiral amplification in BTAs

Alkyl substituted BTAs self-assemble upon increasing the concentration c or decreasing the temperature T into helical supramolecular polymers, which are stabilized by threefold hydrogen bonding between the amides of consecutive discs. The presence of directional intermolecular hydrogen bonding leads to the formation of two different helical senses, *P* and *M*. In the absence of chiral information, these two helical senses have equal stabilities, thus they are formed in equal amounts (Figure 1.12). The introduction of one stereogenic centre into one alkyl side chain of the BTAs suffices to fully bias one helical sense.

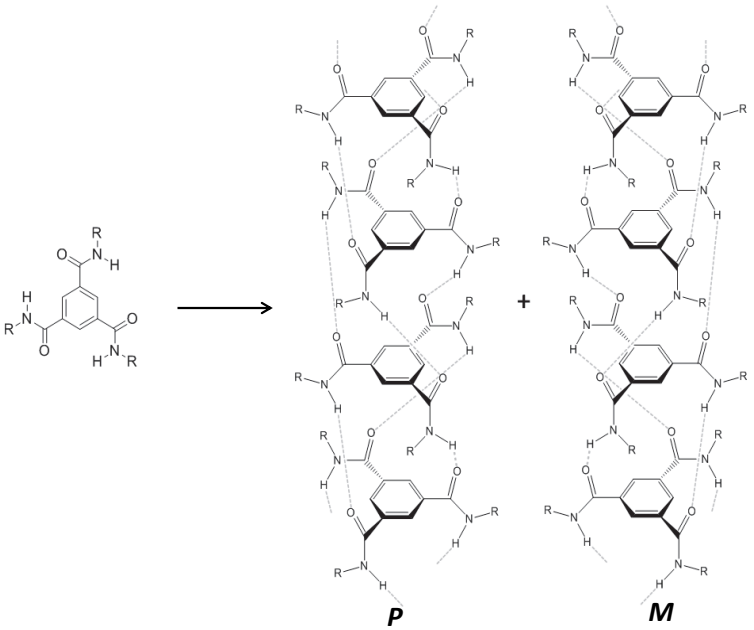

Figure 1.12: Self-assembly of BTAs into right- (*P*) and left-handed (*M*) supramolecular polymers.

The self-assembly of BTAs equipped with achiral and chiral aliphatic side chains, has been studied using a wide variety of different spectroscopic techniques in dilute apolar solvents such as methylcyclohexane (MCH) and heptane. For example, helical supramolecular polymers formed by chiral symmetric BTA, (*R*)-**12**, are analyzed by temperature-dependent UV-vis and circular dichroism (CD) spectroscopy.[56] The UV-vis spectrum of (*R*)-**12** in heptane (c = 1.4×10^{-5} M) revealed a hypsochromic shift in the absorption maximum. According to the exciton theory, a relatively blue shifted curve (λ = 193 nm) in comparison to the monomer peak (λ = 207 nm) is commonly assigned to H-type aggregates (Figure 1.13A). Furthermore, the CD spectrum exhibited a bisignated Cotton effect ($\Delta\varepsilon \approx 40$ L mol^{-1} cm^{-1} at λ = 223 nm where $\Delta\varepsilon$ is molar ellipticity and = CD maximum/32980 c *l* where c = concentration in M and *l* = path length in cm) arising from π-π^* (λ = 193 nm) and n-π^* transition (λ = 223 nm) upon cooling (Figure 1.13B). The CD effect monitored at λ = 223 nm as a function of temperature showed a strong non-sigmoidal shape (Figure 1.13C) and a clear elongation temperature (T_e), reflecting the cooperative nature of the self-assembly process.[35] Furthermore, the degree of aggregation, probed by UV-vis spectroscopy, coincides with the net helicity, probed by CD spectroscopy, suggesting that aggregation and expression of one helical sense are coupled processes.

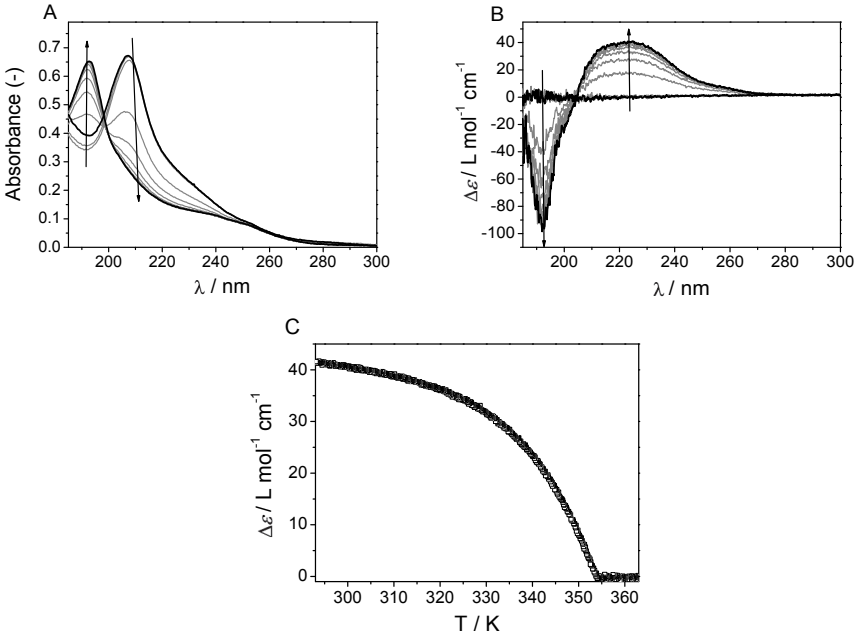

Figure 1.13: A) UV-vis, B) CD spectra of (*R*)-**12** in heptane (c = 1.45×10^{-5} M) between 363 and 293 K measured at intervals of 10 °C. Arrow shows the decrease in the temperature. C) Molar ellipticity ($\Delta\varepsilon$ = CD maximum/32980 c *l* where c = concentration in M (mol L^{-1}) and *l* = path length in cm) as a function of temperature monitored at λ = 223 nm at a cooling rate of 1 K min^{-1} for (*R*)-**12** in heptane; c = 4×10^{-5} M.[56]

The cooperative self-assembly of BTAs can be described quantitatively by a nucleation-growth model.[54] Temperature dependent UV-vis or CD measurements performed for different concentrations revealed that the self-assembly of BTAs proceeds *via* two regimes; nucleation and elongation. At elevated temperatures, BTA monomers are at molecularly dissolved state. Upon cooling, an unfavored nucleation takes place which is followed by a favored elongation giving rise to a non-sigmoidal cooling curve (Figure 1.13C). A detailed study on dilute solutions of chiral BTA **12** employing a combination of vibrational circular dichroism (VCD)[132] and CD[56], supported by DFT calculations[133] confirms the correspondence between the reported[134] crystal structure and the structure of the helical aggregates formed in dilute, apolar solutions. Importantly, VCD experiments performed in solution and density functional theory (DFT) calculations are in good agreement and clearly provide evidence for a nonzero twist angle between the amide plane and the benzene plane for BTA monomers present in the helical aggregate. As intermolecular hydrogen bonding is the dominant interaction responsible for BTA self-assembly, addition of competing solvents such as acetonitrile results in complete depolymerization of the helical aggregates.[56] Interestingly,

side-chains that can compete with the threefold hydrogen bonding of the BTA core (e.g., in **24** and **25**) *via* intramolecular back-folding cause a diminished degree of aggregation as evidenced by UV-Vis and CD studies.[126,135]

Furthermore, the effect of the position of the stereocenter in the side alkyl chains of BTAs on the self-assembly behavior was investigated.[55] BTAs comprising two *n*-octyl and one chiral methyl-alkyl side chain in which the position (methyl at either α, β-, γ- or δ position) and the absolute configuration (*R* or *S*) of the stereogenic centre were systematically varied. Mirror image CD spectra of the enantiomeric BTAs revealed that these enantiomers self-assemble in opposite helical senses. In addition, a positive Cotton effect resulting from *(R)*-methyl substituent at the α- or γ-position and a negative Cotton effect arising from the *(R)*-methyl substituent at the β- and δ-position revealed the presence of a pronounced odd-even effect in the sign of the Cotton effect. This remarkable result indicates that the helical sense preference changes upon moving the methyl from an odd to an even position. The stability of the aggregates increases when the methyl group is closer to the amide function.

Chiral amplification behavior in BTA-based supramolecular polymers has been investigated for more than a decade. The first example of supramolecular polymer showing chiral amplification behavior is bipyridyl substituted BTAs (**9**) as mentioned in the previous section.[87] After that, chiral amplification was analyzed in great detail for various BTA molecules and the effect was quantified by using mathematical models. The sergeants-and-soldiers experiment was performed by mixing achiral BTA **11** (soldier) with chiral BTA analogue (*S*)-**12** (sergeant)[56] and majority-rules experiment[136] was performed by mixing of two enantiomeric BTAs (S)-**12** and (*R*)-**12**. Both experiments result in a strong nonlinear relationship between observed net helicity and both the fraction of chiral sergeant and the *e.e.* indicating a strong amplification of supramolecular chirality (Figure 1.14A-B). In supramolecular chemistry the term 'amplification of chirality' implies full expression of a chiral superstructure at the supramolecular level, regardless of the *e.e.* of the monomers used. In contrast, in asymmetric synthesis, amplification of chirality implies the increase of the *e.e* of the reaction product relative to the substrate or catalyst used. Chiral amplification in BTAs is quantified by using the model developed by van Gestel[88,137] and is described in terms of two (free) energy penalties (i.e., the helix reversal penalty, *HRP*) that reflects the barrier to helix reversal within a stack and the mismatch penalty (*MMP*) which represents a mismatch energy when a chiral monomer is introduced into a stack of its unpreferred helicity (Figure 1.14C). The *HRP* value determined for methyl substituted BTAs is approximately 12 kJ mol^{-1} whereas the *MMP* value typically lies in the range of 1–2 kJ mol^{-1}.[136]

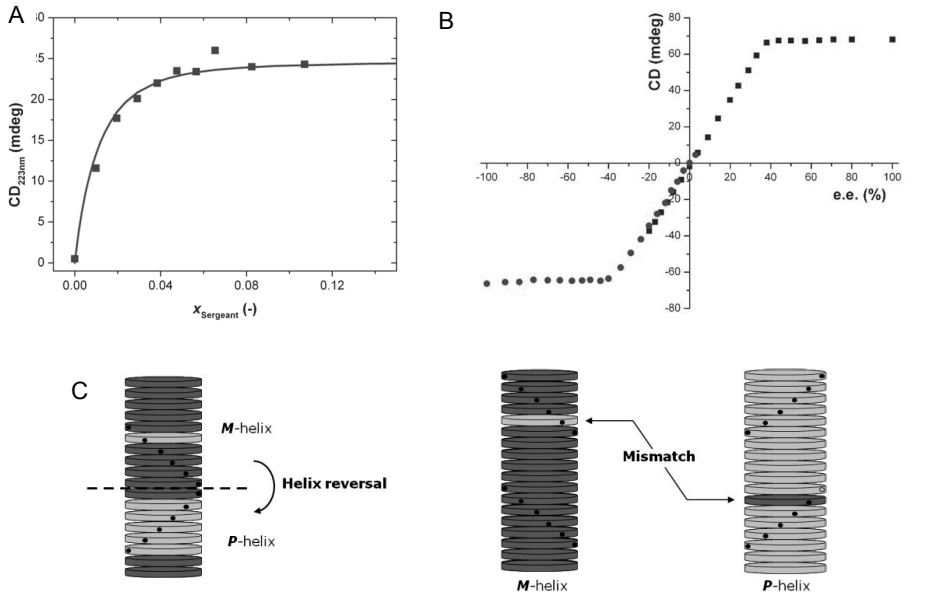

Figure 1.14: A) CD effect (at λ = 223 nm) as a function of sergeant fraction, data based on the sergeants-and-soldiers experiment performed by using achiral BTA **11** and (*R*)-**12**, c = 1.4×10^{-5} M in heptane.[56] The line is to guide the eye. B) CD effect as a function of enantiomeric excess, data extracted from majority-rules experiment by using various ratios of (*R*)-**12** and (*S*)-**12**.[137] C) Schematic representation of helix reversal and mismatch penalties in BTA-based supramolecular polymers.

1.6 Aim and outline of the thesis

Considering the profound importance of cooperativity and chirality observed in biological systems, it is both scientifically fascinating and technologically relevant to study synthetic supramolecular polymers in order to gain insights into the fundamentals of complex molecular systems. Furthermore, unraveling complexity in multi-component systems provides valuable information for the rational design of molecules that assemble into nano-objects of defined structure, stability and shape. Benzene-1,3,5-tricarboxamide (BTA) molecules are particularly appealing building blocks owing to their cooperative self-assembly behavior in dilute solutions, expression of supramolecular chirality and synthetic accessibility. The self-assembly mechanism of BTAs has been studied for more than a decade both experimentally and theoretically. Studies revealed that BTA monomers self-assemble *via* a cooperative mechanism by means of intermolecular hydrogen bonding, and they display chiral amplification behavior which implies a full expression of a chiral superstructure at the supramolecular level, regardless of the enantiomeric excess of the monomers used. In this dissertation, the limits of supramolecular chirality in BTA-based supramolecular polymers

are targeted. Moreover, the research aims at combining covalent chemistry with noncovalent interactions to enter the intriguing area of complex molecular systems. Therefore, the influence of subtle structural changes in BTA monomers on the cooperative self-assembly and chiral amplification behaviour are analyzed. The introduction of chirality inducing isotopes into BTAs, solvent effects on BTA self-assembly and the consequences of introducing a racemization reaction in a self-assembled BTA system are investigated. Studies reveal that cooperative interactions may be responsible for magnified effects at the supramolecular level which are almost negligible at the molecular level.

Chapter 2 describes a synthetic approach towards isotopically chiral BTAs. The enantioselective synthesis of chiral deuterated octyl alcohols and amines by making use of enzymatic asymmetric reduction is depicted. Two enzymatic reduction methods for the synthesis of chiral, mono-deuterated octyl alcohols are applied and the efficiencies of the two are compared. The enantiomeric excesses of the compounds formed are accurately determined by using Mosher's acid method. Chiral alcohols are converted to the corresponding chiral amines which are subsequently used for the synthesis of BTA molecules. Chapter 3 addresses the questions 'how far can we push the supramolecular chirality?' 'how does isotope chirality reflect at the supramolecular level?' 'how do these systems compare to the covalent analogues?'. A detailed analysis on the α-deuterated-BTA self-assembly carried out in dodecane solvent reveals that the result of isotopic substitution is remarkably similar in noncovalent and covalent polymers despite the differences in the formation mechanisms of the two. Chapter 4 describes an unprecedented solvent effect on self-assembly. The α-deuterated-BTA motif is used to demonstrate that relatively small structural differences in the alkane solvents result in remarkable changes in the expression of supramolecular chirality and the preferred conformation of the supramolecular polymer. The observed effects are attributed to the active participation of the solvent molecules in the self-assembly process. Chapter 5 describes the racemization reaction in a cooperative self-assembled system and investigates the kinetics of racemization and the nature of the final state of a racemizing supramolecular system in the presence of a chiral auxiliary. Chapter 6 gives an outlook on increasing complexity in self-assembled systems by combining covalent synthesis with noncovalent synthesis in supramolecular polymerizations. Abstraction of an amide hydrogen in a BTA derivative in the presence of an organic base results in partial depolymerization and leads to oscillatory optical properties when combined with sudden temperature changes in the system. This chapter summarizes the preliminary observations and discusses what the combination of covalent and noncovalent chemistry brings to the field of supramolecular chemistry in the future.

1.7 References

[1] J. R. Williamson, *Nat. Chem. Bio.* **2008**, *4*, 458.
[2] C. A. Hunter, H. L. Anderson, *Angew. Chem. Int. Ed*. **2009**, *48*, 7488.
[3] A. Guijarro, M. Yus, in *The Origin of Chirality in the Molecules of Life: A Revision from Awareness to the Current Theories and Perspectives of this Unsolved Problem*, The Royal Society of Chemistry Publishing, Cambridge, **2009**.
[4] E. Shakhnovich, *Chem. Rev.* **2006**, *106*, 1559.
[5] D. Zhao, J. S. Moore, *Org. Biomol. Chem.* **2003**, *1*, 3471.
[6] I. Kinetics, *Biophys. J*. **1963**, *3*, 239.
[7] F. Oosawa, M. Kasai, *J. Mol. Biol.* **1962**, *4*, 10.
[8] F. Oosawa, S. Asakura, in *Thermodynamics of the Polymerization of Protein*; Academic Press: London, U.K., **1975**.
[9] H. Flyvbjerg, E. Jobs, S. Leibler, *Proc. Natl. Acad. Sci. U. S. A.* **1996**, *93*, 5975.
[10] F. A. Ferrone, J. Hofrichter, H. R. Sunshine, W. A. Eaton, *Biophys. J*. **1980**, *32*, 361.
[11] F. A. Ferrone, J. Hofrichter, W. A. Eaton, *J. Mol. Biol.* **1985**, *183*, 591.
[12] S. Mocklinghoff, W. A. L. van Otterlo, R. Rose, S. Fuchs, T. J. Zimmermann, M. D. Seoane, H. Waldmann, C. Ottmann, L. Brunsveld, *J. Med. Chem.* **2011**, *54*, 2005.
[13] J. W. F. Schwabe, L. Chapman, J. T. Finch, D. Rhodes, *Cell* **1993**, *75*, 567.
[14] R. D. Hancock, B. J. Tarbet, *J. Chem. Ed*. **2000**, *77*, 988.
[15] E. L. Eliel, S. H. Wilen, in *Stereochemistry of Organic Compounds*, New York, **1994**.
[16] R. C. de L. Milton, S. C. F. Milton, S. B. H. Kent, *Science* **1992**, *256*, 1445.
[17] C. Viedma, B. J. V. Verkuijl, J. E. Ortiz, T. d. Torres, R. M. Kellogg, D. G. Blackmond, *Chem. Eur. J*. **2010**, *16*, 4932.
[18] S. F. Mason, *Nature* **1984**, *311*, 19.
[19] M. Calvin, in *Chemical Evolution*, Oxford Press, **1969**.
[20] M. M. Green, V. Jain, *Orig. Life Evol. Biosph.* **2010**, *40*, 111.
[21] I. Weissbuch, L. Leiserowitz, M. Lahav, *Top. Curr. Chem*. **2005**, *123*, 2569.
[22] W. A. Bonner, *Orig. Life Evol. Biosph*. **1991**, *21*, 59.
[23] P. L. Luisi, in *The Emergence of Life: From Chemical Origins to Synthetic Biology*, Cambridge University Press, Cambridge, **2006**.
[24] A. J. Bur, L. Fetters, *J. Chem. Rev.* **1976**, *76*, 727.
[25] M. M. Green, K. –S. Cheon, S. –Y. Yang, J. –W. Park, S. Swansburg, W. Liu, *Acc. Chem. Res*. **2001**, *34*, 672.
[26] K. –S. Cheon, M. M. Green, *J. Label. Compd. Radiopharm.* **2007**, *50*, 961.
[27] M. M. Green, S. Lifson, A. Teramoto, *Chirality* **1991**, *3*, 285.
[28] M. B. Bellot, L. Bouteiller, *Langmuir* **2008**, *24*, 14176.
[29] M. Roman, C. Cannizzo, T. Pinault, B. Isare, B. Andrioletti, P. van der Schoot, L. Bouteiller, *J. Am. Chem. Soc.* **2010**, *132*, 16818.
[30] T. Pinault, B. Isare, L. Bouteiller, *Chem. Phys. Chem*. **2006**, *7*, 816.
[31] B. Isare, M. Linares, R. Lazzaroni, L. Bouteiller, *J. Phys. Chem. B* **2009**, *113*, 3360.
[32] L. Brunsveld, H. Zhang, M. Glasbeek, J. A. J. M. Vekemans, E. W. Meijer, *J. Am. Chem. Soc*. **2000**, *122*, 6175.
[33] J. van Gestel, P. van der Schoot, M. A. J. Michels, *J. Phys. Chem. B* **2001**, *105*, 10691.
[34] J. van Gestel, P. van der Schoot, M. A. J. Michels, *Langmuir* **2003**, *19*, 1375.
[35] T. F. A. de Greef, M. M. J. Smulders, M. Wolffs, A. P. H. J. Schenning, R. P. Sijbesma, E. W. Meijer, *Chem. Rev*. **2009**, *109*, 5687.
[36] E. H. Braswell, *J. Phys. Chem*. **1984**, *88*, 3653.
[37] N. D. Coggeshall, E. L. Saier, *J. Am. Chem. Soc.* **1951**, *73*, 5414.
[38] A. Bierzynski, H. Kozlowska, K. L. Wierzchowski, *Biophys. Chem.* **1977**, *6*, 213.
[39] A. D. Broom, M. P. Schweizer, P. O. P. Ts'o, *J. Am. Chem. Soc.* **1967**, *89*, 3612.
[40] T. J. Gilligan, G. Schwarz, *Biophys. Chem.* **1976**, *4*, 55.
[41] S. Boileau, L. Bouteiller, F. Lauprêtre, F. Lortie, *New. J. Chem*. **2000**, *24*, 845.
[42] P. R. Stoesser, S. J. Gill, J. *Phys. Chem.* **1967**, *71*, 564.
[43] R. B. Martin, *Chem. Rev*. **1996**, *96*, 3043.
[44] P. van der Schoot, in *Theory of Supramolecular Polym*., Vol. 2 (Ed.: A. Ciferri), Taylor & Francis, London, **2005**.
[45] D. Zhao, J. S. Moore, *Org. Biomol. Chem*. **2003**, *1*, 3471.
[46] A. J. Markvoort, H. M. M. ten Eikelder, P. A. J. Hilbers, T. F. A. de Greef, E. W. Meijer, *Nat. Commun*. **2011**, *2*, 59.
[47] L. A. LaPlanche, H. B. Thomson, M. T. Rogers, *J. Phys. Chem.* **1965**, *69*, 1482.
[48] N. Kobbo, J. J. Dannenberg, *J. Phys. Chem A* **2003**, *107*, 10389.

[49] H. P. Erickson, D. Pantaloni, *Biophys. J.* **1981**, *34*, 293.
[50] D. L. Caspar, *Biophys. J.* **1980**, *32*, 103.
[51] D. Chandler, *Nature* **2005**, *437*, 640.
[52] T. M. Raschke, J. Tsai, M. Levitt, *Proc. Natl. Acad. Sci. U. S. A.* **2001**, *98*, 5965.
[53] T. Metzroth, A. Hoffmann, R. Martin-Rapùn, M. M. J. Smulders, K. Pieterse, A. R. A. Palmans, J. A. J. M. Vekemans, E. W. Meijer, H. W. Spiess, J. Gauss, *Chem. Sci.* **2011**, *2*, 69.
[54] P. Jonkheijm, P. van der Schoot, A. P. H. J. Schenning, E. W. Meijer, *Science* **2006**, *313*, 80.
[55] P. J. M. Stals, M. M. J. Smulders, R. Martin-Rapùn, A. R. A. Palmans, E. W. Meijer, *Chem. Eur. J.* **2009**, *15*, 2071.
[56] M. M. J. Smulders, A. P. H. J. Schenning, E. W. Meijer, *J. Am. Chem. Soc.* **2008**, *130*, 606.
[57] F. C. Frank, *Biochem. Biophys. Acta* **1953**, *11*, 459.
[58] B. L. Feringa, R. A. Delden, *Angew. Chem. Int. Ed.* **1999**, *38*, 3418.
[59] K. Soai, I. Sato, T. Shibata, S. Komiya, M. Hayashi, Y. Matsueda, H. Imamura, T. Hayase, H. Morioka, H. Tabira, J. Yamamoto, Y. Kowata, *Tetrahedron: Asymmetry* **2003**, *14*, 185.
[60] T. Shibata, S. Yonekubo, K. Soai, *Angew. Chem. Int. Ed.* **1999**, *38*, 659.
[61] T. Shibata H. Morioka , T. Hayase, K. Choji, K. Soai, *J. Am. Chem. Soc.* **1996**, *118*, 471.
[62] K. Soai, I. Sato, T. Shibata, *Chem. Rec.* **2001**, *1*, 321.
[63] K. Soai, T. Shibata, I. Sato, *Acc. Chem. Res.* **2000**, *33*, 382.
[64] H. Wynberg, *J. Macromol. Sci. -Chem.* **1989**, *A26*, 1033.
[65] K. Soai, S. Niwa, *Chem Rev.* **1992**, *92*, 833.
[66] The reaction gives almost quantitative yield (> 99%).
[67] K. Soai, S. Osanai, K. Kadowaki, S. Yonekubo, T. Shibata, I. Sato, *J. Am. Chem. Soc.* **1999**, *121*, 11235.
[68] I. Sato, K. Kadowaki, K. Soai, *Angew. Chem. Int. Ed*. **2000**, *39*, 1510.
[69] I. Sato, R. Yamashima, K. Kadowaki, J. Yamamoto, T. Shibata, K. Soai, *Angew. Chem. Int. Ed*. **2001**, *40*, 1096.
[70] I. Sato, D. Omiya, T. Saito, K. Soai, *J. Am. Chem. Soc.* **2000**, *122*, 11739.
[71] T. Kawasaki, M. Shimizu, D. Nishiyama, M. Ito, H. Ozawa, K. Soai, *Chem. Commun.* **2009**, 4396.
[72] T. Kawasaki, Y. Matsumura, T. Tsutsumi, K. Suzuki, M. Ito, K. Soai, *Science* **2009**, *324*, 492.
[73] D. G. Blackmond, C. R. McMillan, S. Ramdeehul, A. Schorm, J. M. Brown, *J. Am. Chem. Soc.* **2001**, *123*, 10103.
[74] D. G. Blackmond, *Adv. Synth. Catal.* **2002**, *344*, 156.
[75] F. G. Buono, D. G. Blackmond, *J. Am. Chem. Soc.* **2003**, *125*, 8978.
[76] F. G. Buono, H. Iwamura, D. G. Blackmond, *Angew. Chem. Int. Ed*. **2004**, *43*, 2099.
[77] L. Schiaffino, G. Ercolani, *Angew. Chem. Int. Ed*. **2008**, *47*, 1.
[78] C. Puchot, O. Samuel, E. Dunach, S. Zhao, C. Agami, H. B. Kagan, *J. Am. Chem. Soc.* **1986**, *108*, 2353.
[79] N. Oguni, Y. Matsuda, T. Kaneko, *J. Am. Chem. Soc.* **1988**, *110*, 7877.
[80] M. Kitamura, S. Okada, S. Suga, R. Noyori, *J. Am. Chem. Soc.* **1989**, *11*, 4028.
[81] C. Girard, H. B. Kagan, *Angew. Chem. Int. Ed*. **1998**, *37*, 2922.
[82] M. Avalos, R. Babiano, P. Cintas, J. L. Jimenez, J. C. Palacios, *Tetrahedron: Asymmetry* **1997**, *8*, 2997.
[83] P. Pino, *Adv. Polym. Sci.* **1965**, *4*, 393.
[84] P. Pino, G. P. Lorenzi, *J. Am. Chem. Soc.* **1960**, *82*, 4745.
[85] M. M. Green, M. P. Reidy, *J. Am. Chem. Soc.* **1989**, *111*, 6452.
[86] M. M. Green, B. A. Garetz, B. Munoz, H. Chang, *J. Am. Chem. Soc.* **1995**, *117*, 4181.
[87] A. R. A. Palmans, J. A. J. M. Vekemans, E. E. Havinga, E. W. Meijer, *Angew. Chem. Int. Ed*. **1997**, *36*, 2648.
[88] J. van Gestel, A. R. A. Palmans, B. Titulaer, J. A. J. M. Vekemans, E. W. Meijer, *J. Am. Chem. Soc.* **2005**, *127*, 5490.
[89] A. R. A. Palmans, J. A. J. M. Vekemans, H. Fischer, R. A. Hikmet, E. W. Meijer, *Chem. Eur. J.* **1997**, *3*, 300.
[90] A. R. A. Palmans, E. W. Meijer, *Angew. Chem. Int. Ed*. **2007**, *46*, 8948.
[91] W. Jin, T. Fukushima, M. Niki, A. Kosaka, N. Ishii, T. Aida, *Proc. Natl. Acad. Sci. U. S. A.* **2005**, *102*, 10801.
[92] N. Katsonis, H. Xu, R. M. Haak, T. Kudernac, Z. Tomovic, S. Geoerge, M. van der Auweraer, A. P. H. J. Schenning, E. W. Meijer, B. L. Feringa, S. de Feyter, *Angew. Chem. Int. Ed*. **2008**, *47*, 4997.
[93] M. Parschau, T. Kampen, K. -H. Ernst, *Chem. Phys. Lett.* **2005**, *407*, 433.
[94] L. Pasteur, *C. R. Hebd. Seanc. Acad. Sci*. Paris, **1848**, *26*, 535.
[95] D. K. Kondepudi, R, Kaufman, N. Singh, *Science* **1990**, *250*, 975.
[96] C. Viedma, *J. Cryst. Growth* **2004**, *261*, 118.
[97] C. Viedma, *Phys. Rev. Lett*. **2005**, 065504-1.
[98] W. L. Noorduin, T. Izumi, A. Millemaggi, M. Leeman, H. Meekes, W. J. P. van Enckevort, R. M. Kellogg, B. Kaptein, E. Vlieg, D. G. Blackmond, *J. Am. Chem. Soc.* **2008**, *130*, 1158.

[99] W. L. Noorduin, H. Meekes, A. A. C. Bode, W. J. P. van Enckevort, B. Kaptein, R. M, Kellog, E. Vlieg, *Cryst. Growth Des.* **2008**, *8*, 1675.
[100] W. L. Noorduin, W. J. P. van Enckevort, H. Meekes, B. Kaptein, R. M. Kellog, J. C. Tully, J. M. McBride, E. Vlieg, *Angew. Chem. Int. Ed*. **2010**, *49*, 8435.
[101] S. B. Tsogoeva, S. Wei, M. Freund, M. Mauksch, *Angew. Chem. Int. Ed*. **2009**, *48*, 590.
[102] M. Mauksch, S. Wei, M. Freund, A. Zamfir, S. B. Tsogoeva, *Orig. Life. Evol. Biosph.* **2010**, *40*, 79.
[103] T. Tsunoda, H. Kaku, M. Nagaku, E. Okuyama, *Tetrahedron Lett.* **1997**, *38*, 7759.
[104] P. J. M. Stals, J. Everts, R. de Bruijn, I. A. W. Filot, M. M. J. Smulders, R. Martin-Rapún, E. A. Pidko, T. F. A. de Greef, A. R. A. Palmans, E. W. Meijer, *Chem. Eur. J.* **2010**, *16*, 810.
[105] J. J. van Gorp, J. A. J. M. Vekemans, E. W. Meijer, *J. Am. Chem. Soc.* **2002**, *124*, 14759.
[106] M. A. J. Veld, D. Haveman, A. R. A. Palmans, E. W. Meijer, *Soft Matter*, **2011**, *7*, 524.
[107] Y. Matsunaga, N. Miyajima, Y. Nakayasu, S. Sakai and M. Yonenaga, *Bull. Chem. Soc. Jpn.* **1988**, *61*, 207.
[108] A. Bernet, R. Q. Albuquerque, M. Behr, S. T. Hoffmann, H. −W. Schmidt, *Soft Matter* **2012**, *8*, 66.
[109] J. Y. Chang, J. H. Baik, C. B. Lee, M. J. Han, *J. Am. Chem. Soc*. **1997**, *119*, 3197.
[110] A. R. A. Palmans, J. A. J. M. Vekemans, E. W. Meijer, H. Kooijmans, A. L. Spek, *Chem. Commun*. **1997**, 2247.
[111] R. van Hameren, R. J. M. Nolte et al. *Science.* **2006**, *314*, 1433.
[112] I. Paraschiv, M. Giesbers, B. van Lagen, F. C. Grozema, R. D. Abellon, L. D. A. Siebbeles, A. T. M. Marcelis, H. Zuilhof, E. J. R. Sudhölter, *Chem. Mater*. **2006**, *18*, 968.
[113] J. van Herrikhuyzen, P. Jonkheijm, A. P. H. J. Schenning, E. W. Meijer, *Org. Biomol. Chem*. **2006**, *4*, 1539.
[114] B. Gong, C. Zheng, Y. Yan, *J. Chem. Cryst*. **1999**, *29-6*, 649.
[115] P. P. Bose, M. G. B. Drew, A. K. Das, A. Banerjee, *Chem. Commun*. **2006**, 3196.
[116] P. Besenius, G. Portale, P. H. H. Bomans, H. M. Janssen, A. R. A. Palmans, E. W. Meijer *Proc. Natl. Acad. Sci. U. S. A.* **2010**, *107*, 17888.
[117] M. Gelinsky, R. Vogler, H. Vahrenkamp, *Inorg. Chem*. **2002**, *41*, 2560.
[118] M. de Loos, J. H. van Esch, R. M. Kellogg, B. L. Feringa, *Tetrahedron* **2007**, *63*, 7285.
[119] K. P. van der Hout, R. Martin-Rapùn, J. A. J. M. Vekemans, E. W. Meijer, *Chem. Eur. J*. **2007**, *13*, 8111.
[120] K. Matsuura, K. Murasato, N. Kimisuka, *J. Am. Chem. Soc.* **2005**, *127*, 10148.
[121] M. Akiyama, A. Katoh, T. Ogawa, *J. Chem. Perkin Trans. II,* **1989**, 1213.
[122] P. J. M. Stals, J. F. Haveman, R. Martin-Rapún, C. F. C. Fitié, A. R. A. Palmans,d E. W. Meijer, *J. Mater. Chem.* **2009**, *19*, 124.
[123] S. Lee, J. −S. Lee, C. H. Lee, Y. −S. Jung, J. −M. Kim, *Langmuir* **2011**, *27*,1560.
[124] T. Shikata, D. Ogata, K. Hanabusa, *J. Phys. Chem. B*, **2004**, *108*, 508.
[125] N. Shi, H. Dong, G. Yin, Z. Xu, S. Li, *Adv. Funct. Mater*. **2007**, *17*, 1837.
[126] C. F. C. Fitié, I. Tomatsu, D. Byelov, W. H. de Jeu, R. P. Sijbesma, *Chem. Mater*. **2008**, *20*, 2394.
[127] P. Besenius, J. L. M. Heynens, R. Straathof, M. M. L. Nieuwenhuizen, P. H. H. Bomans, E. Terreno, S. Aime, G. J. Strijkers, K. Nicolay, E. W. Meijer, *Contrast Media Mol. Imaging* **2012**, DOI 10.1002/cmmi.498.
[128] M. Blomenhofer, S. Ganzleben, D. Hanft, H. –W. Schmidt, M. Kristiansen, P. Smith, K. Stoll, D. Maeder, K. Hoffmann, *Macromolecules* **2005**, *38*, 3688.
[129] K. E. Broaders, S. J. Pastine, S. Grandhe, J. M. J. Fréchet, *Chem. Commun*. **2011**, *47*, 665.
[130] L. Brunsveld, B. G. G. Lohmeijer, J. A. J. M. Vekemans, E. W. Meijer, *Chem. Commun*. **2000**, 2305.
[131] K. R. West, K. D. Bake, S. Otto, *Org. Lett.* **2005**, *7*, 2615.
[132] M. M. J. Smulders, T. Buffeteau, D. Cavagnat, M. Wolffs, A. P. H. J. Schenning, E. W. Meijer, *Chirality* **2008**, *28*, 1016.
[133] I. A. W. Filot, A. R. A. Palmans, P. A. J. Hilbers, R. A. van Santen, E. A. Pidko, T. F. A. de Greef, *J. Phys. Chem. B* **2010**, *114*, 13667.
[134] M. P. Lightfoot, F. S. Mair, R. G. Pritchard, J. E. Warren, *Chem. Commun.* **1999**, 1945.
[135] T. F. A. de Greef, M. M. L. Nieuwenhuizen, P. J. M. Stals, C. F. C. Fitié, A. R. A. Palmans, R. P. Sijbesma, E. W. Meijer, *Chem. Commun.* **2008**, 4306.
[136] M. M. J. Smulders, P. J. M. Stals, T. Mes, T. F. E. Paffen, A. P. H. J. Schenning, A. R. A. Palmans, E. W. Meijer, *J. Am. Chem. Soc.* **2010**, *132*, 620.
[137] J. van Gestel, *Macromolecules* **2004**, *37*, 3894.

2

SYNTHESIS OF A STEREOSELECTIVELY DEUTERATED BUILDING BLOCK FOR CHIRAL SELF-ASSEMBLY

Abstract. C_3-symmetrical α-deuterated benzene-1,3,5-tricarboxamides were synthesized from the appropriate α-deuterated octyl amines, which were derived from chiral, α-deuterated octyl alcohols. The enzymatic reduction of mono-deuterated octanal in the presence of alcohol dehydrogenases as the biocatalysts and nicotinamide adenine dinucleotide phosphate as the cofactor gave rise to the formation of the desired, chiral deuterated octanols in high yields and with high enantiomeric excesses (*e.e.*). To simplify the synthetic route, the direct reduction of octanal by using the same enzymes and the same cofactor but adding deuterated isopropanol was explored. By using this method, α-deuterated octanol was synthesized in high yield and with high *e.e.* in a single step. The alcohols were subsequently converted to their corresponding amines by tosylation, azidation and reduction. The *e.e.* of the alcohols and amines were > 90% as determined by the Mosher's acid method. Furthermore, chiral β-deuterated octyl amine was synthesized from deuterated octyl alcohol *via* tosylation, cyanation and reduction. The chiral amines obtained were subsequently converted to C_3-symmetrical α− and β-deuterated benzene-1,3,5-tricarboxamides.

Part of this work has been published:

D. W. R. Balkenende, S. Cantekin, C. J. Duxbury, M. H. P. van Genderen, E. W. Meijer, A. R. A. Palmans, *Synth. Commun.* **2012**, *42*, 563.

S. Cantekin, D. W. R. Balkenende, M. M. J. Smulders, A. R. A. Palmans, E. W. Meijer, *Nature Chem.* **2011**, *3*, 42.

2.1 Introduction

Chiral, deuterated compounds are useful mechanistic probes to elucidate chemical and biological pathways.[1,2] Also in the field of macromolecules, exchanging hydrogen with deuterium has provided insight into the origin of polymer miscibility[2] and polymer crystallization.[3,4] Deuterated polyisocyanates, a class of dynamic helical polymers, were studied in detail by Green and coworkers.[5] In contrast to the deuterated isocyanate monomer that showed hardly any optical activity, the corresponding polymers revealed remarkably strong Cotton effects and high optical rotations as a result of a pronounced helical sense preference.

We are interested in exploring the limits of chiral amplification in supramolecular systems and how this compares to the amplification of chirality in covalent helical polymers.[6] As a result, both enantiomers of α-deuterated-benzene-1,3,5-tricarboxamide (BTA) and the (*S*)-enantiomer of β-deuterated BTA were synthesized ((*R*)-**1**, (*S*)-**1** and (*S*)-**2**; Figure 2.1)*. Bearing minute chiral information, α- and β-deuterated BTA molecules provide valuable information about chirality at the supramolecular level, which will be discussed further in Chapter 3.

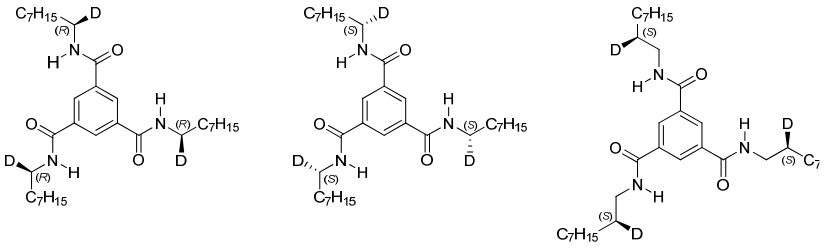

Figure 2.1: Structures of (*R*)- and (*S*)-α- and (*S*)-β-deuterated benzene-1,3,5-tricarboxamides.

The synthesis of deuterated BTAs requires access to chiral (*R*)- and (*S*)-1-^{2}H-1-octanol ((*R*)-**3** and (*S*)-**3**, Figure 2.2) of high enantiomeric purity. Although several chemical reductions are known to afford deuterated alcohols enantioselectively, the enantiomeric excesses (*e.e.*) are typically moderate to good (typically *e.e.* < 92%).[7-13] Moreover, the synthesis of enantioenriched (*S*)-1-^{2}H-1-hexanol *via* the reduction of 1-^{2}H-hexanal with Baker's yeast, a well-known alcohol dehydrogenase, was described by Green et al.; however, the *e.e.* of the product was not determined.[5] Later, Bradshaw et al. reduced hexanal with alcohol dehydrogenases from horse liver (HL-ADH) and *Pseudomonas* (PADH) using a deuterated cofactor to the corresponding (*R*)-1-^{2}H-1-hexanol and (*S*)-1-^{2}H-1-hexanol, respectively. Here,

* Although there are three stereocentra in these BTA molecules, instead of naming them (*S,S,S*)-**1**, (*R,R,R*)-**1** or (*S,S,S*)-**2**, (*S*)-**1**, (*R*)-**1** and (*S*)-**2** are used for simplicity.

the deuterated cofactor is generated by the deuterium transfer from a deuterated solvent such as isopropanol-d_8 or ethanol- d_6. The *e.e.* values of the deuterated alcohols were > 97% but long reaction times were required to reach modest conversion (50% to 89%).[14]

Recently, highly active alcohol dehydrogenases from *Lactobacillus brevis* (ADH-LB, (*R*)-selective) and *Thermoanaerobacter sp.* (ADH-T, (*S*)-selective) have become commercially available.[15] These enzymes exhibit excellent enantioselectivity in the reduction of ketones (> 99%). Here, we describe the use of ADH-T and ADH-LB in the reduction of 1-^{2}H-octanal. Moreover, we combine Bradshaw's method to apply a deuterated cofactor with ADH-T and ADH-LB in order to reduce octanal to enantiopure (*R*)- and (*S*)-1-^{2}H-1-octanol ((*R*)-**3'** and (*S*)-**3'**) with high *e.e.* and in one step. The *e.e.* values of these alcohols were determined by using Mosher's acid method.[8,9] The alcohols were then converted into the corresponding amines ((*R*)-**4**, (*S*)-**4**, and (*S*)-**4'**, Figure 2.2) and the influence of this synthetic strategy on the *e.e.* was investigated. Chiral β-deuterated amine ((*S*)-**5**) was synthesized starting from (*R*)-1-^{2}H-1-octanol ((*R*)-**3**). Finally, chiral amines ((*R*)-**4**, (*S*)-**4'** and (*S*)-**5**) were converted into the corresponding α- and β-deuterated BTAs.

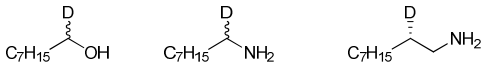

(*R*)-**3** (*S*)-**3** (*R*)-**4** (*S*)-**4** (*S*)-**5**

Figure 2.2: Structures of (*R*)- and (*S*)-α- and (*S*)-β-deuterated octyl alcohols and amines.

2.2 Enantioselective synthesis of (*R*)- and (*S*)-1-^{2}H-1-octanol

Chiral deuterated alcohols (*R*)-**3** and (*S*)-**3** were synthesized by the reduction of deuterated octanal **8** with ADH-T and ADH-LB. In order to synthesize deuterated octanal **8**, commercially available ethyl octanoate (**6**) was first reduced with $LiAlD_4$ in diethyl ether to form deuterated alcohol **7** (Scheme 2.1).[16] After that, compound **7** was oxidized with pyridinium chlorochromate (PCC) in dichloromethane to give deuterated octanal **8**. This oxidation method is general for obtaining aldehydes. However, the low yield (44%) is presumably due to the condensation reactions taking place during the distillation of compound **8**. In order to improve the yield of the oxidation step, we used other oxidizing agents such as Dess-Martin periodinane[17,18] and (2,2,6,6-tetramethylpiperidin-1-yl)oxidanyl (TEMPO).[19] The oxidation of compound **7** to the corresponding aldehyde with Dess-Martin periodinane was effective, providing mild reaction conditions and a simple work-up procedure; however, it was a costly process. TEMPO-catalyzed oxidations required longer reaction times (28 h) and led to a substantial amount of side products.

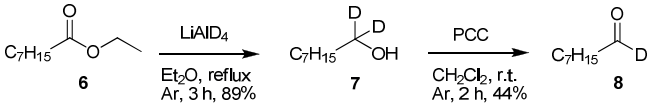

Scheme 2.1: Synthesis of deuterated octanal.

Deuterated octanal **8** was reduced with either ADH-LB or ADH-T affording (*R*)- and (*S*)-1-^{2}H-1-octanol ((*R*)-**3** and (*S*)-**3**), respectively (Scheme 2.2). Both enzymes depend on nicotinamide adenine dinucleotide phosphate (NADPH) as a cofactor in this reduction reaction, which serves as reduction equivalent.[15] However, both enzymes are also able to oxidize isopropanol for cofactor regeneration, and therefore, only catalytic amounts of $NADP^+$ are needed. The reaction equilibrium is driven by excess of isopropanol in buffer. Moreover, the high isopropanol content enhances the solubility of the lipophilic substrate in water. The reductions of deuterated octanal were performed in isopropanol (IPA) and potassium phosphate buffer (pH = 7, 23-29% v/v, IPA/H_2O) at substrate concentrations of 46-48 mM (Table 2.1). The reactions were monitored by gas chromatography-mass spectrometry (GC-MS) and after 4 days the conversions were > 98%. The alcohols were isolated in high yields and high purity as evidenced by NMR spectroscopy and GC-MS. The ^{2}H-NMR spectrum of (*R*)-**3** confirmed the formation of the desired alcohol by indicating the ^{2}H signal at 3.65 ppm as a broad singlet (Figure 2.3).

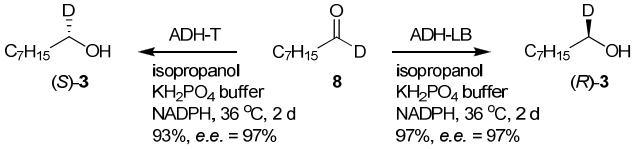

Scheme 2.2: Enantioselective synthesis of (*R*)- and (*S*)-deuterated octanol *via* enzymatic reduction of deuterated octanal.

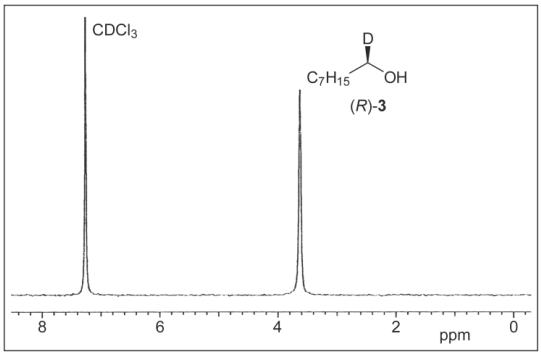

Figure 2.3: ^{2}H-NMR spectrum of (*R*)-**3**.

Preparing deuterated octanal requires a rather tedious, multi-step synthetic process. Furthermore, the PCC oxidation of **7** results in low yields. Therefore, we evaluated the procedure reported by Bradshaw in order to obtain enantiopure alcohols starting from octanal (**9**) (Scheme 2.3).[14] The reduction of octanal is anticipated to give similar results in one step by using isopropanol-d_8, ADH enzymes and NADPH (Scheme 2.3).

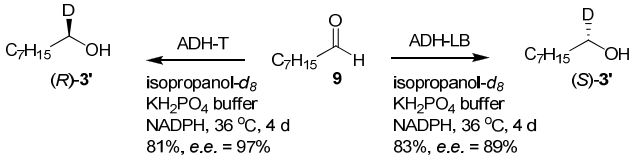

Scheme 2.3: Enantioselective synthesis of (*R*)- and (*S*)-deuterated octanol *via* direct enzymatic reduction of octanal.

Isopropanol-d_8 serves as the deuteride (D^-) source during reduction and additionally enhances the solubility of octanal, as mentioned previously. As shown in Figure 2.4, the deuterated cofactor (NADPD) is generated in a one enzyme system where the deuterium is transferred to the cofactor from isopropanol-d_8 (Figure 2.4).

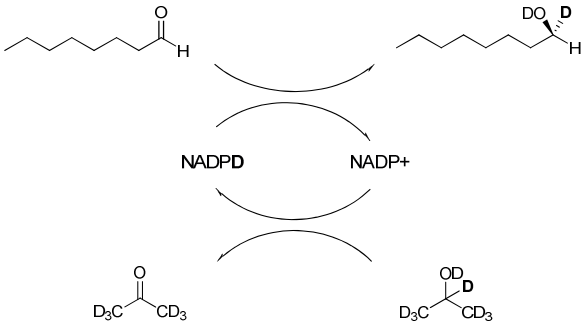

Figure 2.4: Cofactor regeneration and the deuterium transfer during the enzymatic reduction.

The reduction of octanal (Scheme 2.3) was performed with a lower isopropanol content and two times higher substrate concentrations in order to decrease the amount of IPA-d_8. Enzymes and cofactor were stable under these conditions; substrate or product inhibition was not observed. Within 4 days, quantitative conversions were obtained and the isolated yields were > 80% (Table 2.1). Both enantiomers were of high purity as evidenced by NMR spectroscopy and GC-MS.

Table 2.1: Enzymatic reduction of (deuterated) octanal.

Substrate	Solvent, %v/v	Concentration (mM)	Enzyme	Alcohol	Isolated yield (%)
octanal-*d*	IPA/H_2O, 23	46	ADH-LB	(*R*)-**3**	97
octanal-*d*	IPA/H_2O, 29	48	ADH-T	(*S*)-**3**	93
Octanal	IPA-d_8/H_2O, 11	93	ADH-T	(*R*)-**3′**	81
Octanal	IPA-d_8/H_2O, 12	103	ADH-LB	(*S*)-**3′**	83

IPA = isopropanol

2.3 Synthesis of (*R*)- and (*S*)-1-^{2}H-1-octylamine

Subsequently, the alcohols (*R*)-**3**, (*R*)-**3′** and (*S*)-**3′** were converted to their corresponding chiral amine derivatives (*S*)-**4**, (*S*)-**4′** and (*R*)-**4′** respectively, following a previously described procedure by tosylation, azidation and reduction (Scheme 2.4).[13] All steps proceeded in high yields and high purity as proved by NMR spectroscopy and GC-MS.

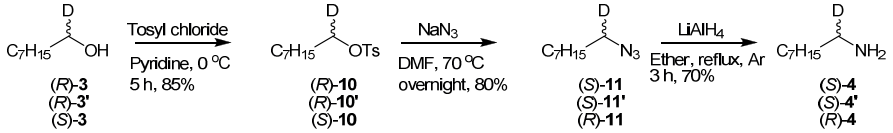

Scheme 2.4: Synthesis of (*R*)- and (*S*)-deuterated amines.

2.4 Determination of the enantiomeric excess (*e.e.*)

The optical purity of the alcohols and amines was assessed by employing the Mosher's acid method. Studies by Mosher et al. showed that α-methoxy-α-trifluoromethylphenylacetyl chloride (MTPA-Cl, **12**) promotes conversion of chiral alcohols and amines into corresponding diastereomeric esters and amides, respectively.[6,7] These esters and amides were analyzed by NMR spectroscopy and the *e.e.* was determined by quantifying the NMR spectra of the diastereomers. This method was adapted to the synthesis of diastereomeric MTPA esters and amides by treating commercially available MTPA-Cl ((*R*)-**12**) with (*R*) and (*S*)-**3**, (*R*) and (*S*)-**3′** and (*S*)-**4** and (*S*)-**4'** (Scheme 2.5).

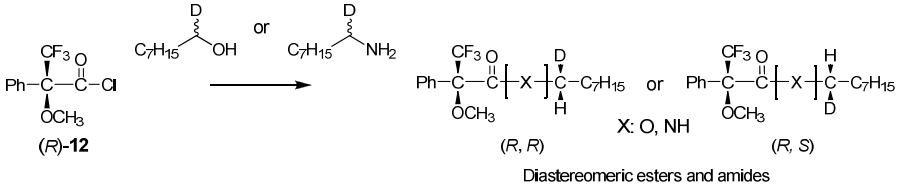

Scheme 2.5: General synthesis of diastereomeric MTPA-esters and amides.

In order to interpret the NMR spectra of the diastereomers accurately, we also synthesized the racemic alcohol (*rac*)-**13** and its amine derivative (*rac*)-**14** as shown in Scheme 2.6. The reduction of octanal (**9**) with $LiAlD_4$ gave (*rac*)-**13** which was subsequently converted to the racemic amine (*rac*)-**14** by following the same synthetic procedure as discussed above. The racemic alcohols and amines were converted to the corresponding MTPA ester ((*rac*)-**15**) and amide derivatives ((*rac*)-**16**).

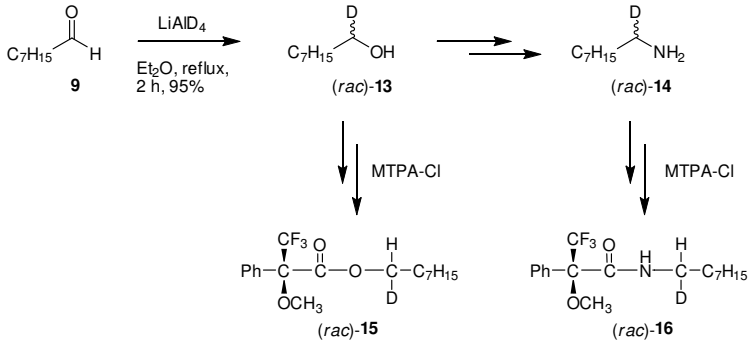

Scheme 2.6: Synthesis of racemic α-deuterated alcohol, amine and corresponding MTPA-ester and amide.

In the ^{1}H-NMR spectrum of MTPA ester (*rac*)-**15**, the -OC*H* proton resonates as two overlapping triplets (at δ = 4.29 ppm) with equal intensity (Figure 2.5a). These overlapping signals hamper the integration thus obtaining the relative proportions of the two diastereomers becomes difficult. In order to prevent this, the –CH_2 protons in (*rac*)-**15** next to the chiral centre were decoupled which resulted in a better separation of the signals with raising decoupler power. However, when the maximum decoupler power was used, the peaks were still not completely separated. Moreover, raising the decoupling energy deteriorated the quality of the ^{1}H-NMR spectra and thus the accuracy of the peak integration.

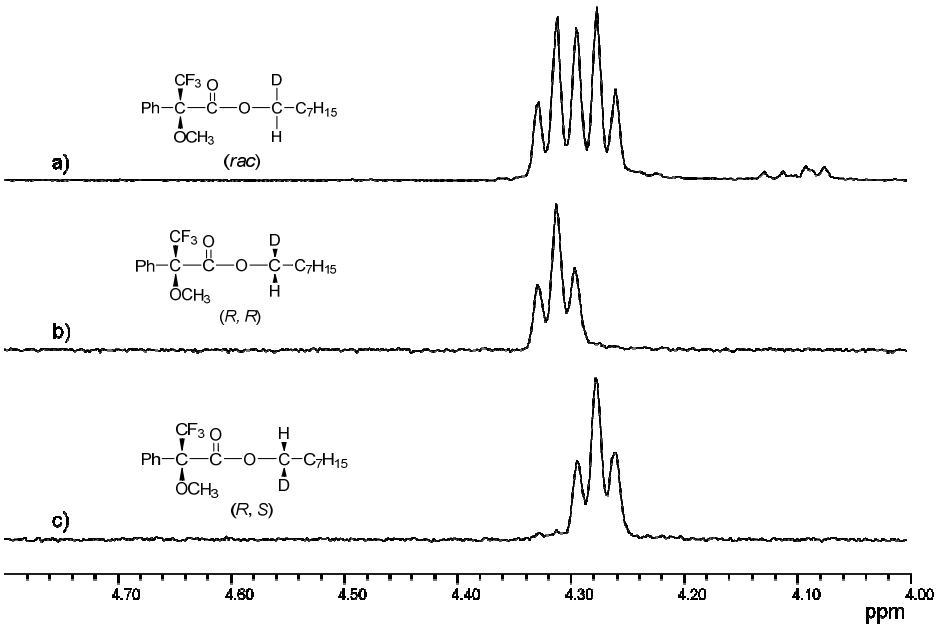

Figure 2.5: ^{1}H-NMR spectra of MTPA-esters produced from a) (*rac*)-**15**, b) (*R*)-**3**, c) (*S*)-**3'**.

In order to separate the overlapping triplets without using the decoupling method, we used a 2D ^{1}H-NMR technique which allowed us to integrate the intensity profiles of both peaks. The application of the method resulted in two triplets at δ = 4.31 and δ = 4.28 ppm having equal magnitude indicating that the *e.e.* of (*rac*)-**15** is 0.0% (Table 2.2, entry 1). However, this method did not give reliable results for the alcohols (*R*)-**3**, (*S*)-**3** and (*R*)-**3′** and (*S*)-**3′** due to difficulties in integration. As a result, we deconvoluted the two triplets in the ^{1}H-NMR spectra of diastereomeric MTPA ester (*rac*)-**15** which gave an *e.e.* of 0% (Table 2.2, entry 1). Following this procedure, the *e.e.* values of (*R*)-**3**, (*S*)-**3** and (*R*)-**3′**, (*S*)-**3′** were measured (Table 2.2, entry 2-5) as 97±1%, 97±1%, 97±1%, and 89±1%, respectively. Alcohol (*R*)-**3′,** which was synthesized *via* a deuterated cofactor, has the same *e.e.* as those synthesized *via* a normal enzymatic reduction process. However, (*S*)-**3′** shows a slightly lower *e.e.* which is presumably the result of non-optimal reduction conditions. The high concentration employed (103 mM) may negatively influence the enantioselectivity of the reduction.

Analysis of (*rac*)-**16** by NMR spectroscopy revealed two signals having quartet multiplicity with equal magnitudes at 3.32 and 3.28 ppm (Figure 2.6a). Signal deconvolution indicated that the *e.e.* of the (*rac*)-**16** was 0% (Table 2.2, entry 6). As for the MTPA amides of (*S*)-**4** and (*S*)-**4′**, ^{1}H-NMR spectra showed a quartet at 3.32 ppm and a small partially overlapping quartet at 3.28 ppm. In this case the *e.e.* values were 90% indicating that the conversion of a chiral alcohol into chiral amine proceeds with high selectivity. The high *e.e.* is preserved during the transformation of the tosylate (*R*)-**10′** to (*S*)-**4′** *via* an S_N2 reaction, during which inversion of configuration occurs.

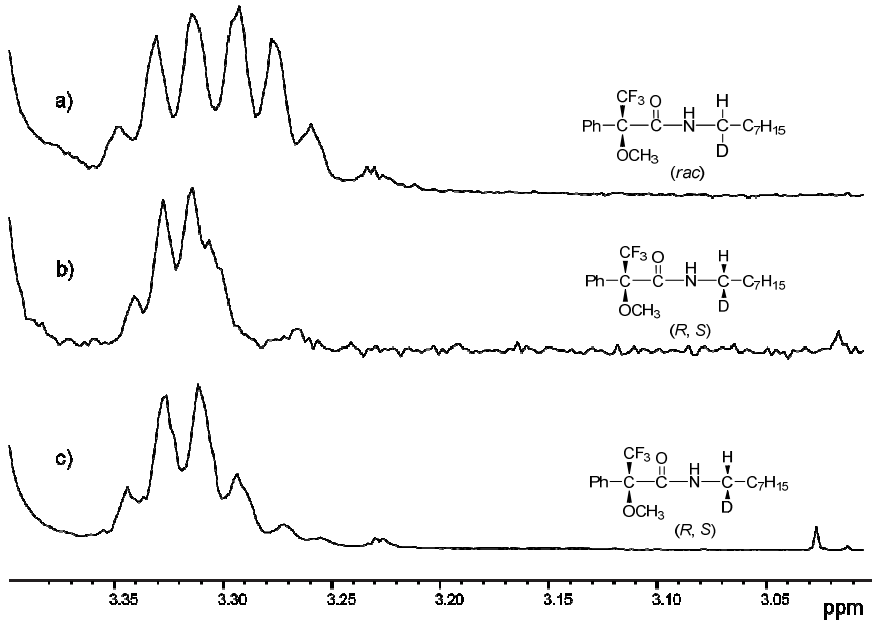

Figure 2.6: ^{1}H-NMR spectra of MTPA-amides produced from a) (*rac*)-**16**, b) (*S*)-**4**, c) (*S*)-**4′**.

Table 2.2: The *e.e.* values of corresponding chiral alcohols and amines.

Entry	Alcohol/amine[a]	*e.e.*[b,c] (%)
1	(*rac*)-**15**	0
2	(*R*)-**3**	97±1
3	(*S*)-**3**	97±1
4	(*R*)-**3′**	97±1
5	(*S*)-**3′**	89±1
6	(*rac*)-**14**	0
7	(*S*)-**4**	89±1
8	(*S*)-**4′**	90±1

[a] All compounds were converted into their MTPA ester or amide derivatives.

[b] *e.e.* (=([*R*]-[*S*])/([*R*]+[*S*])) was calculated from the intensities of –XC*H*– signals in the ^{1}H-NMR spectra of the diastereomeric MTPA derivatives by using deconvolution to resolve overlapping peaks.

[c] The error on the *e.e.* by deconvolution of the spectra was determined by performing an error propagation analysis assuming that the intensity of the ^{1}H-NMR signals possesses an uncertainty of 10%.

2.5 Synthesis of (*R*)- and (*S*)-α-deuterated benzene-1,3,5-tricarboxamide

The target compounds (*R*)- and (*S*)-α-deuterated BTA ((*R*)-**1**) and (*S*)-**1**) (Figure 2.1) were synthesized by functionalizing commercially available benzene-1,3,5-tricarbonyl trichloride with the appropriate chiral amines, (*R*)- and (*S*)-1-^{2}H-1-octylamine ((*R*)-**4** and (*S*)-**4′**), which were obtained from corresponding alcohols (*S*)- and (*R*)-1-^{2}H-1-octanol ((*S*)-**3** and (*R*)-**3′**), respectively. (*R*)-**1** and (*S*)-**1** were obtained in high purity as evidenced by ^{1}H-NMR, ^{2}H-NMR, ^{13}C-NMR, FT-IR and MALDI-TOF MS analysis. The ^{13}C-APT experiment for (*S*)-**1** showed a triplet with a negative amplitude at 40 ppm which is resulting from -C*H*D tertiary carbon (Figure 2.7A). In addition, the presence of deuterium in the molecule was confirmed by the ^{2}H-NMR spectrum of (*S*)-**1**, which gave rise to a broad singlet at 3.45 ppm for deuterium (-CH*D*) (Figure 2.7B).

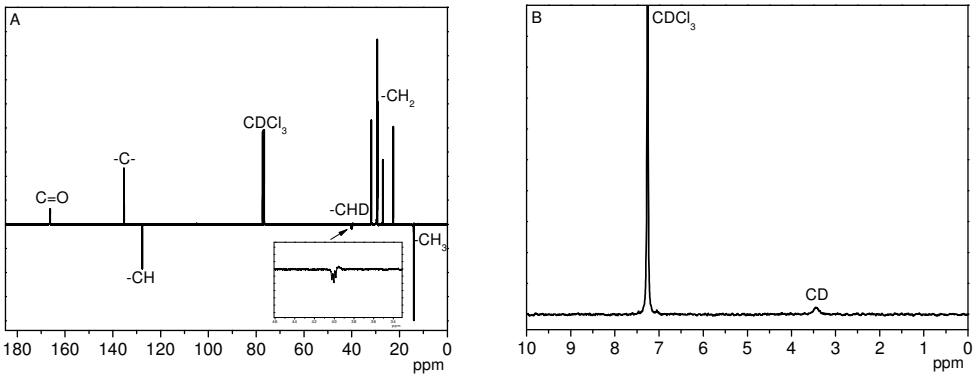

Figure 2.7: A) ^{13}C-APT-NMR spectrum; B) ^{2}H-NMR spectrum of (*S*)-**1**.

2.6 Synthesis of (*S*)-β-deuterated benzene-1,3,5-tricarboxamide

The chiral amine, (*S*)-2-^{2}H-1-aminononane ((*S*)-**5**), was synthesized starting from deuterated alcohol (*R*)-**3′**. The alcohol was first converted into tosylate (*R*)-**17′** using tosyl chloride in pyridine. The cyanation of (*R*)-**17′** with NaCN in DMSO provided (*S*)-**18**. The cyano group was then reduced and the desired β-deuterated amine ((*S*)-**5**) was obtained in a yield of 60%. The conversion of the cyano group into amine was followed by FT-IR and GC-MS. (*S*)-β-deuterated BTA ((*S*)-**2**) was obtained in good yield by treating commercially available benzene-1,3,5-tricarbonyl trichloride with (*S*)-**5** (Scheme 2.7). The *e.e.* of the β-deuterated amine could not be determined.

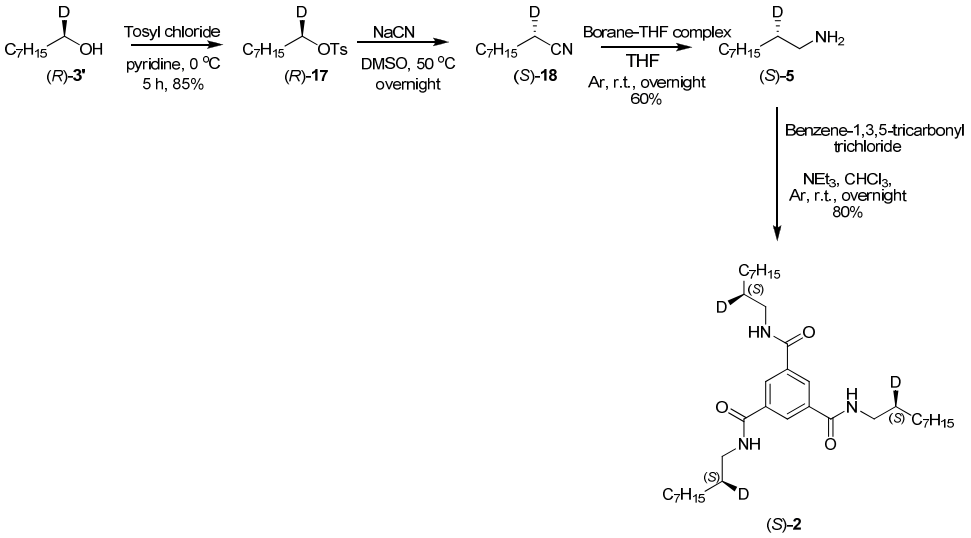

Scheme 2.7: Synthesis of (*S*)-β-deuterated BTA.

2.7 Conclusions

(*R*) and (*S*)-*α*-deuterated BTAs are appealing building blocks for investigating the influence of isotope substitution on the supramolecular chirality. Therefore, it is important to obtain chiral, deuterated precursors with high *e.e.* values. We first evaluated the enzymatic asymmetric reduction of deuterated octanal by using alcohol dehydrogenases (ADH-T and ADH-LB) and the cofactor nicotinamide adenine dinucleotide phosphate (NADPH). While this method gave deuterated alcohols in high yields and purity, it required four-step synthesis of deuterated octanal. We then evaluated the reduction of octanal by using the same enzymes and deuterated isopropanol that served as the deuterium source. By means of this new reduction route, the chiral, deuterated alcohols were obtained from octanal in a single step with comparable yield and purity. The conversion of the deuterated alcohols into deuterated amines was accomplished by tosylation, azidation and reduction in high yields. The *e.e.* of the alcohols and amines obtained were determined by applying the Mosher's acid method. The alcohols and amines were converted into their diastereomeric ester and amide derivatives and the quantification of the ^{1}H-NMR spectra of these compounds by signal deconvolution provided the *e.e.* values of the chiral, deuterated alcohols and amines accurately. Furthermore, β-deuterated amines were obtained from deuterated alcohols via tosylation, cyanation and reduction. (*S*)-β-deuterated BTA was synthesized in good yield from (*S*)-β-deuterated amine. The effect of the deuterium position on the self-assembly of deuterated BTAs will be discussed in the next chapter.

2.8 Experimental

2.8.1 General

^{1}H-NMR (400 MHz and 500 MHz), ^{2}H-NMR (500 MHz), ^{13}C-NMR (100 MHz) and 2D-NMR (400 MHz) spectra were recorded on Varian spectrometers (Varian Mercury V×400 or Varian Unity Inova 500) in deuterated chloroform unless stated otherwise. ^{2}H-NMR was measured on a Varian Unity Inova 500 spectrometer by dissolving the sample in chloroform and adding 10 μL of deuterated chloroform in the NMR tube. Chemical shifts (δ) are reported in ppm and referenced to tetramethylsilane (TMS). Peaks are indicated as singlet (s), doublet (d), triplet (t), quartet (q), quintet (qui), heptet (h), or multiplet (m) broadened peaks are indicated as (br). Deconvolution was performed by using the linefit in MestReNova version 6.0.3-5604. GC-MS was performed on a Shimazu GCMS-QP5000 equiped with a Zebron ZB-5 column and an autosampler. All GC-MS measurements were done with injector temperature = 300 °C, detector temperature = 300 °C. IR spectra were recorded on a Perkin–Elmer spectrum 1 using a universal ATR.

Deuterated octanal was prepared according to ref 5. Octanal, ethyl octanoate, $LiAlD_4$, phosphate buffered saline and isopropanol-d_8 were obtained from Sigma-Aldrich. Cofactor NADPH and alcohol dehydrogenases from *Lactobacillus brevis* (ADH-LB, (*R*)-selective, 4100 U/mL) and *Thermoanaerobacter sp.* (ADH-T, (*S*)-selective, 331 U/mL) were purchased from Julich Chiral Solutions GmbH. (*R*)-(-)-α-Methoxy-α-trifluoromethylphenylacetyl chloride ((*R*)-(−)-MTPA-Cl) and triethylamine were purchased from Acros. All other chemicals were purchased from Sigma-Aldrich and used as received unless otherwise noted. All used solvents were obtained from Biosolve. Diethyl ether and chloroform were dried over molecular sieves and triethylamine was stored on KOH pellets.

Phosphate buffered saline was dissolved in deionized water to prepare phosphate buffer solution (pH 7.4, 50 mM) and was used for the enzymatic reduction reactions. All alcohols and amines were converted to their diastereomeric MTPA ester and amide derivatives by treating them with commercially available (*R*)-(−)-MTPA-Cl following a modified literature procedure.[8]

2.8.2 Synthesis

1,1-Di^{2}H-1-octanol (7): Ethyl octanoate (27.60 g, 160 mmol) in dry diethyl ether (60 mL) was added dropwise to a solution of $LiAlD_4$ (5.0 g, 119 mmol) in dry diethyl ether (200 mL) at 0°C under argon atmosphere. The mixture was refluxed for 1 h and cooled down using an ice bath. Cold water was added slowly to the reaction mixture until bubbling stopped. Subsequently, aqueous H_2SO_4 (10%) solution was added. The mixture was extracted with diethyl ether (3×50 mL). The combined organic layers were washed with water, and dried over $MgSO_4$. The removal of the solvent yielded the isolated product as clear oil (20.84 g,

89%). ^{1}H-NMR (400 MHz, $CDCl_3$): δ = 2.20 (br s, 1H, -CH_2CD_2OH), 1.51 (t, J = 6.6 Hz, 2H, -$(CH_2)_5CH_2CD_2OH$), 1.29 (m, 10H, $CH_3(CH_2)_5CH_2$-), 0.85 (t, J = 6.2 Hz, 3H, $CH_3(CH_2)_5$-) ppm. ^{2}H-NMR (500 MHz, $CDCl_3$): δ = 3.62 (s, -CD) ppm. ^{13}C-NMR (100 MHz, $CDCl_3$): δ = 61.7 (qui), 32.4, 31.8, 29.4, 29.2, 25.7, 22.6, 14.0 ppm. GC-MS temperature program: 50 °C | 15 min → 300 °C, 10 °C/min. t_R = 2.24 min, purity > 99.5%, major peaks: [M^+-CD_2OH] = 99, [M^+-CH_2CD_2OH] = 84, [M^+-$C_2H_4CD_2OH$] = 70, [M^+-$C_3H_6CD_2OH$] = 56, [M^+-$C_4H_8CD_2OH$] = 41.

1-^{2}H-1-Octanal (8): Pyridinium chlorochromate (15.64 g, 73 mmol) and alcohol **7** (9.65 g, 66 mmol) were dissolved in dichloromethane (150 mL) in a round bottom flask under argon. The reaction mixture was stirred at room temperature for 1.5 h. Subsequently, diethyl ether (200 mL) was added to the reaction mixture. After decanting the reaction mixture, the remaining black solid was washed thoroughly with diethyl ether (3×50 mL). The solvent was removed and the residue was filtered over silica (100 g, Et_2O). The solvent was removed, and the remaining black oil was distilled at 30 mbar with rapid heating (heating gun) to avoid aldol condensations. The product was a clear oil (4.13 g, 44%). ^{1}H-NMR (400 MHz, $CDCl_3$): δ = 2.36 (t, J = 7.4 Hz, 2H, -$(CH_2)_5CH_2CDO$), 1.57 (qui, J = 7.2 Hz, 2H, -$(CH_2)_4CH_2CH_2CDO$), 1.24 (m, 10H, $CH_3(CH_2)_5CH_2$-), 0.85 (t, J = 6.2 Hz, 3H, $CH_3(CH_2)_5$-) ppm. ^{13}C-NMR (100 MHz, $CDCl_3$): δ = 201.5 (t), 43.7, 31.6, 29.1, 28.9, 22.5, 22.0, 14.0 ppm. GC-MS temperature program: 50 °C | 15 min → 300 °C, 10 °C/min. t_R = 1.72 min, purity > 99.5%, major peaks: [M^+-CDO] = 100, [M^+-CH_2CDO] = 86, [M^+-C_2H_4CDO] = 72, [M^+-C_3H_6CDO] = 57, [M^+-C_4H_8CDO] = 43.

(*R*)-1-^{2}H-1-Octanol ((*R*)-3): Deuterated octanal **8** (1.16 g, 9 mmol) was dissolved in isopropanol (45 mL). To this mixture, phosphate buffer solution (150 mL) and NADPH (265 mg) were added. Then a few drops of $MgCl_2$ solution in distilled water (0.1 M) were added to the reaction mixture and mild heating was applied. When the temperature was set to 36 °C, the enzyme ADH-LB (308 U) was added to the reaction mixture. The mixture was left stirring at that temperature for 48 h. The mixture was washed with diethyl ether (3×50 mL) and the combined organic layers were dried with $MgSO_4$. After the removal of the solvent, (*R*)-**3** was obtained as colorless oil (1.14 g, 97%). *e.e.* = 97±1%. ^{1}H-NMR (400 MHz, $CDCl_3$): δ = 3.56 (tt, J = 6.8 and 1.2 Hz, 1H, -CH_2CHDOH), 1.51 (q, J = 6.8 Hz, 2H, -$(CH_2)_5CH_2CHDOH$), 1.27 (m, 10H, $CH_3(CH_2)_5CH_2$-), 0.84 (t, J = 6.8 Hz, 3H, $CH_3(CH_2)_5$-) ppm. ^{2}H-NMR (500 MHz, $CDCl_3$): δ = 3.65 (s, -CD) ppm. ^{13}C-NMR (100 MHz, $CDCl_3$): δ = 62.0 (t), 32.5, 31.7, 29.3, 29.1, 25.6, 22.5, 14.0 ppm. GC-MS temperature program: 50 °C | 15 min → 300 °C, 10 °C/min. t_R = 2.64 min, purity > 99.5%, major peaks: [M^+-CH_2OD] = 99, [M^+-C_2H_4OD] = 85, [M^+-C_3H_6OD] = 71, [M^+-C_4H_8OD] = 57, [M^+-$C_5H_{10}OD$] = 43. FT-IR: ν = 3336 (br), 2956 (s), 2856 (s), 2157 (w), 1711 (s), 1466 (m), 1069 (m), 939 (m), 723 (w).

(*S*)-1-^{2}H-1-Octanol ((*S*)-3): Deuterated octanal **8** (1.29 g, 10 mmol) was dissolved in isopropanol (60 mL). To this mixture, phosphate buffer solution (150 mL) and NADPH (326 mg) were added. Instead of using ADH-LB for the reduction, ADH-T (155 U) was used. $MgCl_2$ solution was not required for this enzyme. (*S*)-**3** was obtained as a colorless oil (1.22 g, 93%). *e.e.* = 97±1%. ^{1}H-NMR (400 MHz, $CDCl_3$): δ = 3.56 (tt, *J* = 6.8 and 1.2 Hz, 1H, -CH_2CHDOH), 1.51 (q, *J* = 6.8 Hz, 2H, -$(CH_2)_5CH_2$CHDOH), 1.27 (m, 10H, $CH_3(CH_2)_5CH_2$-), 0.84 (t, *J* = 6.8 Hz, 3H, $CH_3(CH_2)_5$-) ppm. ^{13}C-NMR (100 MHz, $CDCl_3$): δ = 62.0 (t), 32.5, 31.7, 29.3, 29.1, 25.6, 22.5, 14.0 ppm. GC-MS temperature program: 50 °C | 15 min → 300 °C, 10 °C/min. t_R = 2.64 min, purity = > 99.5%, major peaks: [M^+ -CH_2OD] = 99, [M^+ - C_2H_4OD] = 85, [M^+ -C_3H_6OD] = 71, [M^+ -C_4H_8OD] = 57, [M^+ -$C_5H_{10}OD$] = 43. FT-IR: ν = 3336 (br), 2956 (s), 2856 (s), 2157 (w), 1711 (s), 1466 (m), 1069 (m), 939 (m), 723 (w).

(*R*)-1-^{2}H-Octyl-4′-methylbenzenesulfonate ((*R*)-10): *p*-Toluenesulfonyl chloride (1.56 g, 8.4 mmol) was dissolved in dry pyridine (10 mL) in a round bottom flask and cooled down to 0°C. (*R*)-**3** (1.0 g, 7.6 mmol) was added dropwise to this mixture. The reaction mixture was left stirring overnight at 4 °C. The mixture was quenched with cold water, and extracted with diethyl ether (3×50 mL). The combined organic layers were consecutively washed with 1 M HCl solution, water and brine. The organic layer was dried over $MgSO_4$ and the solvent was removed. The isolated product was a yellowish oil (1.95 g, 89%). ^{1}H-NMR (400 MHz, $CDCl_3$): δ = 7.78 (d, *J* = 8.4 Hz, 2H, -$SO_2C(CH$CH)$_2$CCH$_3$), 7.33 (d, *J* = 8.4 Hz, 2H, -$SO_2C(CHCH$)$_2$CCH$_3$), 4.00 (t, *J* = 6.6 Hz, 1H, -CH_2CHDO-), 2.45 (s, 3H, -$SO_2C(CHCH)_2CCH_3$), 1.66 (q, *J* = 6.6 Hz, 2H, $(CH_2)_5CH_2$CHDO), 1.23 (m, 10H, $CH_3(CH_2)_5CH_2$), 0.86 (t, *J* = 6.8 Hz, 3H, $CH_3(CH_2)_5$-) ppm. ^{13}C-NMR (100 MHz, $CDCl_3$): δ = 144.6, 133.2, 129.8, 127.8, 71.5 (t), 31.7, 29.0, 28.8, 28.5, 25.3, 22.5, 21.6, 14.0 ppm. GC-MS temperature program: 50 °C | 15 min → 300 °C, 10 °C/min. t_R = 7.39 min, purity = > 99.5%, major peaks: [M^+-$C_7H_7O_3SD$] = 113, [M^+ -$C_8H_9O_3SD$] = 99, [M^+-- $C_9H_{11}O_3SD$] = 85, [M^+-$C_{10}H_{13}O_3SD$] = 71, [M^+ -$C_{11}H_{15}O_3SD$] = 57, [M^+ -$C_{12}H_{17}O_3SD$] = 43.

(*S*)-1-^{2}H-Octylazide ((*S*)-11): (*R*)-10 (1.95 g, 6.8 mmol) was dissolved in DMF (30 mL). While stirring the reaction mixture at room temperature, NaN_3 (4.4 g, 68 mmol) was added in one portion to this solution. The reaction mixture was left stirring at 70 °C overnight. Subsequently, the mixture was poured into cold water (200 mL) and extracted with diethyl ether (3×50 mL). The combined organic layers were washed with water and brine. The organic layer was dried over $MgSO_4$. After removal of the solvent, the product was obtained as a clear oil (0.9 g, 85%). ^{1}H-NMR (400 MHz, $CDCl_3$): δ = 3.23 (tt, *J* = 7.2 and 1.6 Hz, 1H, -CH_2CHN$_3$), 1.56 (q, *J* = 7.2 Hz, 2H, -$(CH_2)_5CH_2$CDHN$_3$), 1.28 (m, 10H, $CH_3(CH_2)_5CH_2$-), 0.85 (t, *J* = 6.4 Hz, 3H, $CH_3(CH_2)_5$-) ppm. ^{13}C-NMR (100 MHz, $CDCl_3$): δ = 51.1 (t), 31.7, 29.2, 29.1, 28.7, 26.7, 22.6, 13.9 ppm. GC-MS temperature program: 50 °C | 15 min → 300 °C, 10 °C/min. t_R = 2.73 min, purity = 88%, major peaks: [M^+-N_2] = 127, [M^+-DN_3] = 113, [M^+-$CHDN_3$] = 99,

[M^+-CH_2CHDN_3] = 85, [M^+-$C_2H_4CHDN_3$] = 70, [M^+-$C_3H_6CHDN_3$] = 57, [M^+-$C_4H_8CHDN_3$] = 43. FT-IR: ν = 2956 (s), 2856 (s), 2157 (w), 2092 (s), 1677 (m), 1466 (m), 1069 (m), 939 (m), 723 (w).

(*S*)-1-^{2}H-Octylamine ((*S*)-4): $LiAlH_4$ solution (9.9 mL, 1.0 M in diethyl ether) was placed in a round bottom flask under argon atmosphere and diluted with additional diethyl ether (10 mL). The mixture was cooled down to 0 °C. To this solution, (*S*)-**11** (0.7 g, 4.5 mmol) in diethyl ether (40 mL) was added dropwise. The mixture was refluxed for 2 h, cooled down by using an ice bath and quenched slowly with cold water. The mixture was extracted with diethyl ether (3×50 mL). The combined organic layers were washed with water, and dried over $MgSO_4$. The solvent was removed under reduced pressure. The product was isolated as a clear oil (0.5 g, 85%). *e.e.* = 89±1%. ^{1}H-NMR (400 MHz, $CDCl_3$): δ = 2.62 (t, *J* = 6.8 Hz, 1H, -$CH_2CD\mathit{H}NH_2$), 1.60 (br. s, 2H, -$CH_2CDHN\mathit{H}_2$), 1.40 (q, *J* = 6.8 Hz, $CH_3(CH_2)_5C\mathit{H}_2CDHNH_2$), 1.20 (m, 10H, $CH_3(C\mathit{H}_2)_5CH_2CDHNH_2$), 0.82 (t, *J* = 6.4, 3H, $C\mathit{H}_3(CH_2)_5CH_2CDHNH_2$) ppm. ^{13}C-NMR (100 MHz, $CDCl_3$): δ = 41.7 (t), 33.6, 31.7, 29.2, 29.0, 26.5, 22.6, 13.9 ppm. GC-MS temperature program: 50 °C | 15 min → 300 °C, 10 °C/min. t_R = 2.00 min, purity = 94%, major peaks: [M^+] = 130, [M^+-DNH_2] = 113, [M^+-CH_2DNH_2] = 99, [M^+-$C_2H_4DNH_2$] = 84, [M^+-$C_3H_6DNH_2$] = 71, [M^+-$C_4H_8DNH_2$] = 57, [M^+-$C_5H_{10}DNH_2$] = 43. FT-IR: ν = 2956 (s), 2856 (s), 2157 (w), 1466 (m), 1069 (m), 939 (m), 723 (w).

(*R*)-1-^{2}H-Octylamine ((*R*)-4): Following the same procedure described above yielded (*R*)-**4** . as clear oil (0.5 g, 85%). ^{1}H-NMR (400 MHz, $CDCl_3$): δ = 2.61 (t, *J* = 6.8 Hz, 1H, -$CH_2CD\mathit{H}NH_2$), 1.60 (br. s, 2H, -$CH_2CDHN\mathit{H}_2$), 1.42 (q, *J* = 6.8 Hz, $CH_3(CH_2)_5C\mathit{H}_2CDHNH_2$), 1.21 (m, 10H, $CH_3(C\mathit{H}_2)_5CH_2CDHNH_2$), 0.80 (t, *J* = 6.4, 3H, $C\mathit{H}_3(CH_2)_5CH_2CDHNH_2$) ppm. ^{13}C-NMR (100 MHz, $CDCl_3$): δ = 41.7 (t), 33.6, 31.7, 29.2, 29.0, 26.5, 22.6, 13.9 ppm. GC-MS temperature program: 50 °C | 15 min → 300 °C, 10 °C/min. t_R = 2.00 min, purity = 94%, major peaks: [M^+] = 130, [M^+-DNH_2] = 113, [M^+-CH_2DNH_2] = 99, [M^+-$C_2H_4DNH_2$] = 84, [M^+-$C_3H_6DNH_2$] = 71, [M^+-$C_4H_8DNH_2$] = 57, [M^+-$C_5H_{10}DNH_2$] = 43. FT-IR: ν = 2956 (s), 2856 (s), 2157 (w), 1466 (m), 1069 (m), 939 (m), 723 (w).

(*R*)-1-^{2}H-1-Octanol ((*R*)-3′): Octanal (**9**) (3.0 g, 23 mmol) was dissolved in isopropanol-d_8 (28 mL). To this solution, phosphate buffer solution (220 mL) and NADPH (1.0 g) were added. Subsequently, the temperature was set to 36 °C; ADH-T (331 U) was added to the reaction mixture which was left stirring at 36 °C for 4 days. The reaction was monitored by GC-MS and NMR spectroscopy. The mixture was extracted with diethyl ether (3×50 mL) and the organic layer was dried over $MgSO_4$. The solvent was evaporated and the desired alcohol (*R*)-**3′** was obtained as colorless oil (2.50 g, 81%). The alcohol was used without further purification. *e.e.* = 97±1%. ^{1}H-NMR (400 MHz, $CDCl_3$): δ = 3.62 (tt, *J* = 6.8 and 1.4 Hz, 1H, -$CH_2C\mathit{H}DOH$), 1.56 (q, *J* = 6.8 Hz, 2H, -$(CH_2)_5C\mathit{H}_2CHDOH$), 1.15 (m, 10H, $CH_3(C\mathit{H}_2)_5CH_2$-),

0.88 (t, *J* = 6.8, 3H, C*H*$_3$(CH$_2$)$_5$-), ^{13}C-NMR (100 MHz, CDCl$_3$): δ = 62.1 (t), 32.3, 31.6, 29.3, 29.2, 25.7, 22.6, 13.9. GC-MS temperature program: 50 °C | 15 min → 300 °C, 10 °C/min. t_R = 2.64 min, purity = > 99.5%, major peaks: [M$^+$-CH$_2$OD] = 99, [M$^+$- C$_2$H$_4$OD] = 85, [M$^+$-C$_3$H$_6$OD] = 71, [M$^+$-C$_4$H$_8$OD] = 57, [M$^+$-C$_5$H$_{10}$OD] = 43. FT-IR: ν = 3336 (br), 2956 (s), 2856 (s), 2157 (w), 1711 (s), 1466 (m), 1069 (m), 939 (m), 723 (w).

(*S*)-1-^{2}H-Octylamine ((*S*)-4′): LiAlH$_4$ (0.16 g, 4.2 mmol) was dissolved in diethyl ether (15 mL) and the solution was cooled down to 0 °C under argon. (*S*)-1-^{2}H-octylazide (which was synthesized *via* consecutive tosylation and azidation of (*R*)-**3′**) (0.30 g, 1.9 mmol) in diethyl ether (10 mL) was added dropwise to the solution under argon at 0 °C. After the addition was complete, the reaction mixture was refluxed for 2 h. Subsequently, the reaction mixture was cooled down to 0 °C and quenched slowly with cold water, diethyl ether was added and the mixture was washed consecutively with 1 M NaOH and water. The aqueous phase was extracted with diethyl ether (3×20 mL) and dried with MgSO$_4$. After the removal of solvent, the desired amine (*S*)-**4′** was obtained as clear oil (0.18 g, 75%). *e.e.* = 90±1%. ^{1}H-NMR (400 MHz, CDCl$_3$): δ = 2.62 (t, *J* = 6.8 Hz, 1H, -CH$_2$CD*H*NH$_2$), 1.60 (br. s, 2H, -CH$_2$CDHN*H*$_2$), 1.40 (q, *J* = 6.8 Hz, CH$_3$(CH$_2$)$_5$C*H*$_2$CDHNH$_2$), 1.20 (m, 10H, CH$_3$(C*H*$_2$)$_5$CH$_2$CDHNH$_2$), 0.82 (t, *J* = 6.4, 3H, C*H*$_3$(CH$_2$)$_5$CH$_2$CDHNH$_2$) ppm. ^{13}C-NMR (100 MHz, CDCl$_3$): δ = 41.7 (t), 33.6, 31.7, 29.2, 26.8, 22.6, 15.2, 13.9 ppm. GC-MS temperature program: 50 °C | 15 min → 300 °C, 10 °C/min. t_R = 2.00 min, purity = 94%, major peaks: [M$^+$] = 130, [M$^+$-DNH$_2$] = 113, [M$^+$-CHDNH$_2$] = 99, [M$^+$-C$_2$H$_4$DNH$_2$] = 84, [M$^+$-C$_3$H$_6$DNH$_2$] = 71, [M$^+$-C$_4$H$_8$DNH$_2$] = 57, [M$^+$-C$_5$H$_{10}$DNH$_2$] = 43. FT-IR: ν = 2956 (s), 2856 (s), 2157 (w), 1466 (m), 1069 (m), 939 (m), 723 (w).

(*S*)-1-^{2}H-1-Octanol ((*S*)-3′): Octanal (**9**) (1.5 g, 11.7 mmol) was dissolved in isopropanol-d_8 (14 mL). To this solution, phosphate buffer solution (100 mL), NADPH (0.5 g) and a few drops of MgCl$_2$ (0.1 M in distilled water) were added. The temperature was set to 36 °C, ADH-LB (380 U) was added and the reaction mixture was left stirring at 36 °C for 4 days. The same procedure was followed to obtain alcohol (*S*)-**3′** as colorless oil (1.25 g, 83%). *e.e.* = 89±1%. ^{1}H-NMR (400 MHz, CDCl$_3$): δ = 3.62 (tt, *J* = 6.8 and 1.4 Hz, 1H, -CH$_2$C*H*DOH), 1.56 (q, *J* = 6.8 Hz, 2H, -(CH$_2$)$_5$C*H*$_2$CHDOH), 1.15 (m, 10H, CH$_3$(C*H*$_2$)$_5$CH$_2$-), 0.88 (t, *J* = 6.8, 3H, C*H*$_3$(CH$_2$)$_5$-), ^{13}C-NMR (100 MHz, CDCl$_3$): δ = 62.1 (t), 32.3, 31.6, 29.3, 29.2, 25.7, 22.6, 13.9. GC-MS temperature program: 50 °C | 15 min → 300 °C, 10 °C/min. t_R = 2.64 min, purity = > 99.5%, major peaks: [M$^+$-CH$_2$OD] = 99, [M$^+$- C$_2$H$_4$OD] = 85, [M$^+$-C$_3$H$_6$OD] = 71, [M$^+$-C$_4$H$_8$OD] = 57, [M$^+$-C$_5$H$_{10}$OD] = 43. FT-IR: ν = 3336 (br), 2956 (s), 2856 (s), 2157 (w), 1711 (s), 1466 (m), 1069 (m), 939 (m), 723 (w).

(*R*)-1-^{2}H-Octylamine ((*R*)-4′): The reduction of the corresponding azide (0.25 g, 1.60 mmol) (which was synthesized *via* tosylation and azidation of (*S*)-**3′** by following the same

procedure as described above yielded the desired amine (*R*)-**4'** as clear oil (0.16 g, 77%). ^{1}H-NMR (400 MHz, $CDCl_3$): δ = 2.62 (t, *J* = 6.8 Hz, 1H, -CH_2CDHNH_2), 1.60 (br. s, 2H, -CH_2CDHNH_2), 1.40 (q, *J* = 6.8 Hz, $CH_3(CH_2)_5CH_2CDHNH_2$), 1.20 (m, 10H, $CH_3(CH_2)_5CH_2CDHNH_2$), 0.82 (t, *J* = 6.4, 3H, $CH_3(CH_2)_5CH_2CDHNH_2$) ppm. ^{13}C-NMR (100 MHz, $CDCl_3$): δ = 41.7 (t), 33.6, 31.7, 29.2, 29.0, 26.8, 22.6, 13.9 ppm. GC-MS temperature program: 50 °C | 15 min → 300 °C, 10 °C/min. t_R = 2.00 min, purity = 94%, major peaks: [M^+] = 130, [M^+-DNH_2] = 113, [M^+-CH_2DNH_2] = 99, [M^+-$C_2H_4DNH_2$] = 84, [M^+-$C_3H_6DNH_2$] = 71, [M^+-$C_4H_8DNH_2$] = 57, [M^+-$C_5H_{10}DNH_2$] = 43. FT-IR: ν = 2956 (s), 2856 (s), 2157 (w), 1466 (m), 1069 (m), 939 (m), 723 (w).

(*rac*)-1-^{2}H-1-Octanol ((*rac*)-13): Octanal (2.0 g, 16.5 mmol) in diethyl ether (20 mL) was added dropwise to a solution of $LiAlD_4$ (0.43 g, 10.1 mmol) in diethyl ether (10 mL) at 0 °C. The reaction mixture was refluxed for 2 h and then quenched with cold water (10 mL) slowly. The mixture was extracted with diethyl ether (3×50 mL). The combined organic layer was washed consecutively with HCl (1 M) solution and water, and dried over $MgSO_4$. The solvent was removed under reduced pressure. The product was isolated as clear oil (1.95 g, 95%). ^{1}H-NMR (400 MHz, $CDCl_3$): δ = 3.62 (tt, *J* = 6.8 and 1.4 Hz, 1H, -CH_2CHDOH), 1.56 (q, *J* = 6.8 Hz, 2H, -$(CH_2)_5CH_2CHDOH$), 1.15 (m, 10H, $CH_3(CH_2)_5CH_2$-), 0.88 (t, *J* = 6.8, 3H, $CH_3(CH_2)_5$-), ^{13}C-NMR (100 MHz, $CDCl_3$): δ = 62.1 (t), 32.3, 31.6, 29.3, 29.2, 25.7, 22.6, 13.9. GC-MS temperature program: 50 °C | 15 min → 300 °C, 10 °C/min. t_R = 2.19 min, purity = 98%, major peaks: [M^+-DOH] = 113, [M^+-CH_2OD] = 99, [M^+-C_2H_4OD] = 85, [M^+-C_3H_6OD] = 71, [M^+-C_4H_8OD] = 57, [M^+-$C_5H_{10}OD$] = 43.

(*rac*)-1-^{2}H-Octylamine ((*rac*)-14): The desired racemic amine **14** was obtained from (*rac*)-**13** (3.53 g, 27 mmol) as yellowish oil (3.50 g, 80%) by following the previous procedure. ^{1}H-NMR (400 MHz, $CDCl_3$): δ = 2.62 (t, *J* = 7.2 Hz, 1H, -CH_2CDHOH), 1.50 (br. s, 2H, -CH_2CDHNH_2), 1.40 (q, *J* = 6.8 Hz, 2H, $CH_3(CH_2)_5CH_2CDHNH_2$), 1.25 (m, 10H, $CH_3(CH_2)_5CH_2CDHNH_2$), 0.85 (t, *J* = 6.8 Hz, 3H, $CH_3(CH_2)_5CH_2CDHNH_2$) ppm. ^{13}C-NMR (100 MHz, $CDCl_3$): δ = 41.7 (t), 33.6, 31.7, 29.2, 29.1, 26.8, 22.6, 13.9 ppm. GC-MS temperature program: 50 °C | 15 min → 300 °C, 10 °C/min. t_R = 2.00 min, purity = 94%, major peaks: [M^+] = 130, [M^+-DNH_2] = 113, [M^+-CH_2DNH_2] = 99, [M^+-$C_2H_4DNH_2$] = 84, [M^+-$C_3H_6DNH_2$] = 71, [M^+-$C_4H_8DNH_2$] = 57, [M^+-$C_5H_{10}DNH_2$] = 43.

General synthesis of Mosher's acid derivatives: The desired alcohol or amine (0.10 mmol) was dissolved in dry chloroform (300 μL) under argon atmosphere. To this solution, dry pyridine (300 μL) and (*R*)-(-)-α-methoxy-α-trifluoromethylphenylacetyl chloride ((*R*)-(−)-MTPA-Cl) (26 μL, 0.14 mmol) were injected using a syringe. The reaction mixture was stirred overnight at room temperature. A few drops of water were added and the mixture was left

stirring for 10 min. The mixture was diluted with diethyl ether (10 mL) and washed with cold HCl (1 M), Na_2CO_3 and saturated brine solution. The combined organic layers were dried on $MgSO_4$ and subsequently the solvent was removed under reduced pressure. The desired Mosher's ester or amide was obtained as colorless oil in quantitative yield. The NMR spectra of these samples were recorded and the ratio of both diastereomers was determined from the integrals of the –C*H*D proton signals.

***N,N′,N′′*-Tri((*R*)-1-^{2}H-octyl)-benzene-1,3,5-tricarboxamide ((*R*)-1):** To a solution of the appropriate amine ((*R*)-**4**) (1 g, 8.0 mmol) and triethylamine (0.9 g, 8.5 mmol) in dry $CHCl_3$ (15 mL) a solution of benzene-1,3,5-tricarbonyl trichloride (640 mg, 2.4 mmol) in $CHCl_3$ (5 mL) was added dropwise at 0 °C under argon atmosphere in 30 min. After the addition was complete, the reaction mixture was allowed to warm to room temperature and stirred overnight at room temperature under argon. The reaction mixture was diluted with $CHCl_3$ (20 mL) and washed with 1 M HCl (25 mL) and water (25 mL), respectively. The aqueous phase was extracted with $CHCl_3$ (3×25 mL). The combined organic extracts were dried over $MgSO_4$ and solvent was removed under reduced pressure. Crystallization from EtOAc-hexane (3:1) yielded (*R*)-**1** as white powder (1.0 g, 77%). ^{1}H-NMR (400 MHz, $CDCl_3$): δ 8.34 ppm (s, 3H, Ar*H*), 6.41 (br. s, 3H, ArCO*NH*CHD$(CH_2)_6CH_3$), 3.45 (q, *J* = 6.8 Hz, 3H, -NHC*H*D$(CH_2)_6CH_3$), 1.60 (m, 6H, -NHCHDC*H*$_2(CH_2)_5CH_3$), 1.35 (m, 30H, -NHCHDCH$_2$($CH_2)_5CH_3$), 0.88 (t, *J* = 6.8 Hz, 9H, -NHCHD$(CH_2)_6CH_3$); ^{2}H-NMR (500 MHz, $CDCl_3$): δ 3.45 (br.s, -NHCH*D*$(CH_2)_6CH_3$); ^{13}C-NMR (100 MHz, $CDCl_3$): δ 165.8, 135.3, 127.9, 40.0 (-CHD), 31.8, 29.4, 29.3, 29.2, 27.0, 22.6, 14.1. FT-IR: ν = 3240, 3071, 2926, 2859, 2175, 1630, 1550, 1466, 1294, 1022, 9054, 691. MALDI-TOF-MS: calculated for $C_{33}H_{54}D_3N_3O_3$ 546.46, observed $C_{33}H_{54}D_6N_3O_3$ 549.54. Overdeuteration was observed occasionally during the reduction of **7** with $LiAlD_4$. This gave rise to a fraction of BTA which included more deuterium content.

***N,N′,N′′*-Tri((*S*)-1-^{2}H-octyl)-benzene-1,3,5-tricarboxamide ((*S*)-1):** The desired BTA (*S*)-**1** was obtained from ((*S*)-**4′**) (1 g, 8.0 mmol) as white powder (0.90 g, 70%) by following the procedure described above. ^{1}H-NMR (400 MHz, $CDCl_3$): δ 8.34 (s, 3H, Ar*H*), 6.41 (br. s, 3H, ArCO*NH*CHD$(CH_2)_6CH_3$), 3.45 (q, *J* = 6.8 Hz, 3H, -NHC*H*D$(CH_2)_6CH_3$), 1.60 (m, 6H, -NHCHDC*H*$_2(CH_2)_5CH_3$), 1.35 (m, 30H, -NHCHDCH$_2$($CH_2)_5CH_3$), 0.88 (t, *J* = 6.8 Hz, 9H, -NHCHD$(CH_2)_6CH_3$); ^{2}H-NMR (500 MHz, $CDCl_3$): δ 3.45 (br.s, -NHCH*D*$(CH_2)_6CH_3$); ^{13}C-NMR (100 MHz, $CDCl_3$): δ 165.8, 135.3, 127.9, 40.0, 31.8, 29.4, 29.3, 29.2, 27.0, 22.6, 14.1; ^{13}C-APT-NMR (100 MHz, $CDCl_3$): δ 165.8, 135.3,127.9, 40.0 (-CHD), 31.8, 29.4, 29.3, 29.2, 27.0, 22.6, 14.1. FT-IR: ν 3242, 3071, 2924, 2855, 2175, 1630, 1550, 1466, 1294, 1022, 954, 691. MALDI-TOF-MS: calculated for $C_{33}H_{54}D_3N_3O_3$ 546.46, observed $C_{33}H_{54}D_3N_3O_3$ 546.69.

(*S*)-1-^{2}H-Octyl cyanide ((*S*)-18): Tosylate (*R*)-**17′** (1.70 g, 9.2 mmol) was dissolved in DMSO (13 mL) under argon atmosphere with a gas wash bottle filled with 1 M NaOH at the end of the gas-flow. The reaction mixture was heated to 50 °C. Subsequently, NaCN (0.40 g, 0.01 mol) was added to the solution and the mixture was stirred overnight at 50 °C under argon. After the reaction was complete, the mixture was allowed to cool down to room temperature, after which it was transferred to a separation funnel and water (60 mL) was added. The aqueous layer was extracted with CH_2Cl_2 (3×50 mL), the organic layers were collected and washed with 1 M KCl (3×30 mL). After evaporation of the solvent, the crude product was obtained as yellowish oil (0.90 g, 70%). GC-MS temperature program: 50 °C | 15 min → 300 °C, 10 °C/min. t_R = 3.73 min, purity = > 99.5%, major peaks: [M^+-C_2H_4CN] = 85, [M^+-C_3H_6DN] = 83, [M^+-C_5H_7DN] = 56, [M^+-C_6H_9DN] = 44. Trace amount of α-deuterated octanol was observed. ^{1}H-NMR (400 MHz, $CDCl_3$): δ = 2.26 (m, 1H, -CH_2CHDCN), 1.58 (q, *J* = 7.4 Hz, 2H, -CH_2CH_2CHDCN), 1.36 (m, 2H, -$CH_2(CH_2)_4CH_2CH_3$), 1.22 (m, 8H, -$CH_2(CH_2)_4CH_2CH_3$), 0.82 (t, *J* = 8.0 Hz, 3H, -$CH_2(CH_2)_5CH_3$) ppm. FT-IR: ν = 3255 (w), 2928 (s), 2858 (s), 2249 (m), 1727 (w), 1466 (m), 1056 (s), 907 (s), 750 (s), 647 (m).

(*S*)-2-^{2}H-1-Aminononane ((*S*)-5): A 50 mL three-necked round bottle flask was charged with a solution of borane-THF-complex (1 M, 15 mL) in dry THF (7 mL), while keeping the solution at 0 °C and under argon atmosphere. To this solution a solution containing (*S*)-**18** (1.00 g, 7 mmol) in dry THF (6 mL) was slowly added *via* a dropping funnel. The mixture was stirred for 30 min at 0 °C, and subsequently, was refluxed for 1 h. Finally, the mixture was stirred overnight at room temperature. After that, the mixture was cooled to 0 °C, and methanol (15 mL) was added dropwise (care should be taken for the hydrogen gas formation). HCl (37% in water, 3 mL) was added slowly; the reaction mixture was stirred for 1 h and subsequently evaporated to dryness under reduced pressure. To the resulting viscous liquid was added 2 M NaOH (25 mL) and this was extracted with diethyl ether (3×30 mL). The organic layers were collected and dried with sodium sulfate, filtered and the solvent was removed under reduced pressure to obtain (*S*)-**5** as yellowish liquid (0.80 g, 80%). GC-MS temperature program: 50 °C | 15 min → 300 °C, 10 °C/min. t_R = 2.80 min, purity = > 99.5%, major peaks: [M^+-C_3H_7DN] = 86, [M^+-$C_6H_{13}DN$] = 44. Trace amount of α-deuterated-octanol was observed. ^{1}H-NMR (400 MHz, $CDCl_3$): δ = 2.65 (d, *J* = 8.0 Hz, 2H, -$CHCH_2NH_2$), 1.90 (br. s, 2H, -CH_2NH_2), 1.38 (qui, *J* = 8.0 Hz, 1H, -CH_2CHDCH$_2$NH$_2$), 1.23 (m, 12H, $CH_3(CH_2)_6$CHDCH$_2$NH$_2$), 0.82 (t, *J* = 8.0 Hz , 3H, $CH_3(CH_2)_6$CHDCH$_2$NH$_2$). FT-IR: ν = 3326 (w), 2925 (s), 2856 (w), 1466 (m), 1260 (w), 1091 (m), 802 (s), 734 (s).

***N*,*N*′,*N*′′-Tri((*S*)-2-^{2}H-nonyl)-benzene-1,3,5-tricarboxamide ((*S*)-2):** To a solution of the amine (*S*)-**5** (0.80 g, 5.6 mmol) and triethylamine (0.66 g, 6.2 mmol) in dry $CHCl_3$ (10 mL) a solution of benzene-1,3,5-tricarbonyl trichloride (0.45 g, 2.4 mmol) in $CHCl_3$ (5 mL) was added

dropwise at 0 °C under argon in 30 min. After the addition was complete, the reaction mixture was allowed to warm to room temperature and stirred overnight at room temperature under inert atmosphere. The reaction mixture was diluted with $CHCl_3$ (10 mL) and washed with 1 M HCl (20 mL) and water (20 mL), respectively. The aqueous phase was extracted with $CHCl_3$ (3×20 mL). The combined organic extracts were dried over $MgSO_4$ and the solvent was removed. Crystallization from EtOAc-hexane (3:1) yielded (*S*)-**2** as a white powder (1.0 g, 80%). ^{1}H-NMR (400 MHz, $CDCl_3$): δ 8.37 ppm (s, 3H, Ar*H*), 6.64 (quasi t, 3H, ArCO*NH*CHD$(CH_2)_6CH_3$), 3.44 (t, *J* = 6.2 Hz, 6H, -NHC*H*$_2$CHD$(CH_2)_6CH_3$), 1.58 (qui, *J* = 6.2 Hz, 3H, -NHCH$_2$C*H*D$(CH_2)_6CH_3$), 1.30 (m, 36H, -NHCH$_2$CHD$(CH_2)_6CH_3$), 0.87 (t, *J* = 7.0 Hz, 9H, -NHCH$_2$CHD$(CH_2)_6$C*H*$_3$). FT-IR: ν = 3252 (w), 3077 (w), 2926 (m), 2856 (m), 2246 (w), 1641 (m), 1556 (m), 1457 (w), 1296 (w), 1220 (m), 906 (s), 772 (s), 733 (s). MALDI-TOF-MS: calculated for $C_{36}H_{60}D_3N_3O_3$ 588.51, observed $C_{36}H_{60}D_3N_3O_3$ 588.36.

2.9 Appendix

2.9.1 Deconvoluted ^{1}H-NMR spectra of MTPA esters and amides

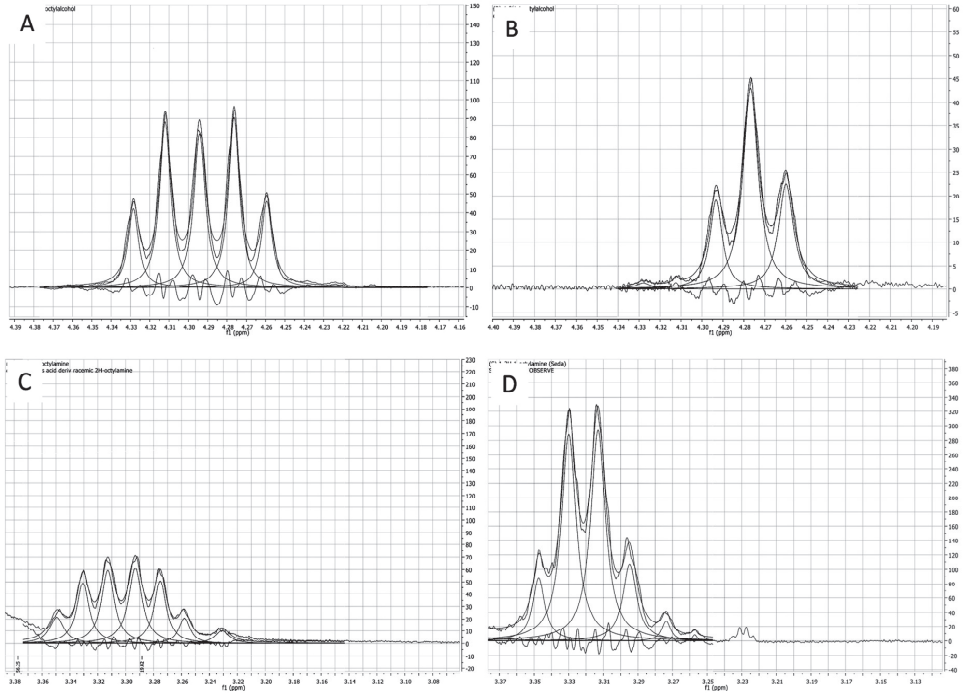

Figure A2.1: Deconvoluted ^{1}H-NMR spectra of MTPA A) ester of (*rac*)-**13**. B) ester of (*R*)-**3**. C) amide of (*rac*)-**14**. D) amide of (*S*)-**4**.

2.9.2 Statistical analysis of the *e.e.*

Statistical analysis of the *e.e.*'s was performed to verify the upper and lower values considering the uncertainty of the ^{1}H-NMR signals. To verify the variation, the following formula was used;

$$e.e. = \frac{a-b}{a+b}\left(1+\frac{a\delta-b\varepsilon}{a-b}-\frac{a\delta+b\varepsilon}{a+b}\right) \qquad (2.1)$$

In equation 2.1, the following parameters have been used:

a: intensity of major peak
b: intensity of minor peak
δ: error for intensity a
ε: error for intensity b

Based on the-NMR theory, the intensity of the ^{1}H-NMR signals possess an uncertainty of 10%. The *e.e.* is calculated with the use of δ = 0 and ε = 0. The upper values correspond to δ = 0.1 and ε = 0.1. The lower value corresponds to δ = -0.1 and ε = -0.1.

Table A2.1. Statistical analysis of the *e.e.* values of corresponding chiral alcohols.

Alcohol[a]	*e.e.*	Upper *e.e.* value (10% error propagation)	Lower *e.e.* value (10% error propagation)
(*R*)-**3**	0.976	0.978	0.973
(*S*)-**3**	0.974	0.977	0.972
(*R*)-**3'**	0.976	0.979	0.974
(*S*)-**3'**	0.895	0.904	0.886

[a]All compounds are converted into their MTPA ester derivative.

Table A2.2. Statistical analysis of the *e.e.* values of corresponding chiral amines.

Amine[b]	*e.e.*	Upper *e.e.* value (10% error propagation)	Lower *e.e.* value (10% error propagation)
(*S*)-**4**	0.894	0.903	0.884
(*S*)-**4'**	0.901	0.910	0.892

[b]All compounds are converted into their MTPA amide derivative.

2.10 References

[1] E. V. Anslyn, D. A. Dougherty, in *Modern Physical Organic Chemistry* **2006**, University Science Books, 421.
[2] S. –I. Inoue, H. Takaya, K. Tani, S. Otsuka, T. Sato, R. Noyori, *J. Am. Chem. Soc.* **1990**, *112*, 4897.
[3] M. M. Green, J. L. White, P. Mirau, M. H. Scheinfeld, *Macromolecules* **2006**, *39*, 5971.
[4] K. R. Reddy, K. Tashiro, T. Sakura, N. Yamagushi, *Macromolecules* **2008**, *41*, 9807.
[5] S. Lifson, C. Andreola, N. C. Peterson, M. M. Green, *J. Am. Chem. Soc.* **1989**, *111*, 8850.
[6] S. Cantekin, D. W. R. Balkenende, M. M. J. Smulders, A. R. A. Palmans, E. W. Meijer, *Nature Chem.* **2011**, *3*, 42.
[7] S. Yamaguchi, H. S. Mosher, *J. Org. Chem.* **1973**, *38*, 1870.
[8] J. A. Dale, D. L. Dull, H. S. Mosher, *J. Org. Chem.* **1969**, *34*, 2543.

[9] J. A. Dale, H. S. Mosher, *J. Am. Chem. Soc.* **1973**, *95*, 512.
[10] E. J. Corey, O. J. Link, *Tetrahedron Lett.* **1989**, *30*, 6275.
[11] R. Noyori, I. Tomino, M. Yamada, M. Nishizawa, *J. Am. Chem. Soc.* **1984**, *106*, 6717.
[12] S. Inoue, H. Takaya, K. Tani, S. Otsuka, T. Sate, S. R. Noyori, *J. Am. Chem. Soc.* **1990**, *112*, 4897.
[13] M. M. Midland, S. Greer, A. Tramontano, S. A. Zderic, *J. Am. Chem. Soc.* **1979**, *101*, 2352.
[14] C. W. Bradshaw, J. J. Lalonde, C. Wong, *Appl. Biochem Biotech.* **1992**, *33*, 15.
[15] C. J. Duxbury, I. Hilker, S. M. A. de Wildeman, A. Heise, *Angew. Chem. Int. Ed.* **2007**, *46*, 8452.
[16] J. H. Boyer, *J. Am. Chem. Soc.* **1951**, *73*, 5865.
[17] D. B. Dess, J. C. Martin, *J. Org. Chem.* **1983**, *48*, 4155.
[18] D. B. Dess, J. C. Martin, *J. Am. Chem. Soc.* **1991**, *113*, 7277.
[19] M. Lei, R. J. Hu, Y. G. Wang, *Tetrahedron* **2006**, *62*, 8928.

3

THE EFFECT OF ISOTOPIC SUBSTITUTION ON THE CHIRALITY OF SELF-ASSEMBLED HELICES

Abstract. *N*,*N*',*N*''-Trialkylbenzene-1,3,5-tricarboxamides (BTAs) self-assemble *via* strong, threefold intermolecular hydrogen bonding into well-defined, helical, 1D columnar aggregates. When a stereogenic centre is introduced into the alkyl side chains of these BTAs, strong Cotton effects are observed in dilute apolar solutions indicating the preference of one helical conformation over the other. This chapter describes the formation of a helical sense preference in self-assembled BTAs by introducing H/D isotope chirality into the alkyl side chains. The relative stabilities of the right- and left-handed helical conformations of these supramolecular polymers are determined by conformational analysis. The result of H/D substitution in BTA-based supramolecular polymers and helical polyisocyanates proves to be highly similar, although the formation mechanisms of the two are different. Furthermore, the effect of the deuterium position on the helical sense preference of BTA aggregates is investigated. The expression of supramolecular chirality decreases significantly when deuterium is placed further from the carboxamide.

Part of this work has been published:

S. Cantekin, D. W. R. Balkenende, M. M. J. Smulders, A. R. A. Palmans, E. W. Meijer, *Nature Chem.* **2011**, *3*, 42.
S. Cantekin, A. R. A. Palmans, *Chemistry Today* **2011**, *29*, 4.

3.1 Introduction

Polymers with the ability to adopt a helical conformation provide valuable insights into cooperative processes and amplification of chirality in macromolecules.[1] Pioneering studies by Green and coworkers on the amplification of chirality in polyisocyanates —a class of dynamic, helical polymers— have led to the discovery that only minute amounts of a chiral seed compound suffice to bias the helical sense and render the polymer homochiral.[2] Green's observation that a preferred helicity in the polymer conformation can be induced solely due to the presence of a deuterium (D) isotope in the monomeric unit represents a milestone in this area.[3] These remarkable findings on amplification of chirality in polyisocyanates have inspired many research groups. Nowadays, amplification of chirality in helical polymers such as poly(phenylacetylene)s, polyisocyanides, polysilanes and polyisocyanates has received extensive attention, both experimentally and theoretically.[4-6] Moreover, the transfer of chiral information through noncovalent interactions to helical polymers by a so-called memory effect is also well-documented.[7] More recently, the interest in these phenomena has been extended to supramolecular chemistry.[8] It appeared that in small molecules, a subtle interplay of noncovalent interactions such as hydrogen bonding, π-π stacking and hydrophobic interactions is sufficient to observe amplification of chirality.

N,*N*',*N*''-Trialkylbenzene-1,3,5-tricarboxamides (BTAs) are simple, easily accessible small organic compounds that self-assemble *via* strong, threefold intermolecular hydrogen bonding into well-defined, helical 1D columnar aggregates.[9] In dilute apolar solutions, strong Cotton effects are observed when a stereogenic centre is introduced into the alkyl side chains.[10,11] Amplification of chirality in these dynamic supramolecular polymers[12-15] is remarkably similar to that observed in helical polyisocyanates. The preference of one helical conformation over the other was confirmed by temperature dependent circular dichroism (CD) spectroscopy as well as vibrational CD (VCD)[16] spectroscopy in dilute apolar solutions. It was shown that helical aggregates of BTAs are formed *via* a cooperative mechanism where a nucleation phase is followed by a more favorable elongation phase, and these phases are separated by a critical temperature of elongation (T_e).[11] The experimental data were modeled which allowed the scope and limitations of the amplification of chirality in this supramolecular array to be predicted.[14,15]

It is, however, important to understand how the limits of the chiral amplification mechanism in the supramolecular system compare to a covalent helical polymer considering the widely divergent mechanisms for the formation of the two helical arrays. We make this comparison using H/D substitution as the source of minute chiral information in BTA-based supramolecular polymers. The α-deuterated BTAs (*S*)-**1** and (*R*)-**1**[*] (Figure 3.1) comprise a

[*] Although the molecules have three stereocentra, instead of naming them (*SSS*) and (*RRR*), (*S*) and (*R*) were used for simplicity.

deuterium substitution on the methylene groups adjacent to the amide group. The syntheses of these deuterated compounds are described in the previous chapter.[17] Chiral amine (*S*)-**4′** (*e.e.* ≈ 90%) was used for the synthesis of (*S*)-**1**, ultimately giving rise to the formation of the deuterated BTA (*S*)-**1** with a diastereomeric ratio (*d.r.*) of 86%[†]. Conformational analysis of the resulting supramolecular polymers employing temperature-dependent UV-vis and CD spectroscopy allows quantitative comparison between the different chiral amplification mechanisms in covalent and supramolecular polymers. In spite of the mechanistic differences between BTA-based supramolecular polymers and helical polyisocyanates, the result of H/D substitution is highly similar.

Furthermore, we investigated the effect of the deuterium position on the supramolecular chirality by analyzing the β-deuterated BTA-based supramolecular polymers formed by ((*S*)-**2**) in solution (Figure 3.1).

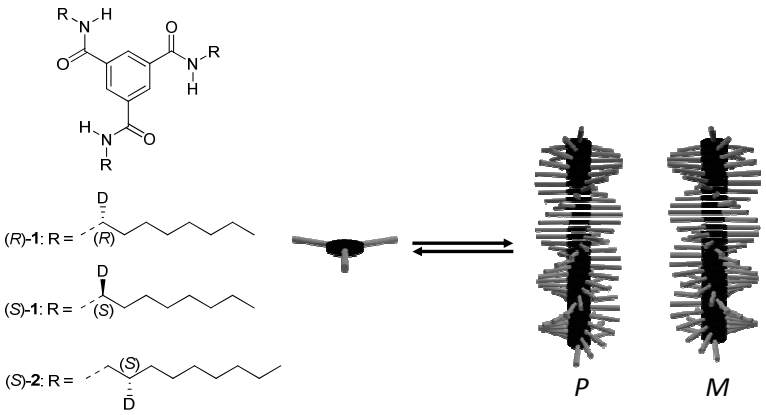

Figure 3.1 Left: Structures of the (*R*)- and (*S*)-α-deuterated and (*S*)-β-deuterated benzene-1,3,5-tricarboxamides. Right: Schematic representation of the deuterated BTA-based supramolecular polymers.

3.2 Self-assembly behavior of (*S*)-α-deuterated benzene-1,3,5-tricarboxamide

The self-assembly of (*S*)-α-deuterated benzene-1,3,5-tricarboxamide (*S*)-**1** was studied by temperature-dependent UV-vis and CD spectroscopy in dilute dodecane solution (c = 5×10^{-5} M). The UV-vis spectrum of (*S*)-**1** at 90 °C shows a λ_{max} = 209 nm and a blue shift upon cooling (Figure 3.2A). This hypsochromic shift is typical for BTA self-assembly in dilute solutions[10,11] and confirms the presence of aggregates at 20 °C. Remarkably, CD spectroscopy shows a significant, negative Cotton effect at λ_{max} = 223 nm at 20 °C (Figure 3.2B). The

[†] There are four possible diastereomers of α-deuterated-BTA such as (*SSS*), (*RRR*). (*SRS*). (*RSR*), the diastereomeric ratio of which is 85.8%, 0.013%, 13.5%, 0.73%, respectively.

spectroscopic data of (*S*)-**1** are consistent with those of various chiral methyl-substituted BTAs and indicate the presence of the supramolecular polymers in solution with a bias towards one helical conformation.[9,11] The negative sign of the Cotton effect suggests that preferably left-handed helical superstructures (*M*) are formed in dodecane.[16] While the shape and the sign of the CD spectrum of (*S*)-**1** are similar to that of (*S*)-methyl substituted-BTA ((*S*)-**3**)[9] (Figure 3.3A), the value for molar ellipticity ($\Delta\varepsilon$ = –16 L mol^{-1} cm^{-1} at 223 nm where $\Delta\varepsilon$ = CD effect/32980 c *l*, c is the concentration in mol L^{-1} and *l* is the pathlength in cm) is approximately three times lower than that of (*S*)-**3** ($\Delta\varepsilon$ = –42 L mol^{-1} cm^{-1} at 223 nm). Previous detailed studies showed that a value of $\Delta\varepsilon$ = –42 L mol^{-1} cm^{-1} indicates complete aggregation into helical stacks of *M* helicity, in which the observed net helicity (i.e., the difference between left- (*M*) and right-handed (*P*) helical aggregates) is equal to 1.[11] The lower value of $\Delta\varepsilon$ observed for (*S*)-**1** presumably arises from a net helicity lower than 1, suggesting that both helical superstructures, *P* and *M*, coexist in dodecane with a preference for *M*. Since $\Delta\varepsilon$ = –42 L mol^{-1} cm^{-1} corresponds to a net helicity of 1, the net helicity of (*S*)-**1** with a $\Delta\varepsilon$ of –16 L mol^{-1} cm^{-1} can be calculated to be 0.38. This corresponds to a diastereomeric excess, *d.e.* = (100×[*M*]–[*P*])/([*M*]+[*P*]), of 38%, where the diastereomeric ratio of *M* helices is equal to 69% and that of *P* is 31%. Different diastereomeric ratios of *P* and *M* result from different free energies (or stabilities) of the two diastereomeric states. (Figure 3.2C).

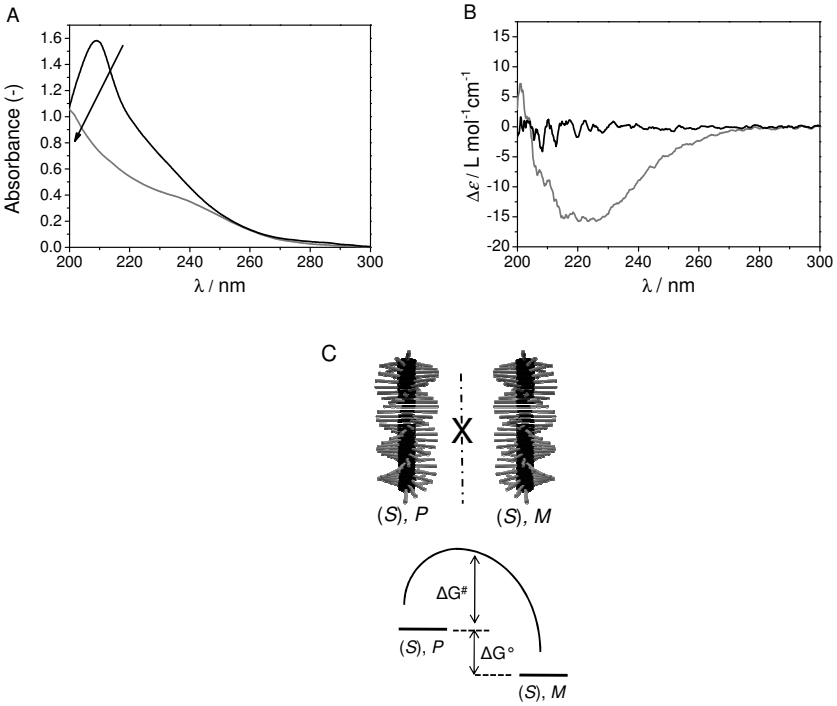

Figure 3.2: A) UV–vis spectrum, B) CD spectrum at 20 °C (gray) and 90 °C (black), of (*S*)-**1**, c = 5×10^{-5} M in dodecane. C) Schematic representation of diastereomeric self-assemblies of (*S*)-**1** and the difference in stabilities of the self-assemblies.

3.3 Chiral amplification in α-deuterated BTAs

"Sergeants-and-soldiers" (SaS) experiments were performed in order to verify the presence of the two supramolecular polymer types, *P* and *M*, with a *d.e.* of 38% favoring *M*. Furthermore, the aim was to amplify the chirality in self-assembled (*S*)-**1**, causing the net helicity to increase to 1. In an SaS experiment, the helicity of large numbers of cooperative achiral units (the soldiers) can be controlled by a few chiral units (the sergeants).[12,18] Here, the chiral (*S*)-α-deuterated benzene-1,3,5-tricarboxamide ((*S*)-**1**) represents the "soldiers", while the chiral methyl-substituted BTAs ((*R*)-**3** or (*S*)-**3**) act as the "sergeants" (Figure 3.3A). Different than in a typical SaS experiment where the soldier has no CD effect, (*S*)-**1** shows an initial $\Delta\varepsilon$ value. Solutions of (*S*)-**1** and (*S*)-**3** in dodecane were mixed in different ratios while keeping the total BTA concentration constant at c = 5×10^{-5} M. An analogous experiment was also performed by mixing the solutions of (*S*)-**1** and (*R*)-**3**. The bottom part of the Figure 3.3B shows that only 4% of (*S*)-**3** suffices to nearly quantitatively bias the helical sense to *M*, as the $\Delta\varepsilon$ reaches a value of –42 L mol^{-1} cm^{-1}. In contrast, 10% (*R*)-**3** is required to dictate the helical

sense towards *P* as shown in the top part of the Figure 3.3B. This result indicates that the preferred helicity of the supramolecular polymers formed by (*S*)-**1** is in accordance with that of (*S*)-**3**, which is, *M*.

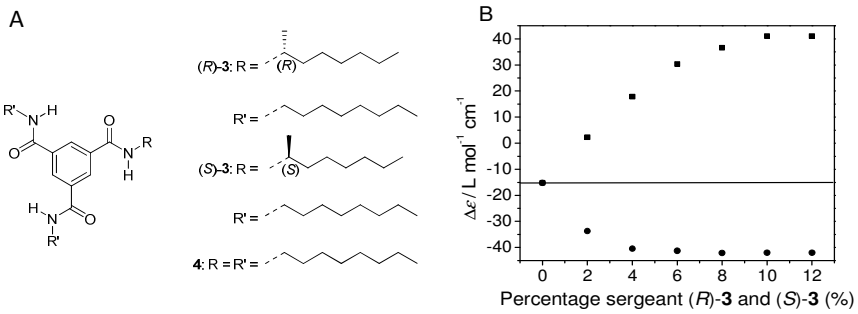

Figure 3.3: A) Structures of (*R*)- and (*S*)-methyl-substituted and achiral benzene-1,3,5-tricarboxamide. B) Sergeants-and-soldiers experiment at 20 °C, c = 5×10^{-5} M in dodecane. Dot: Change in $\Delta\varepsilon$ at λ = 223 nm upon mixing the solutions of (*S*)-**1** and (*S*)-**3**. Square: Change in $\Delta\varepsilon$ at λ = 223 nm upon mixing the solutions of (*S*)-**1** and (*R*)-**3**.

"Majority rules"[19] experiments are tremendously valuable because they give access to quantitative data regarding amplification of chirality processes.[13,15,20] The data extracted from majority rules experiments by using the model developed by van Gestel[20] can be described in terms of two (free) energy penalties i.e., the helix reversal penalty (*HRP*) that reflects the barrier to helix reversal within a stack and the mismatch penalty (*MMP*) which represents a mismatch energy when a chiral monomer is introduced into a stack of its unpreferred helicity. In the majority rules experiment, the major enantiomer dictates the dominant helical preference, ultimately forcing the minor enantiomer to adjust in spite of the apparent energetic penalty. Majority rules experiments were performed by mixing the solutions of the two enantiomers, (*S*)-**1** and (*R*)-**1** in different ratios. Mirror image CD spectra indicate that enantiomeric forms of deuterated BTAs have a bias for helical aggregates with opposite handedness (Figure 3.4A). The CD effect at λ = 223 nm of scalemic mixtures of the two enantiomers was evaluated as a function of the enantiomeric excess (*e.e.*), which revealed a linear relationship (Figure 3.4B). This result is in sharp contrast to chiral methyl-substituted BTAs, which typically exhibit a strong nonlinear relationship between the CD effect and the *e.e.* However, a linear relationship was anticipated for BTAs having very small *MMP*s or with very high *HRP*s.[15]

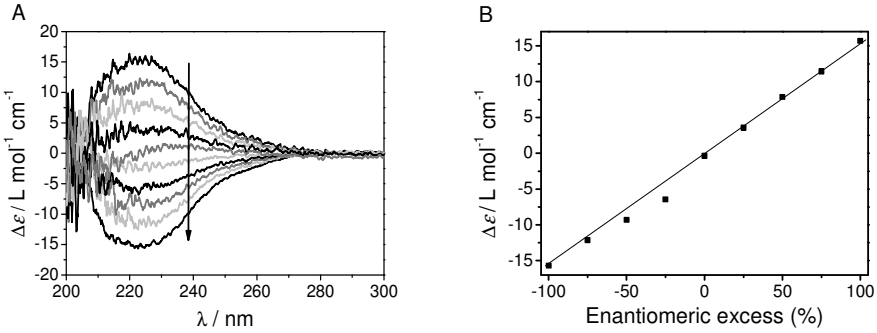

Figure 3.4: Majority rules experiment at 20 °C, c = 5×10^{-5} M in dodecane. A) CD spectra of scalemic mixtures of (*S*)-**1** and (*R*)-**1**. Arrow indicates increasing amount of (*S*)-**1**, starting with pure (*R*)-**1** and ending with pure (*S*)-**1**. B) $\Delta\varepsilon$ at 223 nm as a function of *e.e.* obtained from mixing the solutions of (*S*)-**1** and (*R*)-**1**. The line is to guide the eye.

Assuming that the H/D substitution would result in a relatively small *MMP*, a simulation was conducted to anticipate the net helicity as a function of *e.e.* for low *MMP* values. Therefore, the *MMP* was set as a variable and ranged from 0 to 60 J mol^{-1} while keeping *HRP* constant at 12 kJ mol^{-1}. This value was previously deduced from experimental data for methyl-substituted BTAs.[15] According to Figure 3.5A, a linear dependence of the CD effect on *e.e.* requires values for the *MMP* lower than 30 J mol^{-1}. This value is approximately 30-60 times smaller than the values for *MMP* typically determined for methyl-substituted BTAs which lie in the range of 1–2 kJ mol^{-1}.[15] For a net helicity of 0.38, the *MMP* can be estimated to be 15 J mol^{-1} for deuterated BTAs (Figure 3.5B). As a consequence of this low *MMP* value, deuterated BTA-based supramolecular polymers never reach a state at room temperature in which only *P* or *M* helical structures are formed.

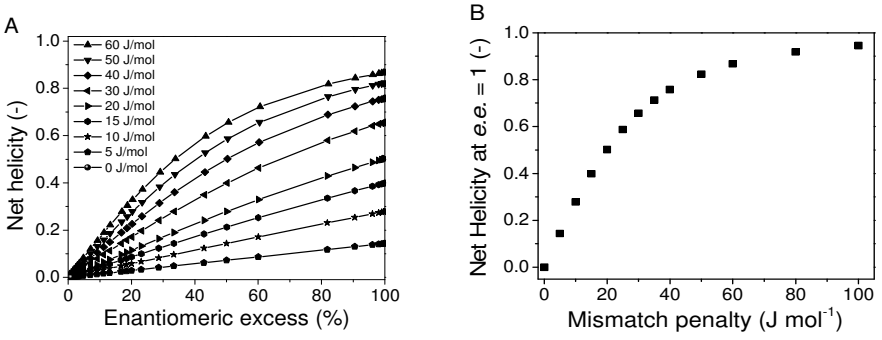

Figure 3.5: A) Simulated net helicity as a function of the *e.e.* for different *MMP* values between 0–60 J mol^{-1} assuming *HRP* = 12 kJ mol^{-1}. B) Simulated net helicity at *e.e.* = 1 as a function of the *MMP* with *HRP* constant at 12 kJ mol^{-1}.

The low *MMP* values also result in diminished directing effects when performing regular SaS experiments with achiral BTA (**4**) and (*S*)-**1**. Applying values of 5–30 J mol^{-1} for the *MMP* and 12 kJ mol^{-1} for the *HRP* to the SaS model results in a nearly linear dependence between the net helicity and the fraction of the sergeant added (Figure 3.6A). Titrating **4** with a solution of (*S*)-**1** in heptane revealed a linear dependence between the CD effect and the fraction of chiral sergeant (Figure 3.6B). This corroborates the low *MMP* value found in the *MR* experiment and suggests that (*S*)-**1** is unable to bias the helical sense in supramolecular polymers of **4**.

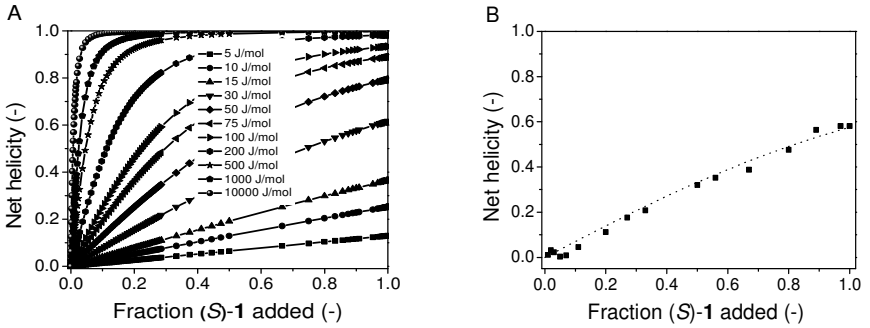

Figure 3.6: A) Simulated net helicity for the "Sergeants-and-Soldiers" experiment as a function of the chiral sergeant fraction; *MMP*s varying from 5 J mol^{-1} to 10 kJ mol^{-1} with *HRP* constant at 12 kJ mol^{-1}. B) Net helicity as a function of the fraction of (*S*)-**1** (sergeant) added. to achiral **4** (soldier) at 20 °C, c = 4.3×10^{-5} M in heptane. The dotted line is the predicted curve for *MMP* = 30 J mol^{-1} and *HRP* = 12 kJ mol^{-1}.

3.4 Conformational analysis of α-deuterated BTA-based supramolecular polymers

The low value of the $\Delta\varepsilon$ for (*S*)-**1** in dodecane at room temperature reveals that *P* and *M* type supramolecular polymers are formed simultaneously, albeit in different ratios. Temperature-dependent CD and UV-vis spectroscopy were performed in order to elucidate the formation mechanism of deuterated BTA-based supramolecular polymers and to gather the quantitative information on the stability difference between the two helical states (i.e., to determine the $\Delta G°$). The intensity of the CD and UV-vis signal at 223 nm was monitored as a function of temperature in dodecane (c = 5×10^{-5} M). A low cooling rate (1 K min^{-1}) was employed to ensure that the self-assembly process is under thermodynamic control. Performing both measurements simultaneously allows a comparison between the CD signal and the UV-vis absorption, which are related to the net helicity and the degree of aggregation, respectively.[11] The UV-vis cooling curve of (*S*)-deuterated BTA ((*S*)-**1**) shows a

sharp transition at a temperature around 353 K and its shape is typical for a cooperative supramolecular polymerization process, as observed in chiral methyl-substituted and achiral BTAs[11] (Figure 3.7A). By applying the nucleation-growth model developed by van der Schoot[21] on the normalized UV-vis cooling curve, the elongation temperature (T_e) and the enthalpy release upon elongation (h_e) were determined to be 353.0 K and –52.0 kJ mol^{-1}, respectively. This model also enables the determination of the degree of cooperativity, expressed by the monomer activation constant K_a, as 1.1×10^{-4}. The thermodynamic parameters derived for (*S*)-**1** are in good agreement with those of achiral BTA (**4**) measured under identical conditions (T_e = 354.0 K, h_e = –56.0 kJ mol^{-1}, K_a = 2.2×10^{-4}). Based on these parameters, the temperature dependence of the number-average degree of polymerization, $<N_n>$[11] was calculated as a function of temperature (Figure 3.7B). At 20 °C, the average number of molecules in the stacks was estimated to be 430 for self-assembled (*S*)-**1**.

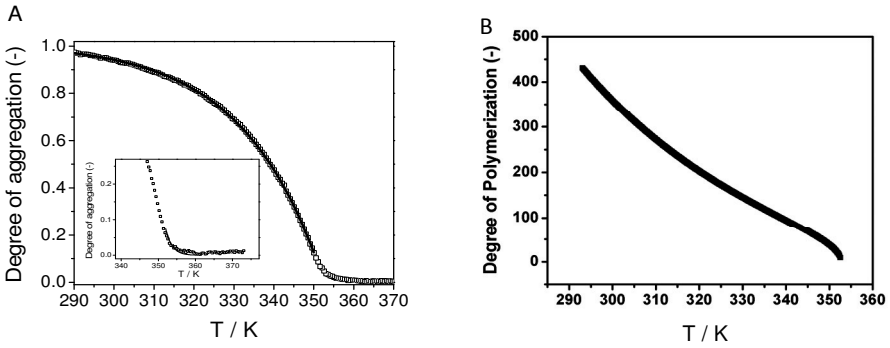

Figure 3.7: A) Normalized UV-vis absorption spectrum as a function of temperature monitored at λ = 223 nm at a cooling rate of 1 K min^{-1} for (*S*)-**1**, c = 5×10^{-5} M in dodecane, with the corresponding fit for the elongation (gray line) and nucleation regime (inset, gray line). B) The average number of molecules in a stack as a function of temperature for (*S*)-**1**, c = 5×10^{-5} M in dodecane, based on the Figure 3.7A.

In contrast to the UV-vis cooling curve, the CD cooling curve of (*S*)-**1** shows a seemingly linear dependence of the CD effect on temperature, lacking the characteristic sharp transition around T_e but with an increase in CD effect starting at around 349 K (Figure 3.8). Hence for (*S*)-**1**, aggregation and preferential formation of one helical sense are not occurring simultaneously.‡ This observation is in sharp contrast to chiral methyl-substituted BTAs, where CD and UV-vis curves are superimposable; suggesting that the aggregation and the formation of one preferred helical sense are intimately coupled.[11]

‡ The same cooling curves were obtained when different cooling rates were applied.

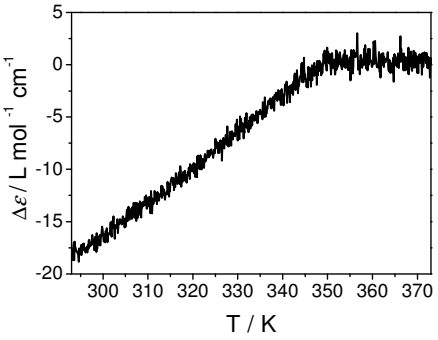

Figure 3.8: $\Delta\varepsilon$ (= CD maximum at 223 nm (mdeg)/32980·c·l where c = concentration in mol L^{-1} (M) and l = path length in cm) as a function of temperature monitored at λ = 223 nm at a cooling rate of 1 K min^{-1} for (*S*)-**1**, c = 5×10^{-5} M in dodecane.

A conformational analysis was performed in order to rationalize that aggregation and preferential formation of one helical sense are not coupled in the supramolecular polymerization of (*S*)-**1**. The supramolecular polymerization of (*S*)-**1** starts at T_e upon cooling, and the two equilibria (i.e., formation of *P* and formation of *M* from (*S*) monomers) occur simultaneously. As shown in Figure 3.9, equilibrium is established between monomers and *P* stacks, and between monomers and *M* stacks. For (*S*)-**1**, the formation of *M* stacks from monomers is slightly more favorable than that of *P* stacks. As a result, the expression of supramolecular chirality can be indeed expected to be less preferred (hence giving rise to an almost linear curve) than aggregation (which gives an exponential curve). Since the system is under thermodynamic control, the product distribution is a function of the stabilities ($G°$) of *P* and *M* (equation 3.1). The equilibrium constant *K* is determined from the ratio of the concentrations of *P* and *M* (equation 3.2) and, therefore, is a function of the disparity in Gibbs free energies ($\Delta G°$).

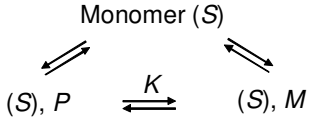

Figure 3.9: The equilibrium between monomers and helical aggregates of (*S*)-**1**.

$$\ln\left(\frac{[M]}{[P]}\right) = \ln K = -\frac{\Delta G°}{RT} \tag{3.1}$$

$$K = \frac{[M]}{[P]} = \frac{1+d.e.}{1-d.e.} \tag{3.2}$$

The relative ratios of *P* and *M* reach a constant value at 20 °C. Theoretically, one can expect that the shift in equilibrium results in the formation of only *M* helical conformers at low enough temperature.

The relative ratios of *P* and *M* during (*S*)-**1** self-assembly were quantified by combining the degree of aggregation based on the UV-vis data and the $\Delta\varepsilon$ for a homochiral stack of 42 L mol^{-1} cm^{-1}, thus creating a theoretical CD cooling curve for a homochiral system for (*S*)-**1,** where *d.e.* is 100% at each temperature. The temperature dependent degree of aggregation based on UV data for (*S*)-**1** (in dodecane, c = 5×10^{-5} M) was multiplied by the $\Delta\varepsilon$ value obtained for methyl-substituted BTAs in dodecane ($\Delta\varepsilon$ = –42 L mol^{-1} cm^{-1}) to obtain the temperature dependent (theoretical) $\Delta\varepsilon$ value corresponding to a fully homochiral supramolecular polymer of (*S*)-**1** (i.e., 100% *M* helicity). Based on this curve and the experimental CD cooling curve (Figure 3.10A), the *d.e.* was calculated at each temperature by dividing the $\Delta\varepsilon$ value of (*S*)-**1** by the theoretical CD curve. Thus;

$$d.e.\ (T) = \frac{\Delta\varepsilon(T)}{\Delta\varepsilon_{theoretical}(T)} \tag{3.3}$$

d.e. is defined as;

$$d.e. = \frac{[M]-[P]}{[M]+[P]} \tag{3.4}$$

where, $[M]+[P]=1$ and $[M]=\frac{1+d.e.}{2}$ (3.5)

Figure 3.10B shows the relative ratios of *P* and *M* and variation of *d.e.* as a function of temperature. From these data, we obtained the equilibrium constant (*K*) which corresponds to an energy difference ($\Delta G°$) of 2.1 kJ mol^{-1} between the two diastereomerically related supramolecular polymers (*P* and *M*), at 20 °C. Taking into account the average stack length of 430 monomers[11] at this temperature, this energy value is in the order of 4.9 J mol^{-1} per monomeric unit, indicating the preference of a stereoselectively deuterated BTA residing in either *P* or *M* type supramolecular polymer. The magnitude of this energy is in the same order with that of the *MMP* determined from the *MR* experiment (*vide supra*). Although the magnitude of this energy difference is relatively small, the chirality inducing isotope substitution is capable of favoring one helical sense over the other, owing to the cooperative nature of the self-assembly process.

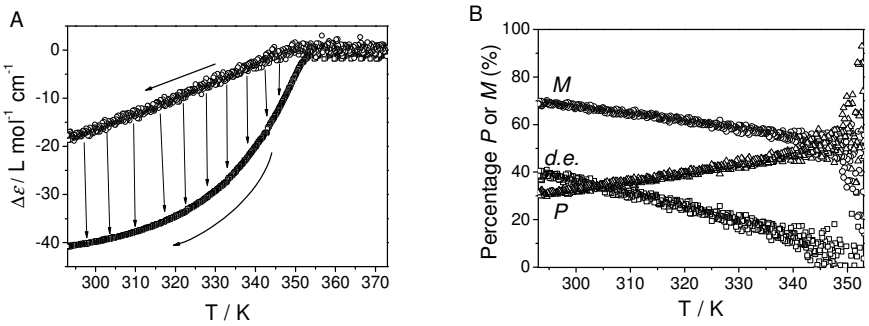

Figure 3.10: A) The overlay of the Figure 3.8 (circle) and the theoretical curve of $\Delta\varepsilon$ (square) as a function of temperature. B) Relative ratios of the *P* (triangle) and *M* (circle) type supramolecular polymers and *d.e.* (square) as a function of temperature.

3.5 Comparison to a helical covalent polymer

The results described above for a deuterated supramolecular polymer show a strong similarity to the results previously reported for poly((*R*)-2-deuterio-*n*-hexylisocyanate (Figure 3.11A).[22,23] The cooperative behavior of these deuterated polyisocyanates has been described by two critical energy parameters, namely the energy of a helical reversal (G_r), being analogous to the *HRP* parameter discussed here, and the energy parameter resulting from a stereospecifically deuterated monomer favoring one helical sense over the other (per unit) (G_h), which can be related to the *MMP* parameter. The values of G_r and G_h are approximately 16.70 kJ mol^{-1} and 4.18 J mol^{-1} (per unit), respectively, as reported previously.[23] Considering these energy values and comparing the covalent and supramolecular systems, it can be concluded that in both systems, due to the high cooperativity (expressed by the high penalty for a helical reversal), the chiral isotope substitution can result in the formation of helical structures with preferred handedness. We further analyzed the data for deuterated polyisocyanates. Based on the previously published data[24], we calculated the net helicity as a function of temperature for poly((*R*)-2-deuterio-*n*-hexylisocyanate) in hexane, where $[\alpha]_{max}$ = 7420×10^{-1} deg cm^2 g^{-1}. We determined the optical rotation $[\alpha]_{300}$ for the polymer with a N_W of 5500 from Figure 5 in ref. 24 and divided it by $[\alpha]_{max}$ (= 7420×10^{-1} deg cm^2 g^{-1}) to obtain the *d.e.* values (Figure 3.11B). The plot of *d.e.* as a function of temperature revealed that the *d.e.* is equal to 43% at 20 °C in hexane for deuterated polyisocyanates which is in the same order as the value reported here for the (*S*)-α-deuterated BTA ((*S*)-**1**). The close similarity of the *d.e.* values is coincidental since the position and the number of deuterium atoms in the repeat unit of the polymers is different in both cases.

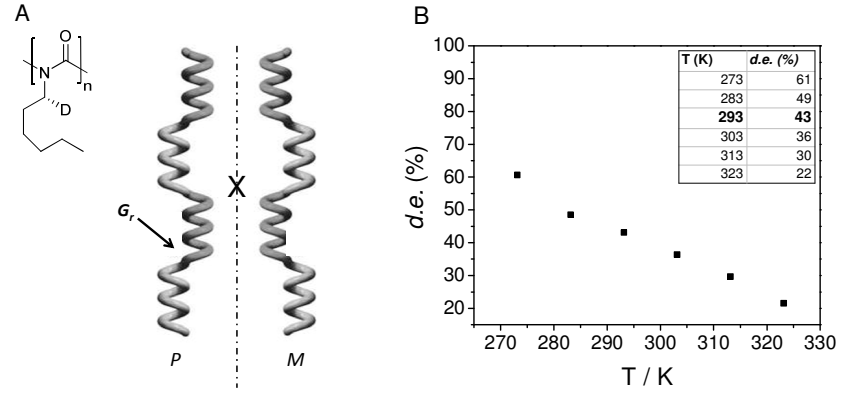

Figure 3.11: A) Structure of poly((*R*)-2-deuterio-*n*-hexylisocyanate and the schematic representation for the helical covalent polymer formed with the helical reversals. B) *d.e.* as a function of temperature for poly((*R*)-2-deuterio-*n*-hexylisocyanate) (N_w = 5500).

Furthermore, the free energy difference between the conformations of deuterated BTA monomers in the self-assembled state may be analogous to that of conformations of cyclohexane molecule at ambient temperature. Mono-deuterium substitution on equatorial or axial position in a cyclohexane ring results in a Gibbs free energy difference, $\Delta G° \approx 1.6$ J mol^{-1} which is in the same order as the $\Delta G°$ obtained for the stabilities of *P* and *M*.[25] These results suggest that the conformational behavior of supramolecular polymers are comparable to those of covalent polymers as well as to small organic molecules.

3.6 Self-assembly behavior of (*S*)-β-deuterated benzene-1,3,5-tricarboxamide

The effect of the position of the stereogenic center in asymmetric BTAs was studied previously.[9] It was reported that the position of the methyl group on the alkyl side chains has a remarkable influence on the organization of the helical stacks in solution which is called the 'odd-even effect'. For instance, BTAs with (*R*)-methyl group on α– and γ– positions give rise to positive Cotton effect with the same shape whereas BTAs with (*R*)-methyl group on β– and δ– positions exhibit a negative Cotton effect with different shapes. The effect of deuterium position was investigated by analyzing the self-assembly behavior of β-deuterated BTAs ((*S*)-**2**)[26] under identical conditions by CD and UV-vis spectroscopy and the results were compared to that of α-deuterated BTAs.

The UV-vis spectrum of (*S*)-**2** in dodecane (c = 5×10^{-5} M) revealed a hypsochromic shift upon cooling from 90 °C to 20 °C. This characteristic hypsochromic shift observed in the UV-vis spectrum upon cooling is a good indication for the formation of H-type aggregates in dodecane at 20 °C and is comparable to that of (*S*)-**1**. The CD spectrum of (*S*)-**2** in dodecane at

20 °C resulted in a small and negative Cotton effect ($\Delta\varepsilon$ = −2.5 L mol^{-1} cm^{-1}), which is significantly smaller than that of α-deuterated BTAs ($\Delta\varepsilon$ = −16 L mol^{-1} cm^{-1}). This suggests that a change in position of the chiral center (i.e., from α- to β-) strongly influences the helical preference of the resulting supramolecular assemblies. The larger distance between the carboxamide and the chiral center in β-deuterated BTAs decreases the free energy difference between *P* and *M* stacks, thus a large helix sense preference is not observed and small Cotton effects are obtained. In addition to the deuterium position, the *e.e.* of the β-deuterated BTA may have an influence on the small Cotton effects observed. The *e.e.* value of the β-deuterated amine (that is used for the synthesis of β-deuterated BTA) was not determined; however, previous studies[24] using the same synthetic strategy for the synthesis of β-deuterated compounds revealed large optical activities (although the *e.e.* values of these compounds were not known) implying a strong helix sense preference. Furthermore, in Chapter 2 it was shown that the *e.e.* is preserved during the transformation of a tosylate into an amine *via* an S_N2 reaction. Therefore, the weak expression of supramolecular chirality in β-deuterated BTA-based supramolecular polymers is not the result of the low *e.e.* but the position of the chirality inducing deuterium atom. Finally, an 'odd-even effect' was not observed in deuterated BTA-based supramolecular polymers unlike the ones formed by methyl-substituted BTAs.

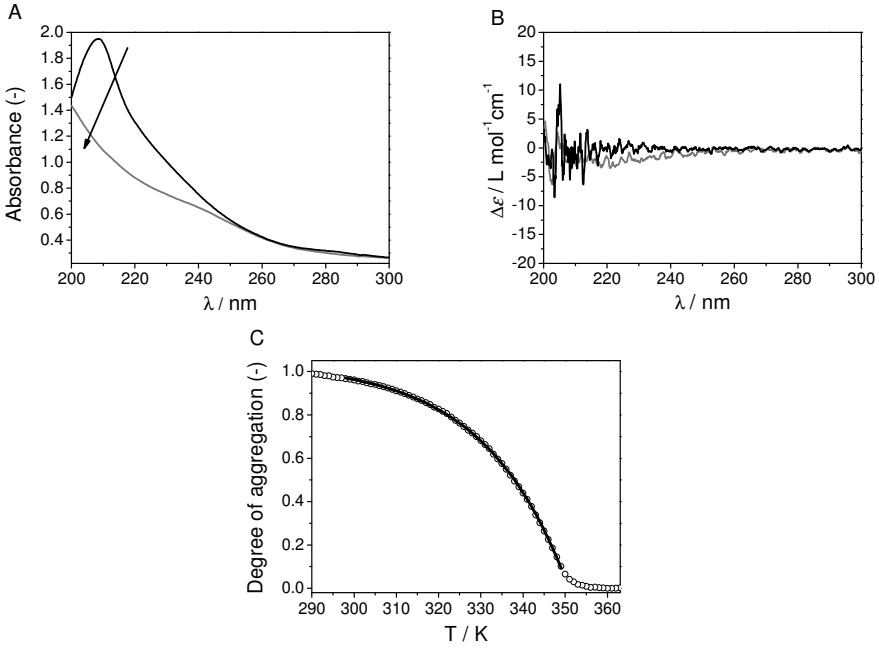

Figure 3.12: A) UV–vis spectrum, B) CD spectrum of (*S*)-**2** at 20 °C (gray) and 90 °C (black), c = 5×10^{-5} M in dodecane. C) The normalized UV–vis spectrum of (*S*)-**2** in dodecane (c = 5×10^{-5}

M) as a function of temperature monitored at λ = 223 nm at a cooling rate of 1 K min^{-1} with the corresponding fit (gray).

Furthermore, we analyzed the formation mechanism of β-deuterated BTA-based supramolecular polymers in dodecane by monitoring the UV-vis absorbance at λ = 223 nm as a function of temperature. As shown in Figure 3.12C, the self-assembly process follows a cooperative mechanism which is similar to that of α–deuterated BTAs. The thermodynamic parameters (T_e, h_e and K_a) determined for (*S*)-**2**-based supramolecular polymers by the nucleation-elongation growth model[11] (T_e = 351 K, h_e = -52 kJ mol^{-1}, K_a = 1.12×10^{-4}) revealed that the aggregation behavior of (*S*)-**1** (*vide supra*) and (*S*)-**2** are remarkably similar.

3.7 Conclusions

In summary, chirality arising from H/D isotope substitution in BTA-based supramolecular polymers results in a preference for one helical conformation. Quantitative analysis of the observed process demonstrates that the left- and right-handed helical supramolecular polymers are formed with only a small difference in stability upon cooling and the *d.e.* is 38% at room temperature. Despite the differences in the formation mechanisms of deuterated polyisocyanates and BTA-based supramolecular polymers, the energy difference between the left- and right-handed helices formed in the two systems is comparable. Furthermore, the position of the deuterium in the alkyl side chains was investigated. The chirality inducing deuterium group at the β position did not lead to a strong preference for one helical sense in the self-assembled state. Furthermore, no 'odd-even effect' was observed in the deuterated BTA self-assembly.

The difference between hydrogen and deuterium is apparently subtle; however, the minute stability difference between the diastereomeric supramolecular polymers formed by the deuterated monomers can be determined by using the properties of cooperative self-assembly.

3.8 Experimental

3.8.1 General

UV-vis and CD measurements were performed on a Jasco J-815 spectropolarimeter where the sensitivity, time constant and scan rate were chosen appropriately. Corresponding temperature dependent measurements were performed with a PFD-425S/15 Peltier-type temperature controller with a temperature range of 263-383 K and adjustable temperature slope. Linear dichroism was not observed in the experiments. Cells with an optical path

length of 1 cm and spectroscopic grade solvents were employed. Dodecane was obtained from Biosolve and heptane from Aldrich in spectroscopic grade (99+%) and used as received. Solutions were prepared by weighing in the required amount of compound for a given concentration, after which this amount was transferred to a volumetric flask (flasks of 5 mL were employed). Then, the flask was filled with the spectroscopic grade solvent and put in an oscillation bath at 40 °C for 20 min, after which the flask was allowed to cool down. Any loss of solvent was compensated for. The molar ellipticity was calculated from: $\Delta\varepsilon$ = CD effect/ (32980 c *l*) in which c is the concentration in mol L^{-1} and *l* is the optical path length in cm. For the majority rules experiment, enantiomeric excesses (*e.e.*) of the mixtures were calculated from the volumes of each identically concentrated stock solution of (*R*)- and (*S*)-deuterated BTA, assuming that each stock solution contains (*R*)- and (*S*)-deuterated BTA at an *e.e.* of 100%.

3.9 Appendix

3.9.1 'Majority rules' and 'Sergeants-and-Soldiers' simulations

The simulated 'sergeants and soldiers' curves were generated using a model developed by van der Schoot et al.[14]

The net helicity η is given by

$$\eta = \frac{z(1-\omega)}{\sqrt{z^2(1-\omega)^2 + 4\sigma(1+z)(1+z\omega)}} \tag{A3.1}$$

The fraction homochiral material *x* follows from

$$x = \frac{z\omega}{(1+z\omega)} + \frac{z(\eta+1)(1-\omega)}{2(1+z)(1+z\omega)} \tag{A3.2}$$

The simulated 'majority rules' curves were generated using the amplification model developed by van Gestel.[20] In this model, the net helicity, η, is given by:

$$\eta - \frac{(z-1)(1-\omega)}{\sqrt{\alpha}} \tag{A3.3}$$

While, the enantiomeric excess *x* is given by:

$$x = \frac{(z-1)(1+\omega)\sqrt{\alpha} + 4\omega\sigma(z^2-1) + (z^2-1)(1-\omega)^2}{[(z+1)(1+\omega) + \sqrt{\alpha}]\sqrt{\alpha}} \quad \text{(A3.4)}$$

In equations A3.1-A3.4 the following parameters have been used:

η: Net helicity

z: Excess fugacity of the homochiral component: a measure for its relative abundance in the solution

ω: Dimensionless mismatch penalty; $\omega = \exp[-MMP/RT]$

MMP: Mismatch penalty (in J mol^{-1})

R: Gas constant = 8.3145 J K^{-1} mol^{-1}

T: Temperature

σ: Dimensionless helix reversal penalty; $\sigma = \exp[-2HRP/RT]$

HRP: Helix reversal penalty (in J mol^{-1})

x: Enantiomeric excess (*e.e.*) or fraction of the homochiral material

α: $\alpha = (z\omega + 1 - \omega - z)^2 + 4\sigma(z\omega + 1)(\omega + z)$

Based on amplification studies on related benzene-1,3,5-tricarboxamide (BTA) derivatives, we found that the helix reversal penalty (*HRP*) (at room temperature) has a constant value of 12 kJ mol^{-1}.[14,15] Hence, for our simulations this value was selected for the *HRP* and was kept constant, while the *MMP* was varied. Using equations A3.1 and A3.2, the simulated 'sergeants and soldiers' curves were generated by plotting the net helicity η as a function of the fraction chiral compound added, x, for different values of the mismatch penalty (Figure 3.6A). Additionally, using equations A3.3 and A3.4, the simulated majority rules curves (Figure 3.5) were generated by plotting the net helicity η as a function of the enantiomeric excess, x, for different values of the mismatch penalty.

3.10 References

[1] M. M. Green, K. –S. Cheon, S. –Y. Yang, J. –W. Park, S. Swansburg, W. Liu, *Acc. Chem. Res*. **2001**, *34*, 672.

[2] M. M. Green J. –W. Park, T. Sato, A. Teramoto, S. Lifson, R. L. B. Selinger, J. V. Selinger, *Angew. Chem. Int. Ed.* **1999**, *38*, 3138.

[3] M. M. Green, C. Andreola, B. Muñoz, M. P. Reidy, *J. Am. Chem. Soc.* **1988**, *110*, 4063.

[4] A. Teramoto, *Progr. Polym. Sci*. **2001**, *26*, 667.

[5] F. Tanaka, *Macromolecules* **2004**, *37*, 605.

[6] E. Yashima, K. Maeda, H. Iida, Y. Furusho, K. Nagai, *Chem. Rev*. **2009**, *109*, 6102.

[7] E. Yashima, K. Maeda, Y. Okamoto, *Nature* **1999**, ***399***, 449.

[8] A. R. A. Palmans, E. W. Meijer, *Angew. Chem. Int. Ed*. **2007**, *46*, 8948.

[9] P. J. M. Stals, M. M. J. Smulders, R. Martìn-Rapùn, A. R. A. Palmans, E. W. Meijer, *Chem. Eur. J.* **2009**, *15*, 2071.

[10] L. Brunsveld, A. P. H. J. Schenning, M. A. C. Broeren, H. M. Janssen, J. A. J. M. Vekemans, E. W. Meijer, *Chem. Lett*. **2000**, 292.

[11] M. M. J. Smulders, A. P. H. J. Schenning, E. W. Meijer, *J. Am. Chem. Soc.* **2008**, *130*, 606.

[12] A. R. A. Palmans, J. A. J. M. Vekemans, E. E. Havinga, E. W. Meijer, *Angew. Chem. Int. Ed*. **1997**, *36*, 2648.
[13] J. van Gestel, A. R. A. Palmans, B. Titulaer, J. A. J. M. Vekemans, E. W. Meijer, *J. Am. Chem. Soc.* **2005**, *127*, 5490.
[14] M. M. J. Smulders, I. A. W. Filot, J. M. A. Leenders, P. van der Schoot, A. R. A. Palmans, A. P. H. J. Schenning, E. W. Meijer, *J. Am. Chem. Soc.* **2010**, *132*, 611.
[15] M. M. J. Smulders, P. J. M. Stals, T. Mes, T. F. E. Paffen, A. P. H. J. Schenning, A. R. A. Palmans, E. W. Meijer, E. W. *J. Am. Chem. Soc.* **2010**, *132*, 620.
[16] M. M. J. Smulders, T. Buffeteau, D. Cavagnat, M. Wolffs, A. P. H. J. Schenning, E. W. Meijer, E. W. *Chirality* **2008**, *28*, 1016.
[17] D. W. R. Balkenende, S. Cantekin, C. J. Duxbury, M. H. P. Van Genderen, E. W. Meijer, A. R. A. Palmans, *Synth. Commun.* **2012**, *42*, 563.
[18] M. M. Green, M. P. Reidy, *J. Am. Chem. Soc.* **1989**, *111*, 6452.
[19] M. M. Green, B. A. Garetz, B. Munoz, H. Chang, *J. Am. Chem. Soc.* **1995**, *117*, 4181.
[20] J. van Gestel, *Macromolecules* **2004**, *37*, 3894.
[21] P. Jonkheijm, P. van der Schoot, A. P. H. J. Schenning, E. W. Meijer, *Science*, **2006**, *313*, 80.
[22] M. M. Green, N. C. Peterson, T. Sato, A. Teramoto, R. Cook, S. A. Lifson, *Science* **1995**, *268*, 1860.
[23] K. –S. Cheon, M. M. Green, *J. Label. Compd. Radiopharm.* **2007**, *50*, 961.
[24] H. Gu, et al., *Macromolecules* **1995**, *28*, 1016.
[25] F. A. L. Anet, M. Kopelevich, *J. Am. Chem. Soc.* **1996**, *108*, 1355.
[26] The *e.e.* of the (*S*)-β–deuterated amine ((*S*)-**5**) which was used to obtain (*S*)-**2** could not be determined.

4

PROBING THE ROLE OF SOLVENT ON THE SELF-ASSEMBLY PROCESSES

Abstract. This chapter describes the use of a stereoselectively deuterated benzene-1,3,5-tricarboxamide molecule as a highly sensitive probe to highlight the role of the solvent structure in self-assembly processes. The experimental findings reveal that small changes in the solvent structure in combination with temperature effects lead to differences in the preferred helix sense and the conformation of the supramolecular polymer. Therefore, solvent plays an active role in the self-assembly processes, and can be used as a tool for controlling the secondary structure and the resulting properties of supramolecular aggregates.

Part of this work has been published:

S. Cantekin, Y. Nakano, J. C. Everts, P. van der Schoot, E.W. Meijer, A. R. A. Palmans, *Chem. Commun*. **2012**, *48*, 3803.

4.1 Introduction

The spontaneous self-assembly of molecules into well-defined aggregates in solution is the result of a subtle interplay of non-covalent interactions between molecules, and solvophobic effects among the molecules, aggregates and the solvent employed. The role of the temperature, concentration and the balance between different interactions on self-assembly processes is well-recognized. Theoretical models can accurately derive the thermodynamic parameters that characterize the self-assembly mechanism, by fitting the concentration and temperature-dependent spectroscopic data.[1,2] The effect of different solvents or solvent mixtures on the self-assembly processes is often rationalized in terms of the differences in polarity and dielectric constant.[3-11] Models that describe supramolecular self-assembly typically treat the solvent as a non-participating, effective continuum. However, the application of chiral, non-racemic solvents can lead to a helical sense preference in self-assembly processes of achiral small molecules, conjugated oligomers and polymers. This remarkable result highlights the active and important role of the solvent in these processes.[12-19] In addition, the small but pronounced effect of the alkane chain length in the solvent molecule on the thermodynamic parameters characterizing the self-assembly of *oligo*-phenylene vinylenes, further emphasizes that an organized layer of solvent molecules explicitly participates in the self-assembly.[20]

Recently, the self-assembly of methyl substituted asymmetric BTAs was studied in various alkane solvents with different chemical structures; *n*-heptane, isooctane, methylcyclohexane (MCH) and decaline as linear, branched, monocyclic and bicyclic aliphatic solvents, respectively.[21] BTA-based supramolecular polymers exhibited two types of helical packing depending on the solvent employed for the self-assembly process which resulted in the differently shaped CD spectra. CD and IR spectroscopy in combination with time-dependent density functional theory (TD-DFT) calculations revealed that differences in the amide dihedral angle, θ, with respect to the central benzene ring leads to the changes in the Cotton effects in the n-π* transition region and the carbonyl stretching pattern in the amide region.[21] A single Cotton effect spectrum arises from the n–π* transition for which the C=O groups are tilted around θ ≈ 45° with respect to the central benzene ring (conformation type 1, H1) while a double Cotton effect is observed for a dihedral angle of θ ≈ 35° (conformation type 2, H2). Moreover, the solvent identity influences the conformational preference.

In order to unravel the remarkable influence of the solvent structure on self-assembly, deuterated BTA molecule (*S*)-**1** was used. This molecule owes its chirality to the introduction of isotopes in the *α*-position of the alkyl side chains stereoselectively (Figure 4.1A). The extent to which the isotope substituent influences the supramolecular chirality proved to be sensitive to several variables, including temperature and solvent. The discussion in the previous chapter showed that a remarkably small energy barrier between the two states of a

single (*S*)-**1** molecule residing in either *P* or *M* type supramolecular polymer (= 4.9 J mol^{-1}) facilitates an easy exchange between these two diastereomerically related supramolecular polymers at room temperature. Here we show that (*S*)-**1** is a highly sensitive probe for investigating the effect of the structure of the alkane solvent in which the self-assembly occurs. Moreover, temperature variation leads to differences in the preferred helix sense and the carboxamide angles, which translates to different spatial relationships between adjacent monomers within the supramolecular polymers (Figure 4.1B, left). We propose that four possible equilibrium states exist for (*S*)-**1**. Furthermore, the preference for a certain state over the others is strongly dependent on the structure of the alkane solvent and the temperature (Figure 4.1B, right). The observed effects can be rationalized by the active participation of the linear alkanes within the self-assembled structures, ultimately inducing a transition within the helical supramolecular polymers.

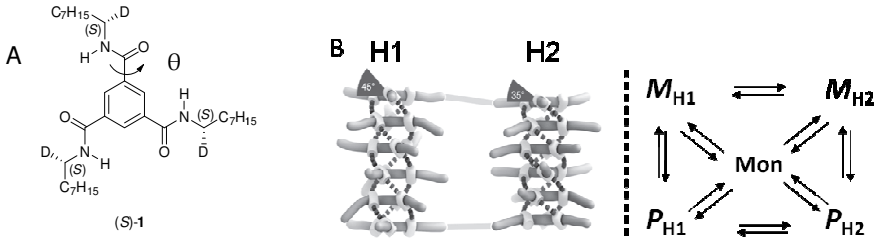

Figure 4.1: A) Structure of α–deuterated BTA and the dihedral angle, θ, between the benzene core and the amide. B) Left: Schematic representation of BTAs present in the two conformers, H1 and H2, both showing *M* type helicity. Right: Equilibrium between the four possible states of the (*S*)-**1** based-supramolecular polymers and the monomers in alkane solvents.

4.2 Self-assembly of α–deuterated BTA in heptane and methylcyclohexane

Two alkane solvents, heptane and methylcyclohexane (MCH) were selected to reveal the influence of solvent structure on self-assembly processes. These solvents have the same number of carbon atoms and have strikingly similar physical properties; however, they have different molecular structures. The self-assembly behavior of (*S*)-**1** in heptane and in MCH (c = 5×10^{-5} M) at 20 °C was investigated by CD and UV-vis spectroscopy, respectively. As shown in Figure 4.2A, the two CD spectra differ in *sign*, *intensity*, and *shape* of the Cotton effect. However, the UV-vis spectra in both solvents are similar (Figure 4.2B). The CD spectrum in MCH gives rise to a small, positive, double Cotton effect with λ_{max} = 216 nm ($\Delta\varepsilon$ ≈ 6 L mol^{-1} cm^{-1}) and a shoulder at 242 nm, while a larger, negative, single Cotton effect with λ_{max} = 223 nm ($\Delta\varepsilon$ ≈ −13 L mol^{-1} cm^{-1}) is observed in heptane. In CD spectroscopy, the *sign* of

the Cotton effect is a qualitative determination for the type of the excess helical sense while the *intensity* of the Cotton effect determines the ratio of this excess helical sense quantitatively. It was previously shown that the characteristic *intensity* of the Cotton effect is $|\Delta\varepsilon| \approx 40$ L mol^{-1} cm^{-1} for chiral alkyl-substituted BTAs in various alkane solvents. This value indicates the formation of one single type of helical supramolecular polymer, i.e., diastereomeric excess (*d.e.*) is 100%.[22,23] In addition, a positive CD effect at λ_{max} = 223 nm is attributed to *P* helical sense.[24] Therefore, it can be concluded that the preferred helical sense of (*S*)-**1** is *P* in MCH with a *d.e.* of 15%, whereas in heptane, *M* is the pronounced helical sense and the *d.e.* is 33%. The *shape* of the CD spectrum is determined by the conformation of the amide bonds of the monomer within the supramolecular polymer. Thus, the single Cotton effect in heptane indicates that the majority of the (*S*)-**1**-based supramolecular polymers demonstrate an H1 conformation in this solvent, whereas the double Cotton effect in MCH suggests the H2 conformation. We propose that there are four different states of (*S*)-**1**-based supramolecular polymers, P_{H1}, P_{H2}, M_{H1}, M_{H2}, in equilibrium at 20 °C. P_{H2} is favored in MCH while M_{H1} is the most pronounced type of supramolecular polymer in heptane.

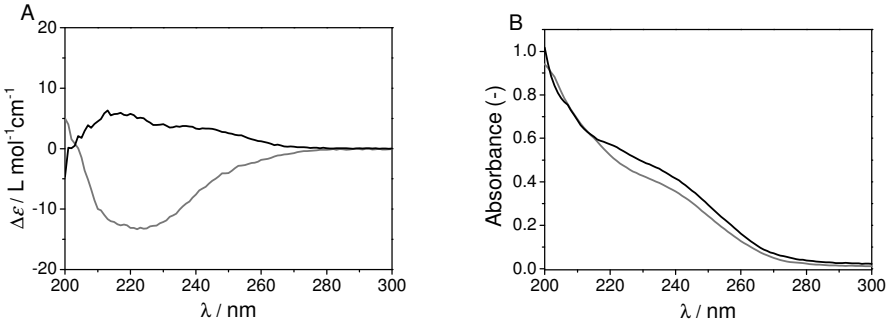

Figure 4.2: A) CD spectra and B) UV-vis spectra of (*S*)-**1** in heptane (gray line) and MCH (black line) at T = 20°C, c = 5×10^{-5} M.

4.3 The self-assembly mechanism of α-deuterated BTAs in heptane and MCH

More detailed information on the (*S*)-**1** self-assembly mechanism in MCH and heptane was gathered by using temperature-dependent UV-vis and CD spectroscopy. The UV cooling curves of (*S*)-**1** in MCH and heptane are similar and typical for a cooperative supramolecular polymerization mechanism. Since the temperature-dependent UV-vis measurements directly relate to the degree of aggregation in a self-assembly process[20,23] (Figure 4.3), the data were used to determine the thermodynamic parameters of this process in each solvent. The values for the temperature of elongation, T_e, the enthalpy of elongation, h_e, and the association constant, K_a, determined by using the nucleation-elongation model, are summarized in Table

4.1. T_e is approximately 12 °C lower in MCH than in heptane. The low value of T_e in MCH indicates that aggregation occurs at lower temperature and that the monomeric state is more favorable in this solvent. The low T_e value in MCH might be an indication for the reduced aggregate stability in this solvent, presumably as a result of slightly higher polarity and dielectric constant of MCH (ε = 2.02 at 20 °C[25]) compared to heptane (ε = 1.92 at 20 °C[26]). Furthermore, the absolute value of h_e is slightly lower in MCH. The dimensionless association constant K_a —a measure of the cooperativity— is smaller in heptane reflecting a higher cooperativity in the aggregation process.

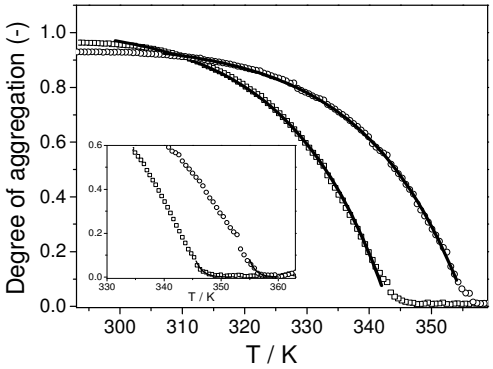

Figure 4.3: Normalized UV-vis absorption spectra monitored at λ = 223 nm at a cooling rate of 1 K min^{-1} for (*S*)-**1** (c = 5×10^{-5} M) in heptane (open circle) and in MCH (open square) with the corresponding fits[20,23] (gray line) of the elongation and nucleation regimes (inset).

Table 4.1: Thermodynamic parameters of the (*S*)-**1** self-assembly derived from temperature-dependent UV-vis data in heptane and MCH (c = 5×10^{-5} M)**.**

Solvent	T_e (K)	h_e (kJ mol^{-1})	K_a (-)
Heptane	355.6	-67.4	1.3×10^{-4} ± 0.3×10^{-4}
MCH	343.4	-63.6	6.8×10^{-4} ± 0.3×10^{-4}

The CD cooling curves are representative for the expression of supramolecular chirality as a function of temperature. As depicted in Figure 4.4, the CD cooling curves of (*S*)-**1** in MCH and heptane differ significantly. The positive sign of the $\Delta\varepsilon$ in MCH increases, then decreases and ends with a small negative value as the temperature decreases. This switch in sign upon cooling (from +5.0 L mol^{-1} cm^{-1} to −1.5 L mol^{-1} cm^{-1}) indicates a change in excess helical sense from *P* to *M*, which can be clearly observed by the CD spectra taken at each temperature

(Figure 4.5A-C). The shape of the CD curve, however, remains the same and the H2 conformer is dominant in this temperature regime.

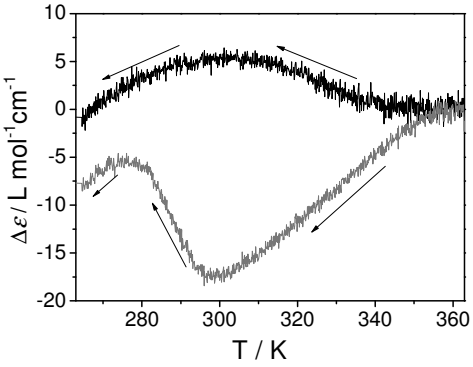

Figure 4.4: A) Molar ellipticity ($\Delta\varepsilon$) as a function of temperature monitored at λ = 223 nm at a cooling rate of 1 K min^{-1} for (*S*)-**1** in MCH (black line) and in heptane (gray line); c = 5×10^{-5} M.

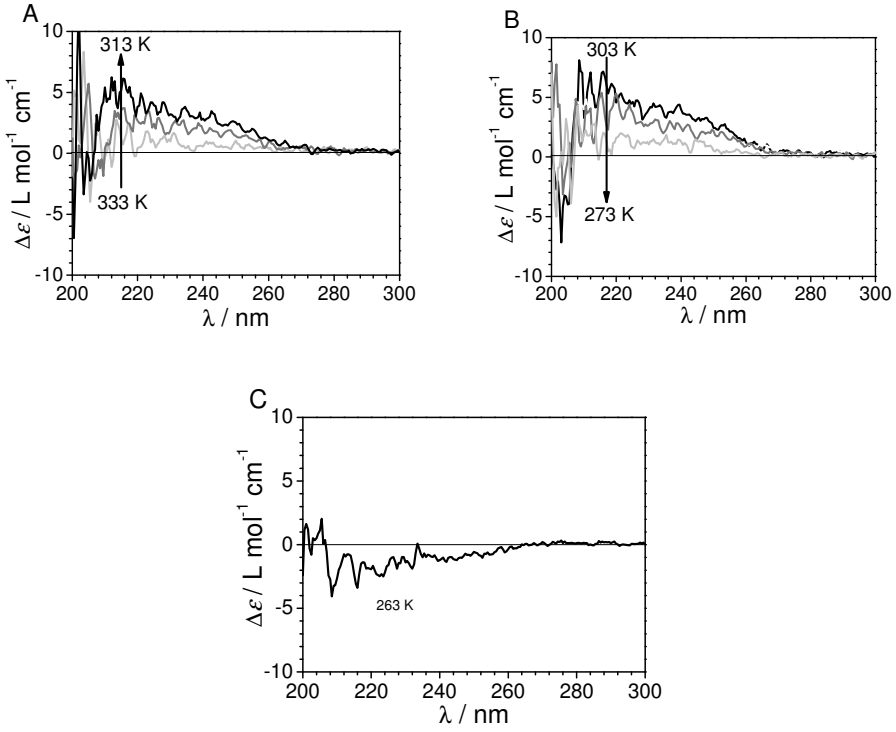

Figure 4.5: The interval CD spectra of (*S*)-**1** in MCH upon cooling (c = 5×10^{-5} M). The arrow shows the decrease in temperature. A) From 333 K to 313 K, B) From 303 K to 273 K, C) At 263 K.

In contrast, in heptane the Cotton effect always displays a negative value as the temperature decreases, suggesting that the *M* type helical sense is in excess at each temperature. However, since the change in the intensity of the Cotton effect is significant upon cooling from 323 K to 263 K in heptane, we analyzed this region in detail (I-III in Figure 4.6A) by measuring the CD spectra at intervals of 3 °C. As shown in Figure 4.6B-D, in addition to the gradual change in the intensity, the shape of the Cotton effect switches from single to double upon cooling from 293 K to 263 K, indicating that the conformation changes from H1 to H2. The cooling curve was monitored at λ = 223 nm, however, measurements performed at 215 nm led to a CD cooling curve of similar shape.

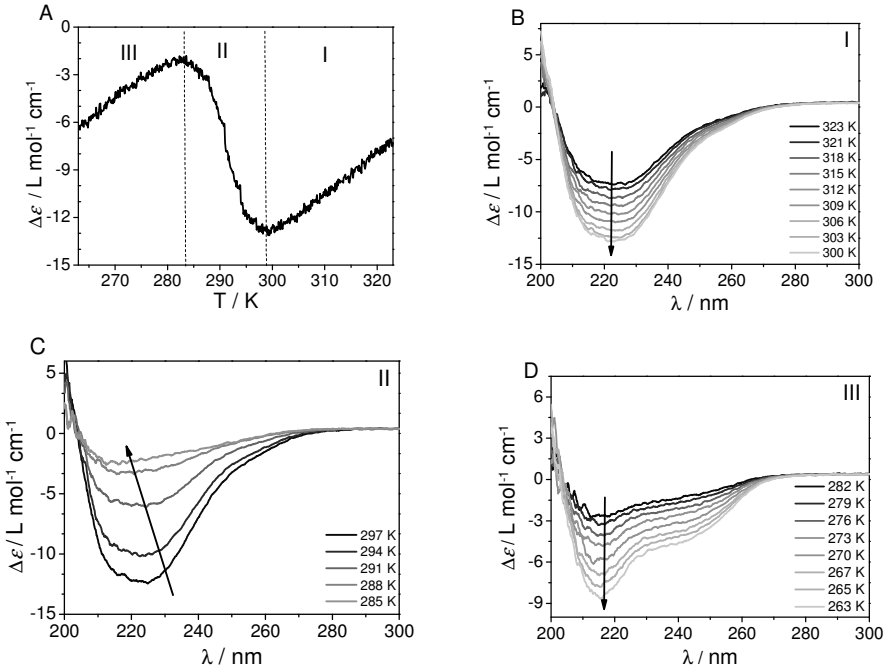

Figure 4.6: A) CD spectrum as a function of temperature between 323 K and 263 K, monitored at λ = 223 nm at a cooling rate of 1 K min^{-1}, for (*S*)-**1** in heptane at c = 5×10^{-5} M. The interval CD spectra of (*S*)-**1** in heptane from B) 323 K to 300 K, C) from 297 K to 285 K, D) 282 K to 263 K.

These results suggest that the four possible conformational states of deuterated BTA-based supramolecular polymers are in thermodynamic equilibrium. The position of the equilibrium depends on the molecular structure of the alkane solvent (cyclic or linear) and the temperature. Figure 4.7 represents an overlay of the UV signal and the CD effect as a function of temperature in MCH (A) and heptane (B). At 343 K in MCH, the monomers

(Mon) form preferably *P* type helical supramolecular polymers with an H2 type conformation (dark gray region). As the temperature decreases, from 293 K to 263 K, the preference for the helical sense shifts from P_{H2} to M_{H2} giving rise to a slight change in UV-vis spectra (light gray region). As for heptane, upon cooling, (*S*)-**1** monomers (Mon) preferably self-assemble into M_{H1} type stacks (dark gray region). In the gray region, from 297 K to 279 K, M_{H1} switches to M_{H2} giving rise to a slight change in the UV signal. Lastly, below 279 K, the most preferred conformation is M_{H2}. Although the two processes are similar in MCH and heptane, the dominant helical sense is always *M* in heptane whereas in MCH it is shifting from *P* to *M*. Moreover, the conformational changes are much more pronounced in heptane than in MCH. The overlay of CD and UV-vis spectra as a function of temperature shows that there is a sharp transition from one conformational state into another as a result of changing the temperature in heptane.

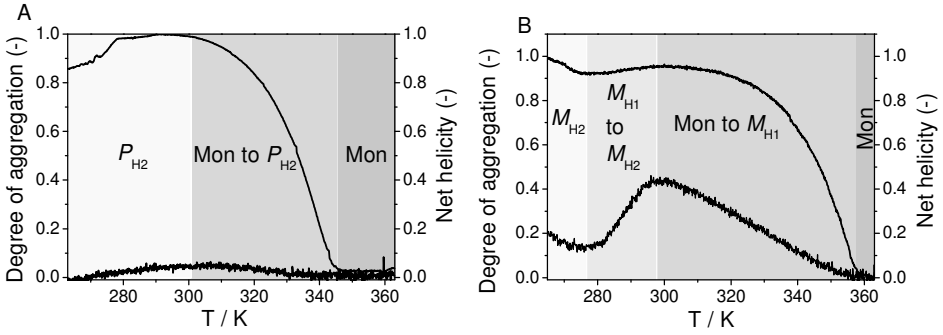

Figure 4.7: Overlay of the net helicity (from the CD cooling curve) and the degree of aggregation (from the UV-vis cooling curve) of (*S*)-**1** as a function of temperature (c = 5×10^{-5} M), λ = 223 nm, cooling rate = 1 K min^{-1}. The color gradient from dark to light shows different regions going from the monomers to supramolecular polymers. A) MCH, B) heptane.

If the transition between two states of a supramolecular polymer is cooperative, theory predicts that this transition is only weakly concentration-dependent.[27,28] At equilibrium, assuming that the average number of monomers in each type of aggregate is large, the chemical potentials of the monomers associated with the two aggregation states are dominated by their respective binding energies. The reason that the concentration dependence drops out is because, on a per monomer basis, it is proportional to the reciprocal aggregation number.[27-29] Thus, we measured concentration-dependent CD cooling curves of (*S*)-**1** in heptane between 1.5×10^{-5} and 35×10^{-5} M (Figure 4.8A). From these data, we derived a pseudo-phase diagram by using the temperature of elongation (T_e) at which monomers (Mon) start forming M_{H1} type supramolecular polymers in excess, the temperature of transition at which M_{H1} switches to M_{H2} and the temperature at which M_{H2} becomes the

dominant conformation (Figure 4.8B). The transition between M_{H1} and M_{H2} starting at 297 K is nearly independent of concentration. A similar concentration independent behavior was observed for the temperature at which M_{H2} becomes the dominant conformation (= 279 K). This result is analogous to that experimentally found for bisurea systems in which a concentration-independent, cooperative filament-to-tube transition occurs and for water soluble bipyridine based discotics in which a nonhelical-to-helical transition was observed.[29-31] In all cases, the experimental pseudo-phase diagrams derived from variable concentration measurements are in excellent agreement with the theoretically predicted phase diagrams for a cooperative transition between supramolecular polymers displaying two different conformations.[27,28]

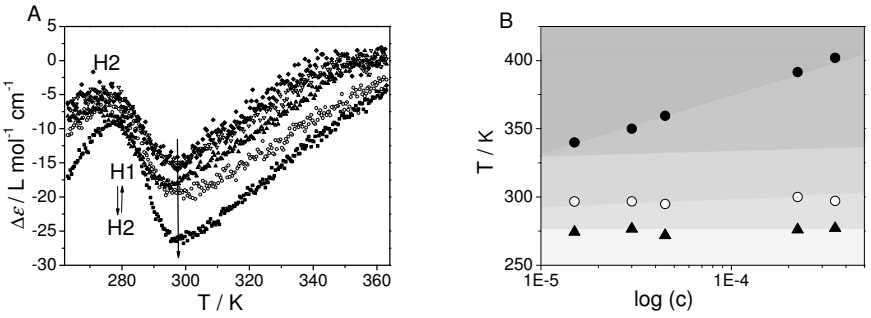

Figure 4.8: A) $\Delta\varepsilon$ as a function of temperature monitored at λ = 223 nm at a cooling rate of 1 K min^{-1}, for (*S*)-**1** in heptane with varying concentrations c = 1.5×10^{-5} M (diamond), 3.1×10^{-5} M (down triangle), 4.5×10^{-5} M (up triangle), 23×10^{-5} M (circle) and 35×10^{-5} M (square). Arrow shows increasing concentration. B) Pseudo-phase diagram derived from Figure 4.8A showing T_e (closed circles), the temperature of transition from H1 to H2 (open circles) and the temperature at which H2 is formed in excess (triangles) as a function of the logarithm of the concentration, c.

4.4 Preferential solvation in mixed solvents

Since the self-assembly of (*S*)-**1** in MCH and heptane shows dramatic differences in terms of the preferred helical sense and the preferred conformation of the supramolecular polymer formed, it is interesting to evaluate whether there is a preferred solvation of one of these solvents in a mixture. For this purpose, we prepared two solutions of (*S*)-**1** in MCH and in heptane with identical concentrations (c = 5×10^{-5} M) and mixed them in varying ratios. The UV-vis and CD spectra of (*S*)-**1** in solutions ranging from pure heptane to a mixture of heptane and MCH (heptane/MCH = 62/38, v/v%) were measured as a function of temperature. The shapes of the UV cooling curves are similar for each mixture (Figure 4.9A)

indicating that the aggregation behavior of (*S*)-**1** is similar in the mixed solvents. However, the temperature of elongation, T_e, shows a slight decrease from 361 K to 358 K as the MCH ratio increases in the mixture suggesting that the monomeric state is more favored as the amount of MCH increases. The CD cooling curves, in contrast, are highly sensitive to the amount of MCH added (Figure 4.9B). The shape of the cooling curves changes gradually as the amount of MCH increases. Moreover, the transition between the conformers H1 and H2 shifts from 296 K to 340 K. Interestingly, MCH dominates the system and after the ratio of this solvent reaches 38%, the cooling curve of (*S*)-**1** in this mixture becomes similar to that in pure MCH. Moreover, below 9.1% MCH, the presence of the single and double Cotton effect depends on the temperature. As the temperature decreases from 293 K to 273 K, the double Cotton effect appears which is similar to the (*S*)-**1** self-assembly in pure heptane (*vide supra*). Interestingly, the pronounced effect of MCH on the *intensity* of the Cotton effect observed at 293 K (open circles, Figure 4.9C) is almost absent at 278 K (closed circles, Figure 4.9C). In fact, MCH only has a pronounced effect on the *intensity* of the Cotton effect in the temperature region where the H1 conformer dominates, i.e., when the amide dihedral angle is around $\theta \approx 45°$.

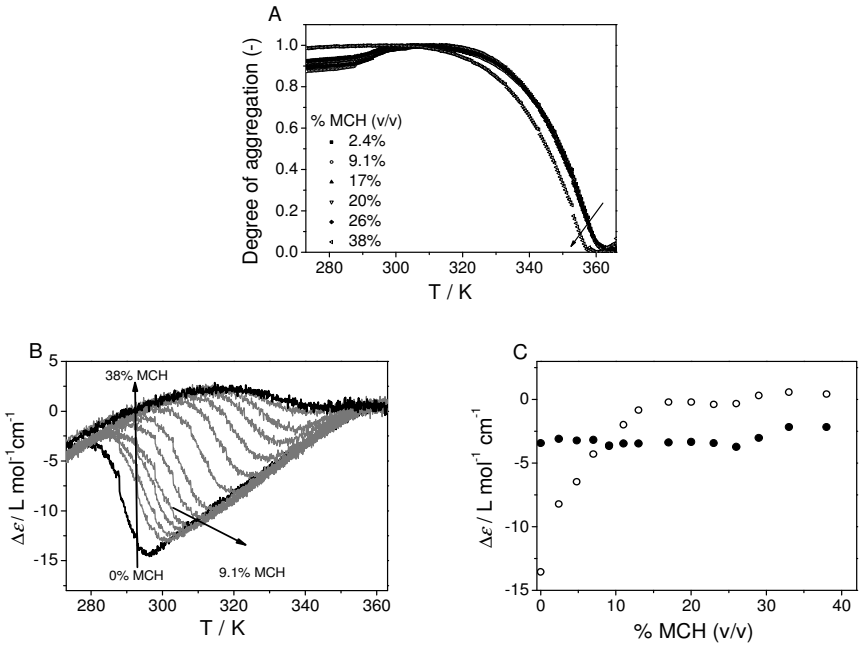

Figure 4.9: A) Normalized absorbance of (*S*)-**1** in heptane-MCH mixture as a function of temperature ($c = 5\times10^{-5}$ M). Monitored at λ = 223 nm, at a cooling rate of 1 K min^{-1}. The arrow shows the increasing amount of MCH. For clarity, only a few measurements are shown. B) $\Delta\varepsilon$ as a function of temperature monitored at λ = 223 nm at a cooling rate of 1 K min^{-1}, for (*S*)-

1 in heptane-MCH mixtures, ranging from 0% MCH (light gray) to 38% MCH (black), with an increment of 3% MCH in each step, c = 5×10^{-5} M. C) Molar ellipticity ($\Delta\varepsilon$) as a function of the vol% of MCH (in MCH-heptane mixture) at 293 K (open circles) and 278 K (closed circles).

We attribute this behavior to the intercalation of heptane between BTA molecules within the stacks. At lower temperatures in pure heptane and at higher MCH concentrations in the heptane-MCH mixture, heptane is expelled from the neighborhood of the stacks, leading to a reduction of the angle, $\theta \approx 35°$, and as a result, H2 becomes the preferred conformer (Figure 4.10). This observation implies that the contribution of the heptane intercalation to the association enthalpy of the monomers within the stacks must be positive rather than negative. This in turn implies that solvent intercalation into the stack is entropy driven, e.g., due to mixing with the side chains and/or enhanced conformational freedom of these side chains due to a larger separation between BTA monomers within the stacks.

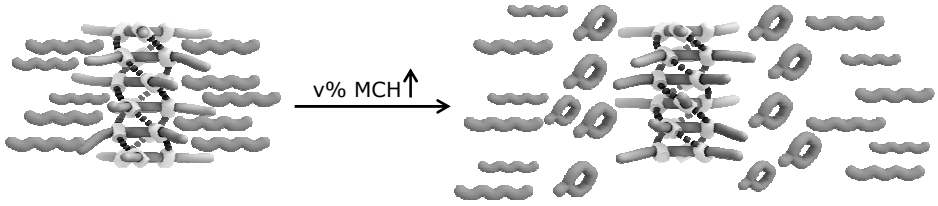

Figure 4.10: Schematic representation of the heptane intercalation between BTA monomers of the supramolecular aggregate. Due to the preferential solvation by MCH, the conformation changes from H1 to H2.

Similar preferential solvation behavior was also observed in heptane-isooctane* mixtures. As the (*S*)-**1** solution in heptane is titrated with (*S*)-**1** in solution in isooctane, the CD spectra changed gradually (Figure 4.11A) while the UV-vis spectra remained almost constant (Figure 4.11B).

* Isooctane: 2,2,4-Trimethylpentane

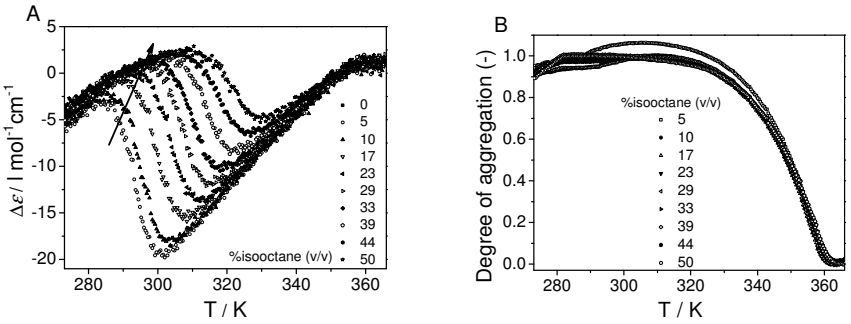

Figure 4.11: A) $\Delta\varepsilon$, B) The normalized absorption as a function of temperature monitored at λ = 223 nm at a cooling rate of 1 K min^{-1} for (*S*)-**1** in heptane-isooctane mixtures. The arrow shows the increasing amount of isooctane.

These results suggest that expression of supramolecular chirality for the (*S*)-**1**-based supramolecular polymers was strongly influenced by isooctane (branched) and MCH (cyclic) concentration in the mixture and the columnar stacks were preferentially solvated by these solvents. A rationale for this behavior may be offered by the formation of a shell-like structure around the stacks which is analogous to the hydration layer on proteins.[32] The intercalation of the solvent molecules in combination with the formation of columnar shell-like structures due to the preferential solvation leads to a change in the conformation from H1 to H2.

4.5 Solvation by linear alkanes

The higher bias caused by heptane is related to an increased amide angle $\theta \approx 45°$ suggesting that a linear solvent effectively helps in biasing one helical sense over the other. A clear preference of (*S*)-**1** for the *M* helical sense is also observed in other linear alkane solvents such as hexane, octane, nonane, decane, undecane[†] and dodecane at 20 °C (Figure 4.12A). Furthermore, the $\Delta\varepsilon$ values measured in different alkane solvents showed an 'odd-even effect' depending on the solvent with an odd or even number of carbon atoms in the alkane chain (Figure 4.12B). A similar 'odd-even effect' was observed in the self-assembly of *oligo*-phenylenevinylenes (OPV) in various linear alkane solvents.[20] The self-assembly mechanism of (*S*)-**1** in these alkane solvents was further investigated by temperature-dependent UV-vis and CD measurements (Figure 4.12C). Temperature-dependent CD spectra revealed that similar transitions take place between M_{H1} and M_{H2} upon cooling and the transition temperatures are different in each solvent. The thermodynamic parameters were determined from the corresponding nucleation-elongation growth fits based on the UV-

[†]Due to the high absorption of undecane in the wavelength region of interest, 0.1 cm path length was applied.

vis spectra.[20,23] As shown in Figure 4.12D, an 'odd-even effect' is also present for T_e values.‡ The T_e values observed for the self-assembly in the alkanes with odd number of carbon atoms (C_7, C_9)§ are higher than those of even ones (C_8, C_{10}, C_{12}) suggesting that the aggregate formation is more favored in those solvents. This observation correlates nicely with the CD spectra taken in these alkanes at 20 °C. Higher $\Delta\varepsilon$ values in C_7, C_9, C_{11} solvents correspond to a larger diastereomeric excess (*d.e*) indicating a larger preference for *M* type supramolecular polymers which is presumably related to a more stable supramolecular polymer with larger persistence length. Almost all physical parameters in alkane solvents depend linearly on the number of carbons in the alkane chain except for properties related to ordering, such as density and melting points of the alkanes.[33,34] Although the differences in the thermodynamic parameters are relatively small, our results suggest that coorganization of the solvent at the periphery of the aggregates plays a direct role in the self-assembly processes as previously reported for the self-assembly of OPVs.[20]

‡Measurements were performed with identical concentrations of (*S*)-**1**; however, there may be small concentration differences which may cause slight deviations in T_e values.

§To eliminate the effect of high absorption of undecane in the wavelength region of interest, high concentration of (*S*)-**1** and a path length of 0.1 cm was applied. The T_e value obtained was not comparable with the data obtained in other alkane solvents.

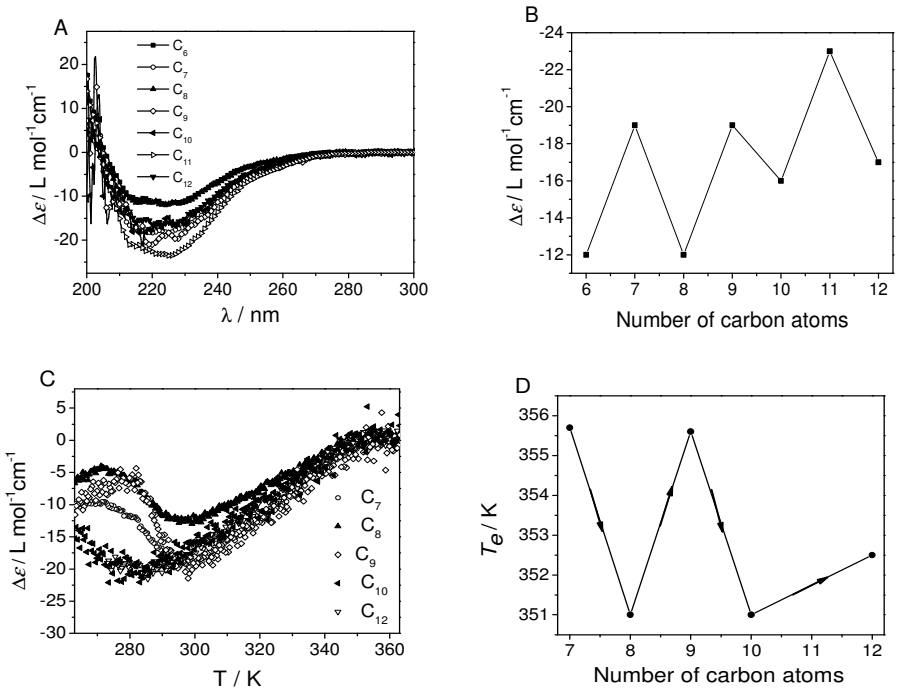

Figure 4.12: A) An overlay of the CD spectra of (*S*)-**1** in linear alkane solvents. c = 5×10^{-5} M, T = 20 °C. B) $\Delta\varepsilon$ as a function of the number of carbons in the alkane solvents. The line is to guide the eye. C) $\Delta\varepsilon$ as a function of temperature monitored at λ = 223 nm at a cooling rate of 1 K min^{-1} for (*S*)-**1** in alkane solvents. D) T_e as a function of the number of carbons in the alkane solvents containing (*S*)-**1** with identical concentrations. The line is to guide the eye.

In contrast, the CD spectra of (*S*)-**1** in branched and cyclic solvents such as isooctane, cyclohexane and decaline show no or only a very small Cotton effect at room temperature (Figure 4.13A-C), although cooling induces small preferences for either *P* or *M* helicity. These observations support that linear alkanes actively participate in the self-assembled structures. Branched and cyclic solvents reduce the ability of the deuterium stereocenter to bias one helicity in (*S*)-**1** aggregates, while linear solvents increase the bias. Thus, weak van der Waals interactions present between the alkane solvent and BTA alkyl chains assist in expressing a preferred helicity. In the absence of this interaction (as is the case with branched/cyclic solvents), the ability of the deuterium to favor one helicity is reduced.

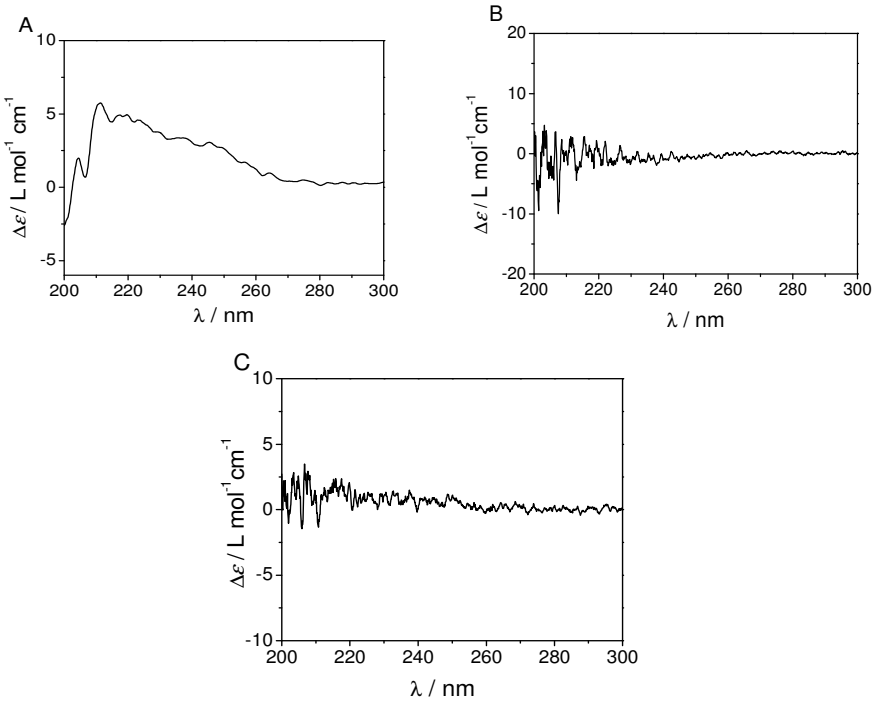

Figure 4.13: CD spectra of (*S*)-**1**, c = 5×10^{-5} M at 20 °C in A) cyclohexane, B) decaline, C) isooctane.

4.6 Origin of the supramolecular chirality in *α*-deuterated-BTAs

Our findings reveal that deuterated-BTA-based supramolecular polymers display a helical sense preference, which is strongly dependent on the structure of the solvent employed as discussed above. Previously, Green and coworkers reported that deuterium substitution on diastereotopic hydrogens of a methylene group lowers the zero point energy (ZPE) of the C-H bond resulting in a favored helical sense from the carbon which places the deuterium in the position with the lower ZPE. The origin of this helical sense preference on the macromolecular level was investigated by applying plane-wave density functional theory (PW-DFT) calculations on the hydrogen bonded BTA chains of (*S*)-**1** and (*R*)-**1** containing up to seven monomers (Figure 4.14).[35]

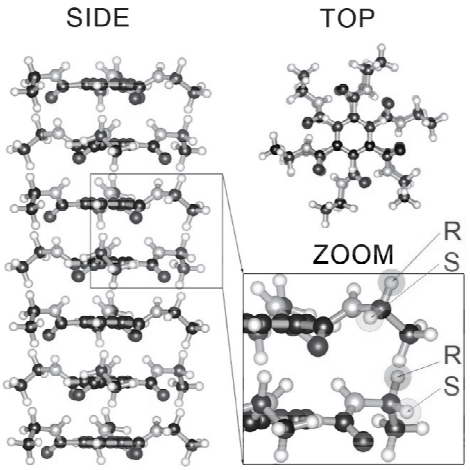

Figure 4.14: Geometry of the *P*-type supramolecular polymer, side view (left) and the top view (right). Indicated are the positions for the deuterium atom to either have an *S* or an *R* configuration. Carbon atoms are shown in black, oxygen atoms in red, nitrogen atoms in blue and hydrogen atoms in white spheres.[**]

DFT calculations performed by Filot, de Greef and Pidko[35] revealed that the difference in the ZPEs originate from the eigenvector orientations of the C-H/C-D bond stretching frequencies. As shown in Figure 4.15, C-H bond vibration can be either in the direction of the oxygen atom (higher electron density, more electronegative atom) or to the perpendicular direction with low electron density. When substituted with deuterium, C-D vibration favors the direction of the higher electron density due to the increase in mass. The overall supramolecular polymer in a *P* conformation is more stable when the C-D vibrations point toward regions of higher electron density and the C-H vibrations point toward regions of lower electron density (Figure 4.15). Given the orientation of a *P*-type helical polymer, the energetically lowest configuration for each of the stereocenters in the supramolecular polymer corresponds to the (*S*) configuration. Although the effect of the solvent is neglected in these calculations, the results presented here show a clear picture to the origin of the preferred helical sense which is in good agreement with our experimental findings in MCH where no solvent intercalation observed.

[**] The experiments discussed here were performed by I. Filot.

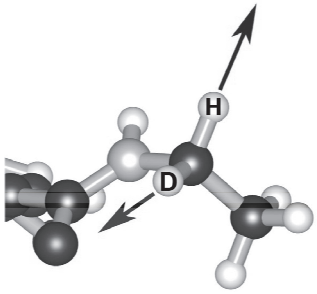

Figure 4.15: Side chain of (*S*)-**1** monomer. The hydrogen eigenvector points to the vacuum, while the deuterium eigenvector points toward the strongly electronegative region of the oxygen atom.

4.7 Origin of the conformation and the helical sense switch

Observations discussed above suggest that heptane molecules intercalate within the monomeric units of supramolecular polymers. However, the presence of MCH molecules even in small concentration is sufficient to disrupt this intercalation. The temperature of elongation is lower in MCH (T_e = 343.4 K) than in heptane (T_e = 355.6 K) suggesting a more favored molecularly dispersed state in MCH. Hence, addition of MCH to heptane solution may result in partial depolymerization of the supramolecular polymer. This mechanistic rationale may be a plausible explanation for the decrease in the intensity of the CD signal observed in the binary mixture experiments performed at 20 °C (Figure 4.9C). However, it is insufficient for unraveling the origin of the conformational and the helical sense changes that are observed in pure heptane and MCH solutions upon cooling, respectively.

The thermodynamic parameters discussed above were determined by using the 'nucleation-elongation growth model' developed by van der Schoot.[20,23] A new mathematical model ('equilibrium model') describing cooperative supramolecular polymerization of a single monomer type was developed recently by Markvoort and ten Eikelder.[36] The two models describe the same process differently; however, the results are similar and both provide valuable information on the mechanism of the processes under investigation. Cooperative supramolecular polymerization is described by the stepwise addition (forward reaction) or removal (backward reaction) of the monomeric unit to a growing supramolecular polymer in Markvoort and ten Eikelder's model. Equilibrium constant (K = $k_{1(\text{addition})}/k_{-1(\text{removal})}$) is directly related to the Gibbs free energy as follows:

$$K = \exp\left(-\Delta G^{\circ}/(RT)\right)$$
$$K = \exp\left(-\left(\Delta H_{e}^{\circ} - \Delta H_{MMP}^{\circ} - T\Delta S_{e}^{\circ}\right)/(RT)\right) \quad (4.1)$$

where $\Delta H°_e$ and $\Delta S°_e$ are the (standard) enthalpy and entropy changes in the elongation phase, respectively.[37] $\Delta H°_{MMP}$ is the energy barrier when a monomer assembles into its unfavorable helical sense or conformation. The mismatch penalty term may be important in determining the proportions of different states of the supramolecular polymers at different temperatures. For example, as the temperature decreases in MCH, the mismatch penalty between the two states, P_{H2} and M_{H2}, increases leading to formation of M_{H2}. This explanation may be also applicable to the conformations, M_{H1} and M_{H2}, which are observed in heptane. Quantitative analysis on the observed process by using the new equilibrium model is under investigation.

Another plausible explanation for the origin of the preferred conformation and the helix sense switch is the size of deuterium changing with temperature. It was reported that deuterium has a smaller van der Waals radius than hydrogen as a result of the lower zero-point energy of deuterium.[38,39] This translates to different racemization rates of the molecules where the hydrogen atoms are replaced with deuterium.[40] Further studies revealed that the size changes of deuterium and hydrogen are influenced differently by temperature.[41] Van der Waals size of the deuterium expands faster than that of hydrogen. The size of deuterium atom as a function of temperature may be effective in deuterated-BTA system. Helical packing might change due to the steric reasons leading to a switch in the helical sense, from *P* to *M* as observed in MCH.

4.8 Solvent effect on (*S*)-β–deuterated BTA self-assembly

The self-assembly behaviour of (*S*)-β–deuterated BTA ((*S*)-**2**, Figure 4.16A) was studied in dodecane by UV-vis and CD spectroscopy as discussed in Chapter 3. We herein investigate the self-assembly of (*S*)-**2** in MCH and compare it with the results obtained in dodecane. The UV-vis spectrum in MCH revealed a hypsochromic shift upon cooling from 90 °C to 20 °C which is a good indication for the formation of H-type aggregates in MCH upon cooling (Figure 4.16B). CD spectrum of (*S*)-**2** in MCH gives rise to a small positive double Cotton effect with a $\Delta\varepsilon$ of +5 L mol^{-1} cm^{-1} (Figure 4.16C). Similar to the CD spectrum obtained in dodecane, the intensity of the Cotton effect in MCH is small. The low intensity of the CD effects in both solvents is probably a result of low helical preference of (*S*)-**2** due to the deuterium position. The CD spectra of (*S*)-**2** in dodecane and MCH were compared to those of (*S*)-**1** at 20 °C. As shown in Figure 4.16D, the CD spectra taken in MCH are similar, whereas in dodecane the intensity of the Cotton effect for (*S*)-**2** is much lower than that of (*S*)-**1**. Furthermore, induction of chirality by the dodecane solvent as a result of solvent intercalation was not observed in (*S*)-**2**-based supramolecular polymers. Obviously, β-deuterated BTA-based supramolecular polymers do not exhibit a preferred helix sense due to the more remote position of the chirality-inducing deuterium center from the benzene core.

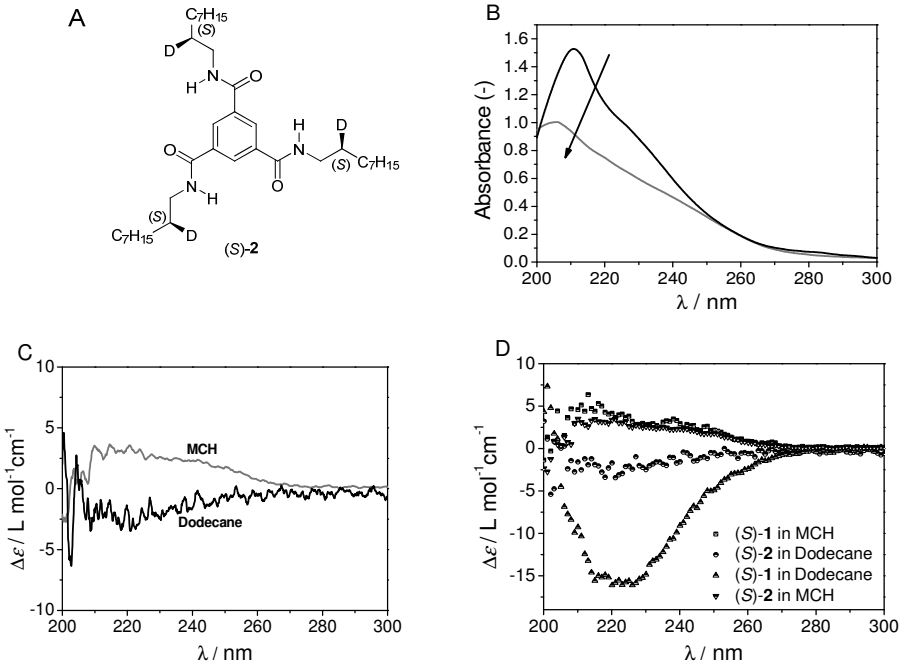

Figure 4.16: A) Chemical structure of (*S*)-β-deuterated BTA. B) UV-vis spectra of (*S*)-**2** in MCH, c = 5×10^{-5} M, at 20 °C (gray) and 90 °C (black). The arrow shows the hypsochromic shift in λ_{max} upon cooling. B) Overlay of the CD spectra of (*S*)-**2** at 20 °C, c = 5×10^{-5} M, in dodecane (black), in MCH (gray). C) Overlay of the CD spectra of (*S*)-**2** and (*S*)-**1** in dodecane and MCH, c = 5×10^{-5} M at 20 °C.

The mechanism of formation of β-deuterated BTA-based supramolecular polymers was analyzed in MCH by monitoring the UV-vis and CD spectra at λ = 223 nm as a function of temperature. As shown in Figure 4.17A, the self-assembly process follows a cooperative mechanism whereas the CD spectrum (Figure 4.17B) has almost a linear dependence on temperature which is similar to that obtained in dodecane (*vide supra*). The thermodynamic parameters were obtained by using the nucleation-elongation growth model[20,23] based on the UV-vis cooling curve. The values for the temperature of elongation (T_e = 345 K) and the enthalpy of elongation (h_e = -45 kJ mol^{-1}) suggested that the stability of the (*S*)-**2**-based supramolecular polymers in MCH may be lower than the ones formed in dodecane.[††] (In dodecane: T_e = 351 K, h_e = -52 kJ mol^{-1}). Furthermore, compared to the self-assembly properties of (*S*)-**1** in MCH (T_e = 343.4 K, h_e = −63.6 kJ mol^{-1}), the T_e values of (*S*)-**1** and (*S*)-**2** are similar.

[††] K_a is not applicable.

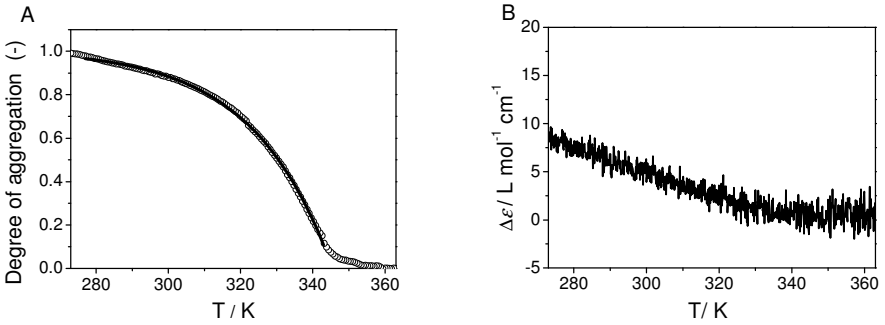

Figure 4.17: A) Normalized UV–vis spectrum, B) $\Delta\varepsilon$ of (*S*)-**2** in MCH (c = 5×10^{-5} M) as a function of temperature, monitored at λ = 223 nm at a cooling rate of 1 K min^{-1}.

4.9 Chiral solvation in achiral BTA self-assembly

Previous studies revealed that optically inactive poly(*n*-hexylisocyanate) gives rise to a large Cotton effect when dissolved in optically active solvents such as (*R*)-2-chloropentane. The CD spectra of optically inactive polymers obtained in optically active solvents are identical in shape and intensity with those obtained from optically active polyisocyanates in which an excess of one helical sense is enforced by chiral stereogenicity in the side chain.[42,43] Similar chiral solvation effects were also observed in polythiophenes[44] and in 3,3′-diamino-2,2′-bipyridine-substituted-BTA supramolecular systems.[12]

We investigate here similar chiral solvation effects in the self-assembly of achiral trioctyl-substituted BTAs. Achiral trioctyl-BTA **3**[‡‡] leads to the formation of *P* and *M* type helical aggregates in equal amounts in solution and a helical sense preference is not observed. The self-assembly of achiral BTA **3** was analyzed in a commercially available optically active solvent, (*R*)-(-)-2,6-dimethyloctane. The UV-vis spectroscopy resulted in strong absorptions due to the impurities present in this solvent.[§§] The enantiomeric, optically active, (*S*)-(+)-2,6-dimethyloctane, was synthesized starting from commercially available (*R*)-(-)-3,7-dimethyloctylbromide and the self-assembly properties of the achiral **3** was investigated in this solvent.[***] The CD spectrum of compound **3** in (*S*)-(+)-2,6-dimethyloctane (c = $2\text{x}10^{-4}$ M) measured at three different temperatures (−10, 20 and 90 °C) resulted in a relatively large Cotton effect (Figure 4.18A). Due to the high absorption below 220 nm, the spectrum is shown only in the region between 220-300 nm. The positive CD effect suggests that (*S*)-(+)-

‡‡ See Appendix 4.12 for the chemical structure of **3**.

§§ The solvent was distilled; however, the impurities could not be removed completely.

*** This chiral alkane solvent contained some impurities that could not be eliminated completely by simple purification methods; however, the intensity of absorption resulting from the alkane solvent was smaller compared to the commercially available (*R*) enantiomer.

2,6-dimethyloctane induces a preference for *P* helical stack in achiral BTA-based supramolecular polymers. The $\Delta\varepsilon$ at λ_{max} = 238 nm is 11.6 L mol^{-1} cm^{-1} at 20°C which is comparable to that of α-deuterated-BTA-based supramolecular polymers in dodecane. Moreover, the temperature-dependent CD spectroscopy revealed a similar linear relationship between the CD effect and the temperature (Figure 4.18B) which was observed in deuterated-BTAs (*vide supra*). This result suggests that due to the small stability difference between the two type supramolecular polymers formed, *P* and *M* are formed simultaneously and the net helicity is lower than 1 as is the case in α–deuterated BTA self-assembly.

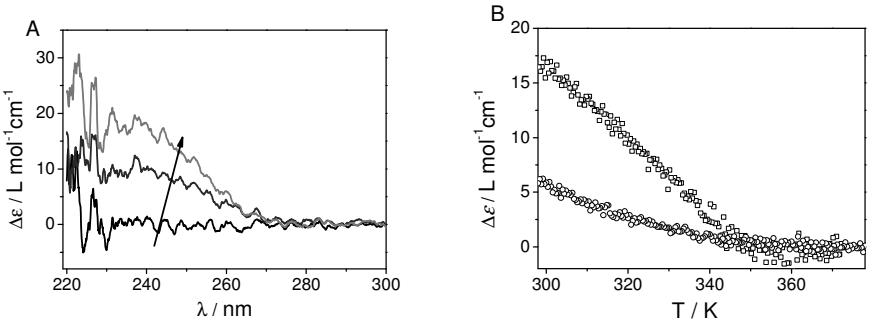

Figure 4.18: A) The CD spectra of **3** in (*S*)-(+)-2,6-dimethyloctane (c = 2x10^{-4} M). The arrow shows the decrease in the temperature, 90, 20, −10 °C. B) The overlay of the CD spectra of (*S*)-**1** (square) in dodecane, c = 5×10^{-5} M, monitored at λ = 223 nm and **3** (circle) in (*S*)-(+)-2,6-dimethyloctane, c = 2×10^{-4} M, monitored at λ = 238 nm as a function of temperature with a cooling rate of 1 K min^{-1}.

4.10 Conclusions

The effect of the solvent on the self-assembly of α-deuterated BTA monomers was investigated. The analysis of the self-assembly mechanism in various solvents as well as in the binary solvent mixtures suggested an active participation of the solvent molecules during the supramolecular polymerization. As a result of the solvent interaction, four different conformational states of the self-assembled structures were deduced. Further analysis on the self-assembly process revealed that temperature has a dominant role on the preferred conformational state of the supramolecular polymer. Self-assembly behavior of the β-deuterated BTAs were investigated in MCH and dodecane solvent. In both cases a very weak helix sense preference was observed. This result was attributed to the reduced effect of deuterium on the supramolecular chirality which becomes smaller when the deuterium center is positioned more remote from the carboxamide. Further evidence on the active participation of the solvent on the self-assembly of BTAs was gathered by analyzing the self-assembly behavior of achiral BTAs in chiral alkane solvents. The results obtained by UV-vis

and CD spectroscopy revealed that supramolecular chirality was induced by the chiral solvent in achiral BTA-based supramolecular polymers. The results presented here provide strong evidence for the existence of a bound solvent shell around or even partially incorporated solvent molecules into structures formed by self-assembling molecules. While in protein folding the role of water is widely recognized to play a dominant role, solvophobic effects may be equally important for self-assembling systems in organic media. Gathering precise knowledge on these additional weak interactions during self-assembly is difficult yet it is important especially when applications in the field of catalysis or organogelators are envisaged.

4.11 Experimental

4.11.1 General

Ultraviolet (UV) and circular dichroism (CD) measurements were simultaneously performed on a Jasco J-815 spectropolarimeter where the sensitivity, time constant and scan rate were chosen appropriately. Corresponding temperature-dependent measurements were performed with a PFD-425S/15 Peltier-type temperature controller with a temperature range of 263-383 K and adjustable temperature slope. In all cases, a temperature slope of 1 K min^{-1} was used. The molar ellipticity $\Delta\varepsilon$ was calculated from the CD effect as follows; $\Delta\varepsilon$ = CD effect/(32980 c *l*) where the CD effect is given in mdeg, c is the concentration in mol L^{-1} and *l* is the optical path length in cm. In all experiments, the linear dichroism was measured and in all cases no linear dichroism was observed. Cells with an optical path length of 1 cm or 1 mm were used. Hexane, heptane, octane, isooctane (spectrophotometric grade) was purchased from Acros and methylcyclohexane (MCH, spectrophotometric grade) was obtained from Aldrich. Dodecane (spectrophotometric grade) was obtained from Biosolve. Nonane, decane and undecane were obtained from Acros and used without further purification. (*R*)-(-)-2,6-dimethyloctane was obtained from Aldrich and was distilled at reduced pressure before using. Solutions were prepared by weighing (S)-**1** after which this amount was transferred to a volumetric flask (flasks of 5 mL were employed). Then the flask was filled with the spectrophotometric grade solvent and put in an oscillation bath at 40 °C for 50 min, after which the flask was allowed to cool down. Any loss of solvent was compensated. All fits of the temperature dependent data to obtain the thermodynamic parameters were performed as previously published.[20,23]

4.11.2 Synthesis of (*S*)-(+)-2,6-dimethyloctane: A mixture of (*R*)-(–)-citronellyl bromide (25.3 g, 115 mmol) and K_2CO_3 (32 g) in methanol (150 mL) was catalytically hydrogenated on 5% Pd/C (0.68 g) in the Parr reactor. After the completion of the reaction, the mixture was filtered over celite and the celite was washed with methanol. The filtrate was diluted with

water and the resulting mixture was extracted by using diethyl ether (3×50 mL). The diethyl ether layer was dried with $MgSO_4$ and the solvent was evaporated to yield the desired compound, (*S*)-(+)-2,6-dimethyloctane (6.0 g, 36%). The product was distilled at reduced pressure. T_b = 50 °C/8.8x10^{-2} mbar. $[\alpha]^{20}_D$ = +5.4° (neat), (lit. +6.3).[45]

4.12 Appendix

4.12.1 Structures of BTAs

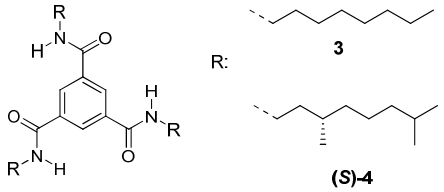

Figure A4.1: Chemical structures of achiral octyl (**3**) and chiral methyl substituted ((*S*)-**4**) BTAs.

4.12.2 Solvation in achiral BTA self-assembly†††

The hypothesis on the selective interaction of the solvent molecules with the supramolecular polymers was corroborated with sergeants-and-soldiers experiment[46,47] performed in heptane and MCH, respectively. Previous studies[48] showed that a helix sense preference can be induced when achiral trioctyl substituted BTAs (**3**, Figure A4.1) is mixed with (*S*)-methyl BTA ((*S*)-**4**) in MCH as a result of chiral amplification in BTAs. This experiment led to the evolution of a double Cotton effect (λ_{max} = 216 nm and a shoulder at λ = 242 nm) upon addition of (*S*)-**4** (Figure A4.2A). A similar experiment was performed in heptane.[49] Mixing achiral BTA **3** with the sergeant (*S*)-**4** resulted in the evolution of a single Cotton effect in heptane with a comparable shape to that of (*S*)-**1** (λ_{max} = 223 nm) in heptane (Figure A4.2B). These results suggest that solvent intercalation is also observed in achiral BTAs giving rise to the formation of two preferred conformations which may be similar to H1 and H2. However, changes in the conformation or the helix sense are not observed upon cooling, in MCH or heptane. (Figure A4.2C-D).

††† These experiments were performed by dr. Y. Nakano.

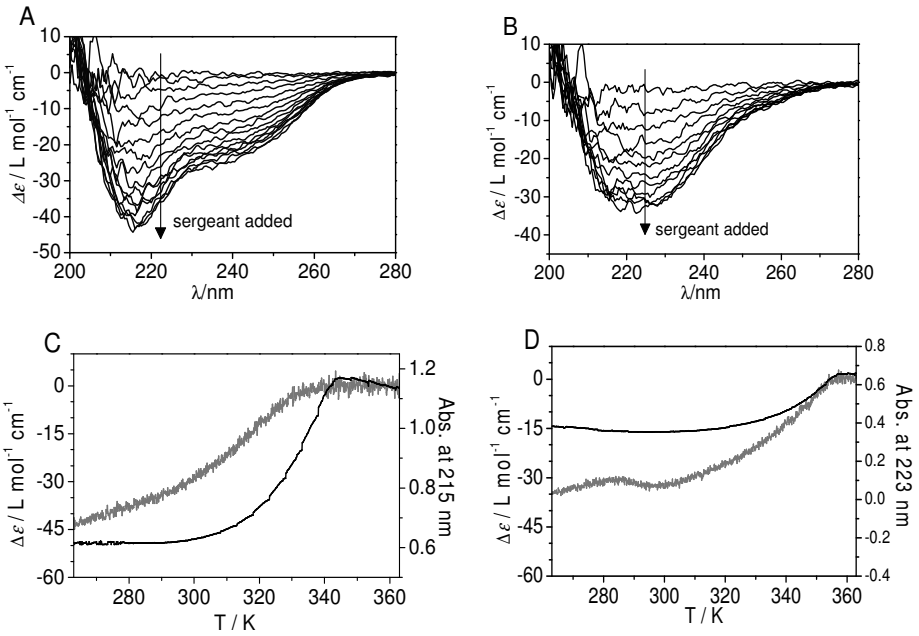

Figure A4.2: CD spectra of **3** upon addition of (*S*)-**4**, c = 3×10^{-5} M, arrow shows increasing amount of (*S*)-**4**. A) MCH, B) heptane. Temperature-dependent UV-vis (black) and CD (gray) spectra as a function of temperature monitored at λ = 223 nm with a cooling rate of 1 K min^{-1}. C) MCH, D) heptane.

4.13 References

[1] T. F. A. de Greef, M. M. J. Smulders, M. M. J. Wolffs, A. P. H. J. Schenning, R. P. Sijbesma, E. W. Meijer, *Chem. Rev.* **2009**, *109*, 5687.

[2] M. M. J. Smulders, M. M. L. Nieuwenhuizen, T. F. A. de Greef, P. van der Schoot, A. P. H. J. Schenning, E. W. Meijer, *Chem. Eur. J.* **2010**, *16*, 362.

[3] T. Pinault, B. Isare, L. Bouteiller, *Chem. Phys. Chem.* **2006**, *7*, 816.

[4] W. Edwards, C. A. Lagadec, D. K. Smith, *Soft Matter* **2011**, *7*, 110.

[5] J. van Esch, F. Schoonbeek, M. de Loos, H. Kooijman, A. L. Spek, R. M. Kellogg, B. L. Feringa, *Chem. Eur. J.* **1999**, *5*, 937.

[6] M. George, G. Tan, V. T. John, R. G. Weiss, *Chem. Eur. J.* **2005**, *11*, 3243.

[7] Y. Jeong, K. Hanabusa, H. Masunaga, I. Akiba, K. Miyoshi, S. Sakurai, K. Sakurai, *Langmuir*, **2005**, *21*, 586.

[8] V. V. Borovkov, G. A. Hembury, Y. Inoue, *Angew. Chem. Int. Ed.* **2003**, *42*, 5310.

[9] M. Hutin, J. Nitschke, *Chem. Commun*. **2006**, 1724.

[10] K. Sakajiri, T. Sugisaki, K. Moriya, S. Kutsumizu, *Org. Biomol. Chem.* **2009**, *7*, 3757.

[11] A. L. Hofacker, J. R. Parquette, *Angew. Chem. Int. Ed*. **2005**, *44*, 1053.

[12] A. R. A. Palmans, J. A. J. M. Vekemans, E. E. Havinga, E. W. Meijer, *Angew. Chem. Int. Ed.* **1997**, *36*, 2648.

[13] B. Isare, M. Linares, L. Zargarian, S. Fermandjian, M. Miura, S. Motohashi, N. Vanthuyne, R. Lazzaroni, L. Bouteiller, *Chem. Eur. J*. **2010**, *16*, 173.

[14] S. J. George, Z. Tomovic, A. P. H. J. Schenning, E. W. Meijer, *Chem. Commun.* **2011**, *47*, 3451.

[15] S. J. George, Z. Tomovic, M. M. J. Smulders, T. F. A. de Greef, P. Leclere, E. W. Meijer, A. P. H. J. Schenning, *Angew. Chem. Int. Ed.* **2007**, *46*, 8206.

[16] H. von Berlepsch, S. Kirstein, C. Bottcher, *J. Phys. Chem. B* **2003**, *107*, 9646.
[17] M. M. Green, N. C. Peterson, T. Sato, A. Teramoto, R. Cook, S. Lifson, *Science* **1995**, *268*, 1860.
[18] Y. Nakano, Y. Liu, M. Fujiki, *Polym. Chem*. **2010**, *1*, 460.
[19] H. Nakashima, J. R. Koe, K. Torimitsu, M. Fujiki, *J. Am. Chem. Soc.* **2001**, *123*, 4847.
[20] P. Jonkheijm, P. van der Schoot, A. P. H. J Schenning, E. W. Meijer, *Science* **2006,** *313*, 80.
[21] Y. Nakano, T. Hirose, P. J. M. Stals, E. W. Meijer, A. R. A. Palmans, *Chem. Sci.* **2012**, *3*, 148.
[22] P. J. M. Stals, M. M. J. Smulders, R. Martin-Rapun, A. R. A. Palmans, E. W. Meijer, *Chem. Eur. J.* **2009,** *15*, 2071.
[23] M. M. J. Smulders, A. P. H. J. Schenning, E. W. Meijer, *J. Am. Chem. Soc.* **2008**, *130*, 606.
[24] M. M. J. Smulders, T. Buffeteau, D. Cavagnat, M. Wolffs, A. P. H. J. Schenning, E. W. Meijer, E. W. *Chirality* **2008**, *28*, 1016.
[25] W. R. Pyle, *Phys. Rev*. **1931**, *38*, 1057.
[26] D. R. Lide, in *Handbook of Organic Solvents*, CRC Press, **1994**.
[27] J. van Gestel, P. van der Schoot, M. A. J. Michels, *J. Phys. Chem. B* **2001**, *105*, 10691.
[28] J. van Gestel, P. van der Schoot, M. A. J. Michels, *Langmuir* **2003**, *19*, 1375.
[29] M. Roman, C. Cannizzo, T. Pinault, B. Isare, B. Andrioletti, P. van der Schoot, L. Bouteiller, *J. Am. Chem. Soc.* **2010**, *132*, 16818.
[30] M. Bellot, L. Bouteiller, *Langmuir* **2008**, *24*, 14176.
[31] P. van der Schoot, M. A. J. Michels, L. Brunsveld, R. P. Sijbesma, A. Ramzi, *Langmuir* **2000**, *16*, 10076.
[32] S. Ebbinghaus, S. J. Kim, M. Heyden, X. Yu, U. Heugen, M. Gruebele, D. M. Leitner, M. Havenith, *Proc. Natl. Acad. Sci. U. S. A* **2007**, *104*, 20749.
[33] R. Boese, H. C. Weiss, D. Blaser, *Angew. Chem. Int. Ed*. **1999**, *38*, 988.
[34] V. R. Thalladi, R. Boese, H. C. Weiss, *Angew. Chem. Int. Ed*. **2000**, *39*, 918.
[35] I. Filot, A. R. A. Palmans, T. F. A. de Greef, E. Pidko, *On the origin of isotope-induced chirality in supramolecular polymers of benzene-1,3,5-tricarboxamides*. Manuscript in preparation.
[36] A. J. Markvoort, H. M.M. ten Eikelder, P. A. J. Hilbers, T. F.A. de Greef, E.W. Meijer, *Nat. Commun*. **2011**, *2*, 59.
[37] The additional parameter in the nucleation phase, ΔH_{nuc} is not mentioned for simplicity.
[38] L. S. Bartell, K. Kuchitsu, R. J. Deneui, *J. Chem. Phys.* **1961**, *35*, 1211.
[39] L. S. Bartell, R. R. Roskos, *J. Chem. Phys.* **1966**, *44*, 457.
[40] K. Mislow, R. Graeve, A. J. Gordon, G. H. Wahl, *J. Am. Chem. Soc.* **1964**, *86*, 1733.
[41] J. D. Dunitz, R. M. Ibberson, *Angew. Chem. Int. Ed.* **2008**, *47*, 4208.
[42] C. A. Khatri, Y. Pavlova, M. M. Green, H. Morawetz, *J. Am. Chem. Soc.* **1997**, *119*, 6991.
[43] M. M. Green, C. Khatri, N. C. Peterson, *J. Am. Chem. Soc.* **1993**, *115*, 4941.
[44] H. Goto, E. Yashima, Y. Okamoto, Chirality **2000**, *12*, 396.
[45] N. M. Kishner, *J. Russ. Phys. Chem. Soc*. **1913**, *45*, 1786.
[46] M. M. Green, M. P. Reidy, *J. Am. Chem. Soc.* **1989**, *111*, 6452.
[47] A. R. A. Palmans, J. A. J. M. Vekemans, E. E. Havinga, E. W. Meijer, *Angew. Chem. Int. Ed*. **1997**, *36*, 2648.
[48] M. M. J. Smulders, P. J. M. Stals, T. Mes, T. F. E. Paffen, A. P. H. J. Schenning, A. R. A. Palmans, E. W. Meijer, *J. Am. Chem. Soc.* **2010**, *132*, 620.
[49] Y. Nakano, S. Cantekin, H. M. M. ten Eikelder, A. J. Markvoort, A. R. A. Palmans, E. W. Meijer, *Thermally induced cooperative helix-to-helix transformation in a dynamic supramolecular polymer*. Manuscript in preparation.

5

CONSEQUENCES OF COOPERATIVITY IN RACEMIZING SUPRAMOLECULAR SYSTEMS

Abstract. This chapter describes a dynamic cooperative supramolecular chiral aggregate of disc-like molecules showing strong nonlinear racemization kinetics in solution, based on the selective susceptibility of free monomers to base-catalyzed racemization. A theoretical model fully describes the consequences of the cooperativity in this racemizing supramolecular system. This model is also used to predict the non-zero enantiomeric excess in deracemization reactions by adding a stable chiral auxiliary that influences the ratio of labile enantiomers in solution. The enantiomeric excess is fully controlled by the ability of the enantiomers to be included in supramolecular aggregates with opposing chirality under thermodynamic control. The model provides design rules to reach different enantiomeric excesses under racemization conditions and can be used to unravel many open questions in the debate on the origin of chirality.

Part of this work has been accepted for publication:

S. Cantekin, H. M. M. ten Eikelder, A. J. Markvoort, M. A. J. Veld, P. A. Korevaar, M. M. Green, A. R. A. Palmans, E. W. Meijer, *Angew. Chem. Int. Ed.* **2012** *DOI 10.1002/anie.201201701.*

5.1 Introduction

Racemization which arises from the reversible interconversion of enantiomers[1] is governed by simple first-order kinetics.[2] Racemization can occur under a variety of conditions[3-7] and is associated with the disappearance of optical activity.[1] On the other hand, the conversion of a racemic mixture into an excess of one enantiomer (i.e., deracemization) is useful to yield non-racemic products out of a racemic mixture without the tedious intermediate separation of materials.[8,9] In the examples of deracemization, chiral auxiliaries are used to favor the non-racemic product, such as chiral catalysts in dynamic kinetic resolution[10-12] or chiral host-guest interactions.[13,14] In some recent examples, attrition-enhanced Ostwald or Viedma ripening were used to obtain enantiomerically pure crystals from racemic mixtures, in which the preference of the handedness is determined by chiral external forces, including chiral seeds.[15-18] Here we present a supramolecular system based on cooperative self-assembled helicity, which exhibits strong chiral amplification and in which racemization and de-racemization processes being under thermodynamic equilibrium take an unprecedented course.

In earlier work, it was observed that enantiomeric *N*,*N*′,*N*″-trialkylbenzene-1,3,5-tricarboxamide (BTA) molecules form helical supramolecular polymers in solution, which show strong majority rules behavior.[19-22] In a system under majority rules control, the major enantiomer dictates the helical sense of the supramolecular polymer, to which the minor enantiomer adjusts. This unique behavior results in a strong nonlinear relationship between the optical activity of the supramolecular polymer and the overall enantiomeric excess (*e.e.*), which can be described and quantified by using one dimensional Ising models adapted from the theory of covalent helical polymers.[23] Recently, we introduced a novel methodology for quantifying chiral amplification in a two-component self-assembling BTA system by taking into account the dynamic equilibrium between free monomers and the supramolecular polymer and the cooperative growth of the corresponding polymer.[24,25] The underlying methodology is based on a common reaction scheme in which supramolecular polymerization is described as a sequence of stepwise monomer addition and dissociation events. In this model, the equilibrium concentrations of the BTA molecules in the free monomer state and in the aggregated state are predicted as a function of the overall *e.e.* by solving the mass-balance equations for the enantiomeric monomers.[24] Calculations reveal that the majority rules principle in BTA-based supramolecular polymers leads to a nonlinear change in the concentration of enantiomeric free monomers as a function of the overall *e.e.* under the conditions at which BTA monomers are mostly aggregated. In other words, the *e.e.* of the enantiomeric units participating in the aggregate differs from the *e.e.* of the free enantiomeric molecules in the solution except at an *e.e.* of either 0 or 100%. Similar nonlinear effects were observed in asymmetric catalysis as reported by Kagan and co-workers.[26,27]

Inspired by these remarkable predictions, we superimpose on this system racemization of the participating enantiomers and elucidate the effects of cooperativity on reaction kinetics and the nature of the final state. We have adapted the structure of BTA to allow racemization by incorporating phenylglycine octyl ester units, judiciously selected since it may racemize in solution upon the addition of 1,8-diazabicycloundec-7-ene (DBU)[16] (Figure 1). The two-component model (describing the majority rules behavior) was extended to the racemizing system, ultimately revealing the model to be capable of a precise quantitative description of the experimental data obtained. In addition, a new three-component model was introduced in order to obtain new insights into the racemization reaction in the presence of a chiral additive. It is noteworthy to mention that the theoretical analysis described in this chapter was performed by dr. A. J. Markvoort and dr. H. M. M. ten Eikelder.

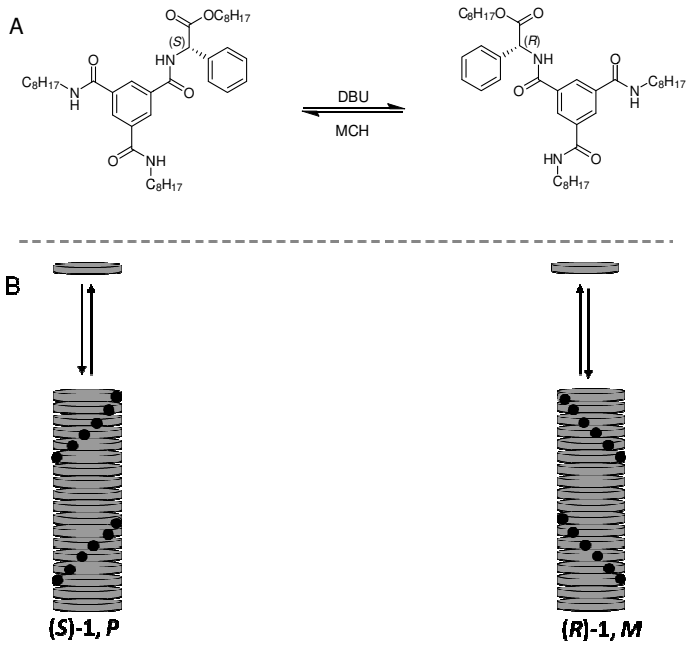

Figure 5.1 A) Chemical structures of *N*-((*R*/*S*)-phenylglycine octyl ester)-*N*',*N*''-di(*n*-octyl)benzene-1,3,5-tricarboxamide (Phg-BTA). Racemization takes place upon addition of DBU in MCH. B) The schematic representation of Phg-BTA-based supramolecular polymers.

5.2 Synthesis and self-assembly of Phg-BTAs

N-((*R*/*S*)-phenylglycine octyl ester)-*N*',*N*''-di(*n*-octyl)benzene-1,3,5-tricarboxamide (Phg-BTA, (*R*)-**1** and (*S*)-**1**) were synthesized by treating 3,5-bis(octylaminocarbonyl)benzoic acid (**3**)[28] with (*R*)- and (*S*)-phenylglycine octyl ester TsOH salt in the presence of carbonyl-1,1'-

diimidazole (CDI) as the coupling agent (Scheme 5.1). The structure and purity of the desired compounds were confirmed by NMR, MALDI-TOF MS and FT-IR spectroscopy. The enantiomeric excess (*e.e.*) of the Phg-BTAs was determined to be 82% for each enantiomer, by using chiral high-performance liquid chromatography (HPLC). After performing preparative HPLC, (*R*)**-1** and (*S*)**-1** were obtained with *e.e.* values of 99.1% and 97%, respectively.

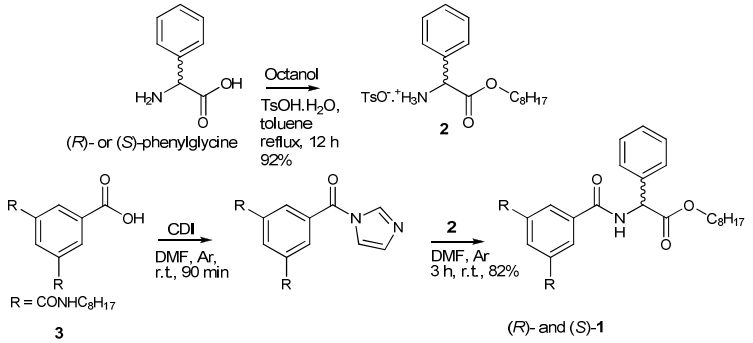

Scheme 5.1. Synthesis of (*R*)- and (*S*)-Phg-BTAs.

The self-assembly behavior of Phg-BTA-based supramolecular polymers was analyzed by UV-vis and CD spectroscopy in methylcyclohexane (MCH) solution (c = 1.2 mM). The hypsochromic shift in the UV-vis spectrum from 216 nm to 206 nm observed for (*S*)**-1** upon cooling from 90 °C to 20 °C strongly suggests the presence of H-type aggregates in solution (Figure 5.2A). Furthermore, (*S*)-**1** and (*R*)-**1** exhibit mirror image CD spectra at 20 °C with $\Delta\varepsilon$ of ±38 L mol^{-1} cm^{-1} at 226 nm (Figure 5.2B) (determined from the samples with *e.e.* > 97%). While the shape and the intensity of the CD spectra are comparable to that of conventional BTAs, the preferred helicity may be different. In contrast to (*S*)-methyl substituted BTAs ((*S*)-**5** in Figure 5.9A)[29,30], (*S*)-**1** exhibits a positive Cotton effect, suggesting the presence of right-handed (*P*) supramolecular polymers. Analogously, (*R*)-**1** shows a negative Cotton effect and indicates the formation of the left-handed (*M*) supramolecular polymers, which is in contrast to that of (*R*)-methyl substituted BTAs ((*R*)-**5** in Figure 5.9A).

[*] Phg-BTAs form stable one-dimensional aggregates in MCH solution which results in reproducible Cotton effects at 20 °C during several months.

[*](*S*)-**1** has one stereocenter while (*S*)-**5** has three and their preferred helix senses are different. *N*-((*S*)-1-methylheptyl)-*N*',*N*''-di(*n*-octyl)benzene-1,3,5-tricarboxamide (asymmetric BTA with one stereocenter positioned next to the carboxamide) forms left-handed (*M*) helical stacks in dilute MCH solution similar to (*S*)-**5**.

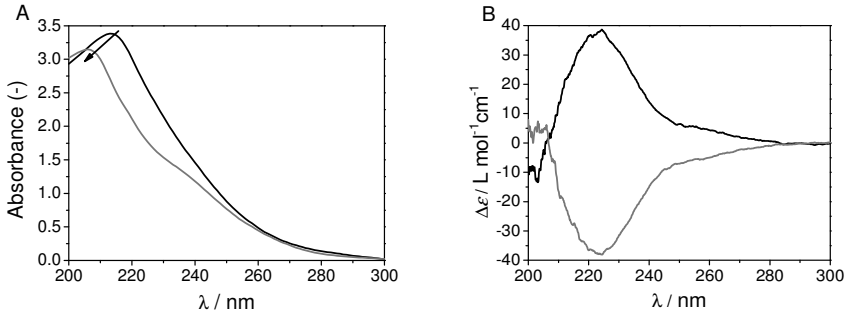

Figure 5.2 A) UV-vis spectra of (*S*)-**1** in MCH (c = 1.2 mM) at 90 °C and 20 °C. The arrow shows the change in λ_{max} from 216 nm to 206 nm upon cooling. B) CD spectra of (*S*)-**1** in MCH (c = 1.2 mM) at 20 °C ($\Delta\varepsilon$ = ±38 L mol^{-1} cm^{-1} at 223 nm). (*S*)-**1** and (*R*)-**1** exhibit mirror image Cotton effects.

5.3 Formation mechanism of the Phg-BTA-based supramolecular polymers

The mechanism of the supramolecular polymerization was investigated with UV-vis and CD spectroscopy as a function of temperature at λ = 225 nm. As evidenced from the spectroscopic data, Phg-BTA-based supramolecular polymers are formed *via* a cooperative mechanism, in which an unfavorable nucleation phase is followed by a favorable elongation phase; the two phases are distinguished by a distinct transition attributed to a temperature of elongation (T_e) (Figure 5.3A and B). Moreover, nearly superimposable temperature-dependent UV-vis and CD spectra indicated that the aggregation and the expression of supramolecular chirality are coupled processes in Phg-BTA system. Temperature-dependent CD cooling curves provide insight into the thermodynamic parameters characterizing the self-assembly mechanism such as the enthalpy of elongation ($\Delta H°_e$), the entropy of elongation ($\Delta S°_e$) and the nucleation penalty ($\Delta H°_{NP}$) by fitting the experimental data with the theoretical model reported by dr. A. J. M. Markvoort and dr. H. M. M. ten Eikelder previously.[24]

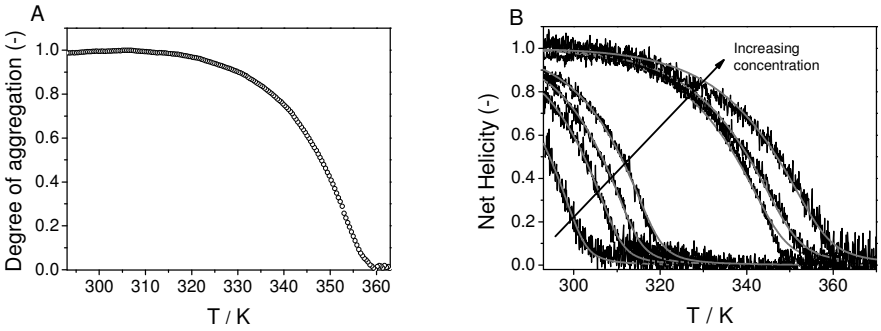

Figure 5.3 A) UV-vis spectra of (*S*)-**1** in MCH (c = 1.2 mM) as a function of temperature monitored at 225 nm with a cooling rate of 1 K min^{-1}. B) Net helicity for (*S*)-**1** in MCH as a function of temperature with varying concentrations (black line) and the corresponding fits (gray line). The arrow shows the increase in the concentration. Concentrations used: 1.4×10^{-5}, 3.0×10^{-5}, 4.4×10^{-5}, 6.5×10^{-5}, 5.8×10^{-4}, 7.2×10^{-4} and 1.2×10^{-3} M. The spectra were monitored at λ = 225 nm with a cooling rate of 1 K min^{-1}. The net helicity is calculated by dividing $\Delta\varepsilon$ by 38 L mol^{-1} cm^{-1}, which is the maximal attainable value for $\Delta\varepsilon$.

In this model, the supramolecular polymerization of (*S*)-**1** into one type of supramolecular polymers (*P*) is considered as a 'single-component system' which consists of a single enantiomer, *S* (for simplicity we use *S* for (*S*)-**1** and *R* for (*R*)-**1**), and forms single type supramolecular polymers, *P*. A cooperative mechanism is assumed, with a nucleus size of two. Thus, the nucleation and the elongation phases are described by the following reactions;

$$S + S \underset{}{\overset{\hat{K}_1}{\rightleftharpoons}} SS \qquad\qquad P + S \underset{}{\overset{K_1}{\rightleftharpoons}} PS$$

(nucleation) (elongation)

The second reaction scheme embodies the elongation phase, during which an arbitrary supramolecular polymer *P* can be extended by addition of *S* monomers. The equilibrium constants $\hat{K}_1$ and K_1 are related to the thermodynamic parameters by

$$\hat{K}_1 = \exp\left(-\left(\Delta H_e^\circ - \Delta H_{NP}^\circ - T\Delta S_e^\circ\right)/\left(RT\right)\right) \tag{5.1}$$

$$K_1 = \exp\left(-\left(\Delta H_e^\circ - T\Delta S_e^\circ\right)/\left(RT\right)\right) \tag{5.2}$$

where $\Delta H°_e$ and $\Delta S°_e$ are the (standard) enthalpy and entropy changes in the elongation phase, respectively, and the enthalpy change in the nucleation phase has an additional nucleation penalty ($\Delta H°_{NP}$) while the entropies in the nucleation and the elongation phases are equal. Nucleation penalty is a measure of cooperativity in systems that self-assemble in a

cooperative fashion; this parameter is considered to have a value of zero for isodesmic self-assembly since nucleation phase does not take place in isodesmic self-assembly.

The equilibrium concentrations of the various polymers and their compositions were computed using the *principle of detailed balance,* which states that in thermodynamic equilibrium, each individual component describing the overall reaction is in equilibrium, as described previously. The corresponding fit of the temperature-dependent CD spectra at various concentrations of (*S*)-**1** in MCH with the theoretical model resulted in the thermodynamic parameters of the self-assembly process as the enthalpy of elongation $\Delta H°_e$ = −72.4 kJ mol^{-1}, entropy of elongation $\Delta S°_e$ = −0.15 kJ mol^{-1} and the nucleation penalty $\Delta H°_{NP}$ = −12.2 kJ mol^{-1}. The thermodynamic parameters determined for the self-assembly of methyl substituted BTA analogue ((*R*)- and (*S*)-**5** in Figure 5.9A) in MCH by using the same 'single-component model' revealed $\Delta H°_e$ = −72.0 kJ mol^{-1}, $\Delta S°_e$ = −0.13 kJ mol^{-1} and $\Delta H°_{NP}$ = −30.0 kJ mol^{-1}. The nucleation penalty ($\Delta H°_{NP}$) is a measure of cooperativity. The enthalpy gain in the elongation step (in a cooperative growth mechanism) is $\Delta H°_e$ and the enthalpy gain in the nucleation step is $\Delta H°_e$-$\Delta H°_{NP}$. Thus, the negatively larger $\Delta H°_{NP}$ makes the enthalpy gain in the nucleation step lower. This means an unfavorable nucleation step and the dimers formed in this step are unstable and they fall apart. Thus the system with a negative, large $\Delta H°_{NP}$ implies a more cooperative system. The negatively larger nucleation penalty suggests that the self-assembly of (*S*)-**5** is more cooperative than that of (*S*)-**1** in MCH.

5.4 Majority rules behavior

Majority rules experiments were performed by mixing solutions of the two enantiomers (*S*)-**1** and (*R*)-**1** in different ratios. Each mixture was analyzed by CD spectroscopy (Figure 5.4A) and the net helicity was plotted (at λ = 225 nm) as a function of the *e.e.* where *e.e.* is defined as the difference between the total enantiomeric monomer concentrations added to the solutions (*e.e.* = ([(*S*)-**1**]-[(*R*)-**1**])/([(*S*)-**1**]+[(*R*)-**1**])×100%) and the net helicity is defined as the difference between the fraction of *M*- and *P*-type helical aggregates (net helicity = ([*P*]-[*M*])/([*P*]+[*M*]).[19-23] The mixing experiment resulted in a nonlinear change in the net helicity as a function of the *e.e.* (Figure 5.4B) suggesting that Phg-BTA-based supramolecular polymers show majority rules behavior when the two enantiomers are mixed in varying ratios. However, the effect is smaller compared to the methyl substituted BTA analogues.[21,22]

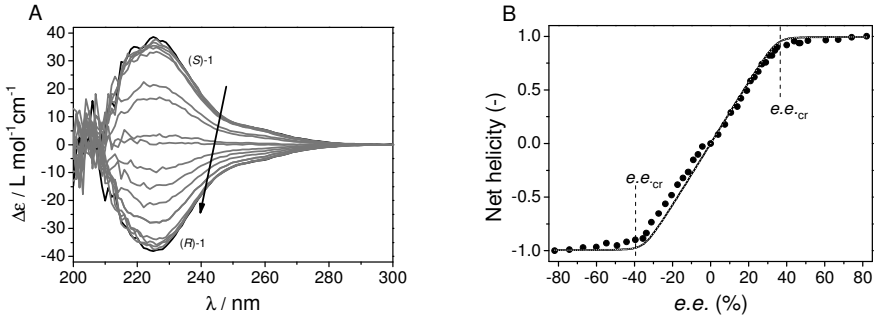

Figure 5.4 A) Majority-rules experiment, CD spectra of scalemic mixtures of (*S*)-**1** and (*R*)-**1** (c = 1.2 mM in MCH) with varying ratios. Arrow indicates increasing amount of (*R*)-**1**, starting from pure (*S*)-**1**. B) The net helicity as a function of the *e.e.* obtained from the majority rules experiment by mixing solutions of (*S*)-**1** and (*R*)-**1** (c = 1.2 mM in MCH) at 20 °C, obtained from Figure 5.4A (black dot) and the corresponding fit (black line). The net helicity is calculated by dividing $\Delta\varepsilon$ at every *e.e.* by 38 L mol^{-1} cm^{-1}, which is the maximal attainable value for $\Delta\varepsilon$.

The origin of this nonlinear behavior may be explained by a theoretical model[24] for a two-component self-assembling Phg-BTA system. In this model, the two enantiomers can aggregate into supramolecular polymers with two types of helicity, where the favorable enthalpy of elongation ($\Delta H°_e$) is reduced by a mismatch penalty ($\Delta H°_{MMP}$)[19-24] when a monomer ((*R*)-**1** or (*S*)-**1**) assembles into its non-preferred helical sense. We determined the value of the $\Delta H°_{MMP}$ (between (*R*)-**1** and (*S*)-**1**) to be -1.7 kJ mol^{-1} for this system by fitting the majority rules experiment described in Figure 5.4B with the two-component model. Application of the same model to the majority rules experiment performed by mixing the enantiomers of methyl substituted BTAs results in a larger absolute value of mismatch penalty ($\Delta H°_{MMP}$ = −2.1 kJ mol^{-1})[24] compared with Phg-BTAs. Studies revealed that a smaller (absolute) value of $\Delta H°_{MMP}$ imply a stronger majority rules effect (i.e., more favorable mixing of the enantiomeric monomers, less conglomerate-like behavior). However, the majority rules effect is weaker in the Phg-BTA system although the absolute value of the $\Delta H°_{MMP}$ is lower than that of conventional BTAs (also evidenced by $e.e._{cr}$ values (≈ 37% for (*S*)-**1** and ≈ 28% for (*S*)-**5** in Figure 9A). A high $e.e._{cr}$ value may imply a less favorable mixing of the enantiomeric monomers, thus weak majority rules effect). This suggests that the molecular structure of the BTA monomers has an influence on the chiral amplification behavior.[†]

Furthermore, the concentrations of the enantiomeric units inside and outside the aggregates were predicted as a function of the *e.e.* (along the abscissa) by the same two-

[†]For *N*-((*R*/*S*)-3,7-dimethyloctyl)-*N*',*N*''-di(*n*-octyl)benzene-1,3,5-tricarboxamide (asymmetric BTA with one stereocenter positioned second carbon next to the carboxamide); $\Delta H°_{MMP}$ = -1 kJ mol^{-1} and $e.e._{cr}$ ≈ 18%.

component model (Figure 5.5). The ordinate in Figure 5.5A gives the predicted concentrations of the monomers that are not residing in the supramolecular polymer. According to this two-component model, two regimes, separated by a certain critical *e.e.* (*e.e.*$_{cr}$), can be distinguished. In the first regime, where $|e.e.| < e.e._{cr}$, the free monomer concentrations of both enantiomers (the black and gray lines) (those not participating in the aggregate) have a weak dependence on *e.e.*, and are almost equal with a slight excess for the major enantiomer. In the second regime, where $|e.e.| > e.e._{cr}$, the free monomer concentration of the major enantiomer increases, whereas the free monomer concentration of the minor enantiomer decreases (i.e., moving to the right along the abscissa) leading to a large difference between the concentrations of the enantiomers in the free monomer state as the overall *e.e.* increases. On the other hand, the concentrations of the enantiomeric units within the aggregated state, the supramolecular polymers, change as seen in the Figure 5.5B. In the first regime, where $|e.e.| < e.e._{cr}$ the number of units entering the major helical sense is increasing (i.e., moving to the right along the abscissa). Both enantiomeric units enter this major aggregate from the solution, while the number of units entering the minor helical sense decreases linearly until the minor aggregate no longer exists at *e.e.*$_{cr}$.

The mathematical model anticipates a nonlinear relationship between the concentration of the free monomers and the *e.e.* Initially, free monomer pool is enriched with (*S*)-**1** monomers. (*R*)-**1** monomers are mixed with (*S*)-**1** giving rise to an increase in the concentration of (*R*)-**1** in the free monomer pool. As a result of the majority rules behavior, (*R*)-**1** monomers assemble into the majority helical sense which is *P* formed by (*S*)-**1**. However, after reaching a certain *e.e.* value (*e.e.*$_{cr}$), the concentration of (*R*)-**1** monomers becomes large enough to form its own helical stacks, which are of the type *M*. Thus, the concentration of *P*-type supramolecular polymers decreases while that of *M* increases. Below the absolute value of the *e.e.*$_{cr}$, the concentration (*R*)-**1** and (*S*)-**1** monomers is almost equal and does not change significantly as a function of *e.e.* The nonlinear change in the free monomer pool is a result of aggregation, where the aggregates exhibit majority rules behavior. Such behavior is also observed in methyl substituted BTA self-assembly.[24] The expression 'nonlinear effects' was used to describe the disproportionality between the *e.e.* of the product and the *e.e.* of the chiral auxiliary in asymmetric synthesis.[26,27] Although the chiral amplification in Phg-BTA-based supramolecular polymers is a different phenomenon than asymmetric synthesis, the observed effects in both cases are coincidentally similar.

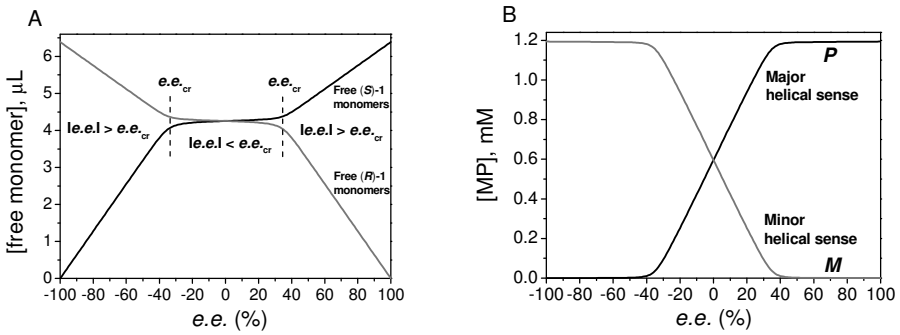

Figure 5.5: A) The computed concentrations of free (*S*)-**1** and (*R*)-**1** monomers, B) the computed concentrations of the monomers participating in the *P* and *M* type supramolecular polymers, as a function of *e.e.* at 20 °C (c_{tot} = 1.2 mM). The calculations are based on the majority rules experiments and are based on following thermodynamic parameters; $\Delta H°_{MMP}$ = −1.7 kJ mol^{-1}, $\Delta H°_{e}$ = −72.4 kJ mol^{-1}, $\Delta H°_{NP}$ = −12.2 kJ mol^{-1}, $\Delta S°_{e}$ = −0.15 kJ mol^{-1} K^{-1}.

5.5 Racemization of Phg-BTAs

We now turn our attention to the experimental consequence of adding a racemization reaction to this system. We investigated the racemization reaction of (*S*)-**1** molecules upon addition of DBU (1 eq.) in MCH. At 80 °C almost all (*S*)-**1** and (*R*)-**1** monomers are in the molecularly dissolved state ($c_{free\ monomer}$ ≈ 9×10^{-4} M) and complete racemization (*e.e.* = 0%) is reached within 3 h. The racemization reaction follows first-order reaction kinetics (i.e., the natural logarithm of the *e.e.* changes linearly as a function of time; Figure 5.6A). However, at 20 °C when (*S*)-**1** molecules are almost fully aggregated and only relatively few free monomers ($c_{free\ monomer}$ ≈ 6×10^{-6} M) are present in solution, the racemization process proceeds extremely slowly and shows a remarkable and unprecedented deviation from first-order reaction kinetics (Figure 5.6B). Although the effect of temperature on the reaction rate is inevitable, the unusually low racemization rate cannot only be explained by the change in temperature. It is proposed that the racemization kinetics at low temperature arise from the fact that only free monomers, those outside the aggregate, can racemize. Furthermore, the shape of the curve for the *e.e.* as a function of time at 20 °C suggests that the racemization of Phg-BTA can be described by two distinct kinetic regimes; one regime ($|e.e.| > e.e._{cr}$) has a higher rate than the other ($|e.e.| < e.e._{cr}$). The *e.e.* value at the interface between the two regimes correlates with the $e.e._{cr}$ observed in the majority rules experiment. Similar two-rate kinetics were observed previously for the racemization of asparagine.[31] It was suggested that asparagine simultaneously hydrolyses into aspartic acid and racemizes during the transformation. The two species, asparagine and aspartic acid, give rise to different

racemization kinetics; an initial high rate resulting from aspartic acid racemization followed by a lower rate due to the asparagine racemization.[31]

By applying the equilibrium model developed by Markvoort and ten Eikelder[24], we determined the racemization rate constant. The racemization rate constant, *k*, and it was found by minimizing the total squared error of the experimentally found and theoretically computed racemization curves. The minimum was found for $k = 0.517\ h^{-1}$, which led to the predicted racemization curve (black line in Figure 5.6B). The predicted racemization curve is in excellent agreement with our experimental findings.

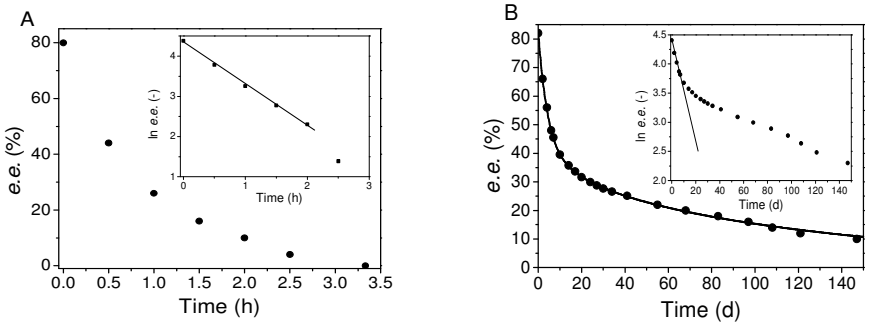

Figure 5.6: A) Racemization of (*S*)-**1** in the presence of DBU (1 eq.) in MCH (c = 1.2 mM) at 80 °C, monitored by chiral HPLC. The inserted graph shows the natural logarithm of *e.e.* as a function of time with corresponding fit for first-order reaction kinetics (black line), $k = 1.03\ h^{-1}$. B) Racemization of (*S*)-**1** upon addition of DBU (1 eq.) in MCH (c = 1.2 mM) at 20 °C (black dot) with predicted *e.e.* values using $k = 0.517\ h^{-1}$ over time (black line). The inserted graph shows the natural logarithm of *e.e.* as a function of time with the corresponding fit for the first-order reaction kinetics (black line).

5.5.1 Racemization of (*R*)-*N*-benzoylphenylglycine octyl ester

The racemization of (*R*)- and (*S*)-*N*-benzoylphenylglycine octyl ester ((*R*)-**4** and (*S*)-**4**) (Scheme 5.2) which is the mono-substituted analogue of (*S*)-**1** was investigated in order to compare the racemization behavior of (*S*)-**1** with a compound that does not self-assemble by means of threefold hydrogen bonding. The formation of helical supramolecular polymers was not observed for (*R*)-**4** as evidenced by CD and UV-vis spectroscopy in MCH (c = 1.2 mM). The racemization of (*R*)-**4** in MCH in the presence of DBU (1 eq.) at 20 °C resulted in first-order reaction kinetics. The complete racemization (*e.e.* = 0%) was achieved in 132 days with a rate constant of $k = 0.02\ h^{-1}$ (Figure 5.7). (*R*)-**4** is essentially molecularly dissolved at 20 °C, and thus has much larger free monomer concentration than that of (*S*)-**1** under the same conditions. However, the difference in the racemization times at 20 °C is insubstantial.

Furthermore, (*R*)-**4** racemizes much more slowly in the presence of DBU (1 eq.) at 80 °C (complete racemization was reached in 25 h, $k = 0.10\ h^{-1}$) while the racemization of (*S*)-**1** is much faster (3 h, $k = 1.03\ h^{-1}$) under the same conditions.

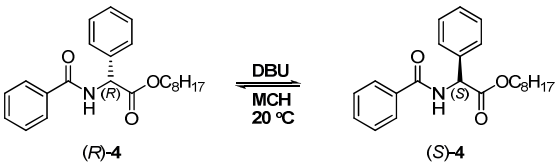

Scheme 5.2: Racemization of (*R*)-**4** in MCH (c = 1.2 mM) at 20 °C.

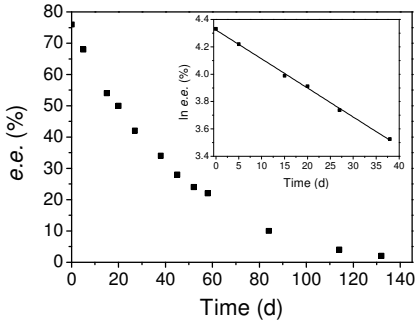

Figure 5.7: Racemization of (*R*)-**4** in MCH (c = 1.2 mM) at 20 °C upon addition of DBU (1 eq.). The inset shows the linear fit for the first-order reaction mechanism the slope of which gives the rate constant, $k = 0.02\ h^{-1}$.

These results suggest that the acidity of the labile hydrogen in (*R*)-**4** is lower than that of (*S*)-**1,** leading to slower reaction kinetics. Possibly, the additional octyl side chains in (*S*)-**1** influence the acidity of the labile proton in the molecule. Similar reactivity differences between mono- and triphenylalanine substituted BTAs towards thermolysin-catalyzed peptide coupling were previously reported.[32] Although the reactivity of (*S*)-**1** and (*R*)-**4** towards DBU is not comparable due to the different chemical structures, the results clearly indicate that in the absence of aggregation first-order racemization kinetics are observed.

5.6 Deracemization of Phg-BTA-based supramolecular polymers

5.6.1 Theoretical approach

The theoretical model discussed above, both with and without racemization provides design rules to reach a non-racemic situation under thermodynamic control during the racemization of Phg-BTA. Chiral additives that form *P* type supramolecular polymers were

used as 'sergeants' in Phg-BTA self-assembly. These additives are similar to (*S*)-**1** except for their chemical stability towards base. The concentrations of the free monomers in Figure 5.8A and the monomer concentrations participating in the aggregates in Figure 5.8B were calculated using the same theory and thermodynamic parameters which had been applied for results in Figure 5.5 but with the addition of 8 mol% of the sergeant indicated by the dashed line. As depicted in Figure 5.8A, the free monomer concentrations in solution change in a non-symmetrical manner as a function of the total *e.e.* because of the presence of the sergeant. In contrast to the results in Figure 5.5A, the concentrations of free (*S*)-**1** (black line) and (*R*)-**1** (gray line) become equal at a non-zero *e.e.* value. As the sergeant preferably forms *P*-type aggregates with monomer (*S*)-**1**, the concentration of free (*S*)-**1** monomers decreases more strongly than that of (*R*)-**1**. Interestingly, this non-zero *e.e.* value is approximately equal to $e.e._{cr}$ from the two-component system.

When adding a racemization reaction to this three-component system, racemization between (*S*)-**1** and (*R*)-**1** will consume free (*R*)-**1** monomers to form (*S*)-**1** monomers as long as the free (*R*)-**1** monomer concentration is higher than the (*S*)-**1** monomer concentration. As a result of this, the total *e.e.* increases to $e.e._{cr}$, including all free enantiomers in solution and the ones participating in the aggregates. Because the sergeant favors the helix (*P*) formed by the (*S*)-**1** monomer, the helices formed have the (*S*)-**1** enantiomer in the majority. The (*R*)-**1** monomers existing in this *P* helix adjust to the major helical sense. In the equilibrium state reached in this process, the free (*S*)-**1** and (*R*)-**1** monomer concentrations are equal. The overall *e.e.* is determined by the *e.e.* value of these free monomers in combination with the *e.e.* value within the aggregates, which favors (*S*)-**1**. The result is a 32% *e.e.* favoring the (*S*)-**1** enantiomer.

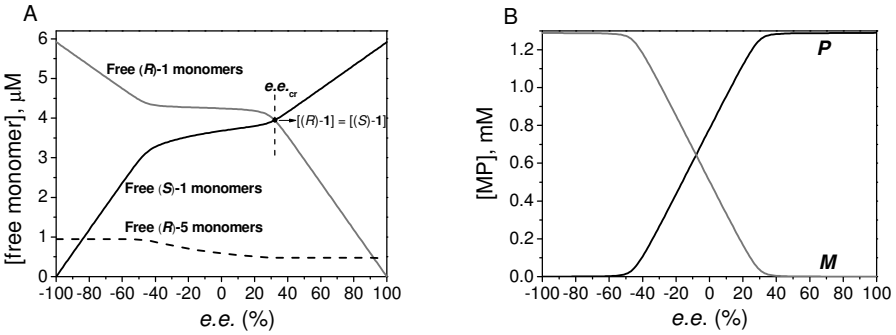

Figure 5.8: A) The computed concentrations of free monomers (*S*)-**1** (black line), (*R*)-**1** (gray line) and (*R*)-**5** (dashed line), B) the computed concentrations of monomers residing in the *P* (black line) and *M* (gray line) type supramolecular polymers, as a function of *e.e.* at 20 °C, c_{tot} (Phg-BTA) = 1.2 mM. $\Delta H°_{MMP}$ (between (*R*)-**1** and (*S*)-**1**) = −1.7 kJ mol^{-1}, $\Delta H°_{e}$ = −72.4 kJ mol^{-1}, $\Delta H°_{NP}$ = −12.2 kJ mol^{-1}, $\Delta S°_{e}$ = −0.15 kJ mol^{-1} K^{-1}, and 8 mol% sergeant. The

thermodynamic parameters for sergeant: $\Delta H°_{MMP,ser}$ (between (*R*)-**1** and sergeant) = −1.7 kJ mol^{-1}, $\Delta H°_{e,ser}$ = −72.4 kJ mol^{-1}, $\Delta S°_{e,ser}$ = −0.15 kJ mol^{-1} K^{-1}.

5.6.2 Experimental approach

The theoretical predictions were validated with experiments by preparing mixtures of (*S*)-**1** and (*R*)-**1** in MCH (c = 1.2 mM) with varying *e.e.* values. A small amount (8 mol%) of non-racemizing (*S*)-methyl-substituted BTA ((*S*)-**5**) was added as 'sergeant' to these solutions (Figure 5.9A). The racemization reaction at room temperature was initiated by adding DBU (1 eq.) to each solution. Samples were collected and the total *e.e.* values were measured by chiral HPLC over time. As shown in the HPLC trace (Figure 5.9B-C), the experiment starts with equal amounts of (*R*)-**1** and (*S*)-**1** (*e.e.* = 0%) and leads to the increase in *e.e.* favoring (*R*)-**1** in the presence of (*S*)-**5** over 40 days.

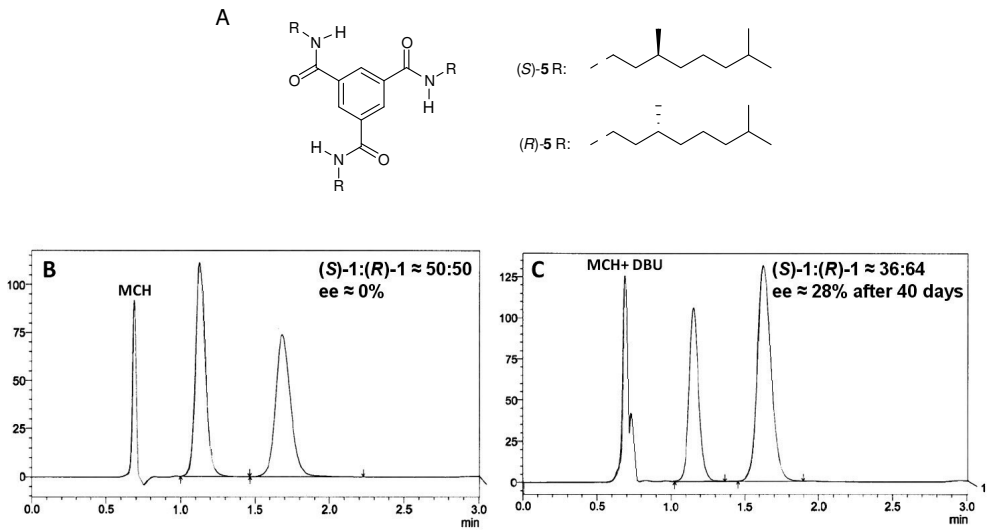

Figure 5.9: A) Molecular structures of 'sergeants', methyl-substituted BTAs. HPLC traces of B) Deracemizing mixture initial state, *e.e.* = 0.26% in the presence of DBU (1 eq.) and (*S*)-**5** (8 mol%). C) The *e.e.* of the mixture after 40 days, *e.e.* = 28% favoring (*R*)-**1** enantiomer.

Racemization in the presence of (*R*)-**5** leads to the formation of (*S*)-Phg-BTA ((*S*)-**1**) in excess and results in an increase in *e.e.* up to 32% independent of the initial total *e.e.* (Figure 5.10A). Similarly, application of (*S*)-methyl-substituted BTA, (*S*)-**5**, as the 'sergeant' resulted in the formation of (*R*)-Phg-BTA ((*R*)-**1**) in excess and the *e.e.* changed to −32% (Figure 5.10B). The racemization process was monitored over 120 days, during which precipitation was not

observed. These experimental results are in excellent agreement with the predicted maximum *e.e.* value that can be retained by the system.

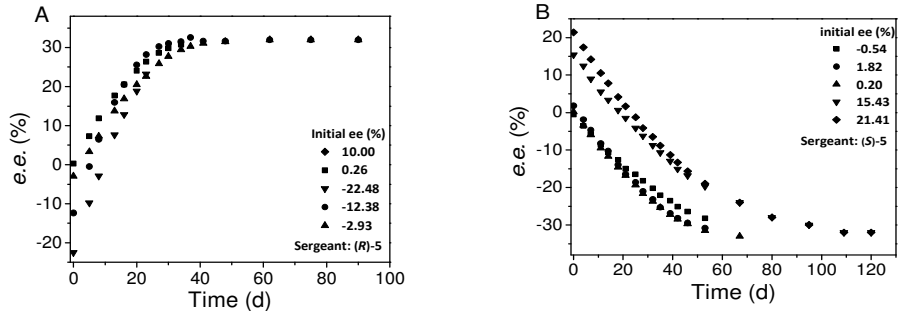

Figure 5.10: The change in *e.e.* in time for mixtures of Phg-BTA with DBU added (1 eq.) and 'sergeant' (8 mol%) at 20 °C, c_{tot} (Phg-BTA) = 1.2 mM in MCH, with different initial *e.e.* values. A) (*R*)-**5** as sergeant. B) (*S*)-**5** as sergeant.

We measured CD spectra of the sample with an initial *e.e.* of 0.26% (including (*R*)-**5** and DBU, c = 1.2 mM in MCH) over time in order to verify the presence of hydrogen bonded helical stacks of (*S*)-**1** in MCH during the deracemization process. The initial Cotton effect is 0 mdeg for the corresponding racemic mixture indicating that the number of *P* and *M* helices in solution is almost equal. As the deracemization reaction proceeds, the concentration of the (*S*)-**1** increases, so does the concentration of *P*-type helical stacks, leading to the evolution of a Cotton effect ($\Delta\varepsilon$ = 10 L mol^{-1} cm^{-1}) over 10 days (Figure 5.11A). The $\Delta\varepsilon$ increases in time and reaches 25 L mol^{-1} cm^{-1} in 16 days as the *e.e.* increases to 20% in favor of the (*S*)**-1** enantiomer. While CD spectroscopy confirms the presence of helical aggregates in solution, UV-vis spectroscopy indicates that the hydrogen bonded assemblies are present. The UV-vis spectra of the corresponding mixture showed that the characteristic absorption at λ_{max} = 206 nm, typical for hydrogen bonded Phg-BTA aggregates, remained constant during deracemization. Since DBU has an absorption in the same region as Phg-BTAs, we observed remarkably large absorptions (Figure 5.11B). Slight changes were detected in the intensity of absorption due to the small changes in concentration over time. In order to determine the change in net helicity over time more accurately, we plotted anisotropy factor ($g = \Delta\varepsilon/\varepsilon$) against time (Figure 5.11C). The linear increase in g value over time confirms the formation of *P* helices predominantly. Only a few measurements are shown in Figure 5.11C for clarity. Only the linear part of the graph is shown and the nonlinear effect due to the majority rules is not visible in the graph.

Furthermore, deracemization experiments performed under the same conditions (1 eq. DBU, 8 mol% sergeant) by using *N*-benzoylphenylglycine octyl ester (*R*)-**4** and (*S*)-**4** led to complete racemization (*e.e.* = 0%) suggesting that the assembly into ordered supramolecular

structures by means of threefold hydrogen bonding is required in the deracemization process discussed here.

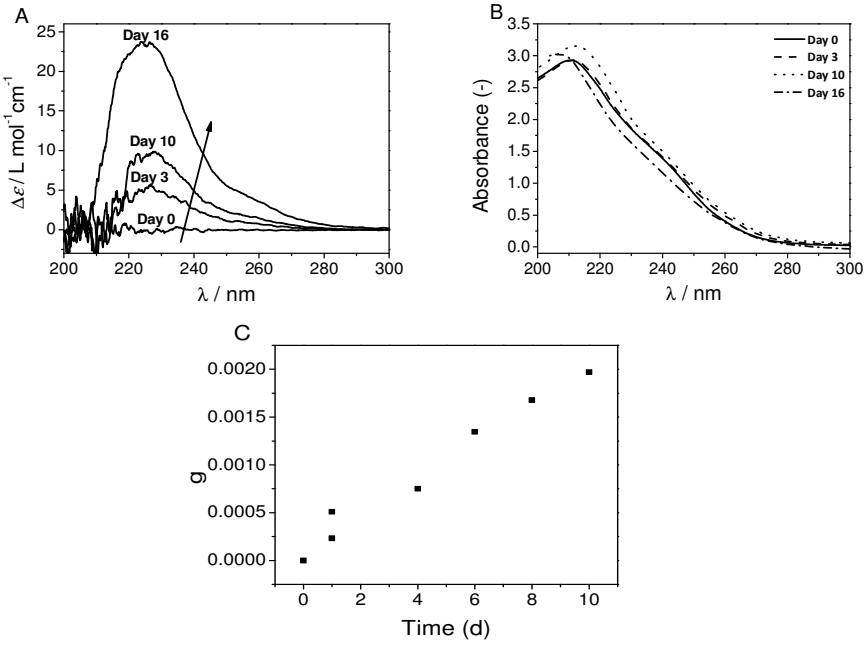

Figure 5.11: A) CD spectra of initially racemic Phg-BTA mixture (*e.e.* = 0.26%) including (*R*)-**5** (8 mol%) and DBU (1 eq.) in MCH (1.2 mM) at 20 °C. The arrow shows the evolution of Cotton effect over time. B) The UV-vis spectra of initially racemic Phg-BTA mixture (*e.e.* = 0.26%) including (*R*)-**5** (8 mol%) and DBU (1 eq.) in MCH (1.2 mM) at 20 °C. C) The change in anisotropy factor (*g*) in time.

5.6.3 Deracemization of Phg-BTA-based supramolecular polymers in stirred solutions

$NaClO_3$ is an achiral compound; however, it crystallizes in enantiomeric D- and L- forms. Studies by Kondepudi and coworkers revealed that crystallization in an unstirred solution produces a statistically equal number of D- and L-crystals. In contrast, crystallization in a *stirred* achiral solution reproducibly results in *e.e* values of the crystals greater than 99%, stochastically (i.e., favoring either D- or L-form).[33,34] The mechanism of this dramatic chiral symmetry breaking of achiral $NaClO_3$ crystals was rationalized by the secondary nucleation which is the production of crystal nuclei from an existing crystal due to the motion of the solution around.[35] The results suggested that stirring as well as the stirring rate[36] has a crucial effect on the chiral symmetry breaking of the racemic or achiral compounds in a

heterogeneous system. Although (de)racemization in Phg-BTA system is homogeneous and crystallization does not take place, the effect of stirring on the corresponding process was investigated. The HPLC analysis of the stirred racemizing (in the presence of 1 eq. DBU, Figure 5.12A) and deracemizing solutions (in the presence of 1 eq. DBU, and 8 mol% sergeant, Figure 5.12B) over time did not lead to any differences in terms of the reaction rate and the final *e.e.* (= 32%) when compared to the unstirred solutions. Our findings confirm that (de)racemization of Phg-BTAs is indeed homogeneous. Stirring, which enhances the growth of enantiomeric crystals and ultimately leads to a divergence from chiral symmetry in heterogeneous systems, is ineffective in a homogeneous system described here. Hence, the Phg-BTA system discussed here is under thermodynamic equilibrium.

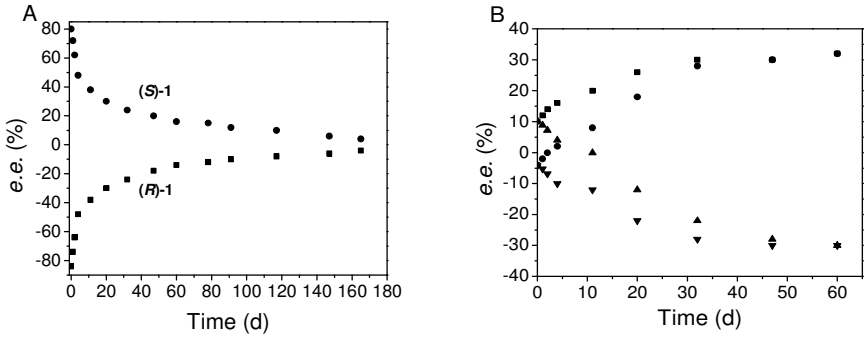

Figure 5.12: A) Racemization of (*S*)-**1** and (*R*)-**1** in MCH (c = 1.2 mM) with DBU (1 eq.) at 20 °C with stirring. B) The change in *e.e.* over time (square: initial *e.e.*: 10%, sergeant: (*R*)-**5**, triangle up: initial *e.e.*: 10%, sergeant: (*S*)-**5**, dot: initial *e.e.*: −4%, sergeant: (*R*)-**5**, triangle down: initial *e.e.*: −4%, sergeant: (*S*)-**5**.

5.7 Factors affecting the final *e.e.* of the Phg-BTA-based supramolecular polymers

5.7.1 Theoretical approach

The *e.e.* of the racemizing Phg-BTA monomers reaches 32% in the presence of a small amount of sergeant as predicted by the theoretical model described above. The factors influencing the maximum *e.e.* value of the system were investigated by using a similar approach. The effect of various parameters such as initial *e.e.* value of the system, concentration of the Phg-BTA, concentration of the sergeant, mismatch penalty between the sergeant and Phg-BTA monomers($\Delta H°_{MMP,ser}$), mismatch penalty between (*R*)-**1** and (*S*)-**1**($\Delta H°_{MMP}$), cooperativity of the system are summarized here, respectively.

Firstly, the initial *e.e.* value of the system was analyzed. As shown in the previous sections, the system reaches the equilibrium *e.e.* value and the racemization stops since the concentration of the enantiomeric monomers is equal at this critical point regardless of the initial *e.e.* value (Figure 5.8). Hence, the initial *e.e.* values do not affect the final *e.e.* retained by the system. Secondly, an increase in the concentration of Phg-BTA monomers does not influence the final *e.e.* of the system. Theory predicts that almost all monomers are in the self-assembled state beyond a critical monomer concentration in a cooperative system (Section 1.3. and Figure 1.6). Thus addition of more monomers into the system –beyond this critical concentration– does not change the concentration of the free monomers (i.e., all additional monomers assemble to form polymers). However, when a low concentration of Phg-BTA is used (i.e., the free monomer concentration is below this critical monomers concentration), the concentration of free monomers is high and that of polymeric species is low. Since the driving force for deracemization is the presence of long aggregates, the increase in the *e.e.* would not be observed at low concentration and the system would racemize completely.

Furthermore, the sergeant concentration does not affect the final *e.e.* value. Figure 5.13A shows that when 20 mol% sergeant is used, the final *e.e.* of the system is the same (= 32%) as the experiment when 8 mol% sergeant was used. Co-assembly of sergeant, methyl-substituted BTA ((*R*)-**5**), and Phg-BTA ((*S*)-**1**) is more favored (than the co-assembly of (*R*)-**5** and (*R*)-**1**) as a result of the mismatch penalty introduced to the system when (*R*)-**5** co-assembles with (*R*)-**1** (*vide supra*). Thus the increase in concentration of (*R*)-**5** leads to only an increase in concentration of free (*R*)-**1** monomers. This may have an influence on the racemization rate of the monomer; however, experimental and theoretical studies on the kinetics of the system have not been performed. Finally, the effect of mismatch penalty between (*R*)-**5** and (*R*)-**1** was investigated. The absolute value of the mismatch penalty $|\Delta H°_{MMP}|$ between the two species was increased from $|\Delta H°_{MMP}|$ = 1.7 kJ mol^{-1} to 5 kJ mol^{-1}. This only led to a larger concentration difference between (*R*)-**1** and (*S*)-**1** while the final *e.e.* remained the same and equals 32% (Figure 5.13B).

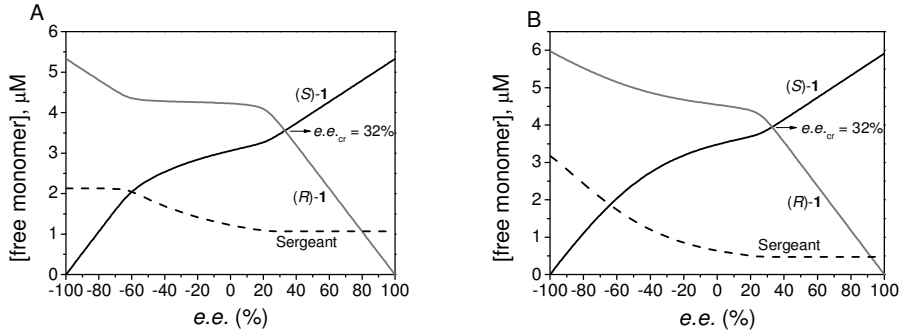

Figure 5.13: A) The computed concentrations of free monomers ((*S*)-**1** (black line), (*R*)-**1** (gray line) and (*R*)-**5** (dashed line)) as a function of *e.e.* at 20 °C, c_{tot} (Phg-BTA) = 1.2 mM, based on the same thermodynamic parameters but 20 mol% sergeant. B) The computed concentration of free monomers ((*S*)-**1** (black line), (*R*)-**1** (gray line) and (*R*)-**5** (dashed line)) as a function of *e.e.* at 20 °C, based on the same thermodynamic parameters but $\Delta H°_{MMP,ser}$ (between (*R*)-**1** and (*R*)-**5**) = −5 kJ mol^{-1}.

The mismatch penalty ($\Delta H°_{MMP}$) between the two enantiomers is the energy barrier when an enantiomeric monomer assembles into its unpreferred helical sense.[21,23] A high (absolute) value of $|\Delta H°_{MMP}|$ in a self-assembled BTA system implies a weak majority rules effect, thus the assembly of an (*R*)- or (*S*)-chiral BTA monomer into its unpreferred helical sense is unfavored. The calculations revealed that the value of the maximum *e.e.* in a deracemizing Phg-BTA system is mainly dependent on the $\Delta H°_{MMP}$ between (*R*)-**1** and (*S*)-**1**. As shown in Figure 5.14A, the model predicts that in a system with a $|\Delta H°_{MMP}|$ increased from the value of the current experiment 1.7 kJ mol^{-1} to 5.0 kJ mol^{-1} an *e.e.* value of 74% in the presence of the sergeant is reached.

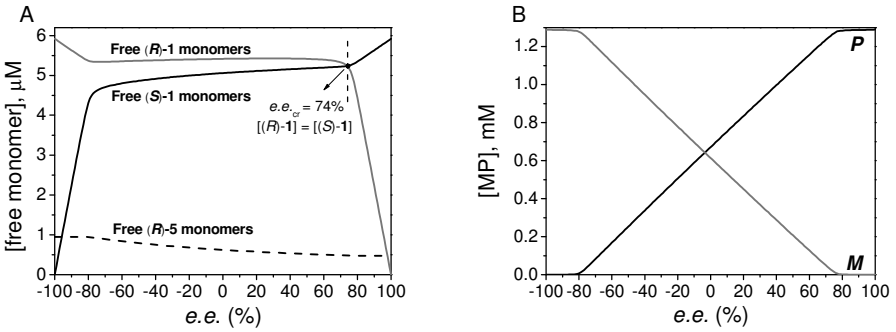

Figure 5.14: A) The computed concentrations of free monomers (*S*)-**1** (black line), (*R*)-**1** (gray line) and (*R*)-**5** (dashed line), B) the concentrations of monomers residing in the *P* (black line) and *M* (gray line) type supramolecular polymers, as a function of *e.e.* at 20 °C, c_{tot} (Phg-BTA) = 1.2 mM. $\Delta H°_{MMP}$ (between (*R*)-**1** and (*S*)-**1**) = −5.0 kJ mol^{-1}, $\Delta H°_{e}$ = −72.4 kJ mol^{-1}, $\Delta H°_{NP}$ = −12.2 kJ mol^{-1}, $\Delta S°_{e}$ = −0.15 kJ mol^{-1} K^{-1}, and 8 mol% sergeant, (*R*)-**5**. The thermodynamic parameters for sergeant are the same.

These results imply that a conglomerate system, in which the mismatch penalty is infinite, is required for reaching high enantiomeric excesses. In conglomerate crystals where every unit cell consists of a single enantiomer, the mismatch penalty between the enantiomeric units is infinitely large. As a result of this infinitely large mismatch penalty, deracemization of racemic conglomerate crystals results in the *e.e.* values larger than 99%.[16-18,32-35] The ultimate goal in the BTA deracemization is the production of new BTA molecules having a large mismatch penalty and forming conglomerate self-assemblies in solution in order to achieve *e.e* > 99%. The introduction of sterically hindered chiral groups in the alkyl side chains of the BTA molecules might lead to large mismatch penalty values, thus large *e.e.* values in deracemization.

The mechanism of self-assembly is another factor affecting the deracemization process. We investigated the effects of the two supramolecular polymerization mechanisms observed in BTA self-assembly; cooperative and isodesmic.[37] In a cooperative supramolecular polymerization, unfavored formation of a nucleus is followed by a favored elongation step, while these two phases are not observed in isodesmic supramolecular polymerizations. The concentration of free monomers inside and outside the supramolecular polymers bearing isodesmic self-assembly behavior as a function of *e.e.* was predicted by applying the same thermodynamic parameters. In the absence of the 'sergeant', concentrations of the free monomers change almost linearly as a function of the *e.e.* value. Moreover, in contrast to the cooperative self-assembly system, the two-regimes which are separated by an $e.e._{cr}$ are not observed in an isodesmic system (Figure 5.15A). In the presence of the 'sergeant' (8 mol%),

the free monomer concentrations become equal at a non-zero *e.e.* value (= 13%) (Figure 5.15B). This value is lower than that of a cooperative system (*vide supra*).

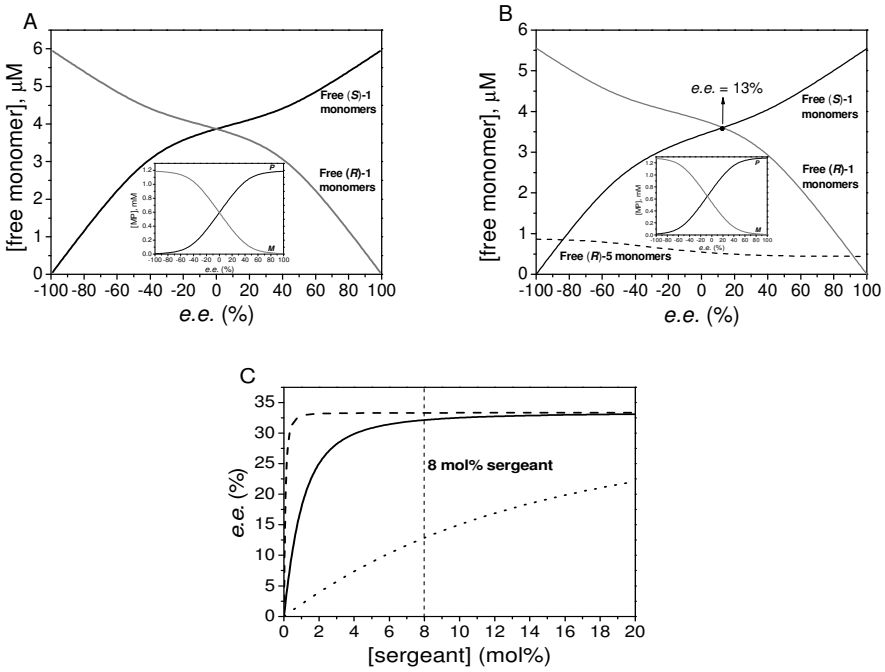

Figure 5.15: The computed concentrations of free enantiomeric monomers ((*S*)-**1** (black line), (*R*)-**1** (gray line) and (*R*)-**5** (dashed line)) as a function of *e.e.* at 20 °C (c_{tot} = 1.2 mM) in an isodesmic system. The inserted figure shows the concentration of the monomers participating in the *P* (black line) and *M* (gray line) type supramolecular polymers as a function of *e.e.* at 20 °C. The calculations are based on the same thermodynamic parameters as the cooperative Phg-BTA system but $\Delta H°_{NP}$ = 0 kJ mol^{-1}; A) in the absence of sergeant, B) in the presence of sergeant (8 mol%) C) The maximum *e.e.* retained by the system as a function of the sergeant added with $\Delta H°_{NP}$ = 0 (isodesmic system, dotted line), $\Delta H°_{NP}$ = −12.2 kJ mol^{-1} (cooperative system, solid line), $\Delta H°_{NP}$ = −24.4 kJ mol^{-1} (cooperative system, dashed line).

Furthermore, the influence of sergeant concentration on the final *e.e.* value in a cooperative and isodesmic system was investigated, respectively. The value of nucleation penalty ($\Delta H°_{NP}$) which is a measure of cooperativity was varied while other thermodynamic parameters were kept constant. In an isodesmic system, $\Delta H°_{NP}$ is 0 whereas a large absolute value of $\Delta H°_{NP}$ implies a high cooperativity in a system.[24] Calculations revealed that the *e.e.* value increases with the increasing fraction of sergeant and reaches a limiting value which

seems to be approximately equal to $e.e._{cr}$ from the two-component model in a cooperative system (dashed and black lines, Figure 5.15C). 8 mol% of sergeant is sufficient in order to reach the limiting value (= 32%) in the system discussed here with a nucleation penalty ($\Delta H°_{NP}$) of −12.2 kJ mol^{-1}. Moreover, less sergeant is needed in order to obtain this value in a system with higher (absolute) value nucleation penalty ($\Delta H°_{NP}$ = −24 kJ mol^{-1}). However, similar processes in a system with isodesmic self-assembly behavior where $\Delta H°_{NP}$ is 0, lead to a much lower *e.e.* value (= 13%) with the same sergeant concentration (= 8 mol%) employed (Figure 5.15C, dotted line). 20 mol% of sergeant is even not sufficient to reach 32% *e.e.* in an isodesmic system.

Chiral-symmetry breaking in crystallization occurs *via* a 'secondary nucleation' phenomenon which involves the generation of a large number of nuclei from the surface of an initially formed crystal i.e., 'mother crystal' in a stirred solution.[1534] In this case, the chiral information of the 'mother crystal' is transferred and amplified to the secondary crystals in the solution leading to a total symmetry breaking. Crystallization in which cooperative mechanism plays a dominant role is a useful tool to generate *e.e.* from a racemic mixture or achiral compound. These results suggest that the cooperative interactions are important in order to obtain high *e.e.* values in chemical systems.

5.7.2 Experimental approach

Deracemization experiments were performed under varying conditions and the final *e.e.* of the system was evaluated. The increase in the sergeant concentration from 8 mol% to 140 mol% did not lead to any significant change in the final *e.e.* of the system (Figure 5.16A). Furthermore, application of much higher Phg-BTA concentration (c = 100 mM) did not change the final *e.e.* value (= 32%) (Figure 5.16B). The deracemization rate was also comparable to experiments performed at lower concentration (c = 1.2 mM). The *e.e.* value was 30% in 100 days. The experimental data showed that the maximum *e.e.* (= 32%) can be obtained under various conditions; however, this value can never be exceeded.

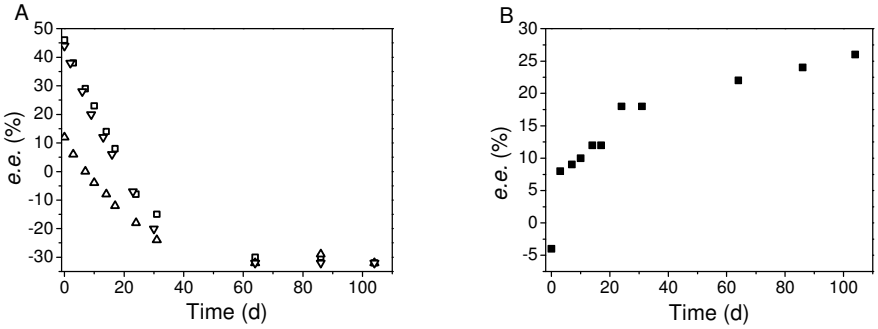

Figure 5.16: The change in *e.e.* over time at 20 °C, 1 eq. DBU added, c = 1.4 mM in MCH. A) Initial *e.e.*: 46%, sergeant: (*S*)-**5** (140 mol%) (square), initial *e.e.*: 44%, sergeant: (*S*)-**5** (8 mol%) (triangle down), initial *e.e.*: 12%, sergeant: (*S*)-**5** (100 mol%) (triangle up). B) c = 100 mM in MCH. Initial *e.e.*: −4%, sergeant: (*R*)-**5** (4 mol%).‡

The experiments described here are in agreement with the theoretical predictions for the corresponding process in terms of the final enantiomeric excess of the system which is reproducibly 32%.

5.8 Conclusions

In conclusion, racemization of a cooperative supramolecular system with a helical conformation was studied. The racemization reaction in the presence of base led to non-first order reaction kinetics in a system under majority rules control. The unusual features of this system were investigated by a theoretical model. One of the features leads to non-first order racemization kinetics, which can have major consequences for the reliability of the dating methods[31], since Nature is built on supramolecular systems. It is also shown how a final *e.e.* different from zero can be obtained under racemizing and thermodynamically controlled conditions by adding a sergeant as auxiliary. This final *e.e.* depends on the mismatch penalty and on the cooperative nature of the aggregating system. The theoretical predictions were validated with the experimental work and transformation of a racemic Phg-BTA mixture into a mixture where one of the enantiomers is present in excess by making use of a chiral sergeant was achieved. A higher *e.e.* value can be reached ultimately in a racemizable self-assembled BTA system with a larger mismatch penalty and a stronger cooperative nature. The formation of conglomerate self-assemblies in solution is required in order to mimic the total symmetry breaking in crystalline systems where *e.e.* > 99%. Porphyrin-based supramolecular polymers were previously reported to form conglomerate stacks in

‡ The sample is heated at 80 °C for 3 h to speed up the racemization process. After that it was cooled down and the *e.e.* values were measured.

solution.[38] Porphyrin structures comprising labile stereocenters may serve as potential candidates for deracemization studies in future.

The stable α–helix conformation is one of the most common conformations in nature hence, racemization and deracemization processes in a cooperative helical self-assembled BTA system provides us with valuable information especially on the origin of homochirality in nature.

5.9 Experimental

5.9.1 General

The chiral amines, (*R*)-**2** and (*S*)-**2**, were synthesized from (*R*)- and (*S*)-2-phenylglycine, respectively. Due to the labile character of the stereocenter in molecules (*R*)-**2** and (*S*)-**2**, these compounds were kept as tosylate salts and used without further purification. Syntheses of the Phg-BTA molecules were carried out under dry argon atmosphere. Synthesis of compounds (*R*)- and (*S*)-**5** was published elsewhere.[30] (*R*)- and (*S*)-2-phenylglycine, 1-octanol, 1,1'-carbonyldiimidazole (CDI) and TsOH.H_2O were purchased from Aldrich. 1,8-diazabicycloundec-7-ene (DBU) was purchased from Acros. Solvents were obtained from Biosolve. Methylcyclohexane (MCH) (spectrophotometric grade) was purchased from Aldrich and used as received. DMF was dried over molecular sieves. All other chemicals were used as received. The *e.e.* determination was performed by HPLC equipped with a chiral column (chiracel OD, eluent: hexane/isopropanol: 90/10, flow rate: 1 mL/min; UV-detector λ = 225 nm). Racemization experiments were performed in MCH at various temperatures in the presence of DBU (1 eq.). Samples were taken over time and injected to the chiral HPLC and *e.e.* values were recorded. Each measurement was repeated three times and the average of the *e.e.* values were taken. For deracemization experiments, *N,N',N"*-tris[(*R*/*S*)-3,7-dimethyloctyl]benzene-1,3,5-carboxamide ((*R*)-**5** and (*S*)-**5**) were used as 'sergeant'. In deracemization experiments, *e.e.* values were recorded every three days by taking samples (100 μL) from the deracemizing solutions. The deracemization experiments were performed at 20 °C with and without stirring which resulted in equal deracemization rates and *e.e.* values. For the majority rules experiment, *e.e.* values of the mixtures were calculated from the volumes of each identically concentrated stock solution of (*S*)**-1** and (*R*)**-1**, assuming that each stock solution contains (*S*)**-1** and (*R*)**-1** at an *e.e.* of 82%, respectively. ^{1}H NMR (400 MHz), ^{13}C NMR (100 MHz) spectra were recorded on a Varian 400 MHz spectrometer in deuterated chloroform unless stated otherwise. Chemical shifts were reported in ppm and referenced to tetramethylsilane (TMS). MALDI-TOF MS spectra were obtained on a Perceptive Biosystems Voyager DE-Pro MALDI-TOF mass spectrometer (accelerating voltage 20 kV; grid voltage 74.0%; guide wire voltage 0.030%; delay 200 ms; low mass gate, 900 amu). IR spectra were recorded on a Perkin–Elmer spectrum 1 using a universal ATR. UV-vis and circular dichroism measurements were performed on a Jasco J-

815 spectropolarimeter where the sensitivity, time constant and scan rate were chosen appropriately. Corresponding temperature dependent measurements were performed with a PFD-425S/15 Peltier-type temperature controller with a temperature range of 263-383 K and adjustable temperature slope. Linear dichroism was not observed in the experiments. Cells with an optical path length of 0.1 cm were employed and spectrophotometric grade methylcyclohexane was employed. Solutions were prepared by weighing Phg-BTA ((*S*)-**1** or (*R*)-**1**) molecule (8.1 mg), after which this amount was transferred to a volumetric flask (flasks of 10 mL were employed). Then, the flask was filled with the spectroscopic grade solvent and put in an oscillation bath at 40 °C for 50 min, after which the flask was allowed to cool down. Any loss of solvent was compensated for. The molar ellipticity was calculated from: $\Delta\varepsilon$ = CD effect/ (32980 c *l*) in which *c* is the concentration in mol L^{-1} and *l* is the optical path length in cm. Matlab© lsqnonlin curve fitting was used as a numerical method.

5.9.2 Synthesis

(*R*)-Phenylglycine octyl ester TsOH salt ((*R*)-2): A 1 L flask was equipped with a stirring bar and Dean-Stark setup. (*R*)-Phenylglycine (7.35 g, 49.8 mmol), 1-octanol (9.49 g, 72.8 mmol, 1.5 eq), and toluenesulfonic acid monohydrate (10.54 g, 55.4 mmol, 1.1 eq) were suspended in toluene (330 mL) and the reaction mixture was subsequently refluxed overnight. All volatiles were removed under reduced pressure and Et_2O (450 mL) was added in a single portion to the sticky residue while stirring vigorously. Stirring was continued for 20 min, after which the precipitate was filtered over a Büchner filter and washed with Et_2O (2×40 mL). The product was dried under vacuum for 30 min and obtained as a fine, white powder (19.86 g, 92 %). The crude product was not further purified and was directly used in subsequent reactions. ^{1}H-NMR (400 MHz, $CDCl_3$): δ 8.63 (br. s., 3H, -N*H*$_3^+$), 7.52 (d, 2H, *J* = 8.0 Hz, -Ar*H*, TsO^-), 7.31 (d, 2H, *J* = 7.5 Hz, -Ar*H*), 7.28-7.21 (m, 1H, -Ar*H*), 7.16 (t, 2H, *J* = 7.5 Hz, -Ar*H*), 7.02 (d, 2H, *J* = 8.0 Hz, Ar*H*, TsO^-), 5.06 (s, 1H, -CONHC*H*-), 3.98 (dt, 1H, A part of the AB-system, *J* = 4.0 and 8.0 Hz, -COOC*H*$_2$-), 3.91 (dt, 1H, B part of the AB-system, *J* = 4.0 and 8.0 Hz, -COOC*H*$_2$-), 2.34 (s, 3H, -C*H*$_3$, TsO^-), 1.40 (qui, 2H, *J* = 8.0 Hz -COOCH$_2$C*H*$_2$-), 1.24 (qui, 2H, *J* = 8.0 Hz, -COOCH$_2$CH$_2$C*H*$_2$-), 1.17-1.01 (m, 8H, -COOCH$_2$CH$_2$CH$_2$(C*H*$_2$)$_4$-), 0.87 (t, 3H, *J* = 7.1 Hz, -COOCH$_2$CH$_2$CH$_2$CH$_2$C*H*$_3$). ^{13}C-NMR (100 MHz, $CDCl_3$): δ 168.2, 141.4, 139.8, 131.8, 129.2, 128.9, 128.6, 128.1, 126.1, 66.5, 56.7, 31.8, 29.0, 28.1, 25.4, 22.6, 21.3, 14.1. IR (cm^{-1}): 3026, 2921, 2855, 2711, 2634, 1741, 1603, 1498, 1458, 1390, 1219, 1173, 1125, 1053, 1037, 1012, 813, 698, 677.

(*S*)-Phenylglycine octyl ester TsOH salt ((*S*)-2): An identical procedure as for the preparation of (*R*)-**2** was followed using (*S*)-phenylglycine (7.56 g, 50.0 mmol), 1-octanol (9.49 g, 72.8 mmol, 1.5 eq.), and toluenesulfonic acid monohydrate (10.47 g, 55.4 mmol, 1.1 eq.) and toluene (330 mL). (*S*)-**2** was isolated as a fine, white powder in good yield (20.44 g, 94%). The

crude product was not further purified and was directly used in subsequent reactions. ^{1}H-NMR (400 MHz, $CDCl_3$): δ 8.61 (br. s., 3H, -NH_3^+), 7.53 (d, 2H, *J* = 8.1 Hz, -Ar*H* TsO^-), 7.32 (d, 2H, *J* = 7.5 Hz, -Ar*H*), 7.28-7.21 (m, 1H, -Ar*H*), 7.19 (t, 2H, *J* = 7.5 Hz, -Ar*H*), 7.02 (d, 2H, *J* = 8.0 Hz, Ar*H*, TsO^-), 5.04 (s, 1H, -CONHC*H*-), 4.00 (dt, 1H, A part of the AB-system, *J* = 4.0 and 8.0 Hz, -COOCH_2-), 3.90 (dt, 1H, B part of the AB-system, *J* = 4.0 and 8.0 Hz, -COOCH_2-), 2.34 (s, 3H, -CH_3, TsO^-), 1.40 (qui, 2H, *J* = 8.0 Hz -COOCH$_2$CH_2-), 1.24 (qui, 2H, *J* = 8.0 Hz, -COOCH$_2$CH$_2$CH_2-), 1.17-1.01 (m, 8H, -COOCH$_2$CH$_2$CH$_2$(CH_2)$_4$-), 0.87 (t, 3H, *J* = 7.1 Hz, -CH_3). ^{13}C-NMR (100 MHz, $CDCl_3$): δ 168.2, 141.4, 139.8, 131.8, 129.2, 128.9, 128.6, 128.1, 126.1, 66.5, 56.7, 31.8, 29.0, 28.1, 25.4, 22.6, 21.3, 14.1. IR (cm^{-1}): 3063, 2921, 2855, 2711, 2635, 1741, 1603, 1498, 1458, 1390, 1219, 1174, 1125, 1053, 1037, 1013, 813, 698, 678.

***N*-((*R*)-phenylglycine octyl ester)-*N*',*N*''-di(*n*-octyl)benzene-1,3,5-tricarboxamide (*R*)-1):** A 25 mL 3-necked flask was equipped with a stirring bar, septum, and argon inlet. The setup was thoroughly dried and kept under an argon atmosphere. Carbonyl-1,1'-diimidazole (CDI, 78.1 mg, 0.48 mmol) was dissolved in dry DMF (5 mL) and the mixture was stirred at room temperature for 5 min. A solution of 3,5-bis(octylaminocarbonyl)benzoic acid[28] (217.8 mg, 0.50 mmol, 0.96 eq.) in DMF (5 mL) was added slowly over a 5 min interval. After stirring at room temperature for 90 min, (*R*)-**2** (525.6 mg, 1.21 mmol, 1.10 eq) was added in a single portion and stirring was continued for exactly 3 h. The reaction mixture was poured into 0.1 M HCl (80 mL) and extracted with Et_2O (2×70 mL). The combined organic layers were washed with saturated KCl (80 mL) and dried over $MgSO_4$. The solvent was removed while keeping the temperature of the water bath below 30 °C, after which the crude product was purified by column chromatography over normal silica gel (EtOAc / heptane (1:2), R_f = 0.28) to give (*R*)-**1** as a white, sticky solid (190 mg, 58%) with an *e.e.* of 82.0%. ^{1}H-NMR (400 MHz, $CDCl_3$): δ 8.35 (s, 2H , -Ar*H*), 8.35 (s, 1H , -Ar*H*), 7.47-7.34 (m, 6H, -Ar*H* Phg + -CON*H*-), 6.35 (d, 2H, *J* = 6.5 Hz, -CON*H*CH-), 5.73 (d, 1H, *J* = 6.5 Hz, -CONHC*H*COO-), 4.17 (t, 2H, *J* = 6.6 Hz, -COOCH_2CH$_2$-), 3.46 (q, 4H, *J* = 8.0 Hz, -CONHCH_2CH$_2$-), 1.64-1.56 (m, 6H, -COOCH$_2$CH_2- + -CONCH$_2$CH_2-), 1.42-1.23 (m, 22H, -CH_2-), 1.20 (br. s, 8H, -CH_2-), 0.88 (m, 9H, -CH_3). ^{13}C-NMR (100 MHz, $CDCl_3$): δ 170.7, 165.6, 165.0, 136.3, 135.6, 134.4, 129.2, 128.9, 128.2, 127.5, 66.3, 57.4, 40.5, 31.9, 31.8, 29.6, 29.4, 29.3, 29.2, 27.0, 22.6, 22.5, 14.1. IR (cm^{-1}): 3243, 3065, 2956, 2924, 2855, 1747, 1637, 1551, 1499, 1466, 1456, 1378, 1295, 1260, 1207, 1173, 1099, 909, 723, 964 cm^{-1}. MALDI-TOF-MS: Calculated for $C_{41}H_{63}N_3O_5$ = 677.48 g/mol, observed m/z =1355.87 [2*M* + H]$^+$, 700.40 [*M* + Na]$^+$, 678.39 [*M* + H]$^+$ g/mol.

***N*-((*S*)-phenylglycine octyl ester)-*N*',*N*''-di(*n*-octyl)benzene-1,3,5-tricarboxamide ((*S*)-1):** An identical procedure as for the preparation of (*S*)-**1** was followed using CDI (77.7 mg, 0.48 mmol), 3,5-bis(octylaminocarbonyl)benzoic acid (215.8 mg, 0.50 mmol, 0.96 eq.), DMF (5+5 mL) , and (*S*)-**2** (214.8 mg, 0.49 mmol, 0.99 eq.). (*S*)**-1** was obtained as a white, sticky solid

(183.0 mg, 56%) and with an *e.e.* of 82.0%. ^{1}H-NMR (400 MHz, $CDCl_3$): δ 8.34 (s, 3H , -Ar*H*), 7.47-7.34 (m, 6H, -Ar*H* Phg + -CON*H*-), 6.37 (d, 2H, *J* = 6.5 Hz, -CON*H*CH-), 5.72 (d, 1H, *J* = 6.5 Hz, -CONHC*H*-), 4.17 (t, 2H, *J* = 6.6 Hz, -COOC*H*$_2$CH$_2$-), 3.45 (q, 4H, *J* = 8.0 Hz, -CONHC*H*$_2$ CH$_2$-), 1.62-1.56 (m, 6H, -COOCH$_2$C*H*$_2$- + -CONCH$_2$C*H*$_2$-), 1.42-1.24 (m, 22H, -C*H*$_2$-), 1.20 (br. s, 8H, -C*H*$_2$-), 0.88 (m, 9H, -C*H*$_3$). ^{13}C-NMR (100 MHz, $CDCl_3$): δ 171.0, 166.0, 165.7, 136.0, 135.4, 134.0, 128.9, 128.6, 128.6, 128.1, 127.6, 66.1, 57.4, 40.4, 31.8, 31.7, 29.5, 29.3, 29.2, 29.1, 29.0, 27.0, 22.6, 22.5, 14.1. IR (cm^{-1}): 3243, 3065, 2956, 2924, 2855, 1747, 1637, 1551, 1499, 1466, 1456, 1378, 1295, 1260, 1207, 1173, 1099, 909, 722, 694. MALDI-TOF-MS: Calculated $C_{41}H_{63}N_3O_5$ = 677.48 g/mol, observed m/z = 1355.91 [2*M* + Na]$^+$, 1357.92 [2*M* + H]$^+$, 700.45 [M + Na]$^+$, 678.43 [*M* + H]$^+$ g/mol.

(*R*)-*N*-Benzoylphenylglycine octyl ester ((*R*)-4): A 25 mL 3-necked flask was equipped with a stirring bar, septum, and argon inlet. The setup was thoroughly dried and kept under an argon atmosphere. Carbonyl-1,1′-diimidazole (CDI, 181.8 mg, 1.12 mmol) was dissolved in dry DMF (9 mL) and stirred at room temperature for 5 min. A solution of benzoic acid (122.1 mg, 1.0 mmol, 0.9 eq.) in DMF (6 mL) was added slowly over a 5 min interval. After stirring at room temperature for 90 min, (*R*)-**2** (525.6 mg, 1.21 mmol, 1.10 eq) was added in a single portion and stirring was continued for exactly 3 h. The reaction mixture was poured into a mixture of water (100 mL), 1.0 M HCl (50 mL) and brine (20 mL) and subsequently extracted with Et_2O (2 × 50 mL). The combined organic layers were washed with saturated KCl solution (100 mL) and dried over $MgSO_4$. The solvent was removed while keeping the temperature of the water bath below 30 °C, after which the crude product was purified by column chromatography over normal silica gel (EtOAc/heptane (1:3), R_f = 0.35) to give (*R*)-**4** as a white solid (230 mg, 63%) and an *e.e.* of 82.0%. ^{1}H-NMR (400 MHz, $CDCl_3$): δ 7.82 (d, 1H, *J* = 5.3 Hz, -CON*H*CH-), 7.60-7.20 (m, 5H, -Ar*H*), 5.78 (d, 1H, *J* = 5.3 Hz, -CONHC*H*-), 4.17 (t, 2H, *J* = 6.6 Hz, -NHCHCOOC*H*$_2$CH$_2$-), 1.62 (m, 2H, -COOCH$_2$C*H*$_2$-), 1.42-1.24 (m, 10H, -C*H*$_2$-), 0.88 (t, *J* = 6.8 Hz, 3H, -C*H*$_3$). IR (cm^{-1}): 3321, 2957, 2923, 2854, 1739, 1533, 1489, 1357, 1293, 1266, 1191, 1099, 1071, 891.

5.10 Appendix

5.10.1 Chiral HPLC analysis

The *e.e.* determination of the compounds was performed by chiral HPLC (chiracel-OD column; *n*-hexane/isopropanol (90:10); 1 mL/min; UV-detector λ = 225 nm). Samples were directly injected in MCH (c = 0.8 mg/mL, injection volume = 1 μL). t_R((*S*)-**1**) : 1.14 min, t_R((*R*)-**1**) : 1.70 min, *e.e.* = 82.0% each.

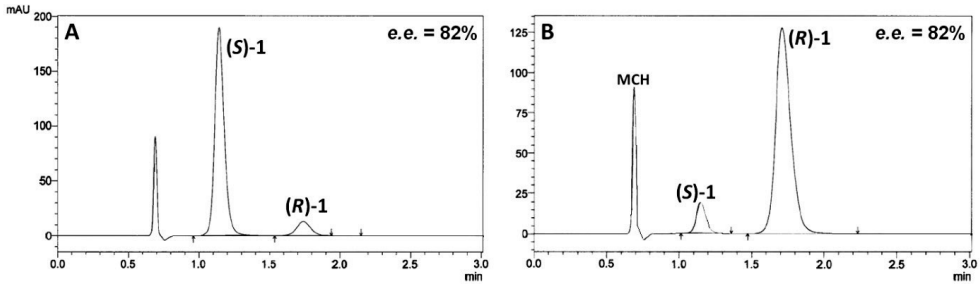

Figure A5.1: HPLC trace of A) (*S*)-**1** and B) (*R*)-**1**.

5.10.2 Preparative HPLC analysis

Preparative HPLC was performed for (*S*)**-1** and (*R*)**-1**, respectively, in order to obtain them in higher optical purity. The same chiral HPLC method was used as mentioned above (chiracel-OD column; *n*-hexane/isopropanol (90:10); 1 mL/min; UV-detector λ = 225 nm) and total run time = 15 min. Samples were dissolved in *n*-hexane/isopropanol (90:10); c = 0.2 mg/mL. The injection was performed manually (100 µL). (*S*)**-1** and (*R*)**-1** were obtained with *e.e.* values 99.1% and 97%, respectively. The figures below display HPLC traces after the preparative HPLC. t_R((*S*)-**1**) : 5.05 min, t_R((*R*)-**1**) : 9.58 min. $\Delta\varepsilon$ of Phg-BTAs was determined by using the samples with *e.e.* ≥ 97%.

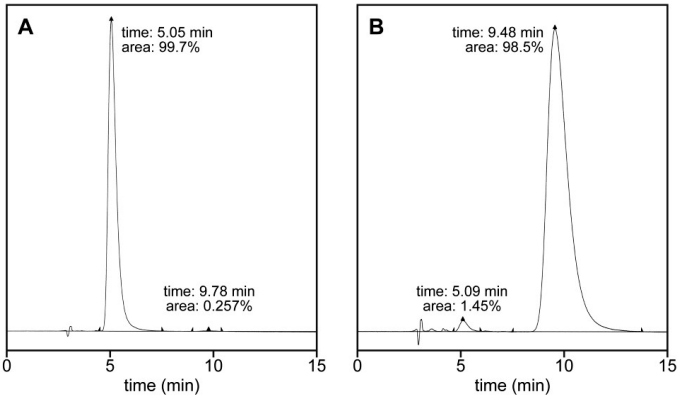

Figure A5.2: HPLC traces of A) (*S*)**-1** and B) (*R*)**-1**.

5.10.3 UV-vis and CD spectra of (*R*)-*N*-benzoylphenylglycine octyl ester ((*R*)-4)

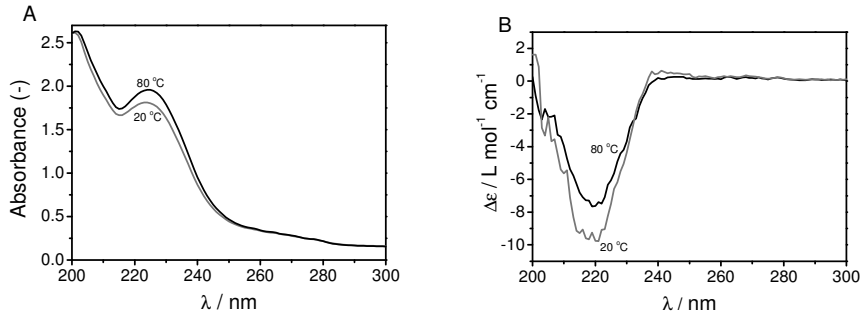

Figure A5.3: A) UV-vis spectrum of (*R*)-**4** in MCH (c = 1.2 mM) at 80 °C (black) and 20 °C (gray). Typical blue shift indicating the presence of H-type aggregates is not observed in the spectra upon cooling. B) The CD spectrum of (*R*)-**4** in MCH (c = 1.2 mM) at 80 °C (black) and 20 °C (gray). $\Delta\varepsilon = -10.0$ L mol^{-1} cm^{-1} at 20 °C.

5.10.3 Theoretical model for racemization

5.10.3.1 Racemization kinetics

In this section, the computation of the racemization kinetics is described in detail. Suppose that during the racemization process, at a time t, the total concentration of the enantiomeric monomers (*i.e.* inside and outside the supramolecular polymers), (*S*)-**1** and (*R*)-**1**, are defined as s_{tot} and r_{tot}, respectively. Since we assume that the racemization reaction is much slower than the dynamic exchange between monomers and supramolecular polymers, the free monomer concentrations $s = [S(\mathbf{1})]$ and $r = [R(\mathbf{1})]$ at time t can be found by solving the equations of the two component model by adapting the current values of s_{tot} and r_{tot}. Now consider the racemization process of the free monomers during a small time interval Δt. This racemization reaction, which is assumed to be a first-order reaction with reaction constant *k*, leads to $\Delta s = k\Delta t\,(r - s)$ for the total concentration of newly produced/used (*S*)-**1** monomers and $\Delta r = k\Delta t\,(s - r)$ for the total concentration of newly produced/used (*R*)-**1** molecules. This means that the total concentrations of (*S*)-**1** and (*R*)-**1** (monomers being inside and outside the supramolecular polymer) at time $t + \Delta t$ are given by $s_{\text{tot}} + \Delta s$ and $r_{\text{tot}} + \Delta r$ respectively. The new corresponding free monomer concentrations $s = [S(\mathbf{1})]$ and $r = [R(\mathbf{1})]$ at time $t + \Delta t$ can be found by solving again the equations of the two component model, using $s_{\text{tot}} + \Delta s$ and $r_{\text{tot}} + \Delta r$ as new total concentrations. The time step is shown in the following table:

Table A5.1: The time step and the corresponding formula

time	$[(S)\text{-}\mathbf{1}]_{tot}$	$[(R)\text{-}\mathbf{1}]_{tot}$	$[(S)\text{-}\mathbf{1}]$	$[(R)\text{-}\mathbf{1}]$	enantiomeric excess
t	s_{tot}	r_{tot}	s	r	*e.e.*
racemization during Δt: $\Delta s = k\Delta t\,(r-s)$ and $\Delta r = k\Delta t\,(s-r)$					
$t+\Delta t$	$s_{tot}+\Delta s$	$r_{tot}+\Delta r$	$\tilde{s}$	$\tilde{r}$	$e.e.-2k\,\Delta t\,(s-r)/(r_{tot}+s_{tot})$

5.10.4. Theoretical model for the self-assembly of three component system ((*R*)-1, (*S*)-1, sergeant)

5.10.4.1 Additional reactions for the sergeant

The three-component model is an extension of the method used for the two-component system described previously.[2424] This three-component model describes the thermodynamic equilibrium of a system that consists of two enantiomers *R* and *S* and an additional sergeant molecule Q. Although both enantiomers can be present in either *P* or *M*, *S* monomers show a preference for *P* and the *R* monomers display a preference for *M*-type supramolecular polymers. The sergeant molecules Q may have a preference for either *P* or *M*, depending on the used thermodynamic parameters. For the addition of sergeant molecules to *P*, the elongation phase has the additional reaction

$$P + \mathrm{Q} \overset{K_4}{\rightleftarrows} P\mathrm{Q},$$

where *P* is an arbitrary *P*-type supramolecular polymer and the equilibrium constant is given by

$$K_4 = \exp\left(-\left(\Delta H^{\circ}_{\mathrm{e,serg}} - T\Delta S^{\circ}_{\mathrm{e,serg}}\right)/\left(RT\right)\right) \tag{A5.1}$$

where $\Delta H^{\circ}_{\mathrm{e,serg}}$ and $\Delta S^{\circ}_{\mathrm{e,serg}}$ are the (standard) elongation enthalpy and elongation entropy for the sergeant molecules, respectively. We now find that the concentration of an arbitrary *P*-type supramolecular polymer of length $i+j+k$ that contains *i* times *S* monomers, *j* times *R* monomers and *k* times Q monomers, is given by

$$p_{i,j,k} = \frac{\sigma}{K_1}\left(K_1 s\right)^i \left(K_2 r\right)^j \left(K_4 q\right)^k \tag{A5.2}$$

where $q = [\mathrm{Q}]$.

The sergeant molecules Q can also occur in *M*-type supramolecular polymers. For the elongation phase this gives the additional reaction

$$M + \mathrm{Q} \underset{}{\overset{K_5}{\rightleftarrows}} M\mathrm{Q}$$

where *M* is an arbitrary *M*-type supramolecular polymer. The corresponding equilibrium constant is given by

$$K_5 = \exp\left(-\left(\Delta H^\circ_{\mathrm{e,serg}} - \Delta H^\circ_{\mathrm{e,serg,MMP}} - T\Delta S^\circ_{\mathrm{e,serg}}\right)/\left(RT\right)\right) \quad , \tag{A5.3}$$

i.e., we introduce an additional mismatch enthalpy $\Delta H^\circ_{\mathrm{e,serg,MMP}}$ for the sergeant molecules when forming *M*-type supramolecular polymer. For the concentration of an arbitrary *M* with a length of $i+j+k$ that contains *i* times *S* monomers, *j* times *R* monomers and *k* times Q monomers, we now obtain

$$m_{i,j,k} = \frac{\sigma}{K_1}\left(K_2 s\right)^i \left(K_1 r\right)^j \left(K_5 q\right)^k \quad . \tag{A5.4}$$

Note that K_4 and K_5 (or $\Delta H^\circ_{\mathrm{e,serg}}$, $\Delta S^\circ_{\mathrm{e,serg}}$ and $\Delta H^\circ_{\mathrm{e,serg,MMP}}$) describe the binding of the sergeant monomers, Q, to the *P* and *M*, respectively. Hence, they are both new parameters, that are independent of the parameters K_1, K_2 and σ, that describe the enantiomeric subsystem.

5.10.4.2 Composition of the supramolecular copolymers

Using the expressions for $p_{i,j,k}$ and $m_{i,j,k}$, as given in equations (A5.2) and (A5.4), we can easily compute the total concentration of the monomers in *P* and *M*, and the composition of these supramolecular polymers. First, we compute the concentration of *P* with length ℓ. Such a polymer may contain *i* times *S*, *j* times *R* and *k* times Q, with $i+j+k=\ell$. However, even for the given values of *i*, *j* and *k* (with $i+j+k=\ell$), many different types of *P* having the required numbers of *R*, *S* and Q molecules might exist. The number of different types of *P* with the required number of monomers is given by the multinomial coefficient $\binom{\ell}{i,j,k}$. Hence the concentration of *P* with length ℓ is given by

$$p_\ell = \sum_{i+j+k=\ell} \binom{\ell}{i,j,k} p_{i,j,k} \tag{A5.5}$$

where the summation is overall combinations of *i*, *j* and *k* with sum ℓ. Using the expression (A5.4) and the multinomial theorem this leads to

$$p_\ell = \frac{\sigma}{K_1} g_{\mathrm{P}}^\ell \qquad (\text{for } \ell = 2,3,\ldots), \tag{A5.6}$$

where $g_{\mathrm{P}} = K_1 s + K_2 r + K_4 q$ is the *elongation factor* for *P*. Clearly $g_{\mathrm{P}} < 1$ to keep the system finite. The total concentration of the monomers in *P* is then given by

$$p_{\mathrm{tot}} = \sum_{\ell=2}^{\infty} \ell \, p_\ell = \frac{\sigma}{K_1} \sum_{\ell=2}^{\infty} \ell \, g_{\mathrm{P}}^{\ell} = \frac{\sigma}{K_1} \frac{g_{\mathrm{P}}^2 (2 - g_{\mathrm{P}})}{(1 - g_{\mathrm{P}})^2} \tag{A5.7}$$

where we have used the identity

$$\sum_{\ell=2}^{\infty} \ell \, a^{\ell} = \frac{a^2 (2 - a)}{(1 - a)^2} \qquad \text{for} \qquad |a| < 1 \tag{A5.8}$$

In the sequel, not only the total concentration of the monomers in *P* is needed, but also the concentration of the different monomers, *R*, *S* and Q, respectively. The total concentration of *S* monomers in *P* of length ℓ is given by

$$s_{p_l} = \sum_{i+j+k=\ell} i \binom{\ell}{i,j,k} p_{i,j,k} = \ell \, \sigma \, s \, g_{\mathrm{P}}^{\ell-1} \quad , \tag{A5.9}$$

where we used again the multinomial theorem. The total concentration of *S* in all *P*-type supramolecular polymers is given by summing this expression over all $\ell \geq 2$, which yields

$$s_{p_{\mathrm{tot}}} = \sum_{\ell=2}^{\infty} s_{\mathrm{P}_\ell} = \sigma \, s \sum_{\ell=2}^{\infty} \ell \, g_{\mathrm{P}}^{\ell-1} = \sigma \, s \frac{g_{\mathrm{P}} (2 - g_{\mathrm{P}})}{(1 - g_{\mathrm{P}})^2}, \tag{A5.10}$$

where we have used the identity $\sum_{\ell=2}^{\infty} \ell a^{\ell-1} = \frac{a(2-a)}{(1-a)^2}$ for $|a| < 1$. In the same way, we can compute the total concentration of *R* and Q molecules in all *P*-type supramolecular polymers, respectively, which results in the following formulas

$$r_{p_{\mathrm{tot}}} = \frac{K_2}{K_1} \sigma \, r \frac{g_{\mathrm{P}} (2 - g_{\mathrm{P}})}{(1 - g_{\mathrm{P}})^2}, \tag{A5.11}$$

$$q_{p_{\mathrm{tot}}} = \frac{K_4}{K_1} \sigma \, q \frac{g_{\mathrm{P}} (2 - g_{\mathrm{P}})}{(1 - g_{\mathrm{P}})^2}. \tag{A5.12}$$

The total concentration of monomers in *M* can be computed in the same way;

$$m_{\mathrm{tot}} = \frac{\sigma}{K_1} \frac{g_{\mathrm{M}}^2 (2 - g_{\mathrm{M}})}{(1 - g_{\mathrm{M}})^2}, \tag{A5.13}$$

where $g_{\mathrm{M}} = K_1 r + K_2 s + K_5 q$ is the elongation factor for *M*. Again g_{M} must be smaller than 1 to keep the system finite. For the total concentration of *R*, *S* and Q monomers in M-type polymers we find

$$r_{m_{\text{tot}}} = \sigma r \frac{g_{\text{M}}(2-g_{\text{M}})}{(1-g_{\text{M}})^2}, \tag{A5.14}$$

$$s_{m_{\text{tot}}} = \frac{K_2}{K_1} \sigma s \frac{g_{\text{M}}(2-g_{\text{M}})}{(1-g_{\text{M}})^2}, \tag{A5.15}$$

$$q_{m_{\text{tot}}} = \frac{K_5}{K_1} \sigma q \frac{g_{\text{M}}(2-g_{\text{M}})}{(1-g_{\text{M}})^2}. \tag{A5.16}$$

5.11 References

[1] K. Mislow, in *Introduction to stereochemistry*, pp 69, Benjamin, New York, **1965**.
[2] E. L. Eliel, S. H. Wilen, in *Stereochemistry of organic compounds*, pp 426, Wiley, New Jersey, **1994**.
[3] L. A. Paquette, T. –Z. Wang, *J. Am. Chem. Soc.* **1988**, *110*, 8192.
[4] C. Roussel, M. Adjimi, A. Chemlal, A. Djafri, *J. Org. Chem.* **1988**, *53*, 5076.
[5] S. K. Massad, L. D. Hawkins, D. C. Baker, *J. Org. Chem.* **1983**, *48*, 5180.
[6] J. March, in *Advanced organic chemistry*, pp 574, Wiley, New York, **1992**.
[7] J. L. Bada, *Ann. Rev. Earth Planet. Sci.* **1985**, 241.
[8] K. Faber, *Chem. Eur. J.* **2001**, *7*, 5004.
[9] D. B. Amabilino, R. M. Kellogg, *Isr. J. Chem.* **2011**, *51*, 1034.
[10] O. Pamies, J. E. Backvall, *Chem. Rev.* **2003**, *103*, 3247.
[11] H. Pellissier, *Adv. Synth. Catal.* **2011**, *353*, 659.
[12] K. M. Wiggins, C. W. Bielawski, *Angew. Chem. Int. Ed*. **2012**, *51*, 1640.
[13] W. H. Pirkle, D. S. Reno, *J. Am. Chem. Soc.* **1987**, *109*, 7189.
[14] H. Kaku, S. Takaoka, T. Tsunoda, *Tetrahedron* **2002**, *58*, 3401.
[15] C. Viedma, *Phys. Rev. Lett.* **2005**, *94*, 1.
[16] W. L. Noorduin, T. Izumi, A. Millemaggi, M. Leeman, H. Meekes, W. J. P. van Enckevort, R. M. Kellogg, B. Kaptein, E. Vlieg, D. G. Blackmond, *J. Am. Chem. Soc.* **2008**, *130*, 1158.
[17] W. L. Noorduin, H. Meekes, A. A. C. Bode, W. J. P. V. Enckevort, B. Kaptein, R. M. Kellogg, E. Vlieg *Cryst. Growth Des*. **2008**, *8*, 1675.
[18] W. L. Noorduin, A. A. C. Bode, M. v. d. Meijden, H. Meekes, A. F. v. Etteger, W. J. P. v. Enckevort, P. C. M. Christianen, B. Kaptein, R. M. Kellogg, T. Rasing, E. Vlieg, *Nature Chem.* **2009**, *1*, 730.
[19] A. R. A. Palmans, E. W. Meijer, *Angew. Chem. Int. Ed*. **2007**, *46*, 8948.
[20] L. Brunsveld, A. P. H. J. Schennning, M. A. C. Broeren, H. M. Janssen, J. A. J. M. Vekemans, E. W. Meijer, *Chem. Lett*. **2000**, 292.
[21] J. van Gestel, A. R. A. Palmans, B. Titulaer, J. A. J. M. Vekemans, E. W. Meijer, *J. Am. Chem. Soc.* **2005**, *127*, 5490.
[22] M. M. J. Smulders, P. J. M. Stals, T. Mes, T. F. E. Paffen, A. P. H. J. Schenning, A. R. A. Palmans, E. W. Meijer, *J. Am. Chem. Soc.* **2010**, *132*, 620.
[23] J. van Gestel, *Macromolecules* **2004**, *37*, 3894.
[24] A. J. Markvoort, H. M. M. ten Eikelder, P. A. J. Hilbers, T. F. A. de Greef, E. W. Meijer, *Nat. Commun*. **2011**, *2*, 59.
[25] H. M. M. ten Eikelder, A. J. Markvoort, T. F. A. De Greef, P. A.J. Hilbers, *J. Phys. Chem. B*, **2012**, *DOI 10.1021/jp300622m.*
[26] M. Tsukamoto, K. Gopalaiah, H. B. Kagan, *J. Phys. Chem. B* **2008**, *112*, 15361.
[27] D. Guillaneux, S. H. Zhao, O. Samuel, D. Rainford, H. B. Kagan, *J. Am. Chem. Soc.* **1994**, *116*, 9430.
[28] J. Roosma, T. Mes, P. Leclere, A. R. A. Palmans, E. W. Meijer, *J. Am. Chem. Soc*. **2008**, *130*, 1120.
[29] M. M. J. Smulders, A. P. H. J. Schenning, E. W. Meijer, *J. Am. Chem. Soc.* **2008**, *130*, 606.
[30] P. J. M Stals, M. M. J Smulders, R. Martin–Rapùn, A. R. A. Palmans, E. W. Meijer, *Chem. Eur. J.* **2009**, *15*, 2071.
[31] J. Robins, M. Jones, E. M. Smith, Amino acid racemization in New Zealand: An overview and bibliography, **2001**.
[32] M. A. J. Veld. (**2010**). *Candida antartica Lipase B catalysis in organic, polymer and supramolecular chemistry*. Ph.D. Thesis. Eindhoven University of Technology: The Netherlands.

[33] D. K. Kondepudi, J. K. Hall, *Physica A* **1992**, *188*, 113.
[34] D. K. Kondepudi, C. Sabanayagam, *Chem. Phys. Lett*. **1994**, *217*, 364.
[35] C. Viedma, *J. Cryst. Growth* **2004**, *261*, 118.
[36] D. K. Kondepudi, K. L. Bullock, J. A. Digits, P. D. Yarborough, *J. Am. Chem. Soc*. **1995**, *117*, 401.
[37] T. F. A. de Greef, M. M. J. Smulders, M. Wolffs, A. P. H. J. Schenning, R. P. Sijbesma, E. W. Meijer, *Chem. Rev.* **2009**, *109*, 5687.
[38] F. Helmich, M. M. J. Smulders, C. C. Lee, A. P. H. J. Schenning, E. W. Meijer, *J. Am. Chem. Soc*. **2011**, *133*, 12238.

6

EPILOGUE AND OUTLOOK

TOWARDS COMBINING COVALENT AND NONCOVALENT SYNTHESIS

6.1 Introduction

In the previous Chapters we show that BTA self-assembly is a versatile model system in which assemblies are formed under thermodynamic equilibrium by directional and reversible noncovalent interactions between monomers. The self-assembly of BTAs adopt a dynamic character and the chiral information at the monomeric level is expressed at the supramolecular level. These properties enable the analysis of the self-assembly behavior of BTAs by chiroptical spectroscopic methods in a straightforward manner. Furthermore, the observed effects can be quantified by making use of valid theoretical models.

One-dimensional self-assembly of synthetic supramolecular polymers under thermodynamic equilibrium is a well-established field.[1] However, kinetic pathways of these processes as well as the processes exhibiting non-equilibrium thermodynamic behavior in supramolecular chemistry are rather new. In future we would like to investigate the limits of the BTA self-assembly and the chiral amplification behavior further and bring these processes to far-from-equilibrium conditions. One way to do this may be combining covalent and noncovalent synthesis by carrying out a chemical reaction during the self-assembly process. The combination of the two may lead to a far-from-equilibrium state and result in an oscillating behavior, when these two processes proceed by inhibiting each other (i.e., giving rise to a negative feedback). This system may then serve as an example of oscillating chemical system and may provide valuable information for non-equilibrium processes in the future.

In the system described in Chapter 5, oscillating behavior was observed occasionally in the racemization reaction of phenylglycine octyl ester substituted-BTA (Phg-BTA) in the presence of 1,8-diazabicycloundec-7-ene (DBU) in methylcyclohexane (MCH). A hot solution of Phg-BTA in MCH (c = 1.2 mM) in the presence of DBU (1 eq.) was cooled down fast (from 243 K to 293 K) and circular dichroism (CD) and UV-vis spectra were measured as a function of time immediately after the Phg-BTA solution reached 293 K. This process led to an oscillatory CD effect and UV-vis absorption over time and both signals subsequently reached a constant value within 30 min. In the outlook/epilogue we want to extent our serendipitous observations that are made in Chapter 5 to another BTA system and we investigate a protonation/deprotonation reaction during a self-assembly process and analyze oscillating chiroptical properties by making use of thio-BTAs as a model system.

6.2 Towards an oscillating self-assembly process

Oscillating reactions are among the most intriguing reactions. In an oscillating reaction, the reaction mixture goes through a sequence of color changes and this sequence repeats periodically as a result of the periodical changes in reactant concentrations.[2,3] This reaction may be analogous to a simple physical oscillator such as a pendulum, oscillations of which

can be attributed to the interconversion between the potential and kinetic energy of the pendulum. Similarly a chemical oscillator may seem to swing through its equilibrium position; however, this comparison is against to the second law of thermodynamics which states that once a chemical system reaches equilibrium it cannot deviate from this condition spontaneously. The origin of oscillating reactions has been examined theoretically to establish the mechanism.[4] The studies reveal that an oscillating chemical system has three common features; 1) the system is far-from-equilibrium and an energy-releasing reaction occurs the energy of which drives the oscillation, 2) the energy-releasing reaction follows at least two different pathways and the reactions periodically switches from one pathway to the other, 3) one of these pathways produces a certain intermediate while the other pathway consumes it. The concentration of this intermediate functions as a trigger from one pathway to the other. When the concentration of the intermediate is low, the reaction follows the producing pathway and vice versa. Eventually the reaction repeatedly switches from one pathway to the other. Chemical oscillators represent an intriguing class of chemical reactions; however, understanding the mechanism of these processes is challenging and the number of examples is limited. We are interested in entering the intriguing area of chemical supramolecular oscillators and combine these processes with self-assembly of BTAs.

6.2.1 Self-assembly of thio-BTAs

Recently, a new class of BTA molecules, benzene-1,3,5-trithioamides (thio-BTAs), (**1**, Figure 6.1A), was introduced by dr. Tristan Mes.[5] The hydrogen bonding ability of thioamides is less strong compared to that of amides which can be explained in terms of electronegativity and bond strength.[6] The C-N bond in thioamides shows more double bond character compared to an amide which results in an increased acidity of the N-H.[7] This leads to strong hydrogen bonding donor ability; however, the sulfide anion exhibits only weak hydrogen bonding acceptor character due to the larger bond distance. This may result in poor aggregation properties of thio-BTAs in solution. Temperature-dependent UV-vis and CD measurements performed in MCH solution (c = 4.2×10^{-5} M), however, demonstrated that thio-BTA monomers self-assemble into helical aggregates by means of intermolecular hydrogen bonding. UV-vis spectroscopy revealed a red shift in the aromatic region (around λ = 300 nm) and a blue shift in the thioamide region (around λ = 239 nm) upon cooling (Figure 6.1B). Furthermore, a large CD effect ($\Delta\varepsilon$ = −60 L mol^{-1} cm^{-1} at λ_{max} = 316 nm) suggested that helical aggregates are formed at 298 K (Figure 6.1C). The thermodynamic parameters of the self-assembly process were determined by fitting the experimental data with the *single-component model* for a nucleus size of two.[8] The enthalpy of elongation (ΔH_e = -54.2 kJ mol^{-1}), and the entropy of elongation (ΔS_e = -56.0 J mol^{-1} K^{-1}) were determined. Despite the fact that thioamides are poor hydrogen bond acceptors, thio-BTAs are able to form aggregates in

solution. The formation of these aggregates may be rationalized by greater contribution of the dipolar resonance structure of the compound (**1a**, Figure 3.1A) which gives rise to better hydrogen bonding ability of thioamide groups in the BTA molecule compared to that of conventional BTAs.

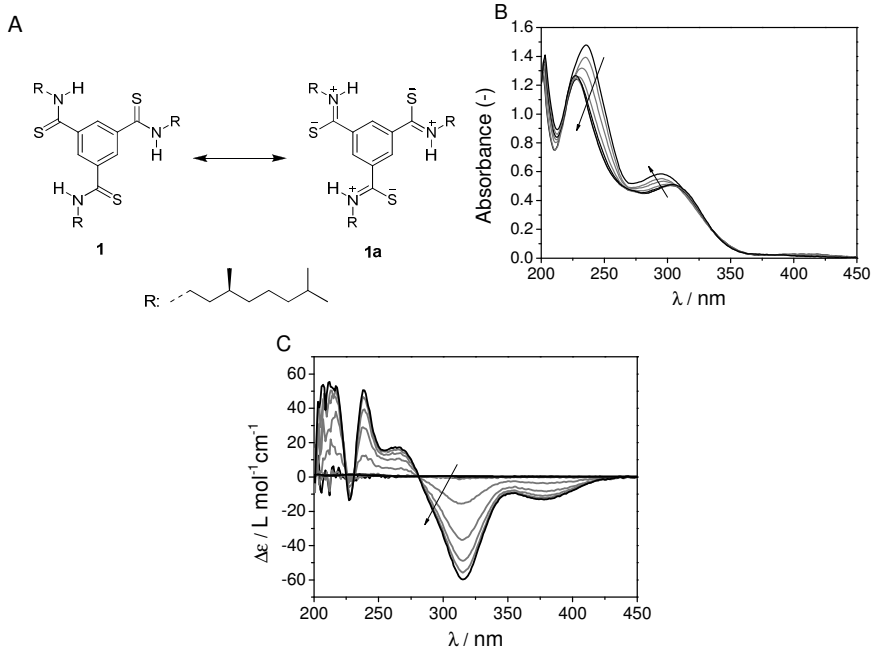

Figure 6.1: A) Resonance structures of thio-BTA **1**. B) UV-vis, C) CD spectra of **1** in MCH (c = 4.2×10^{-5} M) between 363 and 293 K measured at intervals of 10 K at a cooling rate of 60 K h^{-1}. The arrows show the observed shifts upon cooling.

The self-assembly behavior of thio-BTAs was studied at a concentration of c = 9×10^{-4} M, in MCH. UV-vis and CD spectroscopy performed at 363 and 293 K, respectively, suggest that partial depolymerization occurs at 363 K, leading to slight changes in the absorption and the intensity of the CD signal at λ = 316 nm. However, since the temperature of elongation (T_e) is high at that concentration (T_e = 455 K as predicted by the *single-component model*), only partial depolymerization is observed at 363 K.

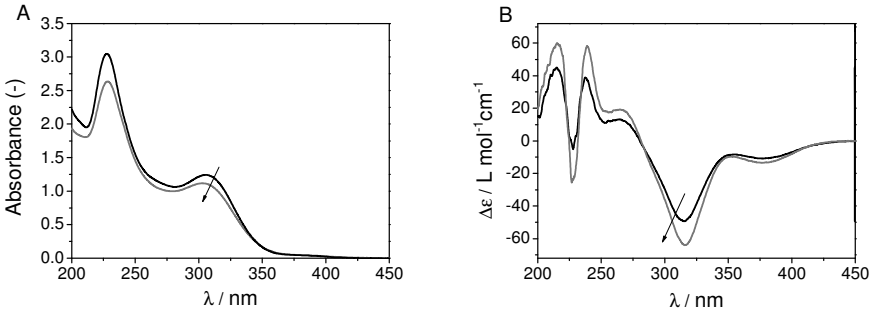

Figure 6.2: A) UV-vis, B) Molar ellipticity ($\Delta\varepsilon$) of **1a** in MCH, c = 9×10^{-4} M, at 363 K (black) and 293 K (gray). Arrow shows the decrease in temperature.

The excellent solubility of thio-BTAs in MCH allows to study the self-assembly behavior at higher concentrations compared to conventional BTAs and make use of other spectroscopic techniques that require high concentrations. Depolarized dynamic light scattering (DDLS) is an effective spectroscopic tool to determine the size distribution of the BTA-based supramolecular polymers in solution, in addition to CD and UV-vis spectroscopy.

The findings on the self-assembly behavior of thio-BTAs were corroborated by DDLS measurements in MCH (c = 9×10^{-4} M). The measurements were performed at three different temperatures, 298, 313 and 333 K. Assuming that the thio-BTA-based supramolecular polymers consist of polydisperse rigid rods, the rotational diffusion coefficients (D_R) were determined by using Broersma's equation[9] [10] from which the stack lengths were estimated at these temperatures. Increasing the temperature resulted in increased D_R values and decreased stack length (Table 6.1). The preliminary results demonstrated a correlation between D_R and the stack length of the supramolecular polymers. The length of the stacks was roughly estimated to be 587 nm at 298 K which equals to 1617 repeating units (assuming that the stack diameter is 0.36 nm). This value can be compared with the number-average degree of polymerization (DP_n) obtained from the *single-component model* based on the temperature-dependent CD and UV-vis data.* DP_n was determined to be 1639 at 298 K (Figure 6.3) which is in excellent agreement with the stack length obtained by DDLS measurements. Considering the DP_n values determined by the *single-component model* and stack length deduced from Broersma's equation are based on different assumptions, the similarity observed between the two is coincidental.

* It is noteworthy to mention that DP_n determined by the *equilibrium model* takes into account not only the monomers within the supramolecular polymers but also the free monomers (outside the supramolecular polymers) in the system.

Table 6.1: Rotational diffusion coefficient (D_R) and stack length (L) deduced from the DDLS data by using Broersma equation.

T (K)	D_R (s^{-1})	L (nm)
298	192	587
313	347	520
333	478	511
298*	306	499

*In the presence of DBU (1 eq.)

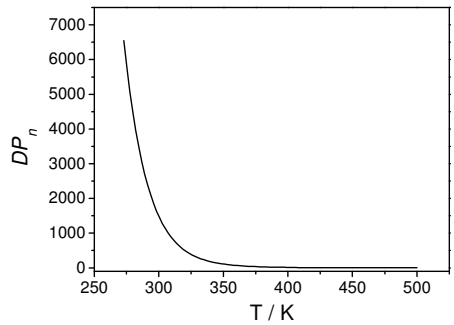

Figure 6.3: The average number of molecules in supramolecular polymers of **1a** as a function of temperature, c = 9×10^{-4} M in MCH, derived from the *single-component model* based on the temperature-dependent CD data.

6.2.2 Self-assembly of thio-BTAs in the presence of base

NH protons in thio-BTAs are acidic and can be readily abstracted by DBU (pK_a = 12) as evidenced by the ^{1}H-NMR spectroscopy performed in $CDCl_3$, DMSO-d_6 and MCH-d_{14}. MCH is a nonpolar alkane solvent; however, protonation/deprotonation equilibrium takes place in this nonpolar solvent as observed in the racemization reaction of Phg-BTAs in Chapter 5. This may result from slightly higher polarity of MCH than that of other alkane solvents and its larger dielectric constant (ε = 2.02 at 293 K).[11] In the absence of DBU, temperature-dependent CD spectra of **1a** in MCH gave rise to typical cooperative curves (Figure 6.3A, square and up triangle) with similar $\Delta\varepsilon$ values regardless of the cooling rate ($\Delta\varepsilon \approx 60$ L mol^{-1} cm^{-1} at 293 K). However, in the presence of DBU (1 eq.) the intensity of the CD effects decreased while the shape of the cooling curves remained non-sigmoidal, thus cooperative (Figure 6.4A, circle and down triangle). The intensity of the CD signal at 293 K decreased

further when the cooling rate was decreased from 60 K h^{-1} to 10 K h^{-1} ($\Delta\varepsilon \approx 50$ L mol^{-1} cm^{-1} at 60 K h^{-1} and 30 L mol^{-1} cm^{-1} at 10 K h^{-1}). These results suggest that base influences the helix sense preference during the supramolecular polymerization when the reaction time is sufficiently long. Interestingly, the UV-vis spectra of **1a** (1 eq.), taken at every 10 K intervals (Figure 6.4B), demonstrated that the aggregation behavior also differs in the presence of base. Similar blue shift was observed around λ = 239 nm upon cooling; however, in the presence of base red shift was not observed around λ = 300 nm. Furthermore, DDLS measurements revealed 15% decrease in the stack length (499 nm) at 298 K in the presence of base. The results suggest that base has an influence on the aggregation behavior and expression of supramolecular chirality; however, the origin of this effect is not elucidated completely for the time being.

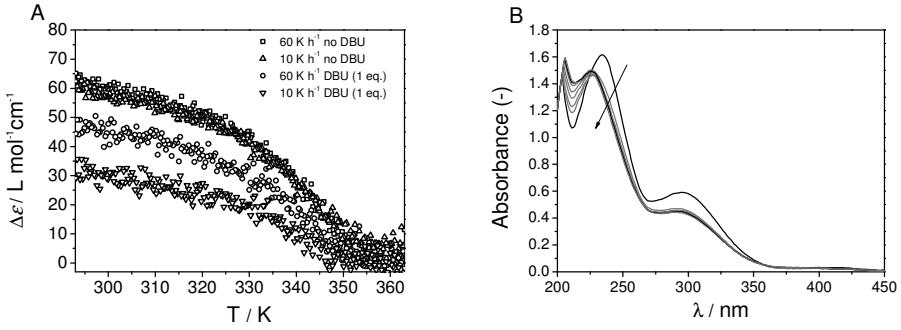

Figure 6.4: The effect of base on the self-assembly of **1a** in MCH. CD and UV-vis spectra as a function of temperature monitored at λ = 237 nm for **1a** in MCH (c = 4.2×10^{-5} M). A) CD spectra at various cooling rates: 60 K h^{-1} (square) and 10 K h^{-1} (up triangle), in the absence of DBU. 60 K h^{-1} (circle) and 10 K h^{-1} (down triangle), in the presence of DBU (1 eq.). B) Interval UV-vis spectra of **1a** in the presence of DBU (1 eq.) as a function of temperature monitored at a cooling rate of 10 K h^{-1} in MCH (c = 4.2×10^{-5} M) measured between 363 K and 293 K at 10 K intervals. The arrow shows the decreasing temperature.

6.2.3 Oscillations

DBU (1 eq.) was added into the solution of **1a** in MCH (c = 9×10^{-4} M) and the solution was heated at 353 K for 2 h. The solution was brought back to 293 K in 2 min and CD and UV-vis spectra were recorded as a function of time as the system reached 293 K. CD and UV-vis spectra gave rise to an oscillating behavior which continues for approximately 80 min (Figure 6.5) after which the system reached thermodynamic equilibrium leading to constant CD and UV-vis signals. This experiment was repeated several times and the oscillations were

reproducible, suggesting that the observed effect is not an artifact. Similar experiments were performed under different conditions i.e., the effect of cooling down to different temperatures, application of more base and stirring[†] on the observed behavior was investigated. In most of the experiments oscillating behavior was observed; however, the amplitude and the number of oscillation cycles were different.

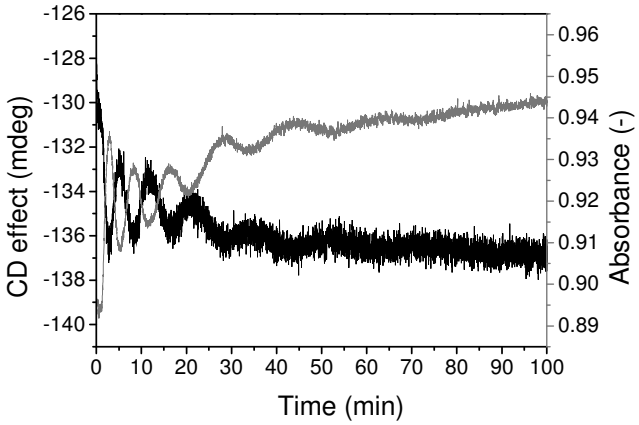

Figure 6.5: CD (black) and UV-vis (gray) spectra of **1a** in MCH as a function of time (c = 9×10^{-4} M, monitored at λ = 316 nm).

6.3 Discussions

The measurements suggest that oscillations may be encountered in this model system when a deprotonation reaction was introduced as an inhibitory step that prevents the monomeric species from assembling into helical stacks. It can be now questioned whether these are real oscillations resulting from two competing processes; deprotonation and self-assembly. The oscillation experiments are reproducible; however, the experiments are very sensitive to physical conditions such as temperature, pH, monomer concentration and stirring. Self-assembly and pK_a are two temperature-dependent phenomena. As the temperature decreases, monomers are withdrawn from the free monomer pool in order to self-assemble (Figure 6.6). Simultaneously, monomers are dissociated by base in order to form anionic species (anionic species can be considered as the intermediate reactants in this system as mentioned before i.e., anions are produced by base but consumed simultaneously by the formation of assemblies). Assuming the two processes have similar rate constants, dissociation of the acidic **1a** by base may act as a negative feedback for the self-assembly

[†] Stirring was performed by adding iron powder in the 0.1 cm cuvette.

process. Deprotonation reaction inhibits self-assembly thus the thermodynamic equilibrium is delayed and an oscillatory response is observed. The theoretical model explaining the oscillating behavior in this system is under investigation. The oscillation behavior of the thioamide-base system, however, is observed in so many different experiments that the observed effect can hardly be an artifact. Hence, the observations made for the system discussed in Chapter 5 could also be the result of the same protonation-deprotonation mechanism.

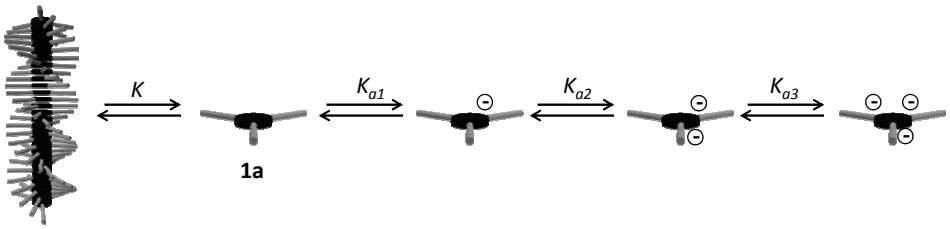

Figure 6.6: Schematic representation of the multiple equilibria as a result of simultaneous deprotonation and self-assembly of BTA **1a**.

6.4 Conclusions and outlook

The design of oscillating reactions is nontrivial yet important since chemical oscillators are intriguing systems that have implications for biology[12], catalysis[13] and fundamental research on understanding the complex self-assembly behavior. Noncovalent synthesis offers a wide range of applications. Combination of noncovalent synthesis with conventional covalent synthesis offers promising routes for bringing the self-assembly process from equilibrium to non-equilibrium. A rational design of the covalent and noncovalent processes may provide valuable information on complex self-assembly systems that are observed in biology. This information can be then used to build self-assembled systems with autocatalytic mechanism, molecular machines or the synthetic mimic of the biological systems.

6.5 Experimental

6.5.1 General

UV-vis and circular dichroism (CD) measurements were performed on a Jasco J-815 spectropolarimeter where the sensitivity, time constant and scan rate were chosen appropriately. Corresponding temperature dependent measurements were performed with a PFD-425S/15 Peltier-type temperature controller with a temperature range of 263-383 K and adjustable temperature slope. Linear dichroism was not observed in the experiments. Cells

with an optical path length of 0.1 cm were employed and spectroscopic grade methylcyclohexane (MCH) were employed. MCH was obtained from Aldrich in spectroscopic grade (99+%) and used as received. Solutions were prepared by weighing the required amount of compound for a given concentration, after which this amount was transferred to a volumetric flask (flasks of 5 mL were employed). Then the flask was filled with the spectroscopic grade solvent and put in an oscillation bath at 313 K for 50 min, after which the flask was allowed to cool down. Any loss of solvent was compensated. The molar circular dichroism was calculated from: $\Delta\varepsilon$ = CD effect/ (32980 c *l*) in which c is the concentration in M (mol L^{-1}) and *l* is the optical path length in cm.

6.6 References

[1] G. M. Whitesides, B. A. Grzybowski, *Science* **2002**, *295*, 2418.
[2] I. R. Epstein, K. Showalter, *J. Phys. Chem. B* **1996,** *100,* 13132.
[3] P. D. Kepper, I. R. Epstein, K. Kustin, *J. Am. Chem. Soc.* **1981**, *103*, 2133.
[4] R. J. Field, F. W. Schneider, *J. Chem. Ed*. **1989**, *66*, 195.
[5] T. Mes, unpublished results.
[6] C. Alemán, *J. Phys. Chem. A* **2001**, *105*, 6717.
[7] F. G. Bordwell, D. J. Algrim, J. A. Harrelson, Jr. *J. Am. Chem. Soc.* **1988**, *110*, 593.
[8] A. J. Markvoort, H. M. M. t. Eikelder, P. A. J. Hilbers, T. F. A. de Greef, E. W. Meijer, *Nat. Commun*. **2011**, *2*, 59.
[9] M. Tirado, J. d. l. T. Garcia. *J. Chem. Phys.* **1980**, *73*.
[10] H. Yamakawa, M. Fujii, *Macromolecules* **1973**, *6*, 407.
[11] W. R. Pyle, *Phys. Rev*. **1931**, *38*, 1057.
[12] M. J. Berridge, *Nature* **1993**, *361*, 315.
[13] Y. H. Hu, E. Ruckenstein, *Ind. Eng. Chem. Res*. **1998**, *37*, 2333.

Consequences of Cooperativity in Supramolecular Polymers

Cooperativity is widely observed in the self-assembled systems that are found in Nature. DNA, RNA, starch and proteins, which are some of the biologically important self-assembled systems in Nature, embody the principles of cooperative self-assembly. The repeating units that form these macromolecular structures are held together by cooperative non-covalent interactions and act harmoniously as a result of this cooperation. In addition to cooperativity, chirality plays a dominant role in Nature. Biologically important molecules such as amino acids, nucleic acids and sugars are homochiral (i.e., they constitute a class of molecules with the same absolute configuration, e.g., all amino acids adopt L-configuration while all sugars bear D-configuration). The enzymatic reactions as well as the pharmaceutical activities depend strongly on the chirality of these molecules. The origin of homochirality in biological molecules is an intriguing research topic among scientists. Several mechanisms propose that a small initial imbalance between the enantiomers (i.e., symmetry-breaking between D and L forms) is followed by an amplification of this imbalance. Considering the profound importance of cooperativity and chirality that are observed in biological systems, it is both scientifically fascinating and technologically relevant to study synthetic supramolecular polymers in order to gain insights into the fundamentals of complex systems in biology. Furthermore, unraveling the complexity in multi-component systems provides valuable information for the rational design of molecules that self-assemble into nano-objects of defined structure, stability and shape by the molecular information stored in the chemical structure. Benzene-1,3,5-tricarboxamide (BTA) molecules are particularly appealing building blocks owing to their cooperative self-assembly behaviour in dilute solutions, expression of supramolecular chirality and synthetic accessibility. This dissertation focuses on the cooperative self-assembly behaviour of BTA molecules in dilute alkane solvents and describes the effects of cooperative interactions between monomers within the aggregates.

Chapter 1 gives a general overview on cooperativity, self-assembly mechanisms and chiral amplification. Cooperativity is defined as based on the interactions of the building blocks within macromolecules that are found in biological and synthetic systems. After that, two general self-assembly mechanisms, cooperative and isodesmic, are briefly discussed. Chiral amplification phenomena are analyzed in different systems such as molecular, macromolecular, solid surfaces and in crystals. Finally, BTA molecules are described as a model system for studying cooperativity and chiral amplification in supramolecular polymers. The structural properties of BTAs and synthetic approaches for BTA procurance are addressed. Cooperative self-assembly behavior and chiral amplification in BTA-based supramolecular polymers are described. Chapter 1 is concluded with the aim and outline of the dissertation.

In Chapter 2 the enantioselective syntheses of chiral, deuterated octyl alcohols and amines are described. Chiral, deuterated octyl alcohols are obtained in high yields and enantiomeric excesses by the enzymatic reduction of deuterated octanal in the presence of alcohol dehydrogenases as the biocatalysts and nicotamide adenine dinucleotide phosphate as the cofactor. This method gives the desired deuterated octyl alcohols in high yields and purity; however, it requires a lengthy synthetic strategy. To shorten the synthetic route, direct reduction of octanal by the same enzymes is applied by using a deuterated cofactor and the efficiency of the two reduction methods is compared. The enantiomeric excesses are accurately determined by using Mosher's acid method. After that, these chiral, deuterated octyl alcohols are converted into the corresponding deuterated amines *via* tosylation, azidation and reduction reactions. Furthermore, β-deuterated amines are obtained from deuterated alcohols by tosylation, cyanation and reduction. These amines are subsequently employed in the synthesis of α− and β−deuterated benzene-1,3,5-tricarboxamide molecules the self-assembly behaviour of which is discussed in Chapter 3.

Chapter 3 addresses the questions 'how far can we push supramolecular chirality?' 'how does isotope chirality reflect at the supramolecular level?' 'how do these systems compare to the covalent analogues?'. A detailed analysis on the self-assembly of α-deuterated-BTA molecules is carried out in dodecane solvent by using temperature-dependent UV-vis and circular dichroism (CD) spectroscopy. The self-assembly of these monomers in dodecane solution gives rise to the formation of helical aggregates. Studies reveal that α-deuterated-BTA monomers form left- (*M*) and right-handed (*P*) helical aggregates in solution at room temperature with a ratio of 69% and 31%, respectively. These results suggest that deuterium chirality is sufficient to bias the formation of a preferred helical sense as a result of cooperative interactions between the monomers. Further comparison between the noncovalent BTA polymers and the conventional helical covalent polymers shows that the result of isotopic substitution is remarkably similar despite the differences in the formation mechanisms of the two.

In Chapter 4 the effect of solvent on the self-assembly behaviour of α-deuterated-BTA motif is investigated by using temperature dependent UV-vis and CD spectroscopy. Two alkane solvents, heptane and methylcyclohexane, which have similar physical properties, are used for the self-assembly process. Experimental findings demonstrate that relatively small structural differences in the alkane solvents result in remarkable changes in the expression of supramolecular chirality and the conformation of the supramolecular polymer. The effects observed are attributed to the active participation of the solvent molecules in the self-assembly process. A number of linear, cyclic and branched alkane solvents are applied for further analysis.

In Chapter 5 the racemization reaction in a cooperative self-assembled system is described. The kinetics of racemization and the nature of the final state of a racemizing supramolecular

system in the presence of a chiral auxiliary are investigated. A new BTA molecule comprising a labile stereocenter is synthesized and the racemization reaction is studied by using an organic base in methylcyclohexane solution. The optical activity of the compounds is monitored by applying high-performance liquid chromatography (HPLC) and CD spectroscopy. The racemization reaction follows first-order reaction kinetics under the conditions that BTA molecules are at the molecularly dispersed state. However, the same reaction follows nonfirst-order reaction kinetics under self-assembly conditions i.e., in the presence of BTA aggregates. This effect is investigated in detail by using a theoretical model and the observed effects are attributed to the changes in the free monomer concentration in solution as a result of *majority-rules principle* in BTA self-assembly. Finally, enantioenriched BTA molecules are obtained from a racemizing solution in the presence of a sergeant molecule which is unreactive towards base.

In Chapter 6 an outlook on increasing complexity in self-assembled systems by combining covalent synthesis with noncovalent synthesis is given. Preliminary studies on a system that undergoes partial depolymerisation upon treatment with base are described. Abstraction of amide hydrogen of a BTA derivative in the presence of an organic base leads to oscillatory chiroptical properties when sudden temperature changes are applied in the system. Chapter 6 summarizes the preliminary observations and discusses what the combination of covalent and noncovalent chemistry brings to the field of supramolecular chemistry in the future.

Süpramoleküler Polimerlerde Kooperativitenin Akibeti

Kovalent olmayan etkileşimler (örneğin hidrojen bağı) ve kooperativite doğada sıklıkla gözlemlenen olgulardır. Mesela, DNA, RNA, nişasta ve protein gibi biyolojik önemi olan makromoleküllerdeki yapı taşları birbine zayıf ve kovalent olmayan bağlarla tutunurlar. Ayrıca, bu yapı taşları bu zayıf etkileşimleri kullanarak, birlikte, uyumlu bir şekilde, yani kooperatif olarak hareket ederler. Kooperativiteye ek olarak, kiralite doğada çok önemli rol oynayan ikinci bir olgudur (kiral moleküllerde karbon atomları 4 farklı sübstitüente sahiptirler. Kiral molekuller ayna görüntüleriyle çakışmazlar). Amino asit, nükleik asit ve şeker gibi biyolojik açidan önem taşıyan yapı taşları homokiral özellik taşırlar (yani bu moleküller−3 boyutlu olarak bakıldığında−ortak bir konfigürasyona sahiptirler, mesela amino asitler L-konfigürasyonu taşırken bütün doğal şekerler D-konfigürasyonuna sahiptirler). Biyolojik sistemlerdeki bütün enzimatik tepkimeler ve farmasötik aktiviteler bu moleküllerdeki konfigürasyona bağlı olarak yürürler. Doğada homokiral moleküllerin oluşumunun akibeti belirsizdir. Yaşamın, rasem, prebiyotik bir karışımdan (yani D- ve L-konfigürasyonlarına sahip moleküllerin eşit oranlarda bulunduğu karmaşık bir çorbadan) başladığını düşünürsek, nasıl olur da bütün şekerler sadece D-konfigürasyonuna sahip olarak evrimleşmiştir? Bu soru bilimsel çevrelerde henüz çözümlenmemiş bir soru olduğundan, son derece ilgi çekici bir çalişma konusudur. Bu soruyu cevaplamak uzere uretilmis bir çok argüman vardır; bunlardan biri bu moleküllerin oluşumunda (yaklaşık 5 milyar yıl önce) D- ve L-yapılarından birinin, diğerine göre çok çok küçük bir farkla daha fazla oluşması ve bu farkın diğer reaksiyonlarda artması (amplifikasyonu) ile ilgilidir.

Kooperatifliği ve kiraliteyi basit ve hayata dair bir örnekle açıklamaya çalışalım; (süpra)polimer kimyasında da sıklıkla kullanılan bir örnek 'asker-çavuş ilişkisi' dir. Bir sentetik polimer sarmal yapıda olabilir. Eğer bu polimer akiral monomerlerden oluşuyorsa, monomerler %50 sağa kıvrılan (*P* konfigürasyonu) veya %50 sola kıvrılan (*M* konfigürasyonu) sarmal yapılar oluşturabilirler. Bu akiral polimerler, katalitik miktarda 'çavuş' polimerler (yani 100% *P* konfigürasyonuna sahip olan polimer) ile karıştırıldığında bütün diğer akiral polimerler 'çavuş' polimerin izlediği sarmalin konfigürasyonunu yani *P*'ye uyum sağlamaktadır. Bir başka deyişle, akiral polimerler %50 *P* ve %50 *M* olmak yerine %100 *P* olmayi tercih ederler. Bu da ancak monomerlerin koopearif bir şekilde hareket etmesi ve kiral bilginin monomerler arasında taşınmasıyla mümkündür.

Kooperatif etkilerin ve kiralitenin doğadaki önemini düşünecek olursak, sentetik süpramoleküler polimerler üzerine çalişmak hem akademik hem de teknolojik açıdan heyecan verici ve önemlidir. Dahası, doğada gözlenen karmaşık yapılar üzerine edindiğimiz temel bilgileri daha sonra çeşitli fonksiyonel sentetik sistemler üretmek üzere kullanabiliriz. Benzen-1,3,5-trikarboksamid (BTA) molekülleri özellikle ilgi çekici moleküllerdir. Bu moleküller derişik çözeltilerde kooperatif olarak ve kendiliğinden bir araya gelip büyük

yapılar (süpramoleküler polimerler) oluştururlar (*self-assembly*), bu küçük moleküllerdeki kiral bilgi büyük yapıların konfigürasyonuna yansir. Örneğin, monomerler (*S*) konfigürasyonuna sahip ise, bu monomerlerin üstüste gelerek oluşturduğu sarmal yapının konfigürasyonu *M*'dir. Dahası, BTA'lar sentetik olarak kolay erişilebilir moleküllerdir. Tum bu özellikler, bu molekülleri çalışmayı pratik ve anlamlı kılar. Bu doktora tezi spesifik olarak BTA'ların derişik organik çözücülerde kooperatif olarak bir araya gelme mekanizmalarını ve bu etkilerin limitlerini inceler.

1. Bölüm'de kooperatif etkiler, moleküllerin bir araya gelme mekanizmaları ve kiral amplifikasyon üzerine genel bir bakış verilir. Kooperatif etkiler, biyolojik ve sentetik sistemlerde, küçük yapı taşları arasındaki etkileşimler göz önüne alınarak incelendikten sonra, iki *supramolekuler polimerizasyon* mekanizması, kooperatif ve izodesmik olarak iki kısımda genel olarak incelenir. Kiral amplifikasyon fenomeni farklı sistemlerde; moleküler, ve makromoleküler düzeyde, katı yüzeyler ve kristal yapılarda ele alınmıştır. Bu bölümde son olarak BTA moleküllerindeki kooperativite ve kiral amplifikasyon özetlenmektedir. BTA'larin yapısal özellikleri ve bu moleküllerin elde edilmesindeki sentetik stratejiler kısaca anlatılır. 1. Bölüm doktora tezinin amacı ve genel taslağıyla son bulur.

2. Bölüm'de ağır hidrojen (döteryum) atomuyla sübstitüye edilmiş oktil alkol ve aminlerin enantiyoselektif sentezi anlatılmıştır. Kiral, monodötero-oktil alkoller enzimatik indirgeme reaksiyonları kullanarak yüksek verimle ve yüksek enantiyomerik saflıkta elde edilmiştir. Enzimatik indirgeme tepkimelerinde alkol dehidrojenaz enzimleri biyokatalist olarak, nikotamid adenin dinucleotit fosfat da kofaktör olarak kullanılmıştır. Bu yöntem kullanılarak istenilen oktil alkoller yüksek verimle ve saflıkta elde edilir; fakat, bu yöntem uzun ve zahmetli bir sentetik yöntemdir. Bu yönteme alternatif olarak, oktanalı direk olarak indirgeme yöntemine gidilmiştir. Bu sentetik stratejide aynı enzimler ve kofaktör kullanılmıştır. Elde edilen alkollerin enantiyomerik saflığı Mosher asit yöntemiyle tayin edilmiştir. İki indirgeme tekniği sonucunda oluşan ürünlerin verimi ve enantiyomerik saflığı karşılaştırılmıştır. Daha sonra, elde edilen monodötero-oktil alkoller sırasıyla tosilleme, azitleme ve azidi amine indirgeme yöntemleriyle kiral, monodötero-amin türevlerine dönüştürülmüştür. Bunun yanında, aynı alkollerin kullanılmasıyla döteryum atomunun β-pozisyonunda olduğu aminler elde edilmiştir. Son olarak bu aminler α- ve β-s bstitüye benzen-1,3,5-trikarboksamid moleküllerine çevirilmiştir, bu moleküllerin süpramoleküler polimer oluşturma davranışları 3. Bölümde incelenecektir.

3. Bölüm şu sorular üzerinde durur; 'süpramoleküler kiralitenin sınırlarını ne kadar zorlayabiliriz?' 'izotop atomuyla elde edilen kiralite süpramoleküler düzeyde nasıl ortaya çıkar?' 'burada elde edilen süpramoleküler sistemler kovalent olan analoglarıyla nasıl farklılıklar ve benzerlikler gösterir?'. α-Mono-dötero sübstitüye BTA moleküllerinin dodekan içerisindeki *self-assembly*'si sıcaklık kontrolu altında UV-vis ve *circular dichorism* (CD) spektroskopisi yardımıyla gözlemlenir. Bu moleküller, derişik dodekan çözeltisinde,

hidrojen bağının yardımıyla, sarmal yapıda olan süpramoleküler polimerler oluştururlar. Oluşan sarmal yapılarda, *M* konfigürasyonu, *P* konfigürasyonuna göre daha çok oluşmuştur ve oda sıcaklığında oranları, *M*:*P* = 69:31'dir. Bu sonuçlar, bir izotop atomunun kiral süpramoleküler polimerler oluşturmak için yeterli olacağına işaret eder. Bu da moleküller arasındakı kooperatif etkileşimin sonucudur. Kiral bilgi moleküller arasında transfer edilir ve sarmal yapıların oluşumunu sağlar. Bu konuda yapılan diğer çalışmalar, kovalent bağlarla birbirine bağlı olmayan fakat polimerik yapıda olan makromoleküllerin, bilinen kovalent polimerlerle çok yakın özellikler gösterdiğini vurgular. Bu iki sistemin (kovalent ve kovalent olmayan polimerler) oluşma mekanizmalari göz önüne alındığında birbirinden oldukça farklı olduğu düşünülürse bu benzerlik çok heyecan vericidir.

4. Bölüm'de α-mono-dötero sübstitüye BTA moleküllerinin *self-assembly*'sinde kullanılan çözücülerin *self-assembly* üzerine etkisi tartışılmaktadır. Bu çalışma, sıcaklık kontrollü, UV-vis ve CD spektroskopisi kullanılarak yapılmıştır. Benzer fiziksel özellikler gösteren heptan ve metilsiklohekzan, BTA'larin *self-assembly*'si için kullanılmıştır. İki çözücü birbinden sadece yapısal olarak ayrılmasına rağmen (heptan lineer ve metilsiklohekzan siklik yapıdadır), BTA bazlı süpramoleküler polimerlerin kiralite özellikleri ciddi farklılıklar gösterir. Aynı şekilde bu süpramoleküler polimerlerin konformasyonunda da değişiklikler gözlemlenir. Bu gözlemler, çözücü moleküllerinin aktif olarak süpramoleküler polimerlerle bir sekilde etkileşim halinde olduğunu önermektedir. Çözücü moleküllerindeki en ufak bir değişiklik, monomer arasındaki kooperatif etkileşim sonucu, süpramoleküler düzeye yansımaktadır. Bunun yanında, daha birçok çözücü üzerinde aynı deneyler denenmiştir ve çıkan sonuçlar bu savımızı destekler yöndedir.

5. Bölüm'de kooperatif *self-assembly* sistemlerine uygulanan rasemizasyon reaksiyonu ele alınmıştır. Bunun için asidik proton taşıyan yeni bir BTA (Phg-BTA) türevi sentezlenmiştir. Asidik proton Phg-BTA'nın kiral merkezi üzerinde olduğundan dolayı, bu molekül metilsiklohekzan çözeltisi içerisinde organik bir bazla muamele edildiğinde rasemikleşmeye müsaittir. Moleküllerin optikçe aktivitesi kromatografik ve spectroskopik yöntemler (HPLC ve CD) aracılığıyla tayin edilmiştir. Burada süpramoleküler polimer oluşumu ve rasemizasyon tepkimesi aynı anda gerçekleşir ve bu durum rasemizasyon reaksiyonunun kinetiğini etkiler. Bu sistemde, Phg-BTA'lar tamamen serbest halde iken rasemizasyon reaksiyonu, birinci derece reaksiyon mekanizmasını izler. Fakat Phg-BTA'lar polimer halinde olduklarında, aynı şartlar altında gerçekleşen rasemizasyon reaksiyonu birinci derece olmaktan çıkar. Bu sonuçlar teorik hesaplamalar da kullanılarak desteklenmiştir. Detaylı araştırmalar, bu etkilerin monomer konsantrasyonundaki değişimler sonucunda ve süpramoleküler polimerlerde gözlenen '*majority rules*' yani 'çoğunluğun hakimiyeti' yasasına dayandığını ortaya çıkarmıştır. Son olarak bu bölümde baza karşı reaktif olmayan kiral moleküller kullanılarak rasem karışımdan enantiyomerik saflığı arttırılmış Phg-BTA molekülleri elde edilmiştir.

6. Bölüm'de BTA bazlı süpramoleküler polimerleri kullanarak gelecekte nelerin yapılabileceği tartışılmaktadır. Daha önceki bölümlerde anlatılan BTA bazlı süpramoleküler yapılar termodinamik kontrol altında oluşurlar. Bu yapıların oluşumu hakkında birçok bilgiye sahibiz ve elde ettiğimiz deneysel sonuçlari kantitatif olarak da çözümleyebiliyoruz. Peki ileride bu sistemleri daha sofistike hale getirebilir miyiz? Bu sistemleri termodinamik dengeden uzaklaştırıp osilasyon yapan sistemler üretebilir miyiz? Bu bölümde bu tür sorulara cevap aranmaktadır ve başka bir BTA türevi olan tritiyoamid bazlı BTA'lar üzerinde gerçekleştirilen ilk deneysel sonuçlar özetlenmektedir. Tiyo-BTA'larda NH hidrojenleri asidiktir, bu protonlar baz yardımıyla koparılabilirler. Bu protonlar koparıldığında oluşan anyonlar bir reaktif ara ürün görevi görür. Nötral halde kalan monomerler bir yandan süpramoleküler polimer yapısına katılırken diğer yandan da baz yardımıyla anyon halinde kalırlar ve oluşan polimerler depolimerize olur. Bu esnada ani bir sıcaklık değişimi uygulandığında sistem hemen termodinamik dengeye ulaşamaz ve osile eden optik özellikler gösterebilir. Bölüm 6, bu konudaki ilk deneyleri özetlerken, kimyasal reaksiyonlarin kovalent olmayan etkileşimlerle birleştirildiginde ne gibi sonuçlar elde edilebileceğini ve bunun süpramoleküler kimya alanına ne gibi faydalar sağlayabileceğini değerlendirmektedir.

Curriculum Vitae

Seda Cantekin was born on March 24, 1981 in Istanbul, Turkey. After secondary education at Kaya Bayazıtoğlu Lisesi in Ankara, she started studying Chemistry at the Middle East Technical University in Ankara. She completed her master's program in the same university at the Graduate School of Natural and Applied Sciences under the supervision of prof. dr. M. Balcı. During her master's research she studied the total synthesis of conduritol derivatives which are biologically active molecules showing antibiotic, antileukemic and glycosidase inhibitory activities. In 2008 she joined the Molecular Science and Technology group and the Institute for Complex Molecular Systems at the Eindhoven University of Technology as a PhD student under the supervision of prof. dr. E. W. Meijer and dr. ir. A. R. A. Palmans. Her PhD research investigates the limits of supramolecular chirality in synthetic supramolecular polymers. The research describes the influence of subtle structural changes in the monomeric level on the cooperative self-assembly and chiral amplification behaviour. Most important results of this research are presented in this dissertation.

List of publications

Consequences of cooperativity in racemizing supramolecular systems
S. Cantekin, H. M. M. ten Eikelder, A. J. Markvoort, M. A. J. Veld, P. A. Korevaar, M. M. Green, A.R.A. Palmans, E. W. Meijer, *Angew. Chem. Int. Ed*. **2012** DOI 10.1002/anie.201201701.

A stereoselectively deuterated supramolecular motif to probe the role of solvent during self-assembly processes
S. Cantekin, Y. Nakano, J. C. Everts, P. van der Schoot, E. W. Meijer, A. R. A. Palmans, *Chem. Commun*. **2012**, *48*, 3803.

Enantioselective synthesis of (R)-and (S)-1-²H-1-Octanol and their corresponding amines
D. W. R. Balkenende, S. Cantekin, C. J. Duxbury, M. van Genderen, E. W. Meijer, A. R. A. Palmans, *Synth. Commun*. **2012,** *42*, 563.

Pushing the limits of amplification of chirality in supramolecular polymers
S. Cantekin, A. R. A. Palmans, *Chemistry Today* **2011**, *29*, 4.

The effect of isotopic substitution on the chirality of a self-assembled helix
S. Cantekin, D. W. R. Balkenende, M. M. J. Smulders, A. R. A. Palmans, E. W. Meijer, *Nature Chem*. **2011**, *3*, 42.

Towards racemizable chiral organogelators
J. –B. Lin, D. Dasgupta, S. Cantekin, A. P. H. J. Schenning, *Beilstein J. Org. Chem*. **2010**, 960.

Synthesis of bromo-conduritol-B and bromo-conduritol-C as glycosidase inhibitors
S. Cantekin, A. Baran, R. Caliskan, M. Balci, *Carbohydr. Res*. **2009**, 426.

Synthesis of phenyl-substituted conduritol B and its mechanism of formation
S. Cantekin, R. Caliskan, E. Sahin, M. Balci, *Helv. Chim. Acta* **2007**, 2227.

(to be) submitted

Benzene-1,3,5-tricarboxamide: a versatile ordering moiety for supramolecular chemistry
S. Cantekin, T. F. A. de Greef, A. R. A. Palmans, submitted to *Chem. Soc. Rev.*

Thermally induced cooperative helix-to-helix transformation in a dynamic supramolecular polymer
Y. Nakano, S. Cantekin, H. M. M. ten Eikelder, A. J. Markvoort, A. R. A. Palmans, E. W. Meijer, to be submitted.

Acknowledgements

Now it is really the end and I am writing the most important part of my dissertation. When I look back I see memorable four years full of excitements, happy days and the joy of performing science. This whole thing would be impossible without having the support of wonderful people around me which made me feel always so special and lucky.

I would like to start with thanking my PhD supervisor prof. dr. Bert Meijer for giving me the opportunity to be a part of MST family and trusting me from the beginning that I can do it. Bert, thank you for opening the doors of supramolecular chemistry wide open to me and letting me in. It was an amazing experience working with you. You have been always open for any kind of ideas, suggestions and have provided me with the opportunities that I can become an independent scientist. No matter how busy you were, your office door has been always open for discussing any single experimental detail. I remember spending three hours on an ordinary busy afternoon for discussing deuterium BTA project with you. Thanks for your helpful suggestions and quick, straightforward solutions to any kind of problems. Thanks for always being so interested. Thanks for being a great teacher and putting your time and effort. I learnt a lot from you all these years.

I would like to thank my PhD co-supervisor dr. Anja Palmans for showing me the way; showing me light at the end of the road and helping me find my way when I am lost. Anja, thanks for always being there to help. Thanks for sharing my enthusiasm on my projects. Thanks for being direct and critical. Your criticism, suggestions and solutions have been very valuable to me and helped me enormously to improve myself both academically and personally. You helped me stay focused during this though adventure. I felt always very motivated and got inspired anytime I talked to you. Thanks also for sharing great time out of work, nice dinners, wine, cocktail parties, and 'ladies nights'.

I would like to thank dr. Jef Vekemans for taking part in my reading and promotion committee. Jef, thanks for being a great teacher and for being always there for answering questions and for nice chats. It has been always a great pleasure to discuss reaction mechanisms and fundamental things in organic chemistry with you. I would like to thank you also for giving me the chance for practicing teaching in the 'werkcollege'. I enjoyed teaching and the 'voorbespreken' sessions a lot.

I would like to express my gratitude to the members of my promotion committee. prof. Blackmond, I am honoured that you took part in my reading committee and came to Eindhoven to participate in my PhD defence. prof. Put, thank you very much for taking part in my reading and promotion committee. Also I would like to thank prof. Sijbesma and dr. Markvoort for participating in my promotion committee.

I would like to thank the analytical team Lou, Ralf and Joost for performing various analyses. I would like to thank especially Joost for helping me with the HPLC measurements that were discussed in Chapter 5. I would like to thank Henk Eding for creating a nice working environment in MST. Thanks for the nice chats in the early morning; I will miss the Eding style coffee. I would like to thank administrative staff for making life much easier (being a Turkish I always had some issues with getting my visa (especially to England☺)). Angela, Joke, Carine, Nora, Jolanda and Sagitta, thanks a lot for helping out with paper work and administrative stuff. I would like to thank Hans Damen for taking care of the chemicals.

I enjoyed working in Lab 2 and have always thought that Lab 2 was the nicest lab to work:P I would like to thank Jolanda for making Lab 2 such a lovely place to work. Thanks for your help and for the nice music (Adele 21☺, all day long!). I would like to thank my lab mates for nice working environment, Marko, Tristan, Patrick, Martijn G., Feng, Matt, Thorsten and Müge. I would like to thank my office mates; Edith, Wilco, Tristan, Müge, Louis and Bram. Thanks for the nice working atmosphere in the office. Thanks for being always very kind and helpful. Bram, thanks for your help with the computer work. I would like to thank especially Tristan for the nice times together at Fort, uitjes and Breckenridge. Thanks for making "*I love organic chemistry*" and '*the singing fish*' kind of symbols of our office☺. I would like to thank you for thio-BTAs which were discussed in Chapter 6 as well. Also thanks a lot for the motivation and support during my writing period. Thanks very much for being my paranymph. I would like to thank Floris for the enjoyable times out of work, chats and lunches and of course for being my other paranymph. I am happy that you guys will wear the suit once more this time for me.☺

During my PhD I had a chance to work with two great mathematicians, dr. Markvoort and dr. ten Eikelder who helped me enormously during Phg-BTA and deuterated BTA projects. I am very happy and feel so lucky that Huub and Bart have been interested in modelling my experimental work. It has been always informative to talk to them. I was lucky that their office were very close to mine. I often went to the BMT department with a bunch of questions in my head. After chatting for a while (sometimes hours) I left the building with a light shining above my head. I got almost all answers to my questions (and many more questions appeared as well), well sometimes I forgot all the explanations till I came back my office but no problem I could always ask again. I even sometimes

think that we actually do not need experiments, we can actually calculate and model everything?!?. Huub and Bart, thank you so much for being very helpful, being available all the time and for all informative e-mails. I appreciate your contribution to my dissertation. I wish you all the best and success!

I would like to thank Maarten Smulders for valuable contributions on the deuterated BTA project. Your comments, suggestions have been very helpful. Thanks also for the nice times in MST and the great time we had in Cambridge. I wish you and Leonie all the best for the future.

I would like to thank Peter and Tom for valuable discussions and helping out with understanding the complex systems. Tom, thanks a lot for sharing my excitement on oscillating self-assembly. I hope one day we can make it happen and show that it is real. I enjoyed writing the review together. It was one of the quickest articles I guess (thanks to Anja!). Also thanks for the tips during my busy writing time, they were quite helpful.

I would like to thank prof. van der Schoot for the contributions on the solvent effect project. I would like to thank Ivo Filot for the permission that I could use some of his unpublished results on the deuterated BTA project. The outcome of the DFT calculations are great!.

I would like to thank Koen Pieterse and the ICMS Animation Studio. Koen, I could impress everyone with the nice animation you made on the racemization project. I always got so nice feedback that sometimes the animation got much more attention than my scientific work:P Koen, thank you very much for creating a beautiful piece of art on BTA work. Also thanks for the great cover you made for the Chemical Communications. And of course thanks for the beautiful cover you made for my dissertation. Thanks for your time and effort and being always available.

During my PhD I had the honour to meet prof. Green and collaborate with him on the deracemization project. He visited us in Eindhoven two times, we met in Liverpool in the chirality conference and we kept contact over many e-mails. Dear prof. Green, I enjoyed talking to you a lot and it was so much fun to discuss science with you. I learnt a lot from you. Your detailed work on chirality in macromolecules has been a milestone in this area. You are a great teacher. I am so happy that I had the chance to meet you. Thanks very much for your interest and input.

I would like to thank Martijn V. for the nice collaboration on Chapter 5 and the famous Phg-BTA molecules. It was fun working with you (and your lab journal is great☺). Thank you Patrick for providing me with some of your alkyl substituted BTAs. It was very handy to have the whole BTA library in the lab, thanks for all your synthetic effort. I would like to thank Bas for synthesizing the thio-BTAs which were discussed in Chapter 6.

I would like to thank Yoko for contributions on Chapter 4 which definitely increased the quality of the project. I always admired your perfection and hard working. Also thank you for your friendship. I wish you and Neal all the best in future!

I would like to thank dr. Albert Schenning and Jian Bin for working together on the Resolve project. It has been so much fun to attend Resolve meetings together.

I would like to thank staff members of MST for being always there for help when needed, Stefan, Marcel, Ilja, Patricia, Martijn, Rene, Rint, Luc, Maarten M. and Tom. Rene and Martijn W., I enjoyed teaching Organic Chemistry A together. Ilja, thanks for your help on DLS measurements discussed in Chapter 6. Marcel, special thanks for your help on the NMR studies discussed in Chapter 2.

I would like to thank Bart Boetzkes for his contributions in the Phg-BTA work described in Chapter 5. Bart, your interest and excitement on this project inspired me a lot. I would like to thank Jeffrey for his detailed and elaborate work on the solvent effects in deuterated BTA self-assembly which is discussed in Chapter 4. Jeffrey, your hard working and motivation helped me enormously. Marcel Scheepstra, thanks for the chiral solvation experiments in Chapter 4. I would like to thank students, Tim, Sabrina, Martijn F., for working together in different projects.

I would like to thank Louis for proof reading my dissertation and for many valuable suggestions. English speaking and writing got another meaning after I met you. I learnt and improved a lot in this short period. I want to cite Hemingway here 'I hate when a text is well-written because I envy it too much!☺. Also thanks a lot for the nice chats, dinners and for always listening to me (mostly my complaints on stupidity in general). I would like to thank Elisa for reading my dissertation (for seeing every small detail). Also thanks for the fun time, nice parties, dancing, chatting.

I would like to thank all my colleagues in MST. Without them it would be impossible to survive the PhD life here in Eindhoven under a grey sky. No matter how far away I was from home I never felt alone. *Der gesellschaft* from the third floor Sascha, Katja, Dana, Micha, Lech, Marcel, Dung, thanks for parties, BBQs and 'just dance'. Isja, Rob, Luc, Marco, Louis, Elisa, Mindaguas, Dominuque, Danielle, Benjamin, Veronique, Ramon, Bob, Martin, Amparo, Thomas, Roxanne, Paco, Pablo, Michel (thanks Michel for the support during my writing period!), Carel, Maartje, Mellany, Sandra, Marie-France, Pol, Takashi, Takaya, Symo-Chem people (Ron, Joris, Michel, Tony),

Davide, Stanislav, Karthik, Janus, Christoph U., thanks for all the nice moments, coffee breaks, lunches, borrels, and Thursday evenings at Fort.

I found myself at the student rowing club E.S.R Thêta Eindhoven just after I'd arrived Eindhoven. Het Eindhovense Kanaal has been the most beautiful place in Eindhoven to me. I spent great time at Thêta and maybe had the most efficient working period in my PhD when I was training 8 times a week as a 'westrijd' rower. I would like to thank Marieke, Rianne, Sietse for helping me joining the club in my first year. I would like to thank Marthe Veenis for training together in the single skull and 2X, and for being a great rowing buddy. Demian, thanks for coaching in my first light weight rowing year. I would like to thank the members of Dames EJD 2010, Tessel, Evelien and Charlotte, the dream team!, top 'stuurman' Marc, and top coaches Mart, Marieke and Dirk. Thanks for the great time, *gezelligheid*, dinners and trainings.

And the habitants of the best student house in Eindhoven, the legendary Antonie Morostraat 4! Folkert, Thomas, Dirk, Roeland and Myrthe, thanks for the *gezelligheid*, BBQs, honger-duurt lang!, pasta rode-pasta groen, wat kan je wel.nl, roeien, mtb, bief stuk, jazz, Dave Brubeck, tuin, appeltaart…Folkert thanks for the holiday at Cinque Terra, alles over Volvo, mtb and your kind friendship. It has been always so much fun spending time with you.

Evet şimdi Türkçe kısmına geçebilirim, yolumuz uzun başlayalım bir an önce. Eindhoven'a alışmamda, ilk günlerin zorluğunu atlatmamda bana yardımcı olan, bu şehri yaşanılır kılan, doktora zamanlarını, tez yazmanın sancılı sürecini benimle birlikte dakika dakika yaşayan, hiçbir zaman desteklerini eksik etmeyen, bana paylaşmanın ve mutluluğun ne demek olduğunu ögreten canım arkadaşlarıma teşekkür etmek isterim.

Eindhoven'a geldiğimde, ilk tanıştığım insanlar, Irmak, Can, Özlem ve Beril. Sizi, sallantılı, gürültülü, her an yıkılacak hissi veren, minik ama sevimli 'spacebox' larda bulduğum için çok şanslıyım. Siz olmasaydınız Eindhoven hayatına bu kadar kolay adapte olabilirmiydim bilmiyorum. 2 Temmuz 2007'de, Eindhoven'da kışın en zorlu sartlar yaşanırken, gri, soğuk ve yağmurlu bir günde, kimya bölümünde tanıştığım, Ece, Barış, Emine, Yusuf, Tuba, beni ilk günlerin şokundan, bunalımından ve karanlığından kurtardığınız için çok teşekkür ederim.

Türk örf ve adetlerinin Eindhoven'daki yılmaz temsilcileri, 'mark günü' müdavimleri, Ece, Seda, Bahar ve Gözde, keyifli sohbetlerimiz, demleme çayla başlayan, kırmızı şarapla devam eden akşamlarımız için çok teşekkür ederim. Bu şehri daha yaşanılır bir hale getirdiğiniz, dostluğunuz ve paylaşımlarınız için teşekkür ederim. Özellikle Bahar ve Gözde, en zor anlarımda yanımda olduğunuz, beni aileden biri gibi sahiplendiğiniz, ne zaman canım sıkılsa iki çift güzel sohbet için hazır olduğunuz için nasıl teşekkür etsem azdır, varlığınız benim için çok ama çok anlamlı. Ayrıca, Bahar, Bölüm 2'deki enzimatik sentez konusundaki yardımların için çok tesekkürler. Doktorayı bitirme sürecinde, size sonsuz başarılar dilerim, yardıma her zaman hazırım, bunu unutmayın!

Abidin ve Başar, bize 'üç silahşörler' demek istiyorum. Aslinda emin de değilim uygun bir benzetme olur mu? Zannetmem☺ hem biz silah kullanmayı da bilmeyiz. Her neyse, en huysuz anlarımda bana katlandığınız, 'hep dayak hep azar' deseniz de benim yanımda olduğunuz, sıcak dostluğunuz için teşekkür ederim. Hatta sizi tebrik ederim. 'bir de böylelerini tebrik mi ediyorsun?'demeyin, ediyorum☺ Bisiklet gezileri, kamplar, bir takım içmeler, piknikler, hepsi için, en önemlisi bana dostluğun, paylaşmanin, ne demek olduğunu öğrettiğiniz için teşekkür ederim. Hiç bişey yapmasak bile sizinle sadece öylece oturmak, sohbet etmek, hayattan ordan buradan konuşmak inanılmaz keyifliydi. Abidin, motivasyon terapileri, omuzda ağlama seansları için, ne olursa olsun her an yardıma hazır olduğun için teşekkür ederim. Başar, konuyu hiç anlamadığın halde tezimin intro ve türkçe özet kısmını kontrol ettiğin için, benimle aylak aylak Eindhoven sokaklarında veya göl kenarında gezdiğin için sonsuz tesekkürler. Abidin&Başar, umarım bundan sonra da birlikte oluruz. Şairin dediği gibi: en güzel deniz henüz gidilmemiş olandır, en güzel çocuk henüz büyümedi, en güzel günlerimiz henüz yaşamadıklarımız...

Serkan ve Müge, sıkıntılı tez yazma saatlerimde bana eşlik ettiğiniz, 'tez odası'ndan bir an da olsa beni çekip kurtardığınız, odamı şenlendirdiğiniz için teşekkür ederim. Serkan, bir yaz günü analitik labında, sen bugün hangi solar cell'i yapsam diye düşünürken, ben de HPLC'de enantiomeric excess'im bugün kaç imiş acaba diye bakarken, yollarımız kesiştiği için çok mutluyum. Seninle gülmek, eğlenmek, film izlemek, geyik yapmak inanılmaz keyifliydi. Mügeee (yada Müjjj mü desem), bir Ocak ayında ansızın hayatıma girdiğin için, ofisime enerji ve neşe getirdiğin için, keyifli sohbetlerin, benimle aynı tabaktan yemek yediğin, aynı havayı soluduğun, Ezginin Günlüğü'yle başlayan Bülent Ortaçgil'le devam eden ve Cengiz Kurtoğlu'yla, saat 23.15 de Helix binasinin STO 4.43 numaralı odasında son bulan calışma saatlerine eşlik ettiğin, tüm bunlara bir anlam kattığın icin çok tesekkür ederim. Herşey çok güzel olacak, hep yanındayım bundan sonra☺ Serkan&Müge hayatınızdaki herşey 'çilekli vanilyalı kwark' tadında olsun!!

Aysegül ve Burcu 'ah şu helix binasının dili olsa da bi konuşsa!:)', kahkaha dolu sohbetlerimiz, geyiklerimiz için çok teşekkür ederim. Tez yazma dönemimde, Ayşegül, beni koridorda bir takım saksı bitkilerinin arkasında,

Burcu, kampüsde elimde bir tez, bir kalem gezerken yakalayıp beni ofisime götürdüğünüz için, keyifli arkadaşlığınız için çok teşekkür ederim.

Sevinç, Zilvermeeuwlaan'daki evimizi bir yuva haline getirdiğin için, tez yazma zamanımdaki desteklerin, çektiğin müthiş fotoğraflar ve akşamları 15 saat calışma sonrası, bir enkaz yığını halinde eve geldiğimde, odandan çıkıp 'Seda, harika gözüküyorsun, günün nasıldı?' diye sorup beni motive ettiğin için teşekkür ederim. Lana içten, dost ve beni kendime getiren gerçek sohbetlerin, desteklerin için çok tesekkur ederim.

Turkish gang'in geri kalan uyeleri, İlkin-Tuba, Kamil, Volkan, Koray, Aydın, Serdar, Doğan, Gökhan, Buket, Selçuk, Fırat, Altuğ, Merve, İlhan, Cem, bir zamanlar yolu Eindhoven semalarından geçen Tuba&Yiğit, süper keyifli zamanlar, öğlen yemekleri, geziler, voleybol maçları, piknikler, barbeküler, partiler, içmeler, için çok teşekkürler.

Doktora sürecim boyunca fiziksel olarak yanımda olmasalar da desteklerini hep yanımda hissettigim, ailem ve dostlarıma teşekkür etmek isterim. Bade, canım dostum, çocukluk arkadaşım, sıra arkadaşım, sırdaşım, biliyorum bu kimya aşkı uğruna çok uzak kaldık, yeterince görüşemedik. Sabrın ve bitmeyen sevgin için çok ama çok teşekkür ederim. Murat ve Beril'e de teşekkür ederim. Beril de bakalim belki bu yollardan gecer, ne de olsa babası ve teyzesi ODTÜ kimyalı☺

Ezgicim, ODTÜ yıllarımın can yoldaşı, Organik kimya sınavı oncesi, Güdaş kantininde, kahve-kola karışımlarının, bitmeyen lab saatlerinin ve arkasından gelen raporların tek ortağı. Kimya kantininde oturup, reaksiyon mekanizmalarını ezberlemeye calışırken bu kadar ileriye gidebileceğimizi tahmin edebilir miydik sence? O günlerden beri hep yanımda olduğun için, aynı yollarda benimle yanyana yürüdüğün için çok teşekkür ederim.

ODTÜ'den bahsetmişken, master danışmanım prof. Balcı'ya, organik kimya macerama başlamamdaki yardımları için, bir kez daha teşekkür etmek isterim. Doktora hayatım boyunca maillerle veya tatillerde sık sık görüştüğüm, desteğini hep hissettiğim, Raşit'e çok teşekkür ederim. 'Herşey tam planladığımız gibi' hocam, selamlar!.

Ankara'daki ailem Sarp ve Şule'ye, en başından beri desteklerini esirgemedikleri, evlerinin kapılarını bana her zaman açtıkları, bana en başından beri güvendikleri için teşekkür ederim.

Görkem ve Pieter, Amsterdam'da geçirdiğimiz güzel zamanlar, keyifli sohbetler için çok teşekkür ederim. Görkemcim, çocukluk arkadaşım, nereye gitsen peşindeyim, bunu biliyosun!. Onca yıldır her zaman benimle olduğun, dostluğun, paylaşımların için ne kadar teşekkür etsem azdır.

I would like to thank my (ex)schoon ouders Myra, Rik, and Rien for being my family in Eindhoven. Thanks for your support and being always there when I needed help. Myra, thanks for your caring and all the nice food you cooked. Hendrikje, thanks for sharing nice moments. Rien, thanks for being my family in Zeeland. I enjoyed the time we spent altogether. It was very special to listen to Dave Brubeck live from you in your living room.

Cok sevgili anne, baba ve biricik kardeşim Ezgi, biliyorum bu beş yıl hepimiz için zor oldu. Birbirimizi çok özledik, istediğimiz her an birbirimizi göremedik ve coğunlukla telefonda kısacık bir konuşmayla yetinmemiz gerekti. Buna katlandığınız, bitmeyen sabrınız, desteğiniz ve sevginiz için size teşekkür ederim. Almadan veren tek şey annelerdir. Annecim; babam, kardeşim ve bana baktığın, bitmez enerjin ve sevgin için çok teşekkürler. Babacım, belki de bilimsel araştırmaya olan merakım senin sayende gelişti, dogmatik olmamayı, kritik olmayı senden öğrendim. Senin sayende çok güzel kitaplar okuma fırsatım oldu. Her zaman cok açık fikirli oluşun, herkesden farklı oluşun için çok teşekkür ederim. Canım kardeşim Ezgi, en iyi arkadaşım, dostum olduğun için, her zaman bütün sevecenliğinle beni sardığın, benden düzgün bir insan yarattığın için çok teşekkür ederim. İyi ki varsın!.

My last words in this part go to Dirk... I still remember the first day I saw you at Thêta, in the ergometer ruimte, probably on one of the AV evenings. You coached me in the single skull and helped me enormously becoming a member at Thêta, planning all the trainings and helping me adapting the life there. It was an amazing experience for me. Afterwards, you helped me joining MST and you were always there for helping me getting along all the problems I faced with. We had great time together, almost four years, full of happy days, share, and unforgettable times. We worked together on the deuterated BTA project which was a great success. You have been always very analytical, rational, direct and open. I learnt a lot from you, a lot about rowing, chemistry, cooking, basically about everything in life. I grew up with you. Your presence meant a lot to me. I would like to thank you for everything, for all great, memorable moments, for caring, sharing, teaching and for being a great person...

Seda